

UNCLASSIFIED

AD NUMBER
AD061591
NEW LIMITATION CHANGE
TO Approved for public release, distribution unlimited
FROM Distribution authorized to U.S. Gov't. agencies and their contractors; Specific Authority; Nov 1954. Other requests shall be referred to WADC, Wright-Patterson, AFB OH.
AUTHORITY
AFAL 1tr 17 Aug 1979

THIS PAGE IS UNCLASSIFIED

AA / CATALOGED BY WCOSI-3

4. Apr 55

4413
WADC TECHNICAL REPORT 52-162

DO NOT DESTROY
RETURN TO
TECHNICAL DOCUMENT
CONTROL SECTION
WCOSI-3

FILE COPY

AD-61591
D-1852

FLUTTER CHARACTERISTICS OF A T-TAIL

C. D. PENGELLEY

L. E. WILSON

T. B. EPPERSON

G. E. RANSLEBEN, JR.

SOUTHWEST RESEARCH INSTITUTE

NOVEMBER 1954

WRIGHT AIR DEVELOPMENT CENTER

20011010015

NOTICE

When Government drawings, specifications, or other data are used for any purpose other than in connection with a definitely related Government procurement operation, the United States Government thereby incurs no responsibility nor any obligation whatsoever; and the fact that the Government may have formulated, furnished, or in any way supplied the said drawings, specifications, or other data, is not to be regarded by implication or otherwise as in any manner licensing the holder or any other person or corporation, or conveying any rights or permission to manufacture, use, or sell any patented invention that may in any way be related thereto.



FLUTTER CHARACTERISTICS OF A T-TAIL

C. D. PENGELLEY
L. E. WILSON
T. B. EPPERSON
G. E. RANSLEBEN, JR.

SOUTHWEST RESEARCH INSTITUTE

NOVEMBER 1954

AIRCRAFT LABORATORY
CONTRACT No. AF 33(038)-18404
RDO No. 459-36

WRIGHT AIR DEVELOPMENT CENTER
AIR RESEARCH AND DEVELOPMENT COMMAND
UNITED STATES AIR FORCE
WRIGHT-PATTERSON AIR FORCE BASE, OHIO

FOREWORD

The work described in this report was conducted by the Aeroelasticity Section, Engineering Mechanics Department, Southwest Research Institute, San Antonio, Texas under United States Air Force Contract AF 33(038)-18404 and Research and Development No. 459-36M, "Wind Tunnel Tests on T-Tail Flutter Models". The project was initiated and sponsored by the Dynamics Branch, Aircraft Laboratory, Wright Air Development Center and was administered by Capt. G. P. Haviland and Mr. L. A. Tolve of the Dynamics Branch.

The authors are indebted to Messrs. W. L. Mynatt and W. A. Strutman for their contributions to the design, construction and testing of the model. Appreciation is also extended to Miss M. Gresham and Mrs. D. Simpson who edited and typed the report.

ABSTRACT

A T-tail flutter model was designed, built and tested by personnel of Southwest Research Institute, San Antonio, Texas. Wind tunnel tests were conducted at the Wright Air Development Center 20 Foot Wind Tunnel during May and June, 1952.

The stabilizer of the model could be located at six different positions on the fin: three different chordwise points at each of two different spanwise stations. The stabilizer rocking frequency, fuselage side bending and torsional frequencies, and rudder rotational frequency could all be varied. Tests involving various combinations of these four degrees of freedom as well as fin bending and torsion were conducted for various stabilizer locations. The stabilizer could be replaced by streamlined weights which simulated the stabilizer in weight, yawing moment of inertia and center of gravity location but not in roll inertia.

Theoretical flutter analyses were conducted for six different model configurations with the number of degrees of freedom involved ranging from two to four. No aspect ratio corrections were employed in the analyses.

Results indicate that for a constant fin bending to fin torsion frequency ratio the critical nondimensional velocity ratio, $V/B_r \omega_f$, for T-tails is relatively independent of stabilizer fore and aft locations in the range of chordwise locations tested. Also for a constant fin bending to fin torsion frequency ratio, the T-tail with stabilizer located at the 58% fin span has a more critical $V/B_r \omega_f$ than when the stabilizer is located at the fin tip. Stabilizer stiffness in roll relative to the fin has a negligible effect on the critical nondimensional velocity ratio, $V/B_r \omega_f$, over the range tested. Reducing the fuselage stiffness in side bending and torsion results generally in a decreased critical nondimensional velocity ratio, $V/B_r \omega_f$.

For constant or fixed fin torsion and bending stiffnesses the critical flutter speed, V , for T-tails decreases appreciably as the stabilizer position is changed from 8 to 48% of the fin chord aft of the fin elastic axis, and increases appreciably when the stabilizer position is changed from the fin tip to the 58% fin span location.

PUBLICATION REVIEW

This report has been reviewed and is approved.

FOR THE COMMANDER:



DANIEL D. MCKEE
Colonel, USAF
Chief, Aircraft Laboratory
Directorate of Laboratories

TABLE OF CONTENTS

<u>Item</u>	<u>Page</u>
LIST OF FIGURES	v
LIST OF TABLES	ix
LIST OF SYMBOLS	x
SUMMARY	xiv
INTRODUCTION AND PURPOSE	xvi
I. PROCEDURE	1
A. Model Design and Construction	1
B. Wind Tunnel Tests	4
C. Theoretical Calculations	8
II. RESULTS	12
III. DISCUSSION	62
A. General	62
B. Experimental Results	63
C. Theoretical Results	68
IV. CONCLUSIONS AND RECOMMENDATIONS	70
A. Conclusions	70
B. Recommendations	71
V. REFERENCES	72
APPENDIX I - DATA	73
APPENDIX II - MODEL DESCRIPTION	91
APPENDIX III - DERIVATION OF DETERMINANT ELEMENTS. . .	120

LIST OF FIGURES

<u>Figure</u>		<u>Page</u>
1.	Effect of Stabilizer C.G. Location on Critical $V/B_r \omega$, <u>Fuselage Locked</u>	23
2.	Effect of Stabilizer C.G. Location on Critical $V/B_r \omega_r$ and V, <u>Fuselage Locked</u>	24
3.	Effect of Stabilizer C.G. Location on Critical ω/ω_r , <u>Fuselage Locked</u>	25
4.	Effect of Stabilizer C.G. Location on Critical $V/B_r \omega$, <u>Fuselage Free</u>	26
5.	Effect of Stabilizer C. G. Location on Critical $V/B_r \omega_r$ and V, <u>Fuselage Free</u>	27
6.	Effect of Stabilizer C.G. Location on Critical ω/ω_r , <u>Fuselage Free</u>	28
7.	Effect of Stabilizer Equivalent Weight C.G. Location on Critical $V/B_r \omega$, <u>Fuselage Locked</u> . . .	29
8.	Effect of Stabilizer Equivalent Weight C.G. Location on Critical $V/B_r \omega_r$ and V, <u>Fuselage Locked</u>	30
9.	Effect of Stabilizer Equivalent Weight C.G. Location on Critical ω/ω_r , <u>Fuselage Locked</u> . . .	31
10.	Effect of Stabilizer Equivalent Weight C. G. Location on Critical $V/B_r \omega$, <u>Fuselage Free</u> . . .	32
11.	Effect of Stabilizer Equivalent Weight C. G. Location on Critical $V/B_r \omega_r$ and V, <u>Fuselage Free</u> . . .	33
12.	Effect of Stabilizer Equivalent Weight C. G. Location on Critical ω/ω_r , <u>Fuselage Free</u>	34
13.	Effect of Stabilizer Rocking Frequency on Critical $V/B_r \omega$, Stabilizer at 100% Fin Span, <u>Fuselage Locked</u>	35
14.	Effect of Stabilizer Rocking Frequency on Critical $V/B_r \omega_r$, Stabilizer at 100% Fin Span, <u>Fuselage Locked</u>	36

LIST OF FIGURES (continued)

Figure		Page
15.	g_r vs. $V/B_r \omega_r$, Fin Bending-Fin Torsion Flutter, Stabilizer C.G. at 100% Fin Span and 48% Fin Chord . . .	37
16.	g_r vs. $V/B_r \omega_r$, Fin Bending - Fin Torsion Flutter, Stabilizer C.G. at 100% Fin Span and 68% Fin Chord . . .	38
17.	g vs. $V/B_r \omega_r$, Fin Bending-Fin Torsion Flutter, Stabilizer Equivalent Weight C.G. at 100% Fin Span and 68% Fin Chord	39
18.	g_r vs. $V/B_r \omega_r$, Fin Bending-Fin Torsion Flutter, Stabilizer C.G. at 100% Fin Span and 88% Fin Chord. . .	40
19.	$V/B_r \omega$ vs. ω_h/ω_r , Fin Bending-Fin Torsion Flutter, Stabilizer C.G. at 100% Fin Span and 48% Fin Chord. . .	41
20.	$V/B_r \omega_r$ vs. ω_h/ω_r , Fin Bending-Fin Torsion Flutter, Stabilizer C.G. at 100% Fin Span and 48% Fin Chord. . .	42
21.	$V/B_r \omega$ vs. ω_h/ω_r , Fin Bending-Fin Torsion Flutter, Stabilizer C.G. at 100% Fin Span and 68% Fin Chord. . .	43
22.	$V/B_r \omega_r$ vs. ω_h/ω_r , Fin Bending- Fin Torsion Flutter, Stabilizer C.G. at 100% Fin Span and 68% Fin Chord. . .	44
23.	$V/B_r \omega$ vs. ω_h/ω_r , Fin Bending-Fin Torsion Flutter, Stabilizer Equivalent Weight C.G. at 100% Fin Span and 68% Fin Chord	45
24.	$V/B_r \omega_r$ vs. ω_h/ω_r , Fin Bending-Fin Torsion Flutter, Stabilizer Equivalent Weight C.G. at 100% Fin Span and 68% Fin Chord	46
25.	$V/B_r \omega$ vs. ω_h/ω_r , Fin Bending-Fin Torsion Flutter, Stabilizer C.G. at 100% Fin Span and 88% Fin Chord. . .	47
26.	$V/B_r \omega_r$ vs. ω_h/ω_r , Fin Bending-Fin Torsion Flutter, Stabilizer C.G. at 100% Fin Span and 88% Fin Chord. . .	48
27.	$V/B_r \omega$ vs. ω_h/ω_r , Fin Bending-Fin Torsion-Stabilizer Rocking Flutter, Stabilizer C.G. at 100% Fin Span and 68% Fin Chord	49

LIST OF FIGURES (continued)

<u>Figure</u>		<u>Page</u>
28.	$V/B_r \omega_r$ vs. $\omega h/\omega_r$, Fin Bending-Fin Torsion - Stabilizer Rocking Flutter, Stabilizer C.G. at 100% Fin Span and 68% Fin Chord	50
29.	$V/B_r \omega$ vs. $\omega h/\omega_r$, Fin Bending-Fin Torsion-Fuselage Side Bending-Fuselage Torsion Flutter, Stabilizer C.G. at 100% Fin Span and 68% Fin Chord . .	51
30.	$V/B_r \omega_r$ vs. $\omega h/\omega_r$, Fin Bending-Fin Torsion-Fuselage Side Bending-Fuselage Torsion Flutter, Stabilizer C.G. at 100% Fin Span and 68% Fin Chord . .	52
31.	Zero Airspeed Vibration Node Lines and Frequencies (CPM)	53
32.	Typical Zero Airspeed and Flutter Oscillograph Records	61
I-1.	Fin-Rudder Weight Distribution	84
I-2.	Fin-Rudder S_y Distribution	85
I-3.	Fin-Rudder I_y Distribution	86
I-4.	Fin EI Distribution	87
I-5.	Fin GJ Distribution	88
I-6.	Fin Bending Mode Shape	89
I-7.	Fin Torsion Mode Shape	90
II-1.	Assembled Model in Test Jig	92
II-2.	Uncovered Model	93
II-3.	Fuselage Flexure Beam and Air Valve Installation . . .	95
II-4.	Fin Spar	96
II-5.	Fin and Fuselage Geometry and Pickup Locations	98

LIST OF FIGURES (concluded)

<u>Figures</u>		<u>Page</u>
II-5a.	Stabilizer Equivalent Weight Geometry.	99
II-6.	Mounted Stabilizer Equivalent Weights.	100
II-7.	Uncovered Stabilizer	101
II-8.	Stabilizer Geometry and Pickup Locations	103
II-9.	Assembled Rudder	104
II-10.	Stabilizer Rocking Fitting Strain Gage Installation. .	107
II-11.	Stabilizer Rocking Strain Gage Installation Characteristics	108
II-12.	Fuselage Side Bending Strain Gage Installation Characteristics	109
II-13.	Fuselage Torsion Strain Gage Installation Characteristics	110
II-14.	Rudder Rotation Strain Gage Installation Characteristics	111
II-15.	Typical Accelerometer Response Curve	112
II-16.	Phase Angle Calibration Curve.	113
II-17.	Schematic Diagram of Air Exciting System	114
II-18.	Model and Safety System, Stabilizer at Fin Tip	116
II-19.	Model and Safety System, Stabilizer at 58% Fin Span. .	117
II-20.	Safety System Cocking Mechanism.	118
II-21.	Model and Safety System for Stabilizer Equivalent Weights Configurations	119
III-1.	Fin and Stabilizer Nomenclature.	121

LIST OF TABLES

<u>Table</u>		<u>Page</u>
1.	Design Geometric and Mass Parameters	2
2.	Design Frequency Parameters	3
3.	Wind Tunnel Test Schedule	6
4.	Additional Tests	9
5.	Summary of Test Results	14
6.	Test Amplitude Ratios	18
7.	Comparison of Theoretical and Experimental Flutter Parameters	21
I-1.	Summary of Model Parameters	74
I-2.	Summary of Uncoupled Frequencies and Damping Coefficients used in Analyses.	78
I-3.	Summary of Numerical Values of Determinant Elements - Infinite Aspect Ratio	79
II-1.	Pickup and Channel Identification.	105

LIST OF SYMBOLS

Symbols other than those listed below are defined in Reference 1.

h Lateral displacement of fin elastic axis, positive to right on inverted model looking forward - in.

h_L Lateral displacement of fin elastic axis at fin tip, positive to right on inverted model looking forward - in.

h' $\frac{\partial h}{\partial s_F}$ - Slope of fin bending curve.

h'_L $\left(\frac{\partial h}{\partial s_F}\right)_L$ - Tip slope of fin bending curve.

δ Rotation about fin elastic axis in plane perpendicular to fin elastic axis, positive counterclockwise looking from root to tip - radians.

δ_L Rotation about fin elastic axis at fin tip in plane perpendicular to fin elastic axis, positive counterclockwise looking from root to tip - radians.

ϕ Fuselage rotation about vertical axis through flexure beam \mathcal{E} , positive counterclockwise looking from fin root to tip - radians.

θ Fuselage rotation about axis through flexure beam longitudinal \mathcal{E} , positive counterclockwise looking forward - radians.

β Rudder rotation about rudder hinge line, positive counterclockwise looking from fin root to tip - radians.

ψ Stabilizer rotation about axis parallel to fuselage \mathcal{E} and at stabilizer \mathcal{E} , positive counterclockwise looking forward - radians.

χ_h $\left(\frac{\partial h}{\partial s_F}\right)_L \cos \angle_F = h'_L \cos \angle_F$ - radians

ψ_δ $\delta_L \sin \angle_F$ - radians

χ_h $\left(\frac{\partial h}{\partial s_F}\right)_L \sin \angle_F = h'_L \sin \angle_F$ - radians

γ $\delta_L \cos \Lambda_F$ - radians

Λ_F Sweepback angle of fin elastic axis.

Λ_S Sweepback angle of stabilizer quarter chord line.

α_F Fin angle of attack (rotation in plane parallel to airstream) positive counterclockwise looking from root to tip - radians.

α_S Stabilizer angle of attack = 0 radians.

S_F Distance measured from fin root along fin elastic axis - in.

L_F Fin tip station on elastic axis = S_{Ftip} - in.

S_S Distance measured from stabilizer root along stabilizer pseudo-elastic axis (line parallel to stabilizer quarter chord line and passing through fin elastic axis trace) - in.

L_S Stabilizer tip station on pseudo-elastic axis = S_{Stip} - in.

B_F Fin semichord parallel to fuselage center line--in. or ft.

B_r Reference semichord (on fin) parallel to fuselage center line, 16.71 in. from fin root = 1.445 ft.

b_F Fin semichord perpendicular to fin elastic axis - in. or ft.

B_S Stabilizer semichord parallel to fuselage center line - in. or ft.

b_S Stabilizer semichord perpendicular to stabilizer pseudo-elastic axis - in. or ft.

$(BX_\gamma)_S = S_S \cos \Lambda_S + B_S(1/2+a) \sin \Lambda_S \cos \Lambda_S$ - in.

r Distance, parallel to fuselage center line, from fin elastic axis at fin tip to stabilizer C.G. - in.

r_F Distance measured from fin elastic axis, perpendicular to fin elastic axis - in.

r_S Distance measured from stabilizer pseudo-elastic axis, perpendicular to pseudo-elastic axis - in.

X_R Distance, perpendicular to fuselage center line, from flexure beam center line to fin root - in.

X_t Distance, perpendicular to fuselage center line, from flexure beam center line to fin tip - in.

Y_R Distance, parallel to fuselage center line, from center of flexure beam to fin elastic axis at fin root - in.

Y_t	Distance, parallel to fuselage center line, from center of flexure beam to fin elastic axis at fin tip - in.
m	Fin-rudder combination mass per unit length along fin elastic axis - $\frac{\text{lb sec}^2}{\text{in.}^2}$
σ	Mass per unit area = $\frac{\text{lb sec}^2}{\text{in.}^3}$
M_F	Total mass of fin-rudder combination - $\frac{\text{lb sec}^2}{\text{in.}}$
M_S	Total mass of stabilizer (both sides) - $\frac{\text{lb sec}^2}{\text{in.}}$
S_γ	Fin-rudder combination static unbalance about fin elastic axis, per unit length along fin elastic axis - $\frac{\text{lb in. sec}^2}{\text{in.}^2}$
S_{γ_s}	Total stabilizer static unbalance about a vertical axis through fin elastic axis trace at fin tip ($=M_S r$) - $\frac{\text{lb in. sec}^2}{\text{in.}}$
I_γ	Fin-rudder moment of inertia about fin elastic axis, per unit length along fin elastic axis - $\frac{\text{lb in.}^2 \text{ sec}^2}{\text{in.}^2}$
I_F	Total moment of inertia of fin-rudder about fin elastic axis - $\frac{\text{lb in.}^2 \text{ sec}^2}{\text{in.}}$
I_R	Total rolling moment of inertia of stabilizer (both sides) about an axis through fin tip parallel to fuselage center line - $\frac{\text{lb in.}^2 \text{ sec}^2}{\text{in.}}$
I_{sy}	Total moment of inertia of stabilizer about a horizontal axis through flexure beam center line, parallel to fuselage center line ($= I_R + M_S X_t^2$) - $\frac{\text{lb in.}^2 \text{ sec}^2}{\text{in.}}$
I_{yaw}	Total yawing moment of inertia of stabilizer (both sides) about a vertical axis through stabilizer C.G. - $\frac{\text{lb in.}^2 \text{ sec}^2}{\text{in.}}$
I_y	Total yawing moment of inertia of stabilizer about a vertical axis through fin elastic axis trace at fin tip ($= I_{yaw} + M_S r^2$) - $\frac{\text{lb in.}^2 \text{ sec}^2}{\text{in.}}$

- I_{sx} Total moment of inertia of stabilizer about a vertical axis through flexure beam center line $(=I_{yaw} + M_s(Y_t + r)^2) - \frac{lb \text{ in.}^2 \text{ sec}^2}{\text{in.}}$
- $I_{\phi x}$ Total moment of inertia of fuselage about a vertical axis through flexure beam center line $- \frac{lb \text{ in.}^2 \text{ sec}^2}{\text{in.}}$
- I_{ey} Total moment of inertia of fuselage about a horizontal axis through flexure beam center line $- \frac{lb \text{ in.}^2 \text{ sec}^2}{\text{in.}}$
- T_F Total fin-rudder combination kinetic energy - lb in.
- T_s Total stabilizer kinetic energy - lb in.
- T_{FUS} Total fuselage kinetic energy - lb in.
- T $T_F + T_s + T_{FUS}$ - Total kinetic energy in system - lb in.
- W_i Work done or potential energy in i degree of freedom by virtue of air forces - lb in.
- $\Omega_i = \left(\frac{\omega_i}{\omega}\right)^2 (1 + jg_i)$
- q_i Generalized coordinate describing motion in i degree of freedom
- $\dot{q}_i = \frac{dq_i}{dt}$
- Q_i Generalized force in i degree of freedom.
- ω_h Natural "circular" uncoupled frequency of fin in bending about an axis perpendicular to the fin elastic axis in the fin chord plane and includes the effects of the rigid stabilizer yawing and rolling moments of inertia - radians per second or cycles per minute.
- ω_r Natural "circular" uncoupled frequency of fin in torsion about the fin elastic axis (chord planes perpendicular to the fin elastic axis) and includes the effects of the rigid stabilizer yawing and rolling moments of inertia - radians per second or cycles per minute.
- ω_y Natural "circular" uncoupled frequency of rigid stabilizer rocking on rigid fin about an axis parallel to the fuselage center line - radians per second or cycles per minute.
- ω_ϕ Natural "circular" uncoupled frequency of fuselage plus rigid empennage in side bending about a vertical axis through center line of the fuselage flexure beam - radians per second or cycles per minute.
- ω_θ Natural "circular" uncoupled frequency of fuselage plus rigid empennage in torsion about the longitudinal axis through the center line of the fuselage flexure beam - radians per second or cycles per minute.

SUMMARY

Flutter characteristics of a T-tail flutter model having variable stabilizer locations as well as variable stiffnesses in the stabilizer rocking, fuselage side bending, fuselage torsion and rudder rotation degrees of freedom are presented. Both fin and stabilizer were swept-back and tapered. The stabilizer could be replaced by equivalent weights in order to eliminate stabilizer aerodynamic damping. Although mass, static unbalance and yaw inertia conditions were satisfied, the roll inertia condition was not simulated. Detailed descriptions of all aspects of the tests and calculations conducted are included.

The following results are contained herein:

1. Tabular results of all wind tunnel tests.
2. Graphical results of wind tunnel tests and calculations showing the effect of stabilizer location on the flutter parameters.
3. Graphical results of wind tunnel tests and calculations showing the effect of stabilizer rocking frequency on the flutter parameters.
4. Calculated flutter characteristics for six configurations involving a maximum of four degrees of freedom.
5. Tabular comparison of experimental and theoretical results.
6. Zero airspeed frequencies and mode shapes for the various configurations.

The results indicate that:

1. For constant fin bending and fin torsion frequencies the critical $V/B_r \omega_f$ for T-tails is quite insensitive to fore and aft stabilizer position but relatively sensitive to spanwise position; the 58% fin span location being more critical than the fin tip location.
2. For constant or fixed fin torsion and bending stiffnesses the critical flutter speed, V , for T-tails decreases appreciably as the stabilizer position is changed from 8 to 48% of the fin chord aft of the fin elastic axis, and increases appreciably when the stabilizer position is changed from the fin tip to the 58% fin span location.

3. Stabilizer stiffness in roll relative to the fin (rocking of the stabilizer on the fin) on this T-tail configuration has a negligible effect on the critical $V/B_r \omega_r$ over the range of stiffnesses tested.
4. Generally, a decrease in critical $V/B_r \omega_r$ results from reducing the fuselage stiffness in side bending and in torsion.
5. The theoretical analyses, in which no aspect ratio corrections were made, of a limited number of the test configurations indicates correlation between test and theoretical values of $V/B_r \omega$ and $V/B_r \omega_r$ ranging from approximately 20% conservative to 20% unconservative; the majority of cases indicating the theoretical results to be unconservative.

INTRODUCTION AND PURPOSE

For some time it has been known that serious flutter difficulties could arise from a wing configuration in which a relatively heavy mass located near the wing tip results in appreciable mass coupling and produces a bending-torsion frequency ratio near unity. Such a condition may result from a T-tail configuration in which the stabilizer is located at or near the fin tip.

A recent Air Force airplane was designed and built with a T-tail configuration; both fin and stabilizer having approximately 35° of sweepback. The sweepback tended to place the center of gravity of the stabilizer aft of the fin elastic axis thus creating a possible serious mass coupling effect from the flutter standpoint. It was recognized, however, that the aerodynamic damping contributed by the stabilizer possibly could offset the adverse mass coupling effect, and thus result in a satisfactorily stable empennage. A flutter analysis of the T-tail configuration should include four or more degrees of freedom, effects of taper, and aspect ratio corrections. Consequently, it was believed that this complicated an analysis, without any experimental check points to be used for comparison purposes, would be unreliable in predicting flutter speeds for such an aircraft. As a result it was considered desirable to design, construct, test and analyze a T-tail wind tunnel flutter model having, in its normal configuration, characteristics roughly similar to an actual airplane.

The purpose of this investigation was to determine by experimental methods the flutter characteristics of a T-tail with emphasis on the effect on the flutter characteristics of (1) stabilizer fore and aft location on the fin, (2) stabilizer spanwise location on the fin, (3) stabilizer rocking stiffness, (4) fuselage side bending and torsional stiffness, and (5) rudder rotational stiffness. The yawing frequency of the stabilizer relative to the fin was kept high as specified in the contract requirements; however, some information recently furnished to the WADC indicates that this flutter parameter is very important for T-tail configurations.

I. PROCEDURE

A. Model Design and Construction

The flutter model was designed to simulate approximately, a full scale airplane in the following degrees of freedom:

1. fin bending
2. fin torsion
3. stabilizer rocking
4. stabilizer bending
5. fuselage side bending
6. fuselage torsion
7. rudder rotation

Other degrees of freedom such as stabilizer yaw, fuselage vertical bending, stabilizer torsion, and elevator rotation were not simulated.

The model was designed and constructed so that the following parameters could be varied:

1. fuselage side bending stiffness
2. fuselage torsional stiffness
3. fin spanwise location of the stabilizer
4. fin chordwise location of the stabilizer
5. stabilizer rocking stiffness
6. rudder rotational stiffness
7. aerodynamic damping of the stabilizer

The parameters on which the design was based are listed in Tables 1 and 2.

As shown in Figure II-1, Appendix II, the aft section of the fuselage was cantilevered from the rigidly supported forward section by means of a flexure beam designed to simulate the fuselage side bending stiffness and the fuselage torsional stiffness of a full scale airplane. Means were incorporated whereby all fuselage motion, both bending and torsion, could be effectively locked out when desired.

Attachment points for the stabilizer were provided at six different points on the fin: three at 58% of the fin span and three at the fin tip. The chordwise positions employed were at 48, 68 and 88% of the local chord for each of the two spanwise stations. The stabilizer was attached to the fin by means of flexure springs which prevented any stabilizer yawing motion relative to the fin but could be altered to produce the various desired rocking stiffnesses. Stabilizer attachments are shown in Figure II-4, Appendix II.

<u>No.</u>	<u>Parameter</u>	<u>Model Parameter</u>
1.	Maximum fuselage depth	31.33 inches
2.	Maximum fuselage width	25.00 inches
3.	Fin height above fuselage	34.50 inches
4.	Fin tip chord	28.67 inches
5.	Fin root chord	41.67 inches
6.	Rudder span	26.67 inches
7.	Stabilizer root chord	26.67 inches
8.	Stabilizer semispan	40.67 inches
9.	Stabilizer tip chord	13.20 inches
10.	Stabilizer - elevator weight per side . . .	8.41 pounds
11.	Fin - rudder weight	19.67 pounds
12.	Rudder weight	2.03 pounds
13.	Rudder moment of inertia about hinge line .	11.88 pounds-inches ²
14.	Stabilizer-elevator C.G., % stabilizer chord	50 %
15.	Stabilizer elastic axis, % stabilizer chord	40 %
16.	Fin elastic axis, % fin-rudder chord . . .	40 %
17.	Fin - rudder C.G., % fin chord	48 %
18.	Moment of inertia of stabilizer - elevator about fin tip 40% chord	56.24 pounds-feet ²
19.	Airfoil thickness ratio	10 % (approximate)

Table 1 - DESIGN GEOMETRIC AND MASS PARAMETERS

<u>No.</u>	<u>Parameter</u>	<u>Model Parameter</u>
1.	Stabilizer rocking frequency relative to rigid fin	Variable (See Table 3)
2.	Uncoupled fin bending frequency with rigidly attached stabilizer and rigid fuselage*	225 cpm approximately
3.	Uncoupled fin torsional frequency with rigidly attached stabilizer and rigid fuselage*	300 cpm
4.	Uncoupled fuselage side bending frequency*	180 cpm
5.	Uncoupled fuselage torsional frequency*	180 cpm
6.	Rudder frequency	Variable (See Table 3)
7.	Stabilizer symmetrical bending frequency	440 cpm
8.	Stabilizer yaw frequency relative to rigid fin	High: at least 2.5 times the uncoupled fin torsional frequency

* Normal Stabilizer Location (Fin tip, 68% fin chord)

Table 2 - DESIGN FREQUENCY PARAMETERS

A variable length torsion spring attached at the rudder root and to the fuselage allowed a wide range of rudder rotational stiffness values to be obtained easily. Streamlined weights (Fig. II-6, Appendix II) which had a C.G. location, weight and yawing moment of inertia equivalent to that of the stabilizer were constructed so that they could be used to replace the stabilizer, thereby eliminating stabilizer aerodynamic damping. A duplicate empennage was constructed, complete with exciter system installation and instrumentation leads, for use in case of damage to the original parts. A maximum tunnel speed of 250 mph was used as a basis of design for all model components.

A compressed air exciting system was installed in the model which consisted of a variable speed motor-driven rotary air valve located in the forward fuselage (Fig. II-3, Appendix II) which fed sinusoidal air pulses through individual tubes imbedded in the model to ports at the stabilizer tips. The ports opened to both the upper and lower surface of the stabilizer, pointing slightly outboard and forward to provide components of air pulses in vertical, lateral, and fore and aft directions. Air was valved to these ports in such a manner as to produce unsymmetrical excitation for the model. The system also included a solenoid shutoff valve, tachometer, and necessary controls.

Eight accelerometers and four strain gage installations were incorporated at strategic points to allow measurements to be made of the motion. William Miller accelerometers, amplifiers and recording equipment were used exclusively.

Following completion of the construction of the model, all uncoupled modes that could be isolated were excited in order to check the design uncoupled frequencies. This was accomplished by tying down various parts of the model with wire so that only the desired motion could take place. A detailed description of the model structure, support system, exciting system, safety system and instrumentation appears in Appendix II.

B. Wind Tunnel Tests

The wind tunnel tests were conducted at the Wright Air Development Center 20-foot Wind Tunnel during the period 14 May to 13 June 1952. Table 3 presents the testing program conducted in the wind tunnel. Tests 1 through 32 were conducted by Southwest Research Institute personnel with the assistance of WADC representatives under terms of the contract. Tests 33 through 66 were later conducted by the WADC Dynamics Branch.

Prior to the start of the wind tunnel test program, shake table calibrations were performed for all accelerometers. Response curves were obtained using a wide range of frequencies and two different amplitude settings. The accelerometers were rendered displacement sensitive by virtue of the amplifier double integration circuits

whereas the strain gage circuits contained no integrators. Since the integrators introduced a phase shift which was a function of frequency, it was necessary to run phase calibrations to determine the relative phase angle between accelerometer and strain gage signals at various frequencies. This was done by installing a strain gage bridge on a flexure beam which was fixed at one end; the other end was forced to move with the shake table. Each accelerometer was calibrated in its respective amplifier channel and the recording oscillograph was used to record simultaneously the eight accelerometer outputs and the strain gage bridge output. A phase calibration curve and a typical accelerometer response curve are included in Appendix II.

The strain gage bridges which were used to measure fuselage side bending, fuselage torsion, stabilizer rocking, and rudder rotation were all subjected to static calibrations. Calibrations, in terms of oscillograph trace amplitude versus angle of rotation, were obtained by applying moments to the various model components.

Before testing each model configuration, the zero airspeed coupled modes were excited and decay records made of each. However, in the cases in which the configuration change involved merely the releasing of the rudder from a locked condition, only a rudder rotation decay record was made. Excitation was accomplished either by using the compressed air exciting system or by manual shaking. The latter method proved more satisfactory for the lower modes due to the lack of fine frequency control of the air vibrator.

During each run the tunnel velocity was increased in steps and with each step the model was excited in the two most prominent coupled modes. The pickup traces were observed on the oscillograph screen during the decay. Simultaneously, a record of the output of one accelerometer, located either in the stabilizer tip or the fin tip, was recorded on a Brush recorder and analyzed immediately. In this manner an approximate velocity-damping record, which proved valuable in predicting the approximate flutter velocity, was kept. This speeded up the tests since a basis for the choice of velocity increments was established. Oscillograph records were made when flutter was obtained. Most of the excitations at finite airspeeds were accomplished manually by jerking a wire attached near the leading edge of the fin and extending through the tunnel wall. This was necessitated by the fact that the compressed air exciting system did not produce a sufficiently strong pulsation to excite the model effectively at high velocities.

Some difficulty was encountered in trimming the stabilizer in roll at high velocities and at the low rocking spring stiffness. This was attributed to the presence of slight differences in geometric twist and incidence of the two halves of the stabilizer which resulted from manufacturing tolerances. The attachment of small aluminum trim tabs to the stabilizer eliminated the difficulty.

Test Number	Stabilizer Location (% Fin Span)	Stabilizer Location (% Fin Chord)	Equivalent Stabilizer Weights	Rudder Rotational Frequency	Stabilizer Rocking Frequency	Fuselage Side-bending Frequency	Fuselage Torsional Frequency
PART A							
1	100	68	-- --	Locked	Locked	Locked	Locked
2	100	68	-- --	0.3 ω	Locked	Locked	Locked
3	100	68	-- --	Locked	.75 ω	Locked	Locked
4	100	68	-- --	Locked	.50 ω	Locked	Locked
5	100	68	-- --	Locked	.75 ω	Free	Locked
6	100	68	-- --	Locked	.75 ω	Free	Free
7	100	68	-- --	.3 ω	.75 ω	Free	Free
8	100	68	-- --	.75 ω	.75 ω	Free	Free
9	100	68	-- --	2.0 ω	.75 ω	Free	Free
10	100	68	On	Locked	Locked	Locked	Locked
11	100	88	On	Locked	Locked	Locked	Locked
12	100	48	On	Locked	Locked	Locked	Locked
PART B							
13	100	48	-- --	Locked	Locked	Locked	Locked
14	100	48	-- --	0.3 ω	Locked	Locked	Locked
15	100	48	-- --	Locked	.75 ω	Locked	Locked
16	100	48	-- --	Locked	.50 ω	Locked	Locked

Table 3 - WIND TUNNEL TEST SCHEDULE

Test Number	Stabilizer Location (% Fin Span)	Stabilizer Location (% Fin Chord)	Equivalent Stabilizer Weights	Rudder Rotational Frequency	Stabilizer Rocking Frequency	Fuselage Side-bending Frequency	Fuselage Torsional Frequency
17	100	88	- - -	Locked	Locked	Locked	Locked
18	100	88	- - -	0.3 ω	Locked	Locked	Locked
19	100	88	- - -	Locked	.75 ω	Locked	Locked
20	100	88	- - -	Locked	.50 ω	Locked	Locked
PART C							
21	58	48	- - -	Locked	Locked	Locked	Locked
22	58	48	- - -	0.3 ω	Locked	Locked	Locked
23	58	48	- - -	Locked	.75 ω	Locked	Locked
24	58	48	- - -	Locked	.50 ω	Locked	Locked
25	58	68	- - -	Locked	Locked	Locked	Locked
26	58	68	- - -	0.3 ω	Locked	Locked	Locked
27	58	68	- - -	Locked	.75 ω	Locked	Locked
28	58	68	- - -	Locked	.50 ω	Locked	Locked
29	58	88	- - -	Locked	Locked	Locked	Locked
30	58	88	- - -	.3 ω	Locked	Locked	Locked
31	58	88	- - -	Locked	.75 ω	Locked	Locked
32	58	88	- - -	Locked	.50 ω	Locked	Locked

Note ω = Uncoupled fin torsion frequency with rigidly attached stabilizer.

Table 3 (continued)

In the process of running the test program, (Table 3), tests 10, 11, and 12 were postponed until the remaining 29 tests were completed. Catastrophic flutter was encountered while conducting Test 10 which resulted in the destruction of the fin and equivalent stabilizer weights. The explosive nature of the flutter encountered in this test and the difficulty experienced in controlling it caused the postponement of the two remaining tests which involved somewhat similar configurations.

The model was refitted with the spare fin and partial instrumentation, and turned over to the WADC Dynamics Branch for additional tests. Some of the tests in the original schedule were repeated and are included in Table 4 with additional tests as Test Numbers 33 through 66.

Reynold's Numbers encountered during the tests ranged from 2.48 to 6.12×10^6 .

C. Theoretical Calculations

Theoretical flutter analyses were conducted for tests 1, 3, 10, 13, 17, and 45 which incorporated combinations of the following degrees of freedom:

1. fin bending
2. fin torsion
3. stabilizer rocking
4. fuselage side bending
5. fuselage torsion

The uncoupled modes used in the analyses are listed in Table I-2. The uncoupled fin bending and fin torsion mode shape and natural frequency calculations were made by means of an iteration process using calculated deflection influence coefficients and measured mass and mass moment of inertia data. These measured data were obtained in the case of the fin by actually sawing the structure into seven sections and measuring the mass properties of each. Experimental uncoupled stabilizer rocking, fuselage side bending and fuselage torsion frequencies and straight line mode shapes were used. All pertinent data are presented in Appendix I.

Prior to conducting the flutter analyses zero airspeed frequency and mode shape checks were performed for each of the six tests for which flutter analyses were to be performed. This was done in order to insure the validity of the determinant elements. In each case the frequency required to make the determinant vanish was determined by successive approximation.

The derivations of determinant elements are presented in Appendix III and the numerical values are tabulated in Table I-3, Appendix I. Determinant solutions were conducted using the Arnold Vector Method of Reference 2. Aspect ratio corrections, which would have been rendered

Test Number	Corresponding Test Number in Table 3	Stabilizer Location (% Fin Span)	Stabilizer Location (% Fin Chord)	Equivalent Stabilizer Weights	Rudder Rotational Frequency	Stabilizer Rocking Frequency	Fuselage Side-bending Frequency	Fuselage Torsional Frequency
33	1	100	68	- - -	Locked	Locked	Locked	Locked
43	6	100	68	- - -	Locked	.75 ω_f	Free	Free
44	3	100	68	- - -	Locked	.75 ω_f	Locked	Locked
45	None	100	68	- - -	Locked	Locked	Free	Free
47	13	100	48	- - -	Locked	Locked	Locked	Locked
48	None	100	48	- - -	Locked	Locked	Free	Free
49	15	100	48	- - -	Locked	.75 ω_f	Locked	Locked
50	None	100	48	- - -	Locked	.75 ω_f	Free	Free
51	17	100	88	- - -	Locked	Locked	Locked	Locked
52	None	100	88	- - -	Locked	Locked	Free	Free
53	19	100	88	- - -	Locked	.75 ω_f	Locked	Locked
54	None	100	88	- - -	Locked	.75 ω_f	Free	Free

Table 4 - ADDITIONAL TESTS

Test Number	Corresponding Test Number in Table 3	Stabilizer Location (% Fin Span)	Stabilizer Location (% Fin Chord)	Equivalent Stabilizer Weights	Rudder Rotational Frequency	Stabilizer Rocking Frequency	Fuselage Side-bending Frequency	Fuselage Torsional Frequency
55	None	58	48	- - -	Locked	Locked	Free	Free
56	21	58	48	- - -	Locked	Locked	Locked	Locked
57	None	58	68	- - -	Locked	Locked	Free	Free
58	25	58	68	- - -	Locked	Locked	Locked	Locked
59	None	58	88	- - -	Locked	Locked	Free	Free
60	29	58	88	- - -	Locked	Locked	Locked	Locked
61	10	100	68	On	Locked	Locked	Locked	Locked
62	None	100	68	On	Locked	Locked	Free	Free
63	None	100	48	On	Locked	Locked	Free	Free
64	None	100	88	On	Locked	Locked	Free	Free
65	11	100	88	On	Locked	Locked	Locked	Locked
66	12	100	48	On	Locked	Locked	Locked	Locked

Note ω_y = Uncoupled fin torsion frequency with rigidly attached stabilizer

Table 4 - (continued)

somewhat complicated by such things as the end plate effect of the stabilizer on the fin, were not desired since the scope of the investigation did not require complete and comparable analyses with and without aspect ratio corrections; consequently aspect ratio corrections were ruled out in favor of a greater number of the more simple infinite aspect ratio solutions. While theoretical spot checks were made of experimental points, the emphasis was generally placed on establishing trends rather than on pin-pointing exact flutter speeds.

II. RESULTS

Experimental and theoretical results are presented in tabular and graphical form in Tables 5 through 7 and Figures 1 through 30 respectively. Table 5 is a summary of test results including both zero air-speed and flutter data. Values of $V/B_r \omega$ and ω/ω_x are based on calculated values of ω_x . Experimental amplitude ratios and associated phase angles are contained in Table 6.

Figures 1 through 6 are graphs of $V/B_r \omega$, $V/B_r \omega_x$, V and ω/ω_x versus stabilizer center of gravity location for both the locked and free fuselage configurations. Similar graphs for the stabilizer equivalent weights are presented in Figures 7 through 12. The effect of stabilizer rocking frequency on the critical $V/B_r \omega$ and $V/B_r \omega_x$ is shown in Figures 13 and 14. Points located at zero frequency ratio are based on an infinitely rigid rocking fitting. Although stabilizer rocking motion could not be completely locked out, the rocking frequency in the locked configuration was several times that of fin torsion. The curves in Figures 1 through 14, although basically experimental results, also include theoretical points.

Theoretical flutter analyses were conducted for six different model configurations which involved a minimum of two and a maximum of four degrees of freedom; the stabilizer or the stabilizer equivalent weights were located at the fin tip in all cases. Graphical results of these theoretical analyses are presented in Figures 15 through 30. The curves of Figures 15, 16, and 18, which are graphs of g_x versus critical $V/B_r \omega_x$ for three model configurations, were obtained by holding g_h constant and varying g_x as it was evident from the graphical solution that variations in g_h had relatively little effect on the results. However, for the case shown in Figure 17 both damping coefficients were varied. Graphs of critical $V/B_r \omega$ and $V/B_r \omega_x$ versus ω_h/ω_x for all six configurations are contained in Figures 19 through 30. The ordinates of the experimental points included in the g_x or g versus $V/B_r \omega_x$ curves were determined by the measured damping coefficient in the coupled mode which most closely approximated fin torsion. In the remaining curves ($V/B_r \omega$ versus ω_h/ω_x and $V/B_r \omega_x$ versus ω_h/ω_x), the experimental $V/B_r \omega$ and $V/B_r \omega_x$ values are plotted versus ratios of calculated fin bending and torsion frequencies.

Table 7 is a tabular comparison of theoretical and experimental flutter results for the six configurations mentioned above. The test amplitude ratios are based on fin tip amplitudes.

All of the aforementioned experimental results are taken from the latter set of test runs (33 through 66) with the exception of amplitude ratios. Four of the six configurations for which flutter analyses were conducted were

tested in the first set of test runs and repeated in the latter set of test runs, the exceptions being Test Numbers 45 and 61 for which there were no corresponding tests conducted in the original schedule (Tests 1 through 32). Lower flutter speeds were obtained at the time these tests were repeated, but no appreciable change was noted in flutter frequencies and amplitude ratios. Since more complete instrumentation was used in the original tests, amplitude ratios were determined from those tests where possible. The amplitude ratios listed for Tests 45 and 61 are approximate as a result of the limited instrumentation. The differences in the results of the two sets of tests are treated in the Discussion.

Figures 31a through 31h are sketches which show the zero airspeed node lines and frequencies for all important model configurations. Many of the model configuration changes involved only the unlocking of the rudder or changing the rudder rotational frequency. Because of the negligible effect of the rudder frequency on the zero airspeed coupled modes, only the cases involving a locked rudder are included. The node lines shown for Test Numbers 33 through 66 are approximate because of the simplified instrumentation used in these runs. However, points on these lines at the intersections of the lines with a line through the fin tip parallel to the air stream are accurate.

Figure 32 is a photograph of a zero airspeed oscillograph record and a flutter record for the same model configuration. These records are typical of the ones obtained throughout the tests.

Model Configuration							Zero Airspeed Measured Coupled Frequencies (cpm)					Flutter Data			
Test No.	Stab. Loc. on Fin (% Span) (1)	Stab. Loc. on Fin (% Chord) (2)	Stab. Rocking Freq. (cpm) (3)	Rudder Freq. (cpm)	Fuselage Side Bend. Freq. (cpm) (3)	Fuselage Torsion Freq. (cpm) (3)	1st Mode	2nd Mode	3rd Mode	4th Mode	Flutter Freq. ω (cpm)	Flutter Speed V (mph)	V/B _r ω (5)	V/B _r ω (5)	ω/ω_N
1	100	68	Locked	Locked	Locked	Locked	176	274	467	---	239	205	8.33	6.87	.824
2	100	68	Locked	100	Locked	Locked	176	274	467	---	178	117	6.39	3.92	.614
3	100	68	214	Locked	Locked	Locked	150	216	393	---	232	214	8.95	7.17	.800
4	100	68	138	Locked	Locked	Locked	122	203	382	---	230	209	8.81	7.00	.794
5	100	68	214	Locked	172	Locked	133	170	308	429	188	198	10.22	6.64	.649
6	100	68	214	Locked	172	258	---	169	300	361	180	195	10.50	6.53	.621
7	100	68	214	100	172	258	---	169	304	364	151	120	7.70	4.02	.521
8	100	68	214	200	172	258	123	169	300	366	150	114	7.37	3.82	.517
9	100	68	214	546	172	258	125	170	305	364	181	188	10.08	6.29	.624
10	100	68	(4)	Locked	Locked	Locked	192	375	---	---	---	---	---	---	---
11	100	88	(4)	Locked	Locked	Locked	(6)	---	---	---	---	---	---	---	---
12	100	48	(4)	Locked	Locked	Locked	(6)	---	---	---	---	---	---	---	---
13	100	48	Locked	Locked	Locked	Locked	177	277	448	---	258	190	7.15	6.11	.854
14	100	48	Locked	100	Locked	Locked	177	276	450	---	181	147	7.88	4.73	.599
15	100	48	214	Locked	Locked	Locked	149	231	383	---	249	212	8.25	6.82	.825

Table 5 - SUMMARY OF TEST RESULTS

Model Configuration						Zero Airspeed Measured Coupled Frequencies (cpm)					Flutter Data				
Test No.	Stab. Loc. On Fin		Stab. Rocking Freq. (cpm)	Rudder Freq. (cpm)	Fuselage Side Bend. Freq. (cpm)	Fuselage Torsion Freq. (cpm)	1st Mode	2nd Mode	3rd Mode	4th Mode	Flutter Freq. ω (cpm)	Flutter Speed V (mph)	V/B ₁ ω (5)	V/B ₂ ω (5)	ω/ω_n
	(% Span) (1)	(% Chord) (2)													
16	100	48	138	Locked	Locked	Locked	120	215	351	---	249	220	8.57	7.08	.825
17	100	88	Locked	Locked	Locked	Locked	167	258	465	---	211	175	8.05	6.34	.788
18	100	88	Locked	96	Locked	Locked	167	257	465	---	174	105	5.85	3.80	.650
19	100	88	214	Locked	Locked	Locked	149	201	402	---	204	176	8.37	6.37	.761
20	100	88	138	Locked	Locked	Locked	120	185	382	---	208	201	9.37	7.29	.776
21	58	48	Locked	Locked	Locked	Locked	230	352	526	---	(7)	---	---	---	---
22	58	48	Locked	102	Locked	Locked	231	352	526	---	(7)	---	---	---	---
23	58	48	214	Locked	Locked	Locked	178	293	486	---	345	252	7.08	5.24	.740
24	58	48	138	Locked	Locked	Locked	131	279	475	---	342	246	6.98	5.12	.734
25	58	68	Locked	Locked	Locked	Locked	226	337	---	---	321	253	7.65	5.58	.730
26	58	68	Locked	102	Locked	Locked	226	337	---	---	306	253	8.01	5.58	.696
27	58	68	214	Locked	Locked	Locked	176	276	487	---	326	246	7.32	5.43	.741
28	58	68	138	Locked	Locked	Locked	133	263	490	---	314	248	7.65	5.47	.714
29	58	88	Locked	Locked	Locked	Locked	218	316	---	---	293	239	7.91	5.84	.739
30	58	88	Locked	102	Locked	Locked	218	310	---	---	(7)	---	---	---	---
31	58	88	214	Locked	Locked	Locked	174	256	486	---	(7)	---	---	---	---
32	58	88	138	Locked	Locked	Locked	131	243	470	---	297	245	8.01	5.99	.748

Table 5 - (continued)

Model Configuration							Zero Airspeed Measured Coupled Frequencies (cpm)				Flutter Data			
Test No.	Stab. Loc. on Fin	Stab. (3) Rocking Freq. (cpm)	Rudder Freq. (cmp)	Fuselage (3) Side Bend. Freq. (cpm)	Fuselage (3) Torsion Freq. (cpm)	1st Mode	2nd Mode	3rd Mode	4th Mode	Flutter Freq. ω (cpm)	Flutter Speed V(mph)	V/B _F ω (5)	V/B _F ω /ω _N	
	(% Span) (1)													(% Chord) (2)
33	100	68	Locked	Locked	Locked	178	272	465	---	238	176	7.16	5.88	.820
43	100	68	214	Locked	258	126	181	302	366	172	162	9.14	5.43	.593
44	100	68	214	Locked	Locked	156	222	395	---	225	179	7.73	5.99	.776
45	100	68	Locked	Locked	258	128	224	313	458	189	167	8.56	5.59	.651
47	100	48	Locked	Locked	Locked	179	275	450	---	248	177	6.91	5.68	.821
48	100	48	Locked	Locked	258	132	220	320	435	193	167	8.38	5.35	.639
49	100	48	214	Locked	Locked	156	233	363	---	243	182	7.27	5.85	.805
50	100	48	214	Locked	258	129	179	313	341	178	162	8.84	5.21	.589
51	100	88	Locked	Locked	Locked	166	256	464	---	209	154	7.14	5.56	.780
52	100	88	Locked	Locked	258	123	223	293	462	184	154	8.10	5.56	.686
53	100	88	214	Locked	Locked	155	207	405	---	200	151	7.32	5.46	.746
54	100	88	214	Locked	258	121	175	288	375	158	141	8.66	5.11	.590
55	58	48	Locked	Locked	258	150	252	388	512	219	206	9.11	4.29	.470
56	58	48	Locked	Locked	Locked	233	353	530	---	336	237	6.83	4.91	.720
57	58	68	Locked	Locked	258	147	249	377	520	208	193	8.99	4.25	.473
58	58	68	Locked	Locked	Locked	226	309	510	---	300	207	6.68	4.55	.682

Table 5 - (continued)

Model Configuration							Zero Airspeed Measured Coupled Frequencies (cpm)				Flutter Data				
Test No.	Stab. Loc. on Fin		Stab. Rocking Freq. (cpm)	Rudder Freq. (cpm)	Fuselage Side Bend. Freq. (cpm)	Fuselage Torsion Freq. (cpm)	1st Mode	2nd Mode	3rd Mode	4th Mode	Flutter Freq. (cpm)	Flutter Speed V (mph)	$V/B \omega$ (5) ^r	$V/B \omega$ (5) ^r	ω/ω_n
	(% Span) (1)	(% Chord) (2)													
59	58	88	Locked	Locked	172	258	141	250	351	510	196	182	8.99	4.44	.494
60	58	88	Locked	Locked	Locked	Locked	218	290	506	---	269	180	6.49	4.40	.678
61	100	68	(4)	Locked	Locked	Locked	195	379	---	---	294	213	7.02	6.09	.867
62	100	68	(4)	Locked	172	258	133	288	361	908	294	183	6.04	5.23	.869
63	100	48	(4)	Locked	172	258	137	286	385	---	269	211	7.60	5.80	.762
64	100	88	(4)	Locked	172	258	127	284	337	908	265	201	7.35	6.22	.846
65	100	88	(4)	Locked	Locked	Locked	179	371	---	---	274	219	7.75	6.78	.875
66	100	48	(4)	Locked	Locked	Locked	204	344	---	---	284	203	6.93	5.58	.805

Table 5 - (concluded)

- (1) Stabilizer location on fin measured from fin root
- (2) Stabilizer CG location on fin measured in percent of fin chord from fin L.E.
- (3) Stabilizer rocking, fuselage side bending and fuselage torsion frequencies are calculated uncoupled frequencies based on static test data. The measured, coupled frequencies are, fuselage side bending 155 cpm, fuselage torsion 210 cpm.
- (4) For Test Nos. 10 and 61-66 the stabilizer was replaced with a steel tube having approximately the same weight and yaw moment of inertia as that of the stabilizer.
- (5) B_r = reference semi-chord (on fin) parallel to fuselage centerline, 16.71 inches from fin root = 1.445 ft.
- (6) Tests cancelled.
- (7) No clear flutter mode established below 250 mph.

Model Configuration					Experimental Amplitude Ratios						
Test No.	Stab. Loc. (% Span) (1)	Stab. Loc. On Fin (% Chord) (2)	Stab Rocking Freq. (cpm) (3)	Rudder Freq. (cpm)	Fuselage Side Bend. Freq. (cpm) (3)	Fuselage Torsion Freq. (cpm) (3)	χ/h (5) rad/in	β/h (5) rad/in	γ/h (5) rad/in	ϕ/h (5) rad/in	θ/h (5) rad/in
1	100	68	Locked	Locked	Locked	Locked	0.0458/15°	0	0	0	0
2	100	68	Locked	100	Locked	Locked	0.000848/0°	0.0925/92°	0	0	0
3	100	68	214	Locked	Locked	Locked	0.0247/0°	0	0.0254/277°	0	0
4	100	68	138	Locked	Locked	Locked	0.0250/32°	0	0.0131/271°	0	0
5	100	68	214	Locked	172	Locked	0.0369/356°	0	0.0477/226°	0.0166/10°	0
6	100	68	214	Locked	172	258	0.0391/37°	0	0.0340/234°	0.0156/10°	0.00488/350°
7	100	68	214	100	172	258	0.0136/345°	0.103/83°	0.0139/155°	0.0238/10°	0.0102/1°
8	100	68	214	200	172	258	0.00465/312°	0.112/82°	0	0.0231/10°	0.0109/1°
9	100	68	214	546	172	258	0.0262/0°	0.0717/3°	0.0445/264°	0.0201/3°	0.00645/14°
10	100	68	(4)	Locked	Locked	Locked	(6)	-----	-----	-----	-----
11	100	88	(4)	Locked	Locked	Locked	(7)	-----	-----	-----	-----
12	100	48	(4)	Locked	Locked	Locked	(7)	-----	-----	-----	-----
13	100	48	Locked	Locked	Locked	Locked	0.0328/31°	0	0	0	0
14	100	48	Locked	100	Locked	Locked	0.00417/180°	0.0898/145°	0	0	0

Table 6 - TEST AMPLITUDE RATIOS

Model Configuration					Experimental Amplitude Ratios						
Test No.	Stab. Loc. on Fin		(3) Stab. Rocking Freq. (cpm)	Rudder Freq. (cpm)	(3) Fuselage Side Bend. Freq. (cpm)	(3) Fuselage Torsion Freq. (cpm)	δ/h (5) rad/in	β/h (5) rad/in	γ/h (5) rad/in	ϕ/h (5) rad/in	θ/h (5) rad/in
	% Span (1)	% Chord (2)									
15	100	48	214	Locked	Locked	Locked	0.0338/22°	0	0.0157/237°	0	0
16	100	48	138	Locked	Locked	Locked	0.037/32°	0	0.0266/305°	0	0
17	100	88	Locked	Locked	Locked	Locked	0.0368/0°	0	0	0	0
18	100	88	Locked	96	Locked	Locked	0.00197/0°	0.0728/113°	0	0	0
19	100	88	214	Locked	Locked	Locked	0.01083/0°	0	0.0168/268°	0	0
20	100	88	138	Locked	Locked	Locked	0.031/9°	0	0.03615/288°	0	0
21	58	48	Locked	Locked	Locked	Locked	(8)	-----	-----	-----	-----
22	58	48	Locked	102	Locked	Locked	(8)	-----	-----	-----	-----
23	58	48	214	Locked	Locked	Locked	0.0488/62°	0	0.0133/78°	0	0
24	58	48	138	Locked	Locked	Locked	0.0694/53°	0	0.0157/99°	0	0
25	58	68	Locked	Locked	Locked	Locked	0.0372/35°	0	0	0	0
26	58	68	Locked	102	Locked	Locked	0.0304/0°	0.0432/56°	0	0	0
27	58	68	214	Locked	Locked	Locked	0.1409/25°	0	0.0403/35°	0	0
28	58	68	138	Locked	Locked	Locked	0.0660/32°	0	0.0237/31°	0	0
29	58	88	Locked	Locked	Locked	Locked	0.0427/7°	0	0	0	0

Table 6 -- (continued)

Model Configuration							Experimental Amplitude Ratios				
Test No.	Stab. Loc. on Fin		Stab. (3) Rocking Freq. (cpm)	Rudder Freq. (cpm)	Fuselage (3) Side Bend. Freq. (cpm)	Fuselage (3) Torsion Freq. (cpm)	δ/h (5) rad/in	β/h (5) rad/in	ν/h (5) rad/in	ϕ/h (5) rad/in	θ/h (5) rad/in
	% Span (1)	% Chord (2)									
30	58	88	Locked	102	Locked	Locked	(8)				
31	58	88	214	Locked	Locked	Locked	(8)				
32	58	88	138	Locked	Locked	Locked	$0.0775/\underline{27^\circ}$	0	$0.0314/\underline{23^\circ}$	0	0

Table 6 - (concluded)

(1)

Stabilizer location on fin measured from fin root.

(2)

Stabilizer CG location on fin measured in percent of fin chord from fin L.E.

(3)

Stabilizer rocking, fuselage side bending and fuselage torsion frequencies are calculated uncoupled frequencies based on static test data. The measured, coupled frequencies are, fuselage side bending 155 cpm, fuselage torsion 210 cpm.

(4)

For Test No. 10 the stabilizer was replaced with a steel tube having approximately the same weight and yaw moment of inertia as that of the stabilizer.

(5)

Phase angles are h leading.

(6)

NC amplitude ratios obtained. See Procedure, Page 11.

(7)

Test cancelled.

(8)

No clear flutter mode established below 250 mph.

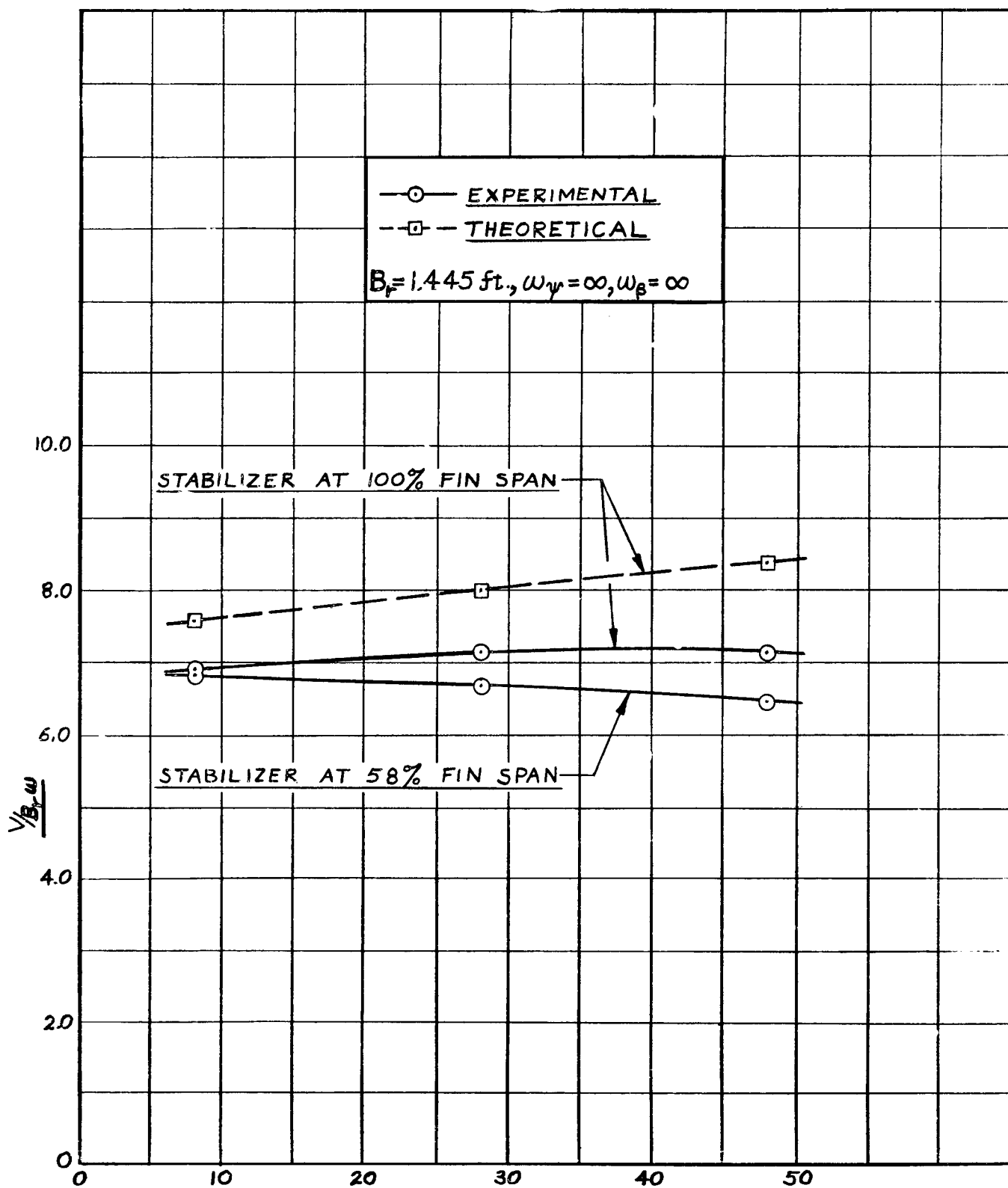
Model Configuration							Flutter Parameter											
Test No.	Stab. Loc. on Fin (% Span) (1)	Stab. Rocking Freq. (cpm) (2)	Stab. (3)	Rudder Freq. (cpm)	Fuselage Side Bend. Freq. (cpm) (3)	Fuselage Torsion Freq. (cpm) (3)	V/B _r ω (5)			V/B _r ω γ (5)			ω/ω _x			V (mph)		
							Calc.	Test	Calc. Test	Calc.	Test	Calc. Test	Calc.	Test	Calc. Test	Calc.	Test.	Calc. Test
47	100	48	Locked	Locked	Locked	Locked	7.58	6.91	1.097	6.70	5.68	1.180	.885	.821	1.078	209	177	1.180
33	100	68	Locked	Locked	Locked	Locked	8.00	7.16	1.118	6.70	5.88	1.140	.837	.820	1.021	200	176	1.140
61	100	68	(4)	Locked	Locked	Locked	7.01	7.02	.999	5.81	6.09	.955	.829	.867	.956	203	213	.955
51	100	88	Locked	Locked	Locked	Locked	8.38	7.14	1.174	6.89	5.56	1.240	.822	.780	1.055	190	154	1.240
44	100	68	214	Locked	Locked	Locked	7.90	7.73	1.023	7.05	5.99	1.178	.893	.777	1.150	211	179	1.178
45	100	68	Locked	Locked	172	258	7.05	8.56	.823	4.95	5.59	.886	.702	.651	1.080	148	167	.886

Table 7 - COMPARISON OF THEORETICAL AND EXPERIMENTAL FLUTTER PARAMETERS

Model Configuration					Amplitude Ratios and Phase Angles (h Leading)							
Test No.	Stab. Loc. on Fin (% Span) (1)	Stab. Loc. on Fin (% Chord) (2)	Stab. Rocking Freq. (cpm) (3)	Rudder Freq. (cpm)	Fuselage Side Bend. Freq. (cpm) (3)	Fuselage Torsion Freq. (cpm) (3)	δ/h rad/in		ψ/h rad/in		ϕ/h rad/in	
							Calc.	Test	Calc.	Test	Calc.	Test
13	100	48	Locked	Locked	Locked	Locked	.0733 /20.4°	.0328 /30.9°	----- -----	----- -----	----- -----	----- -----
1	100	68	Locked	Locked	Locked	Locked	.080 /18.1°	.0458 /14.8°	----- -----	----- -----	----- -----	----- -----
61	100	68	(4)	Locked	Locked	Locked	.173 /25.2°	.0526 /99.1°	----- -----	----- -----	----- -----	----- -----
17	100	88	Locked	Locked	Locked	Locked	.088 /16.0°	.0368 /0°	----- -----	----- -----	----- -----	----- -----
3	100	68	214	Locked	Locked	Locked	.1325 /21.4°	.000848 /0°	.0284 /28.2°	.0925 /92°	----- -----	----- -----
45	100	68	Locked	Locked	172	258	.0364 /348.6°	.0498 /15.3°	----- -----	----- -----	.008 /346.8°	.0113 /12.4°
											.0102 /204.2°	.00156 /304.4°

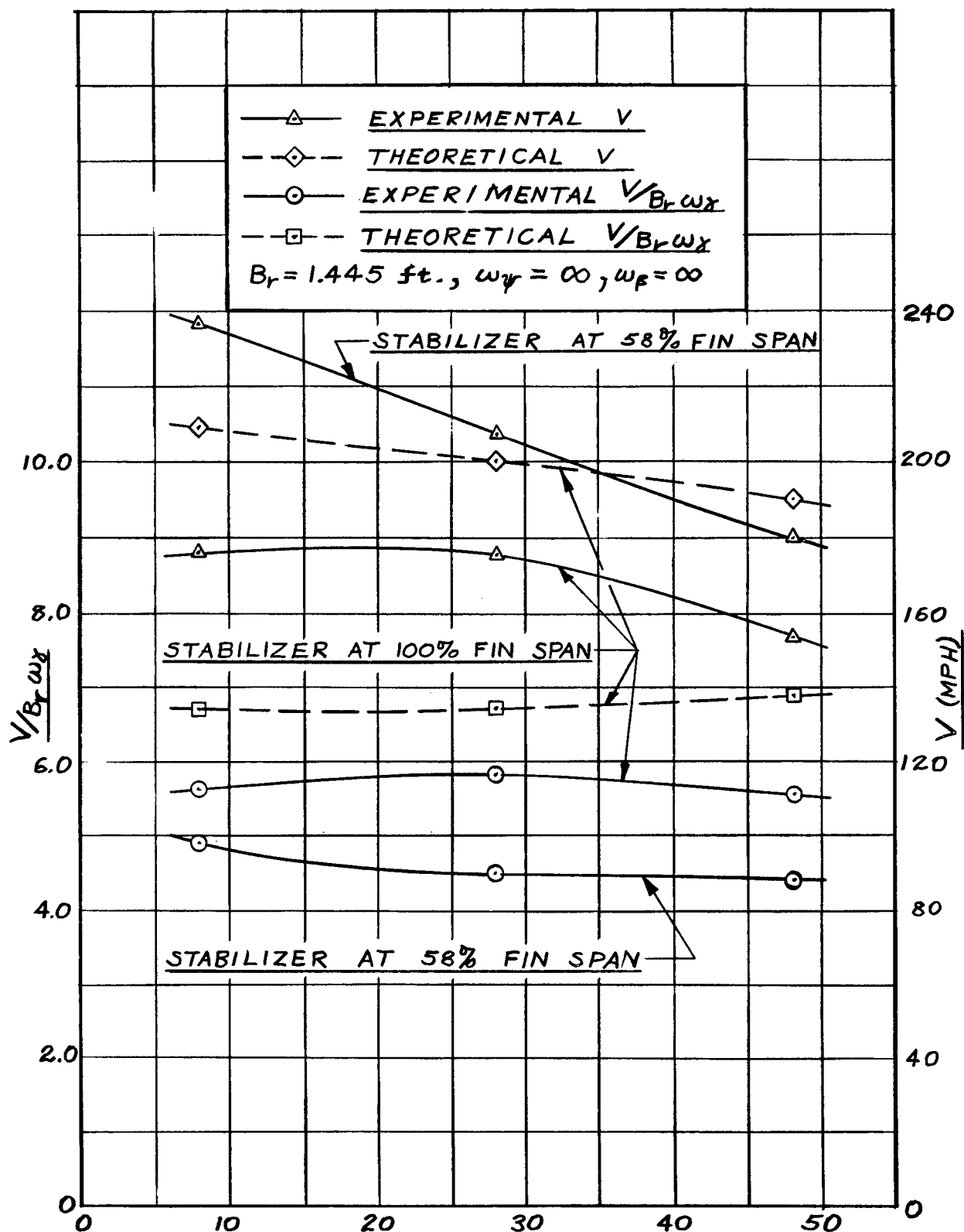
Table 7 - (continued)

- (1) Stabilizer location on fin measured from fin root.
- (2) Stabilizer CG location on fin measured in percent of fin chord from fin L.E.
- (3) Stabilizer rocking, fuselage side bending and fuselage torsion frequencies based on static test data. The measured, coupled frequencies are, fuselage side bending 155 cpm, fuselage torsion 210 cpm.
- (4) For Test No. 61 the stabilizer was replaced with a steel tube having approximately the same weight and yaw moment of inertia as that of the stabilizer.
- (5) B_T = reference semi-chord (on fin) parallel to fuselage centerline, 16.71 inches from fin root = 1.445 ft.



Stabilizer C.G. Location in Per Cent Fin Chord Aft of Elastic Axis

Fig. 1 Effect of Stabilizer C.G. Location on Critical $V/B_r \omega$
Fuselage Locked



Stabilizer C. G. Location in Per Cent Fin Chord Aft of Elastic Axis

Fig. 2 Effect of Stabilizer C.G. Location on Critical $V/B_r \omega_x$ and V ,
Fuselage Locked

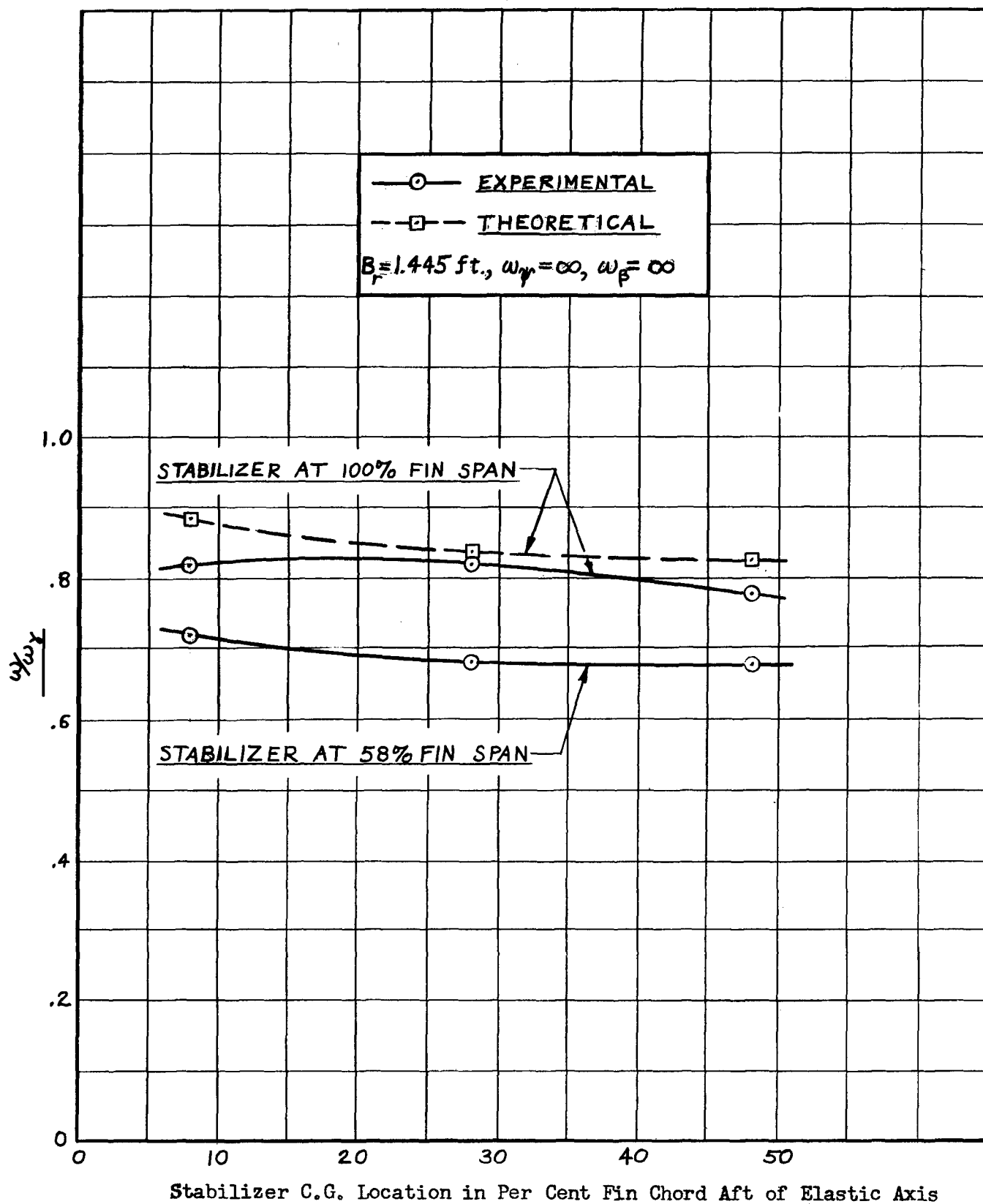
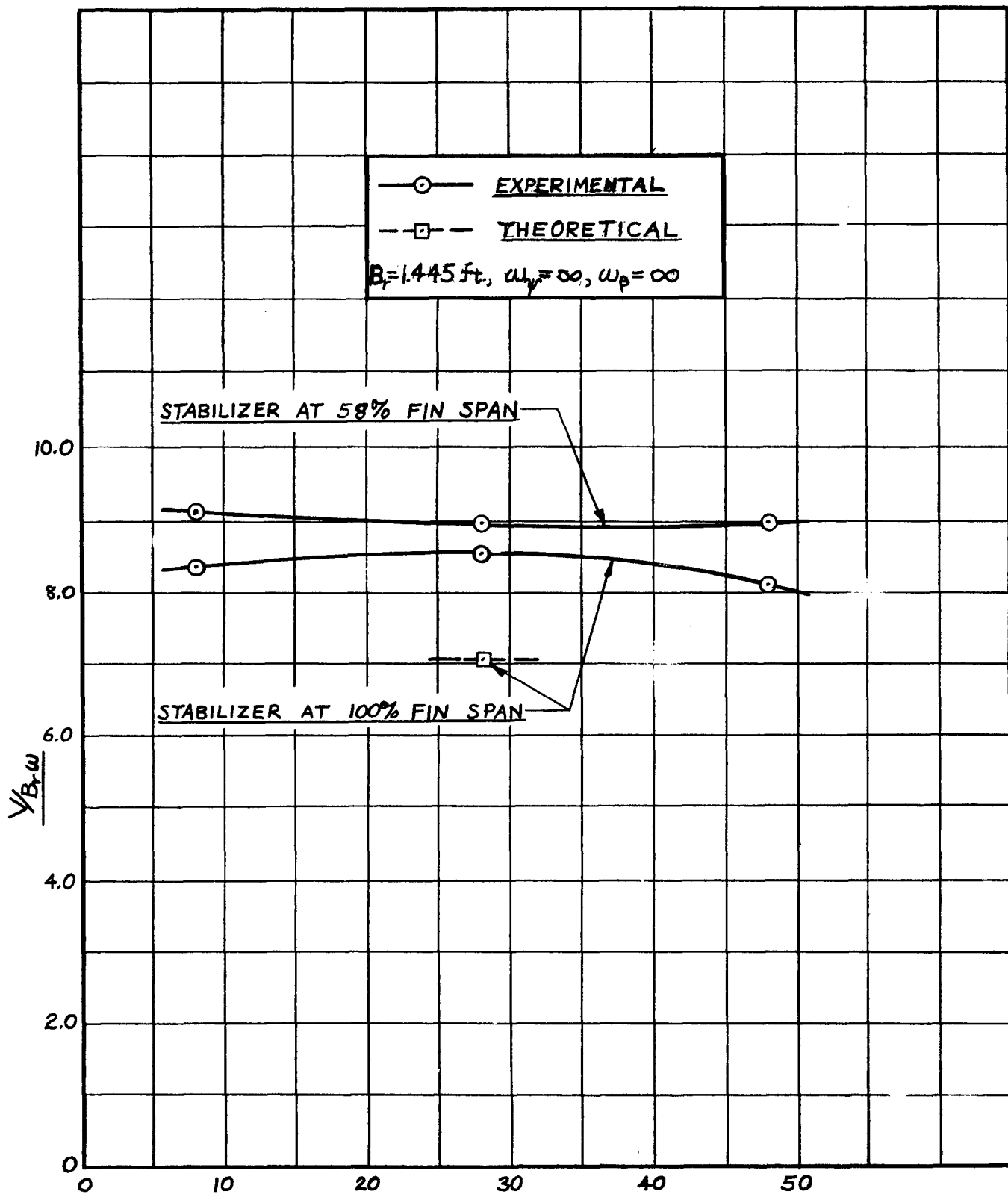
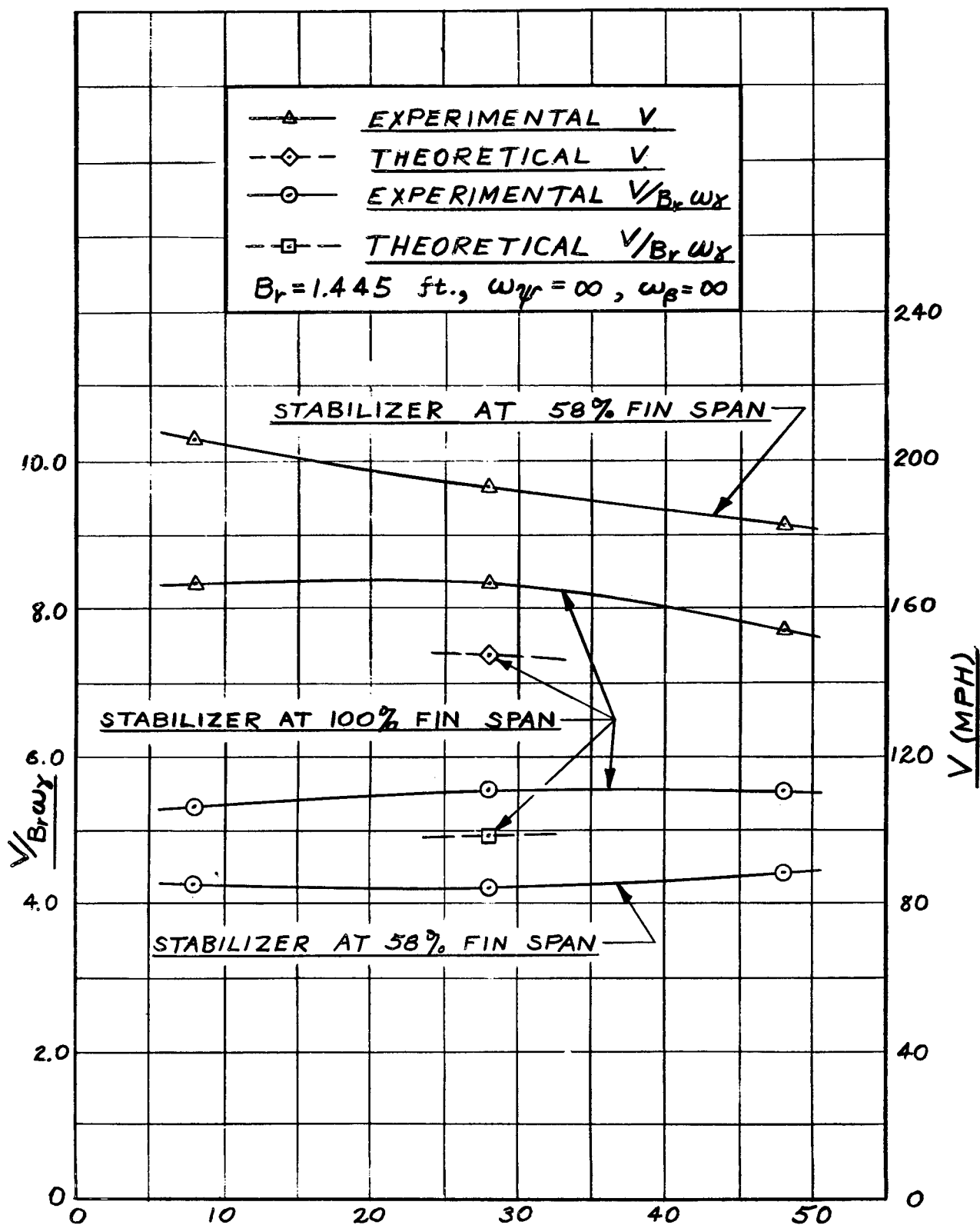


Fig. 3 Effect of Stabilizer C.G. Location on Critical ω/ω_δ ,
Fuselage Locked



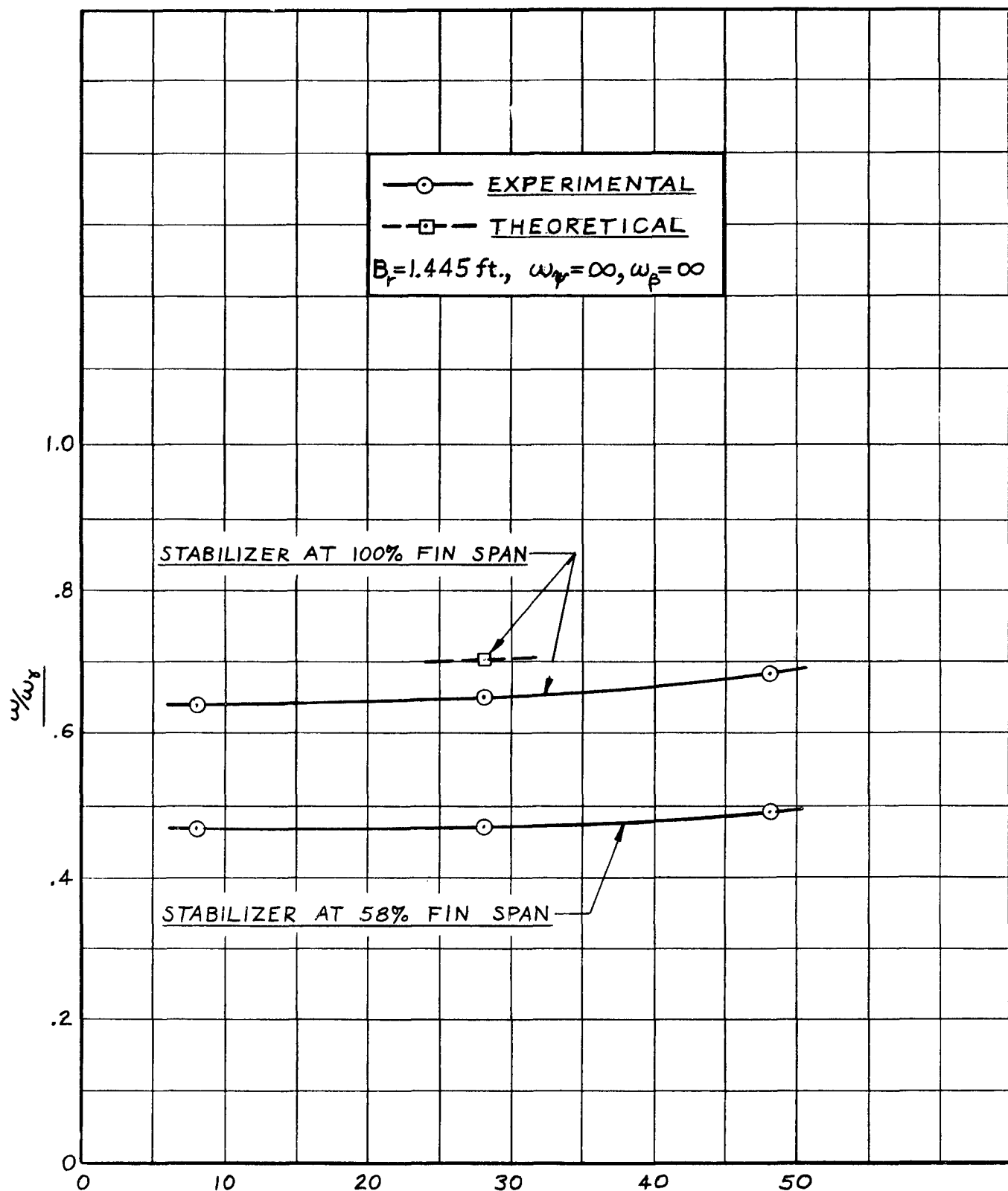
Stabilizer C.G. Location in Per Cent Fin Chord Aft of Elastic Axis

Fig. 4 Effect of Stabilizer C.G. Location on Critical $V/B_T \omega$
Fuselage Free



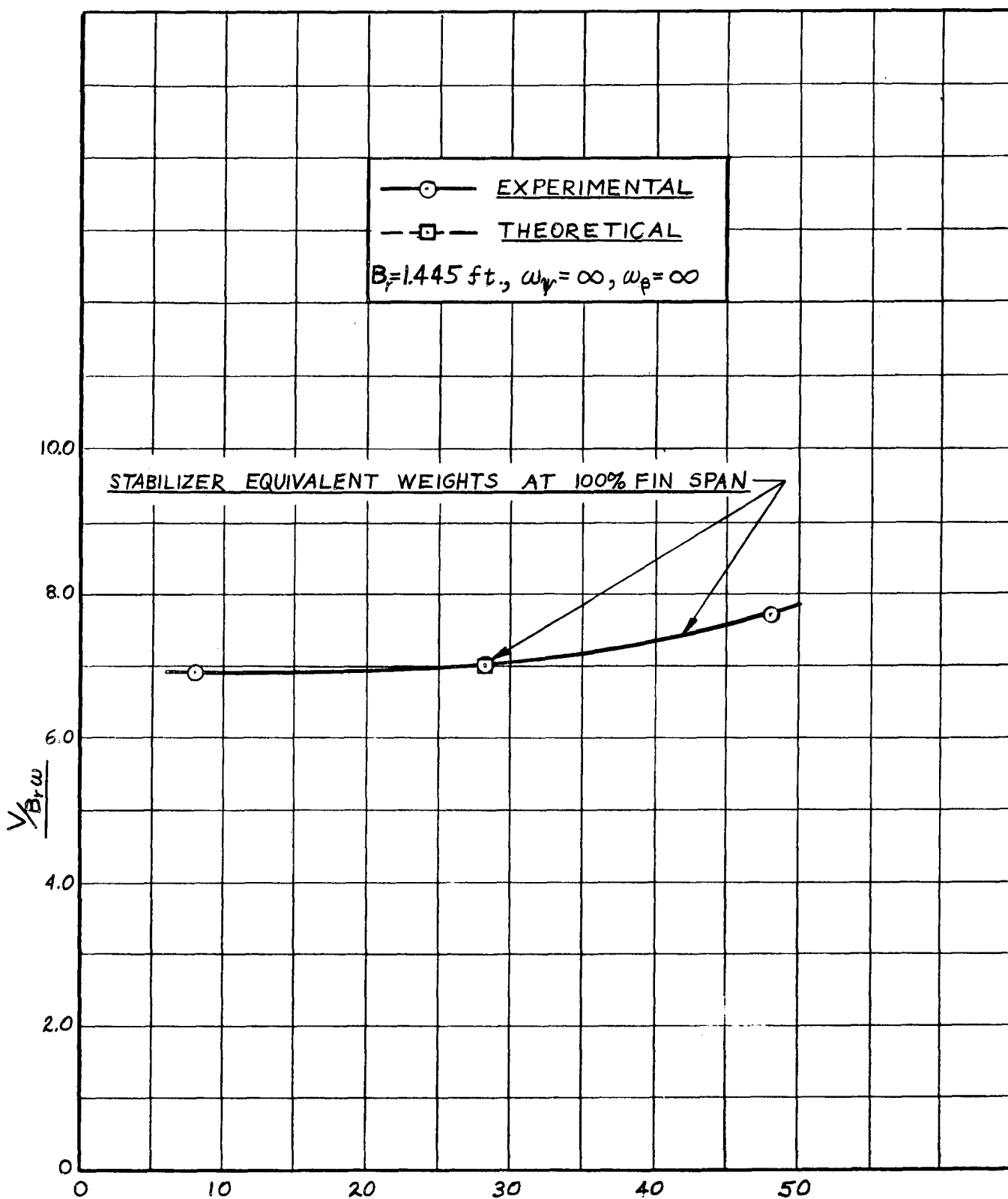
Stabilizer C.G. Location in Per Cent Fin Chord Aft of Elastic Axis

Fig. 5 Effect of Stabilizer C.G. Location on Critical $V/B_r \omega_{\gamma}$ and V ,
Fuselage Free



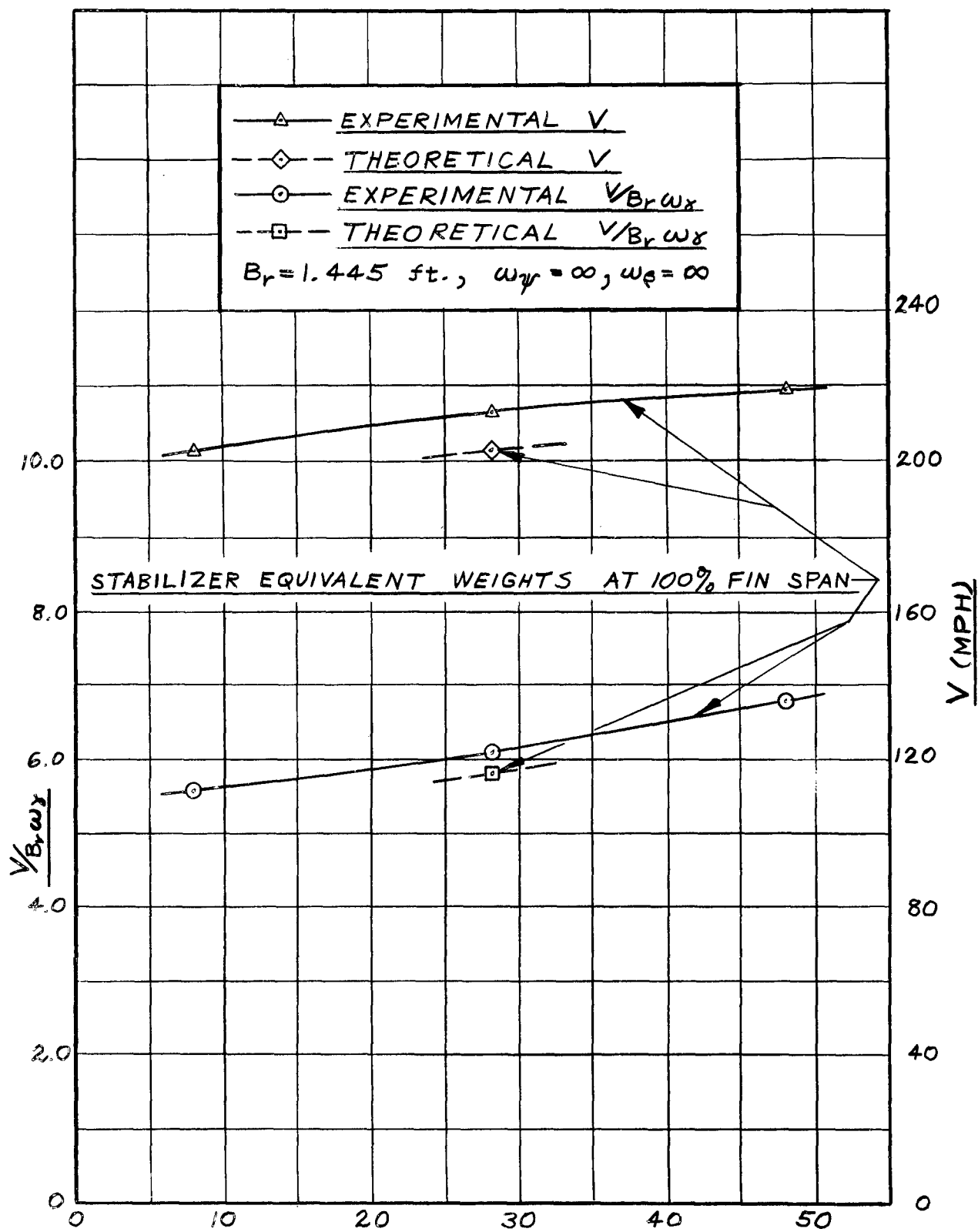
Stabilizer C.G. Location in Per Cent Fin Chord Aft of Elastic Axis

Fig. 6 Effect of Stabilizer C.G. Location on Critical ω/ω_y ,
Fuselage Free



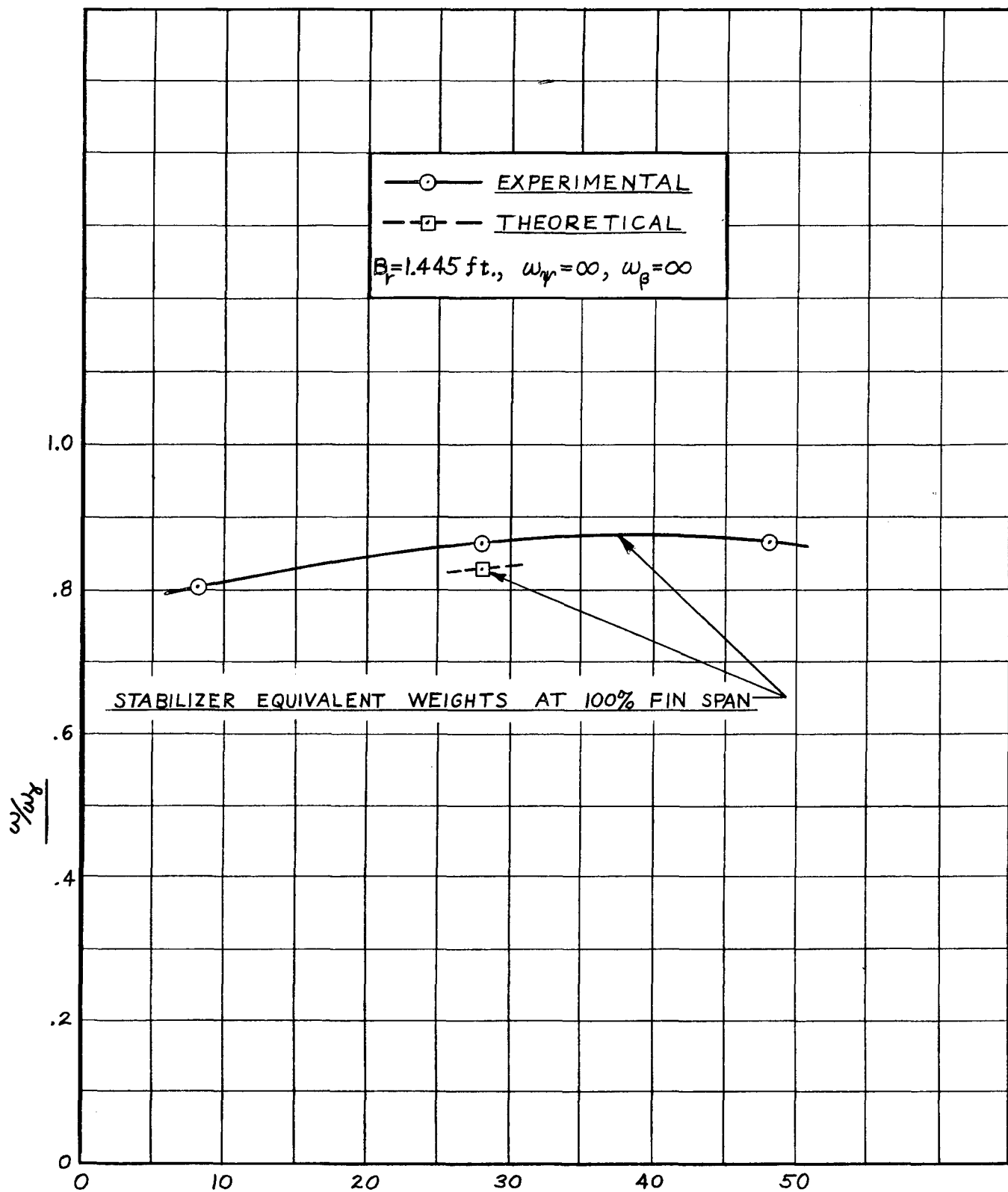
Equivalent Weight C.G. Location in Per Cent Fin Chord Aft of Elastic Axis

Fig. 7 Effect of Stabilizer Equivalent Weight C.G. Location on Critical $V/B_r \omega$, Fuselage Locked



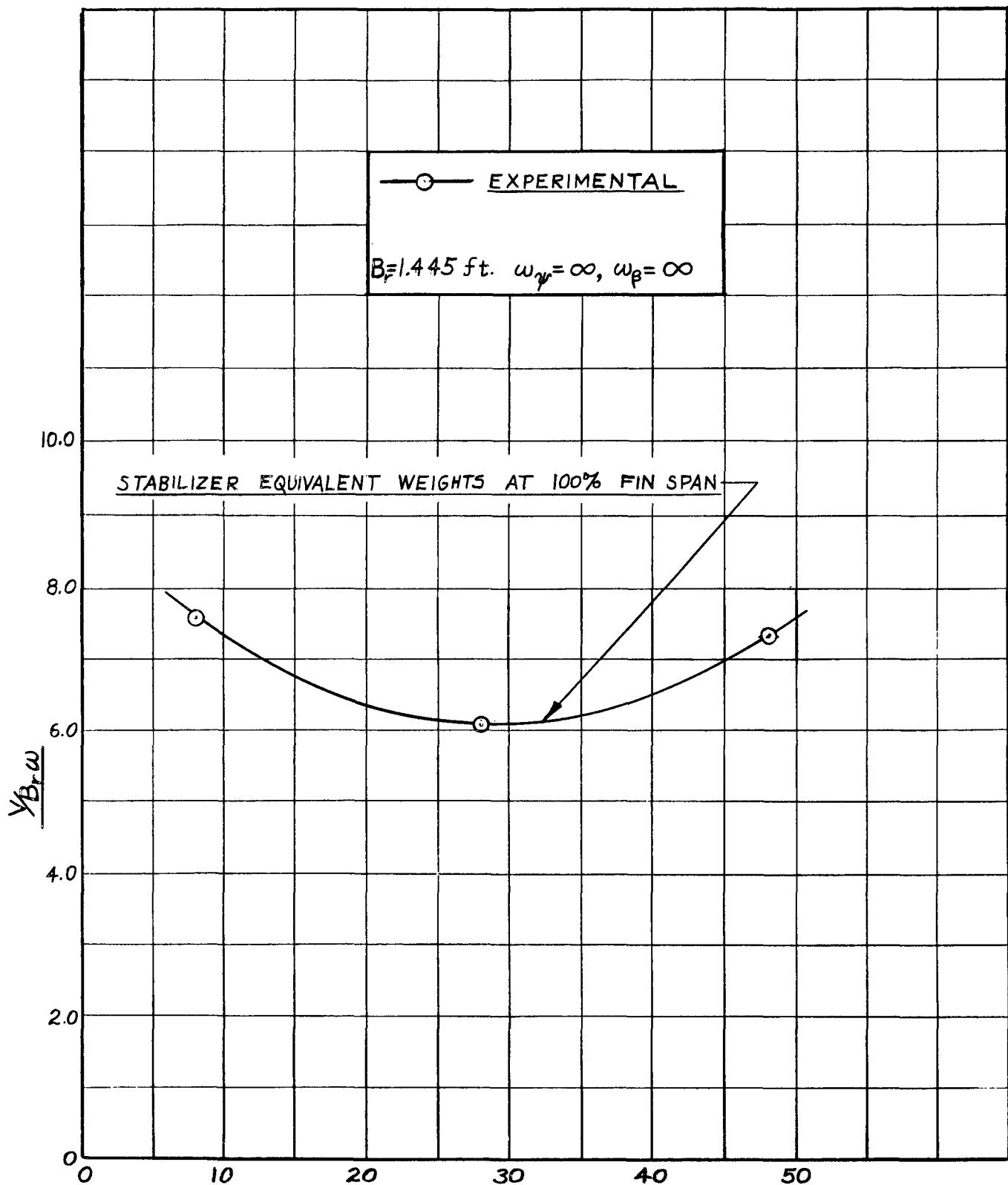
Equivalent Weight C.G. Location in Per Cent Fin Chord Aft of Elastic Axis

Fig. 8 Effect of Stabilizer Equivalent Weight C. G. Location on Critical $V/B_r \omega_x$ and V , Fuselage Locked



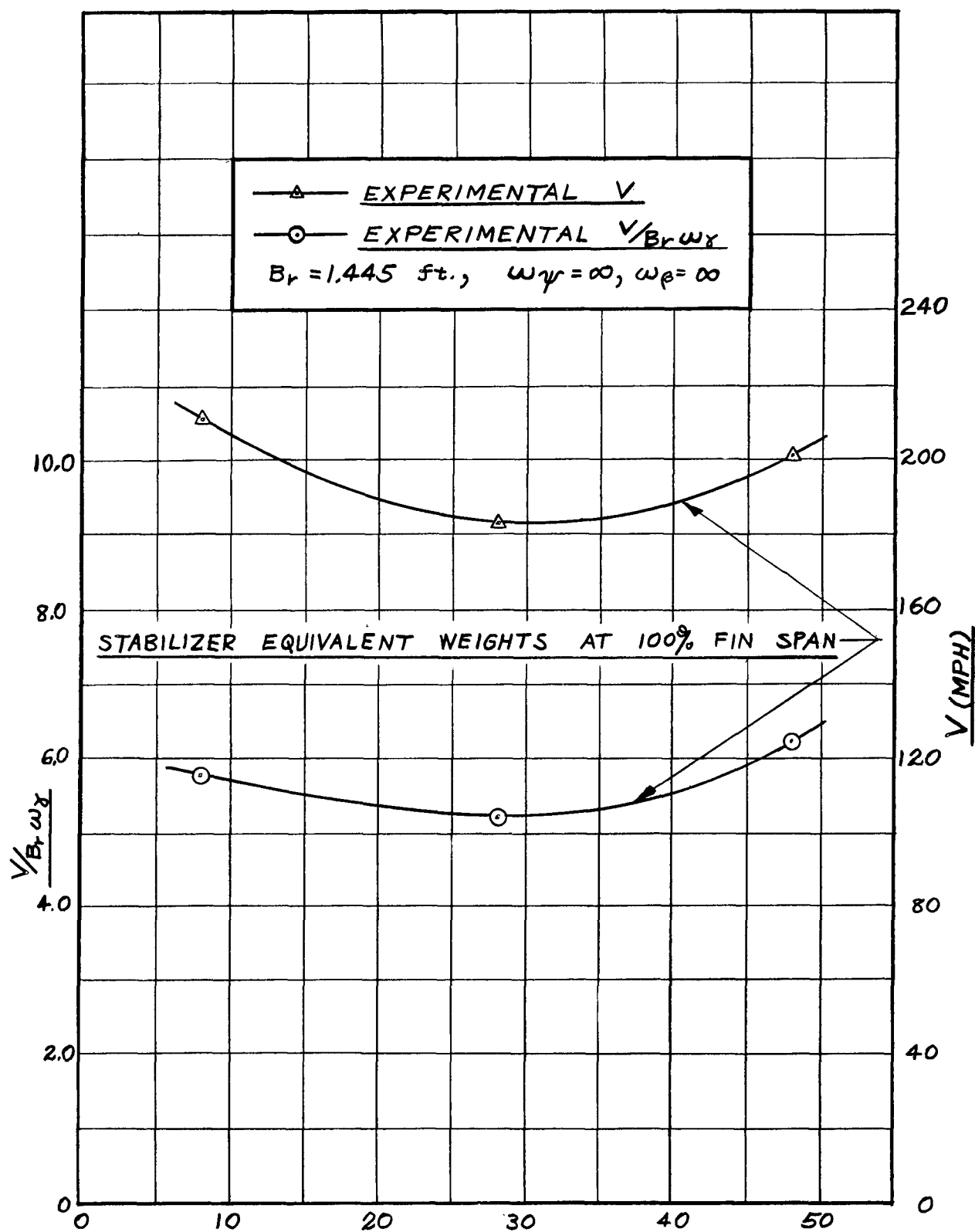
Equivalent Weight C.G. Location in Per Cent Fin Chord Aft of Elastic Axis

Fig. 9 Effect of Stabilizer Equivalent Weight C.G. Location on Critical w/w_f , Fuselage Locked



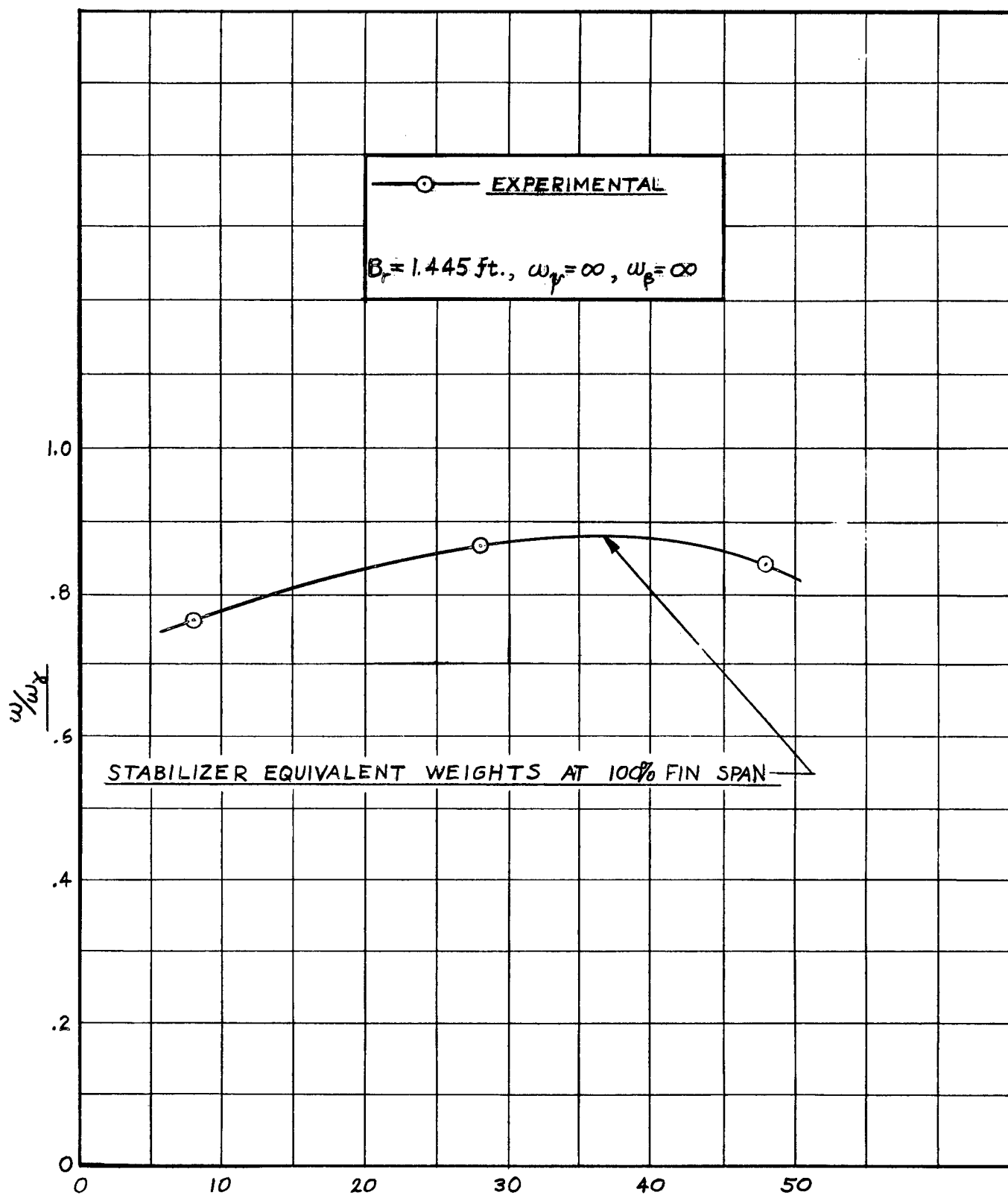
Equivalent Weight C.G. Location in Per Cent Fin Chord Aft of Elastic Axis

Fig. 10 Effect of Stabilizer Equivalent Weight C.G. Location on
Critical $V/B_r \omega$ Fuselage Free



Equivalent Weight C.G. Location in Per Cent Fin Chord Aft of Elastic Axis

Fig. 11 Effect of Stabilizer Equivalent Weight C.G. Location on Critical $V/B_r \omega_\gamma$, and V , Fuselage Free



Equivalent Weight C. G. Location in Per Cent Fin Chord Aft of Elastic Axis

Fig. 12 Effect of Stabilizer Equivalent Weight C.G. Location on Critical ω/ω_r , Fuselage Free

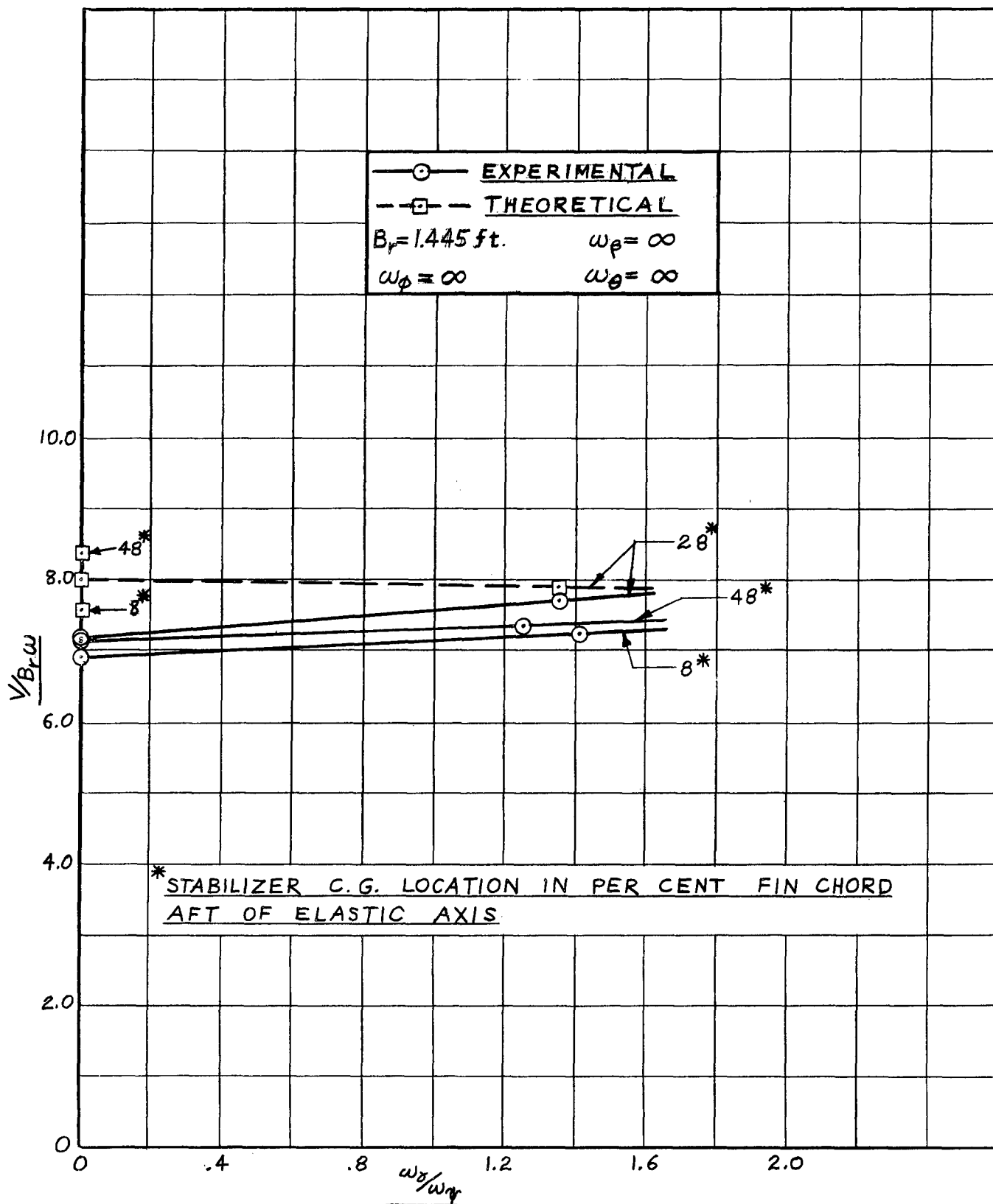


Fig. 13 Effect of Stabilizer Rocking Frequency on
 Critical $V/B_r \omega$, Stabilizer at 100% Fin Span,
Fuselage Locked

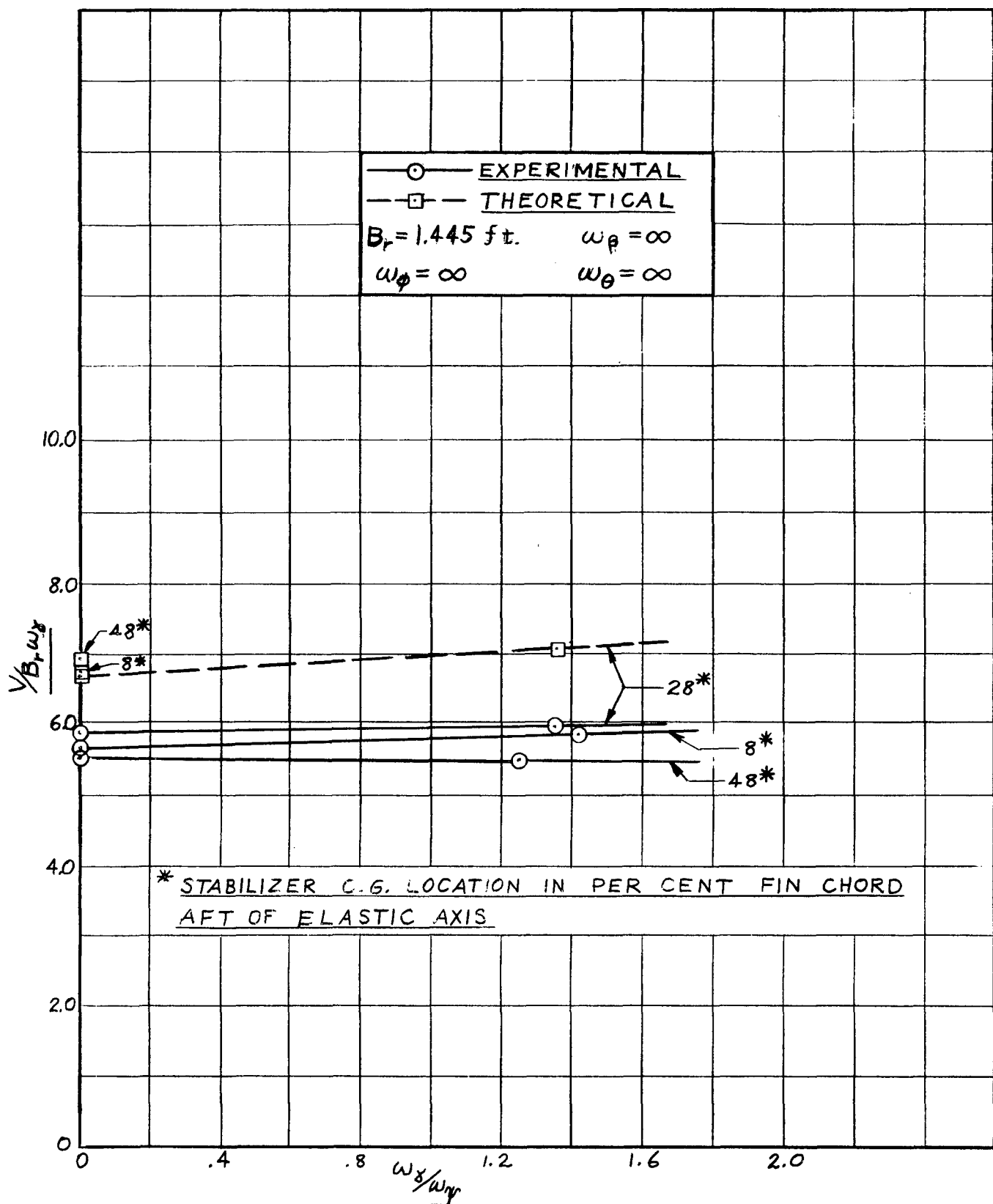


Fig. 14 Effect of Stabilizer Rocking Frequency on Critical $V/B_r \omega_y$,
 Stabilizer at 100% Fin Span, Fuselage Locked

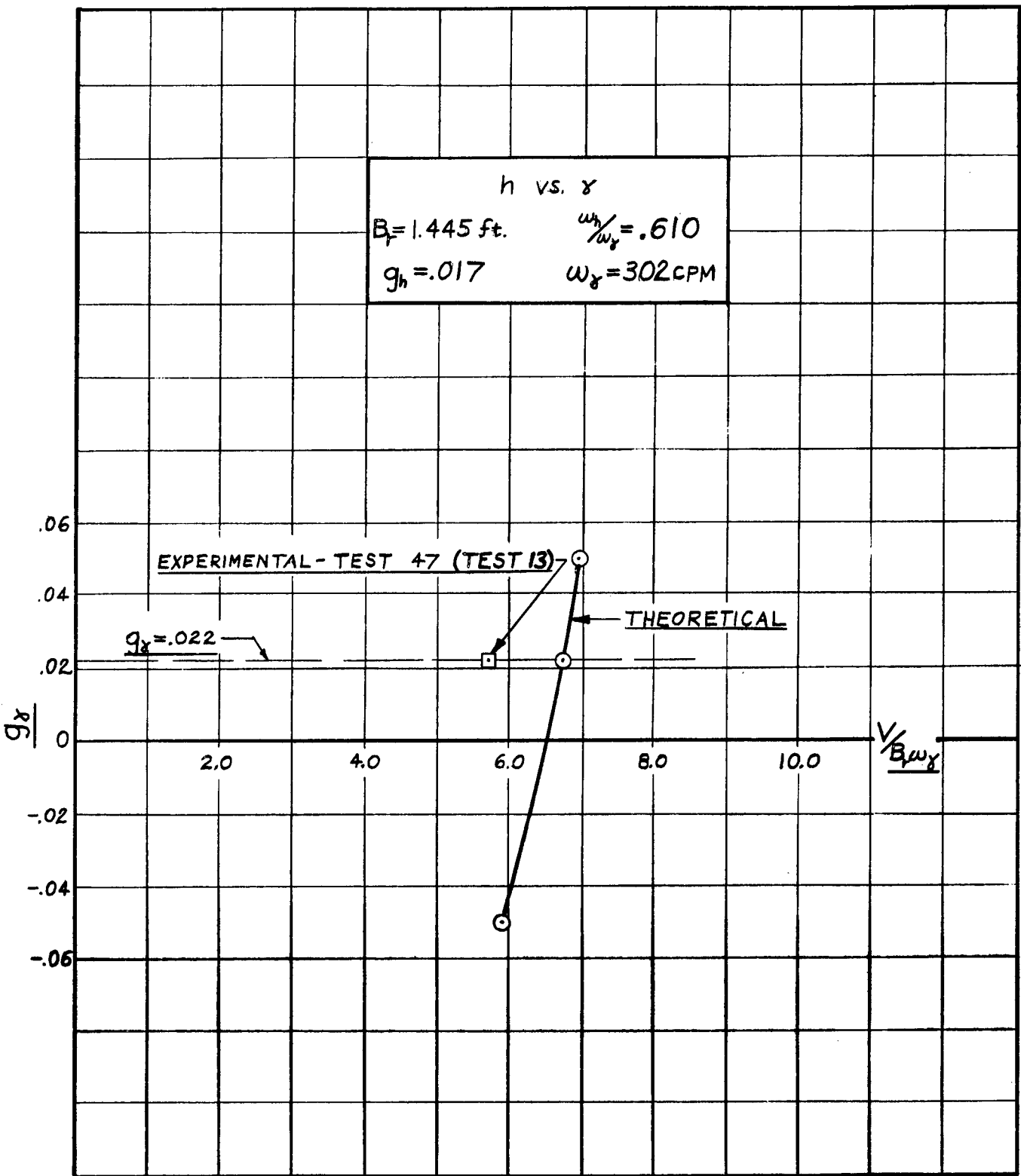


Fig. 15 g_γ vs $V/B_f\omega_\gamma$ Fin Bending-Fin Torsion Flutter,
 Stabilizer C.G. at 100% Fin Span and 48% Fin Chord

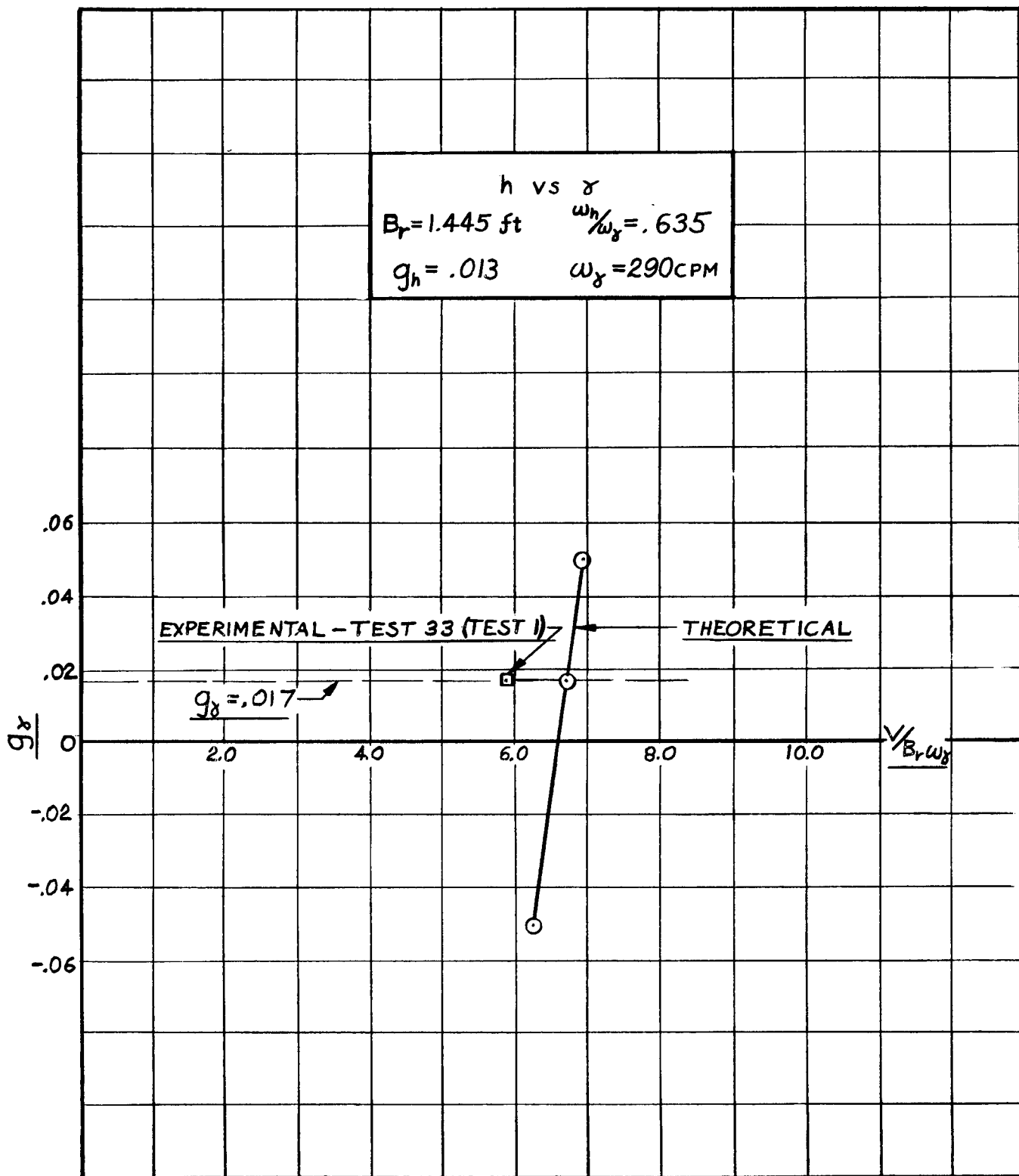


Fig. 16 g_γ vs $V/B_r \omega_\gamma$, Fin Bending-Fin Torsion Flutter,
 Stabilizer C.G. at 100% Fin Span and 68% Fin Chord

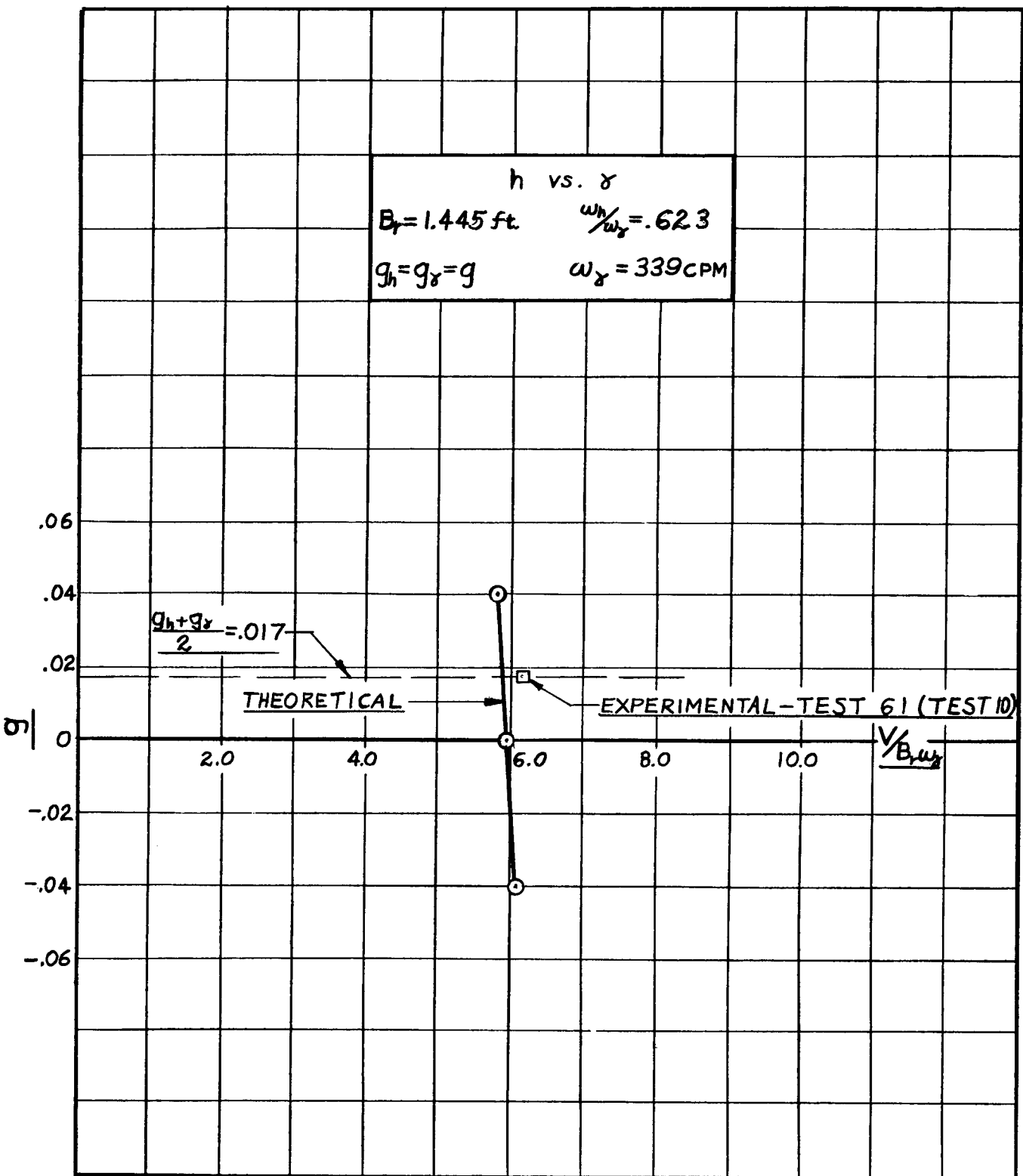


Fig. 17 g vs $V/B_r \omega_y$ Fin Bending-Fin Torsion Flutter,
 Stabilizer Equivalent Weight C.G. at 100% Fin Span
 and 68% Fin Chord

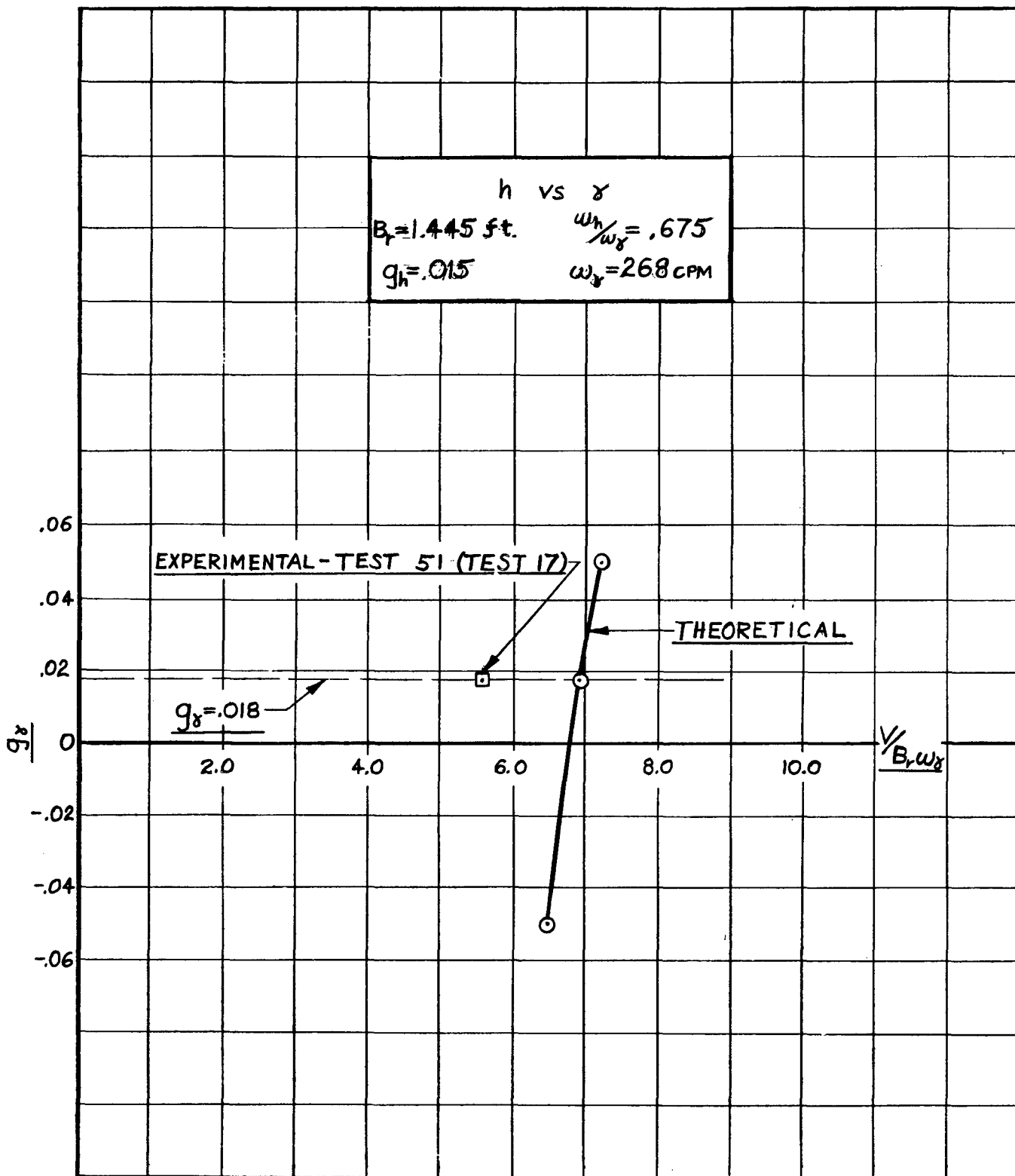


Fig. 18 g_γ vs. $V/B_r\omega_\gamma$, Fin Bending-Fin Torsion Flutter,
 Stabilizer C.G. at 100% Fin Span and 88% Fin Chord

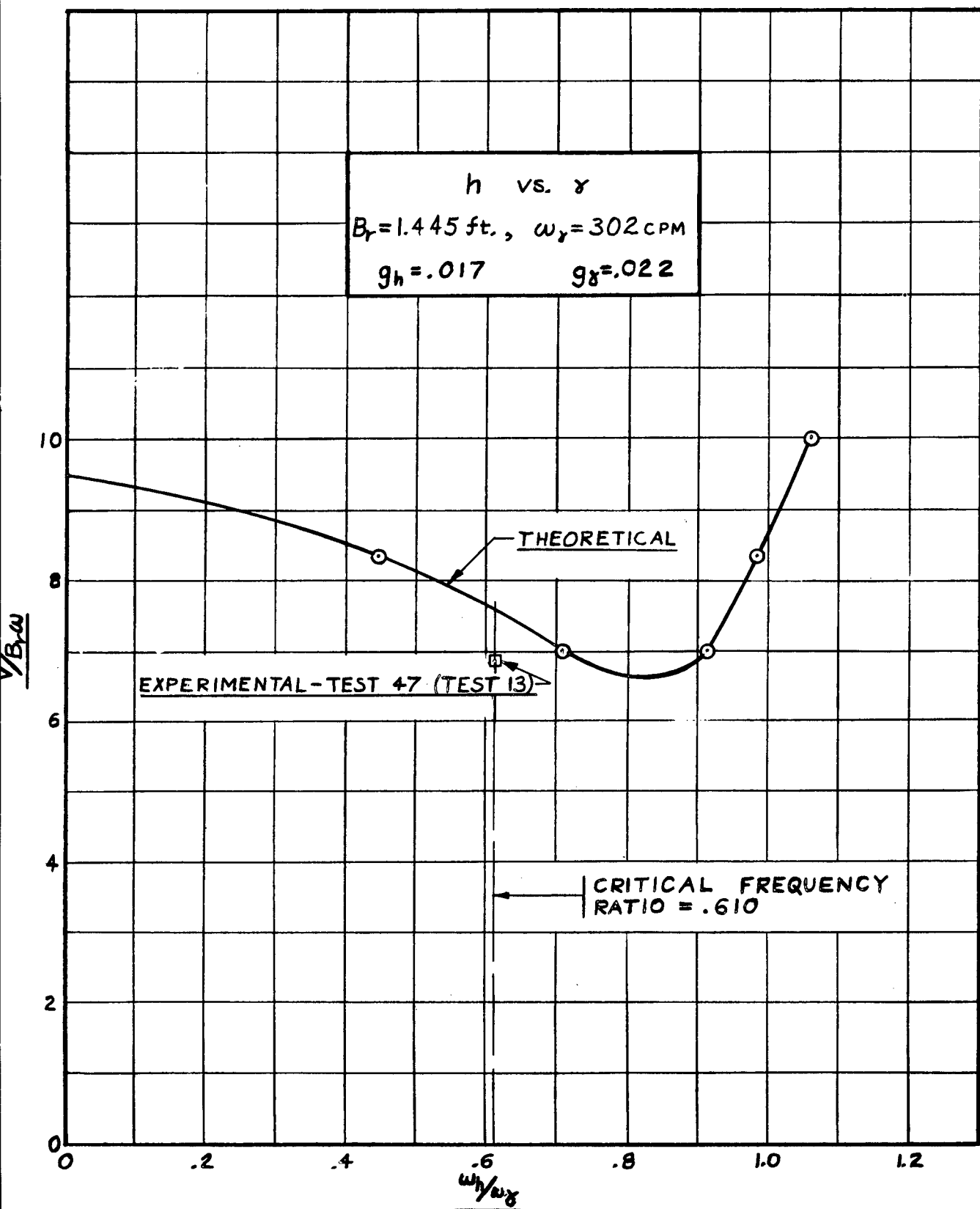


Fig. 19 $V/B_1\omega$ vs ω_h/ω_γ , Fin Bending-Fin Torsion Flutter, Stabilizer C.G. at 100% Fin Span and 48% Fin Chord

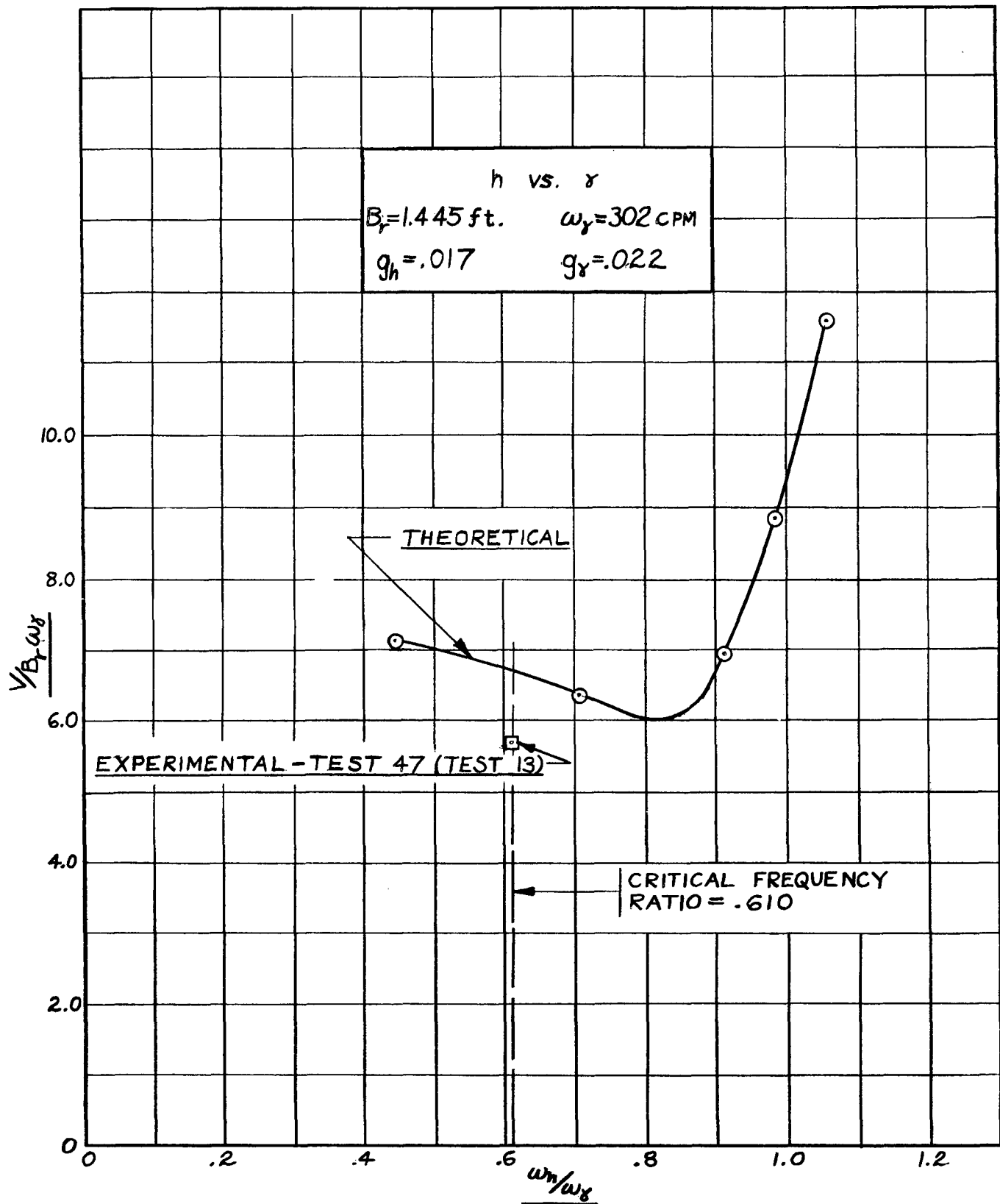


Fig. 20 $V/B_f \omega_\gamma$ vs ω_h/ω_γ Fin Bending-Fin Torsion Flutter,
 Stabilizer C.G. at 100% Fin Span and 48% Fin Chord

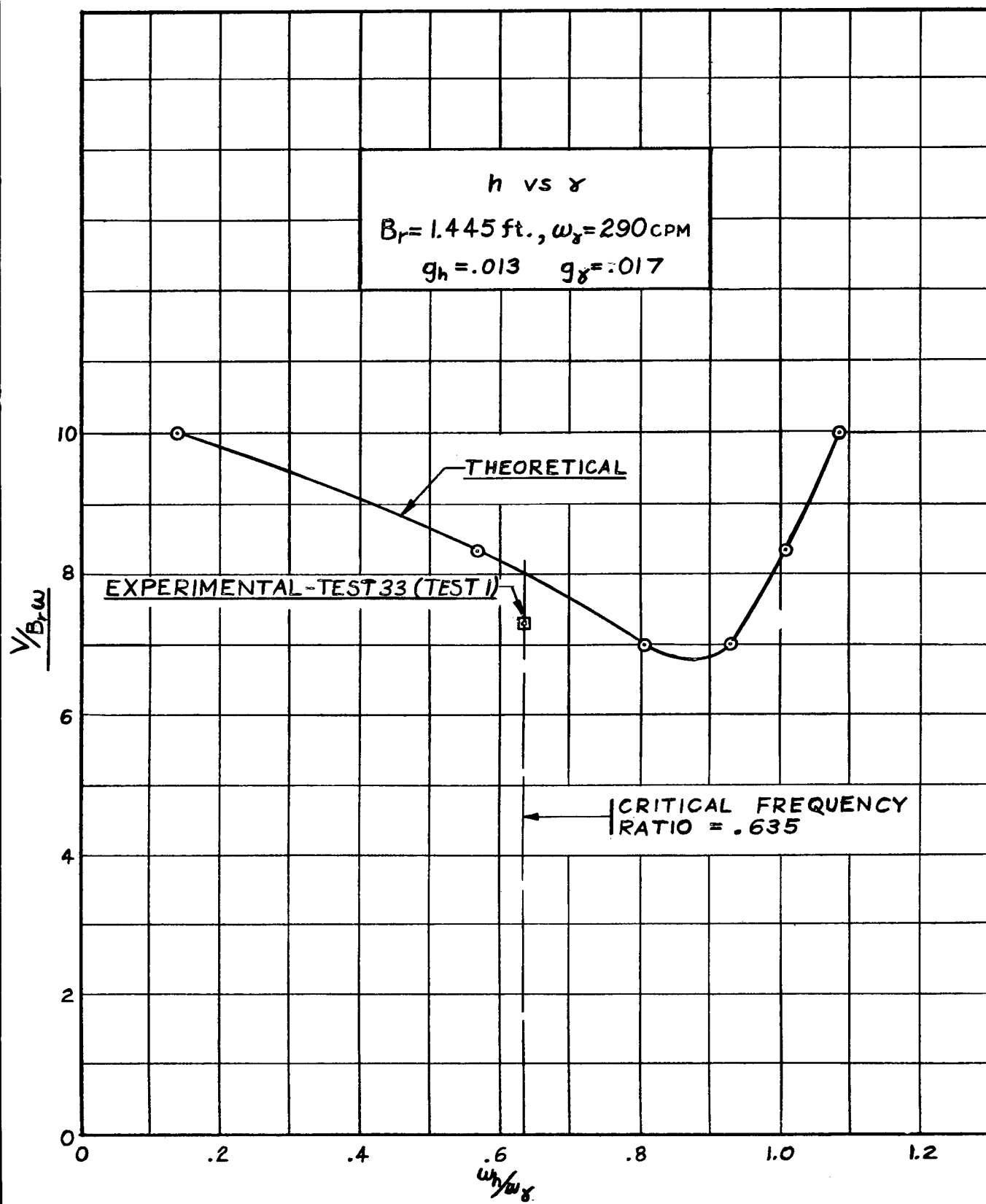


Fig. 21 $V/B_r \omega$ vs ω_h/ω_γ , Fin Bending-Fin Torsion Flutter,
 Stabilizer C.G. at 100% Fin Span and 68% Fin Chord

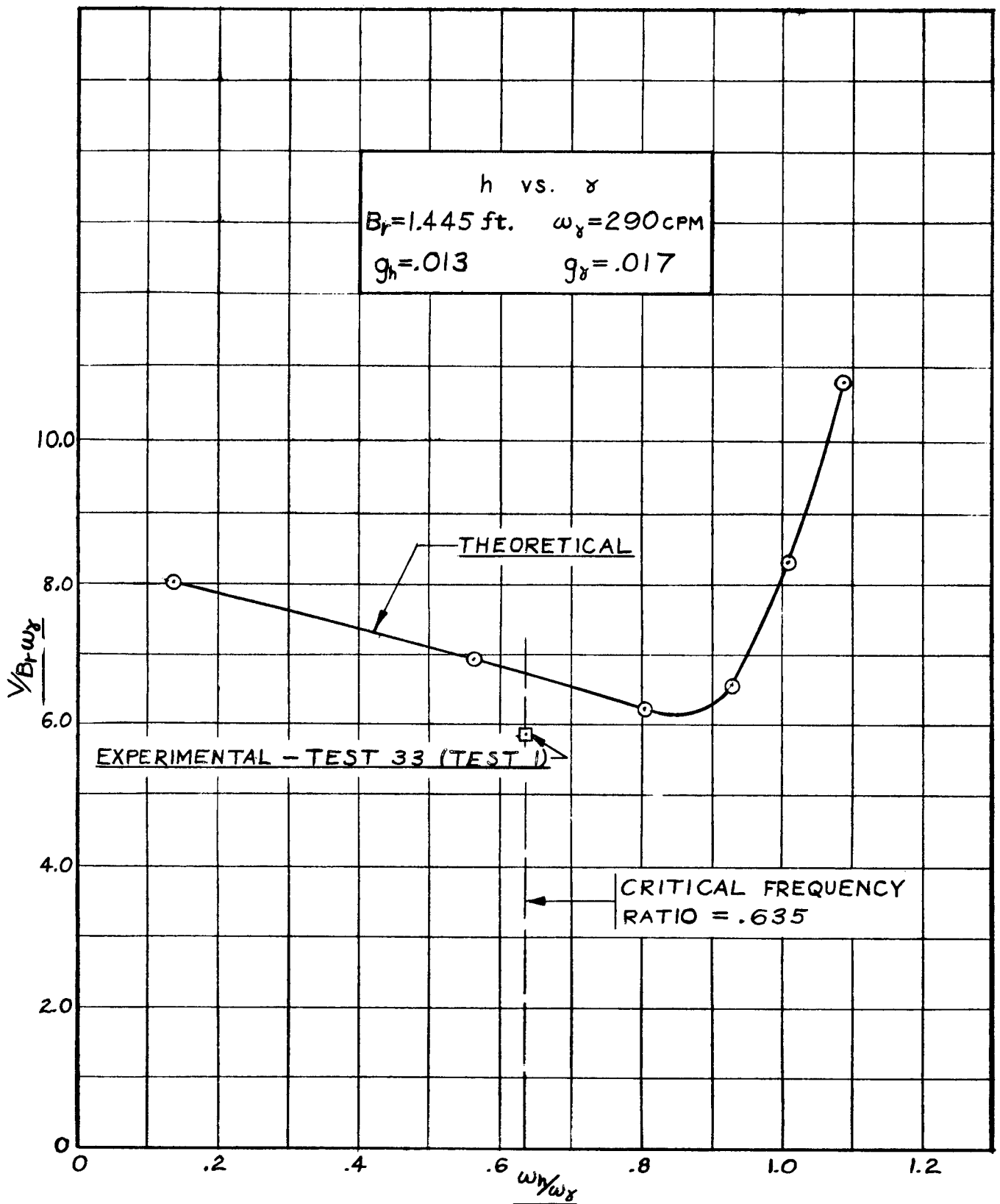


Fig. 22 $V/B_r \omega_\gamma$ vs ω_h/ω_γ , Fin Bending-Fin Torsion Flutter, Stabilizer C.G. at 100% Fin Span and 68% Fin Chord

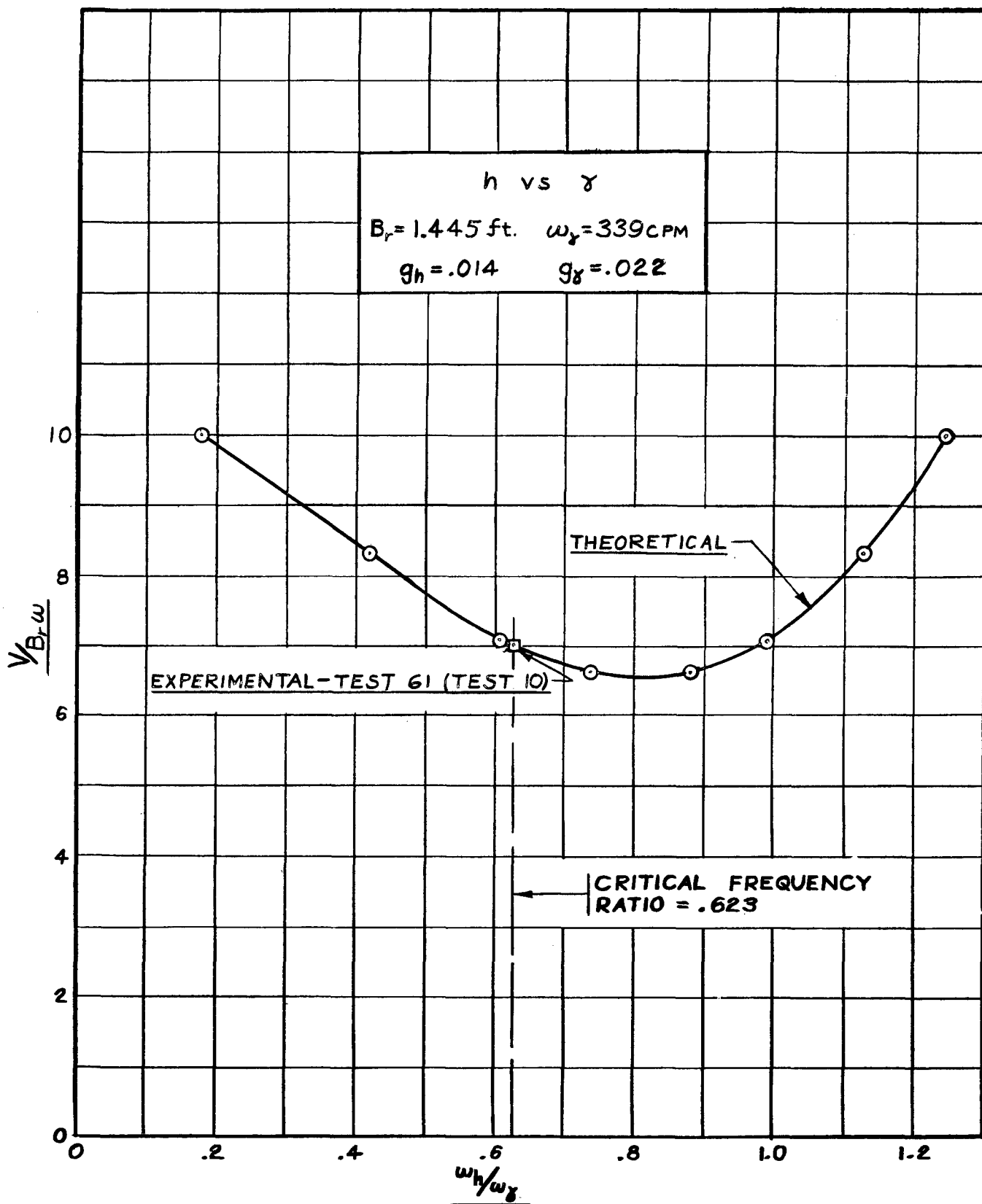


Fig. 23 $V/B_r\omega$ vs ω_h/ω_γ , Fin Bending-Fin Torsion Flutter, Stabilizer
Equivalent Weight C.G. at 100% Fin Span and 68% Fin Chord

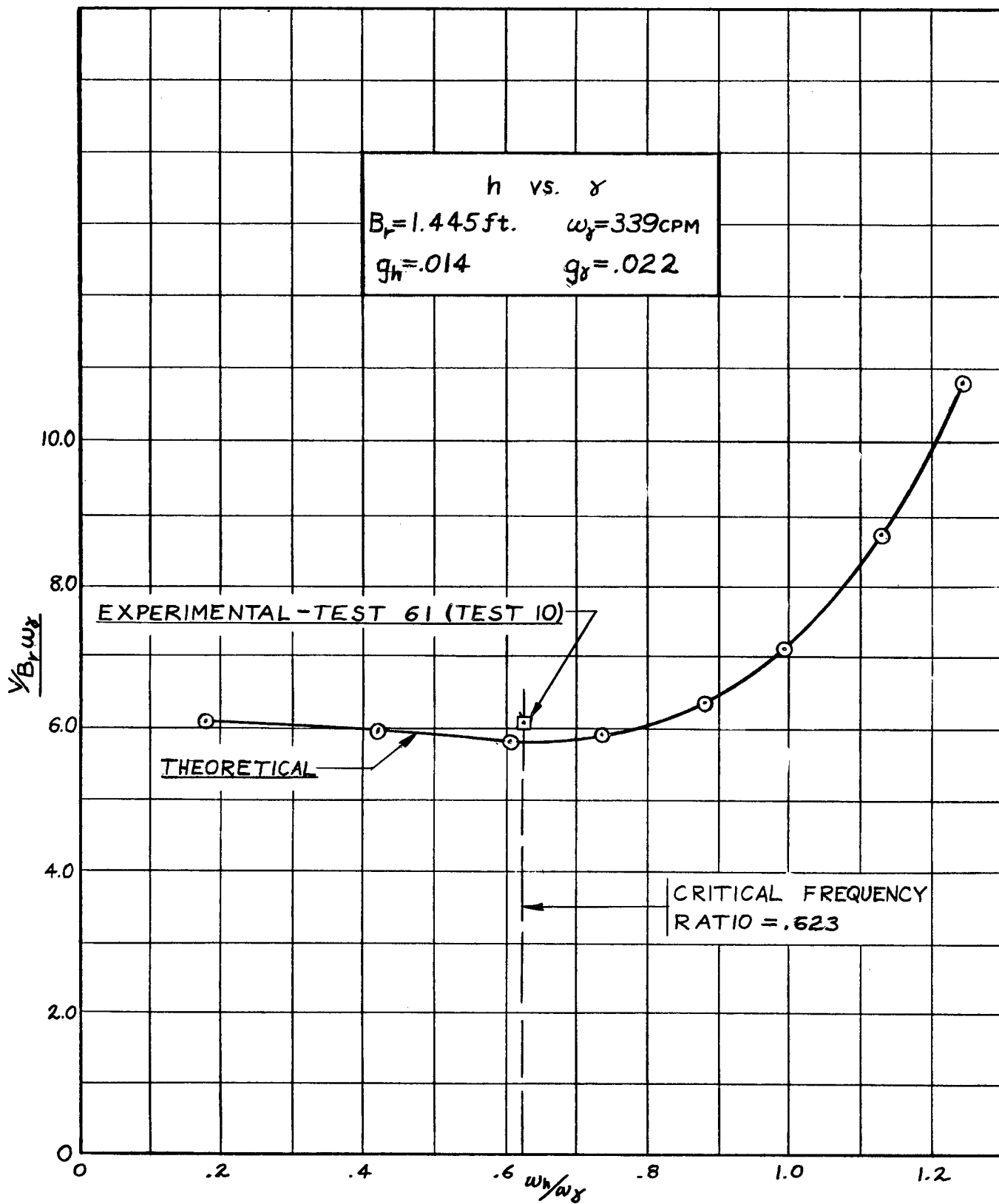


Fig. 24 $V/B_r \omega_f$ vs ω_h/ω_f , Fin Bending-Fin Torsion Flutter, Stabilizer Equivalent Weight C.G. at 100% Fin Span and 68% Fin Chord

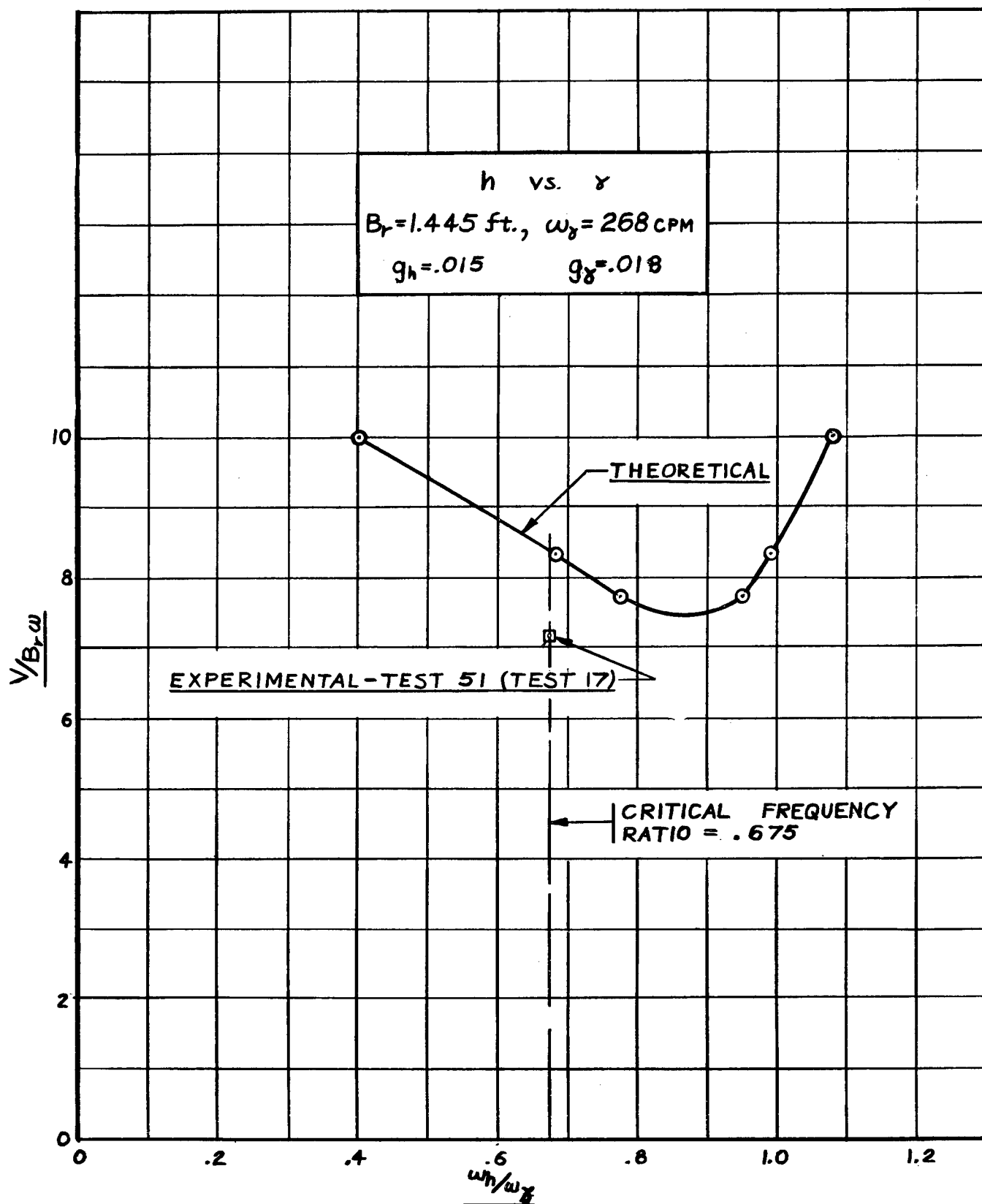


Fig. 25 $V/B_r\omega$ vs ω_h/ω_y , Fin Bending-Fin Torsion Flutter,
 Stabilizer C.G. at 100% Fin Span and 88% Fin Chord

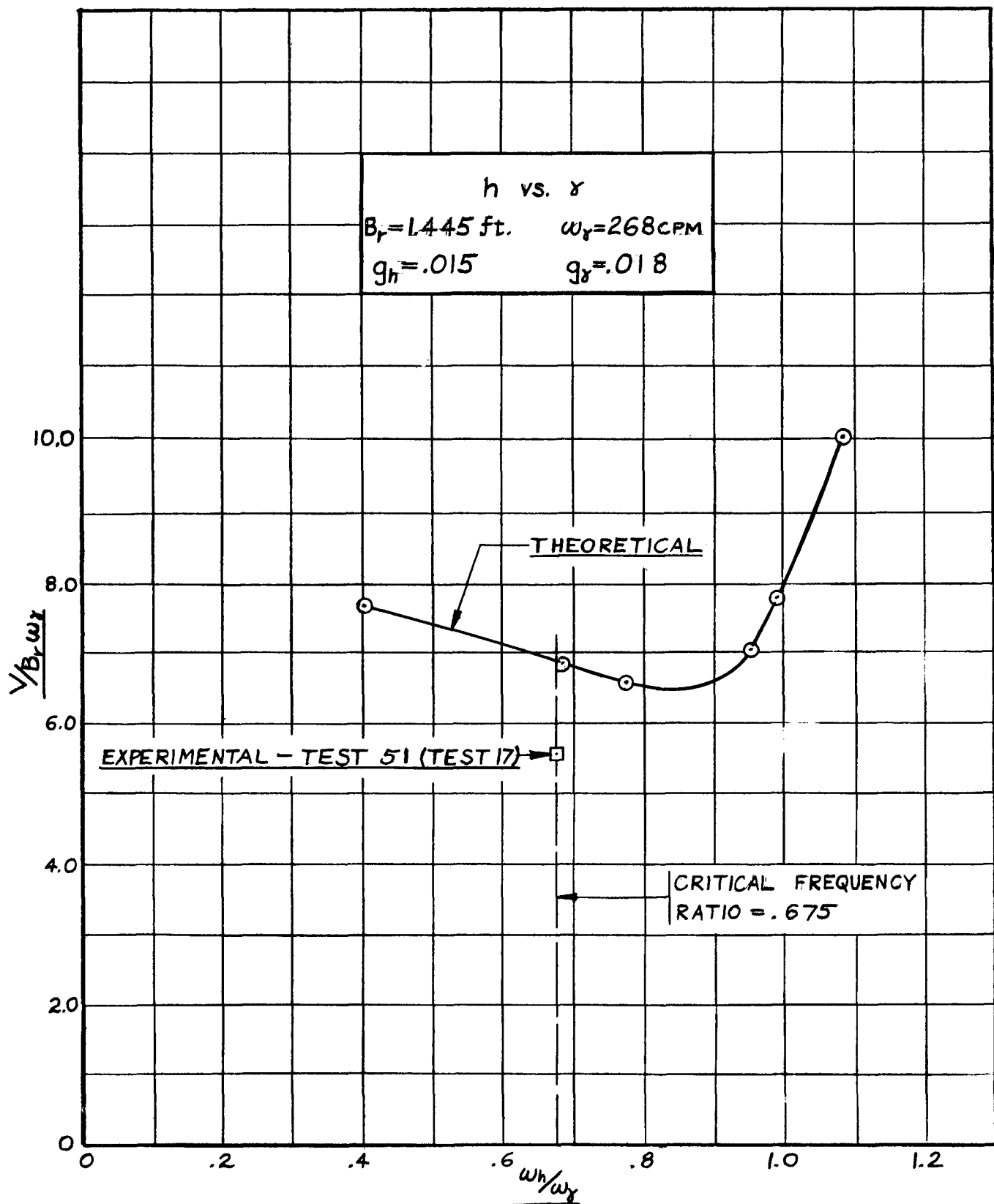


Fig. 26 $V/B_r\omega_\gamma$ vs ω_h/ω_γ , Fin Bending-Fin Torsion Flutter, Stabilizer C. G. at 100% Fin Span and 88% Fin Chord

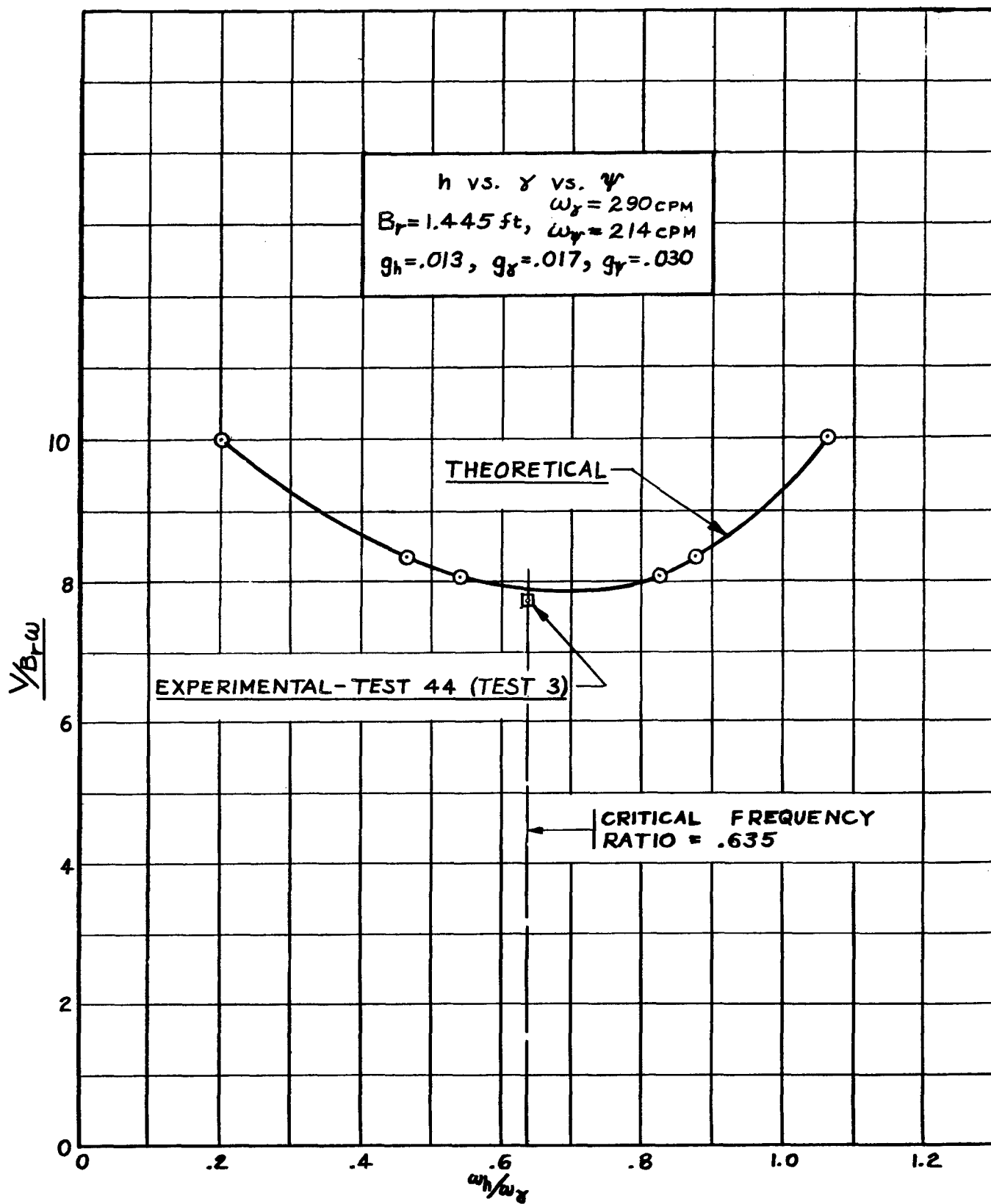


Fig. 27 $V/B_T \omega$ vs ω_h/ω_γ , Fin Bending-Fin Torsion-Stabilizer Rocking Flutter, Stabilizer C.G. at 100% Fin Span and 68% Fin Chord

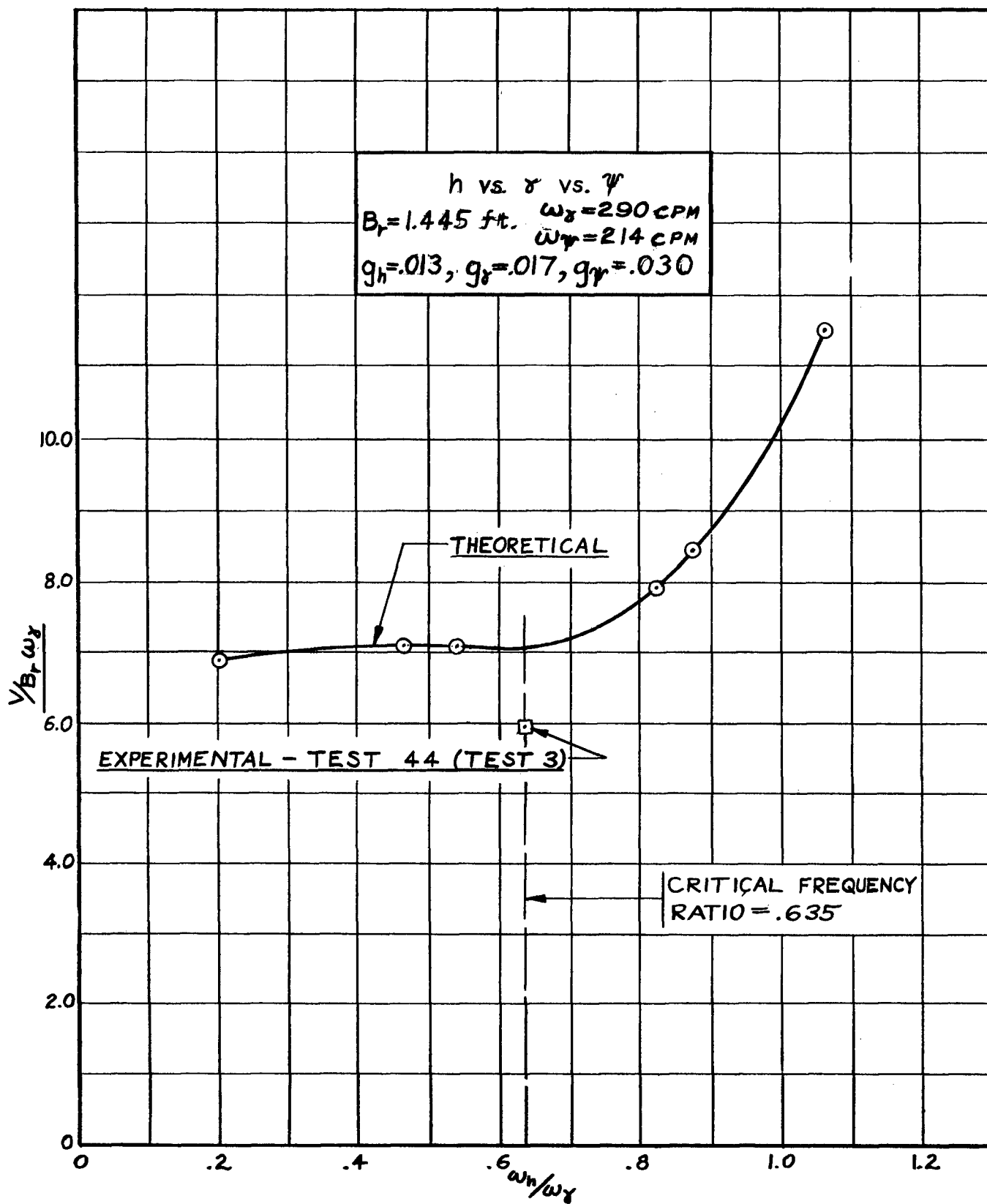


Fig. 28 $V/B_r \omega_\delta$ vs ω_h/ω_δ , Fin Bending-Fin Torsion-Stabilizer Rocking Flutter, Stabilizer C. G. at 100% Fin Span and 68% Fin Chord

h vs. δ vs. ϕ vs. θ
 $B_f = 1.445$ ft. $\omega_y = 290$ CPM
 $\omega_\phi = 172$ CPM $\omega_\theta = 210$ CPM
 $g_h = 0.13$, $g_y = 0.17$, $g_\phi = 0.020$, $g_\theta = 0.14$

EXPERIMENTAL - TEST 45

THEORETICAL

CRITICAL FREQUENCY
RATIO = .635

$\sqrt{B_r \omega}$

ω_h / ω_y

Fig. 29 $\sqrt{B_r \omega}$ vs. ω_h / ω_y Fin Bending-Fin Torsion-Fuselage Side Bending-Fuselage Torsion Flutter,
 Stabilizer C.G. at 100% Fin Span and 68% Fin Chord

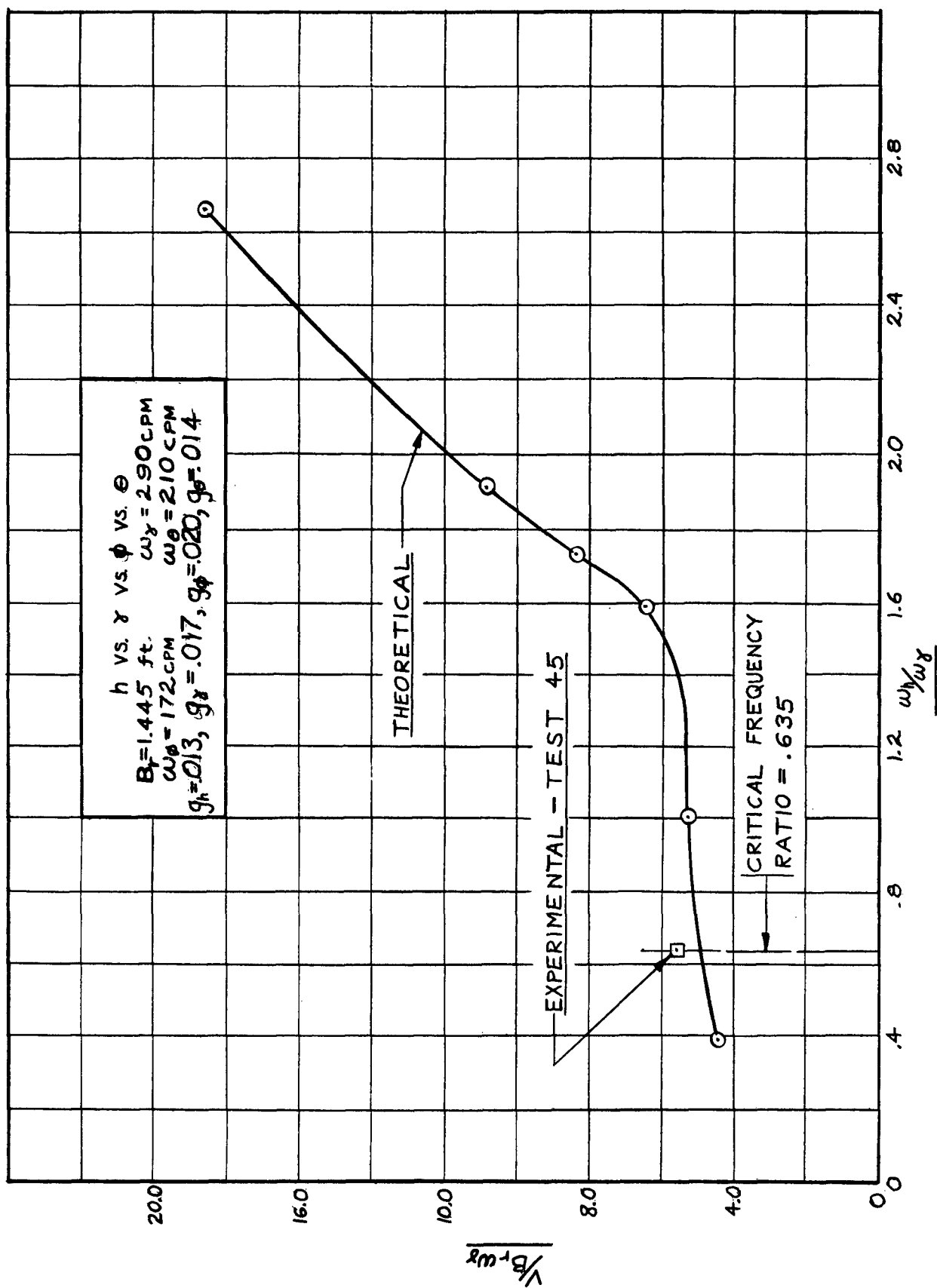


Fig. 30 $V/B_r \omega_r$ vs. ω_r/ω_r , Fin Bending-Fin Torsion-Fuselage Side Bending-Fuselage Torsion Flutter, Stabilizer C.G. at 100% Fin Span and 68% Fin Chord

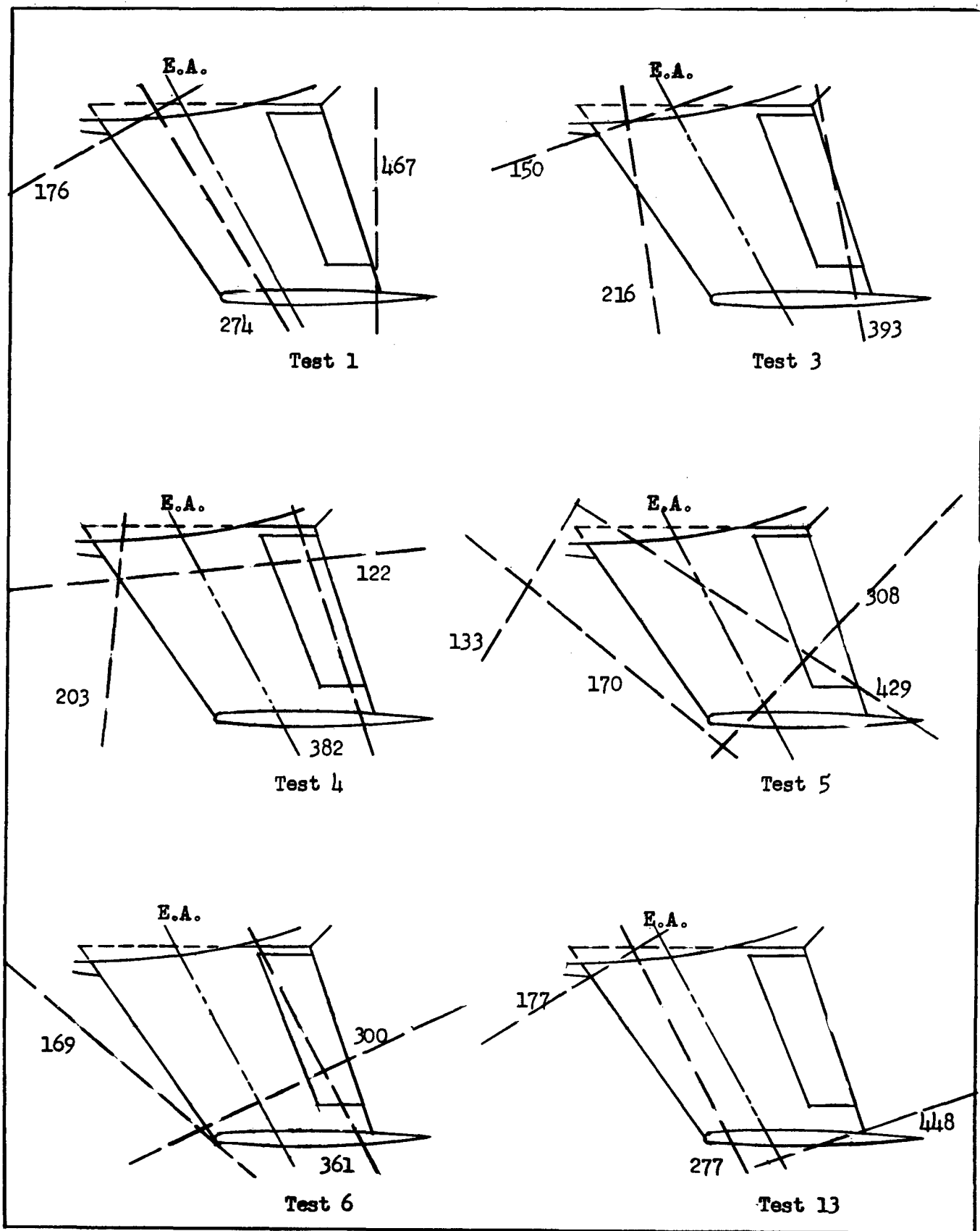


Fig. 31a Zero Airspeed Vibration Node Lines and Frequencies (CPM)

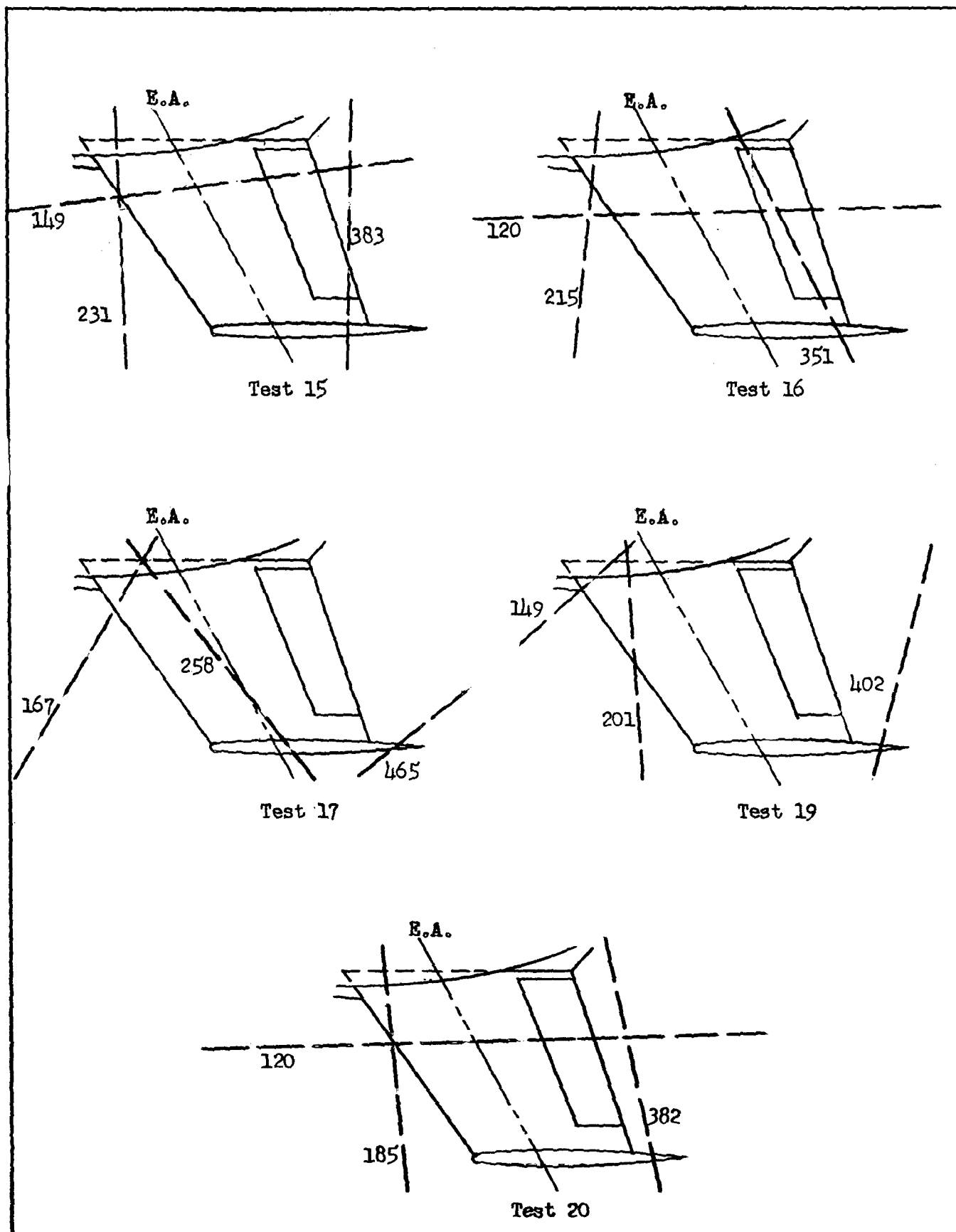


Fig. 31b Zero Airspeed Vibration Node Lines and Frequencies (CPM)

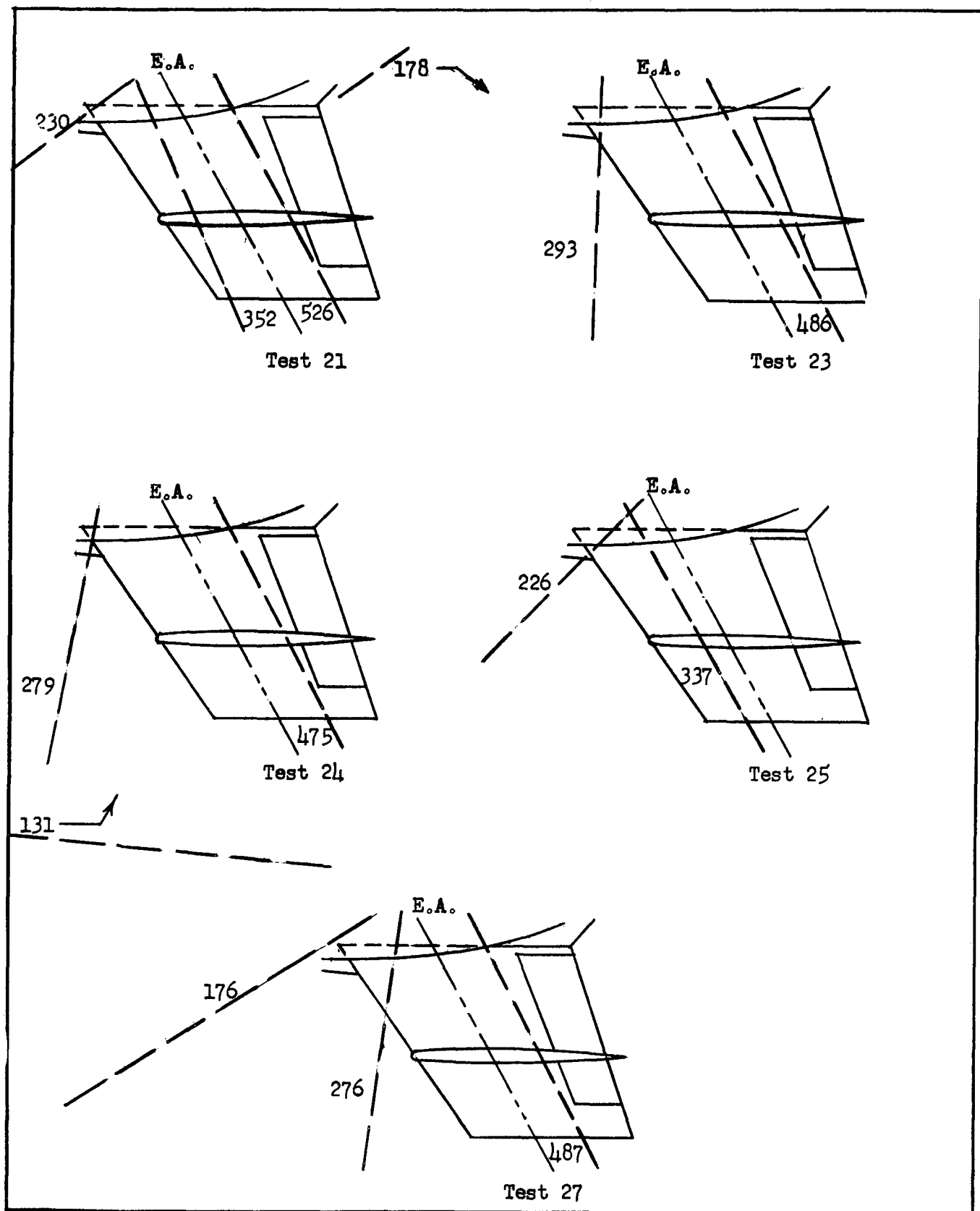


Fig. 31c Zero Airspeed Vibration Node Lines and Frequencies (CPM)

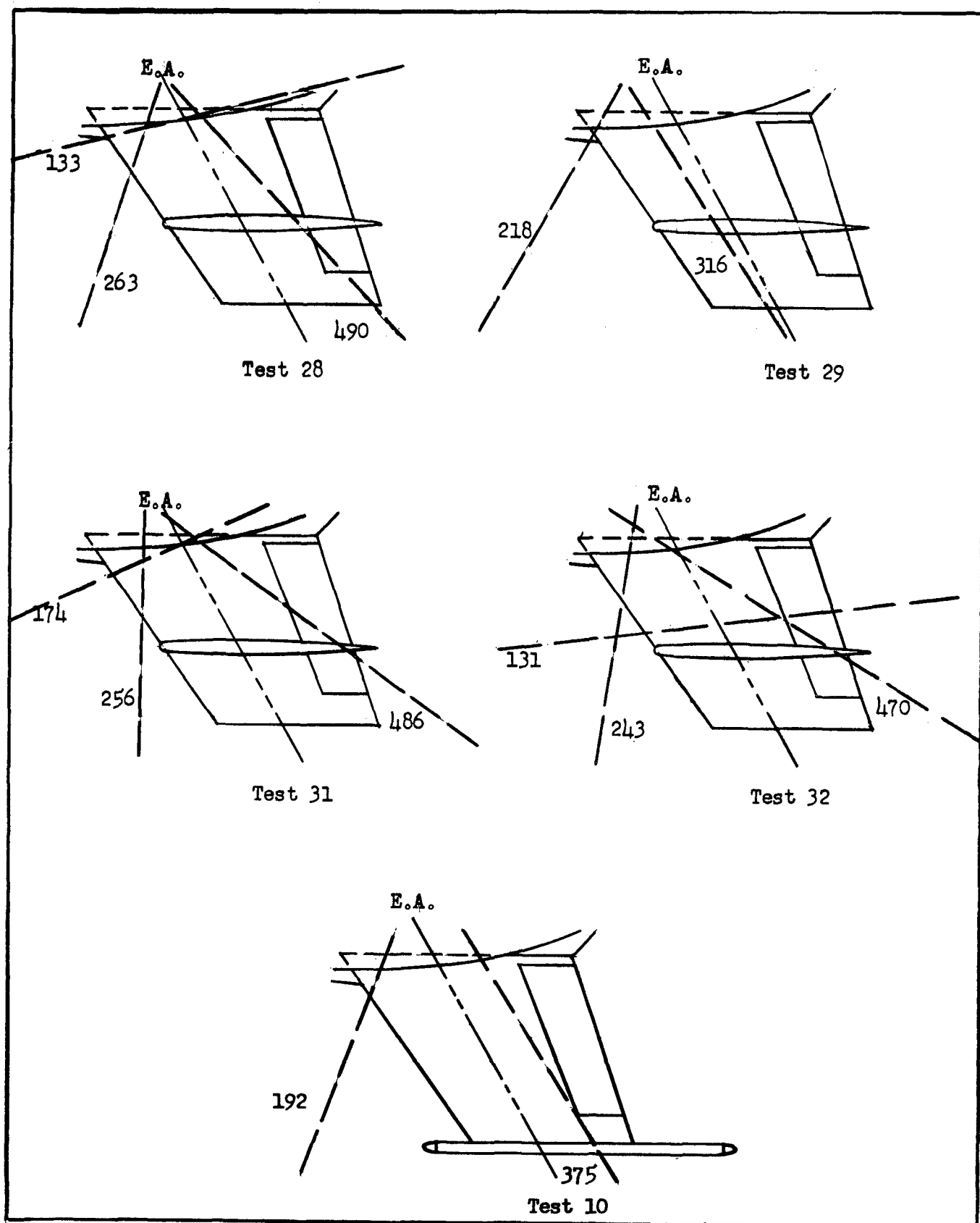


Fig. 3ld Zero Airspeed Vibration Node Lines
And Frequencies (CPM)

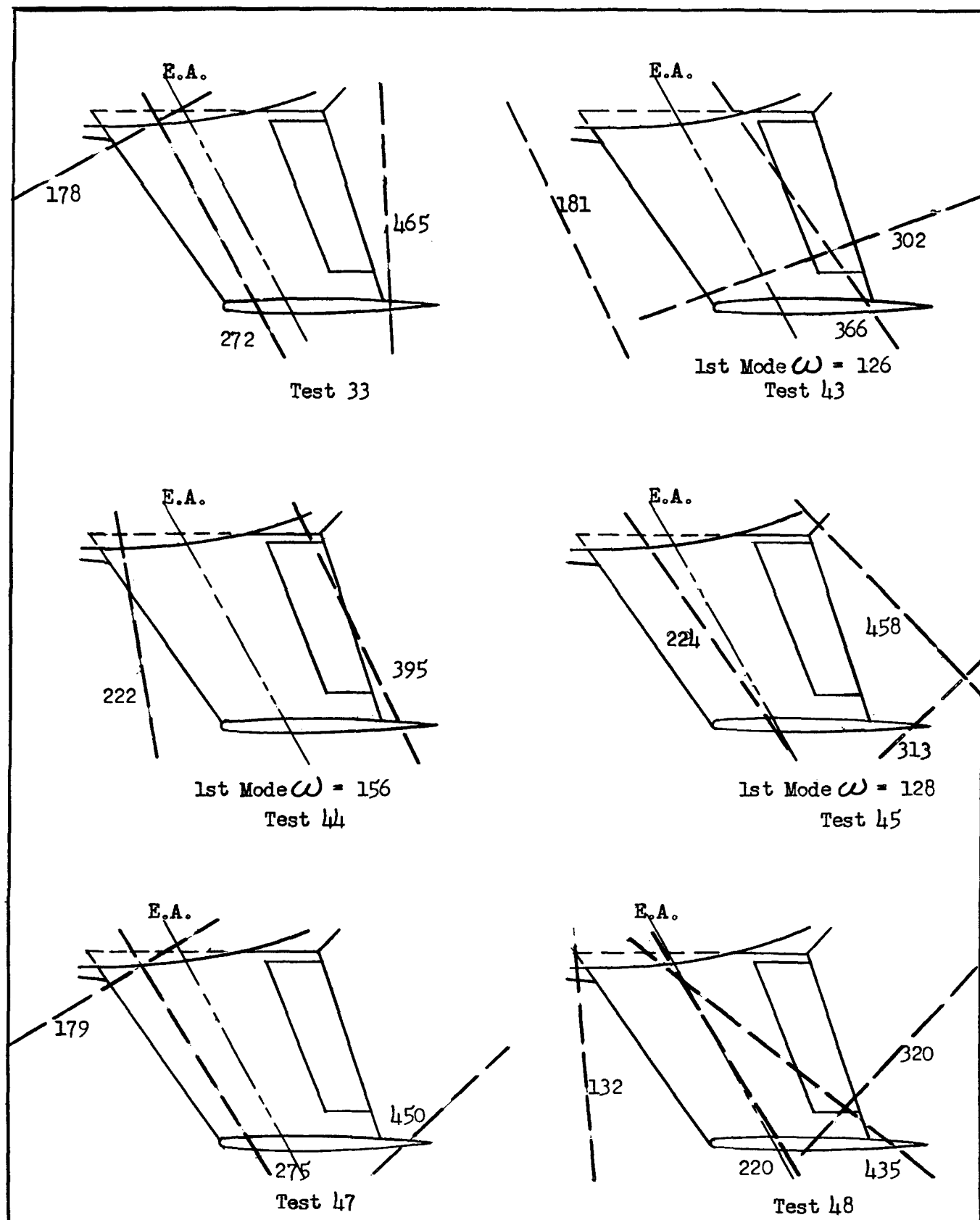


Fig. 31e Zero Airspeed Vibration Node Lines and Frequencies (CPM)

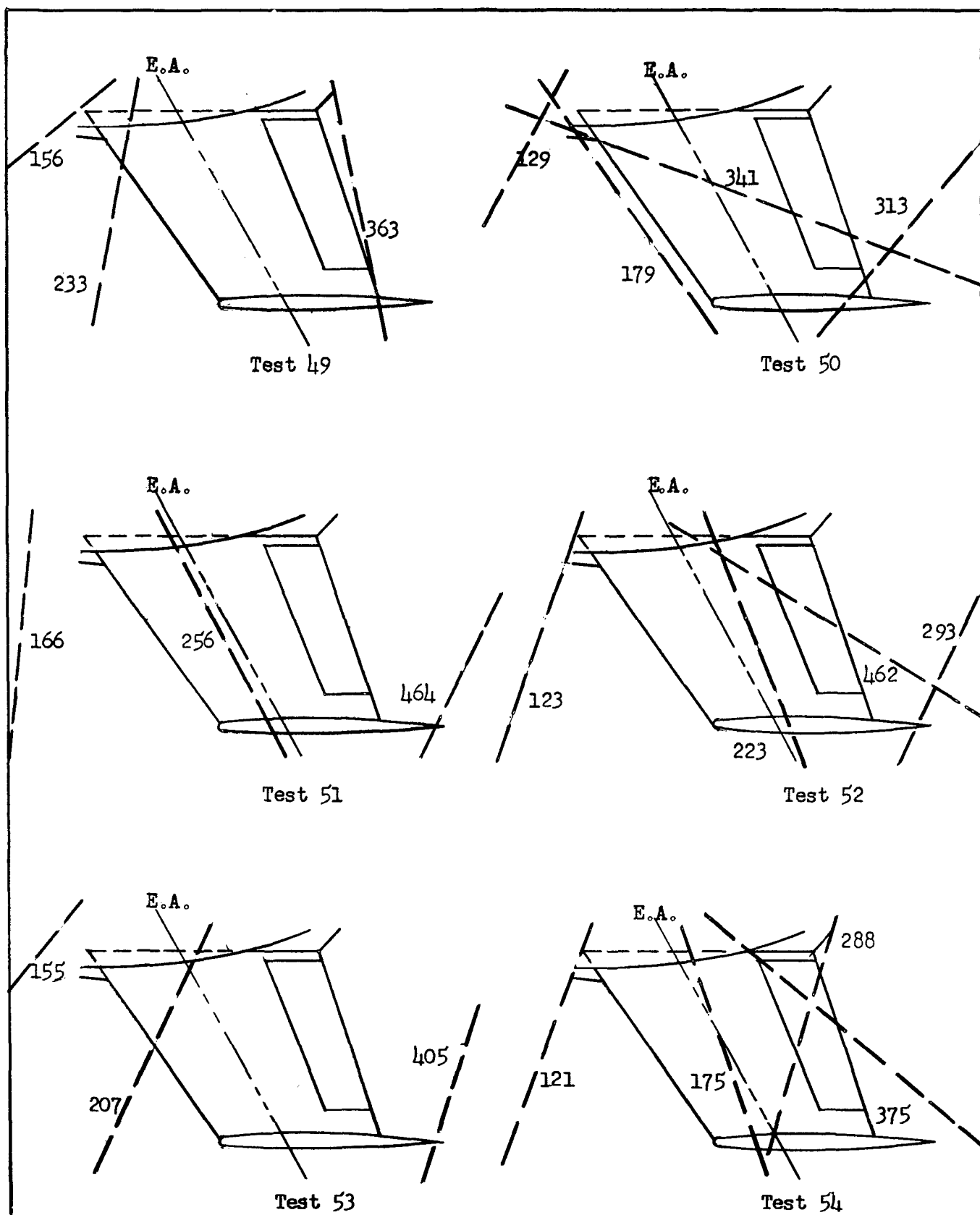


Fig. 31f Zero Airspeed Vibration Node Lines and Frequencies (CPM)

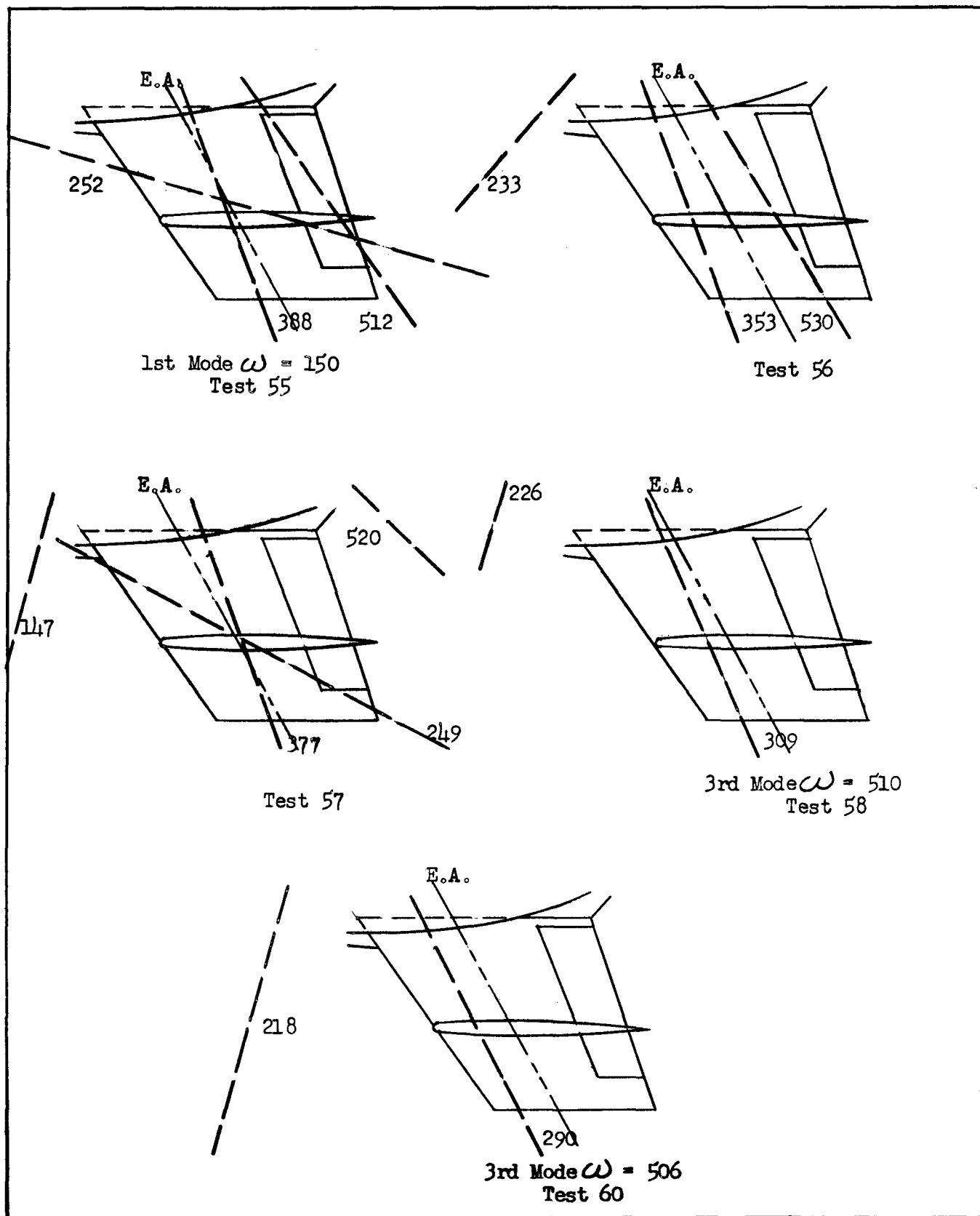


Fig. 3lg Zero Airspeed Vibration Node Lines and Frequencies (CPM)

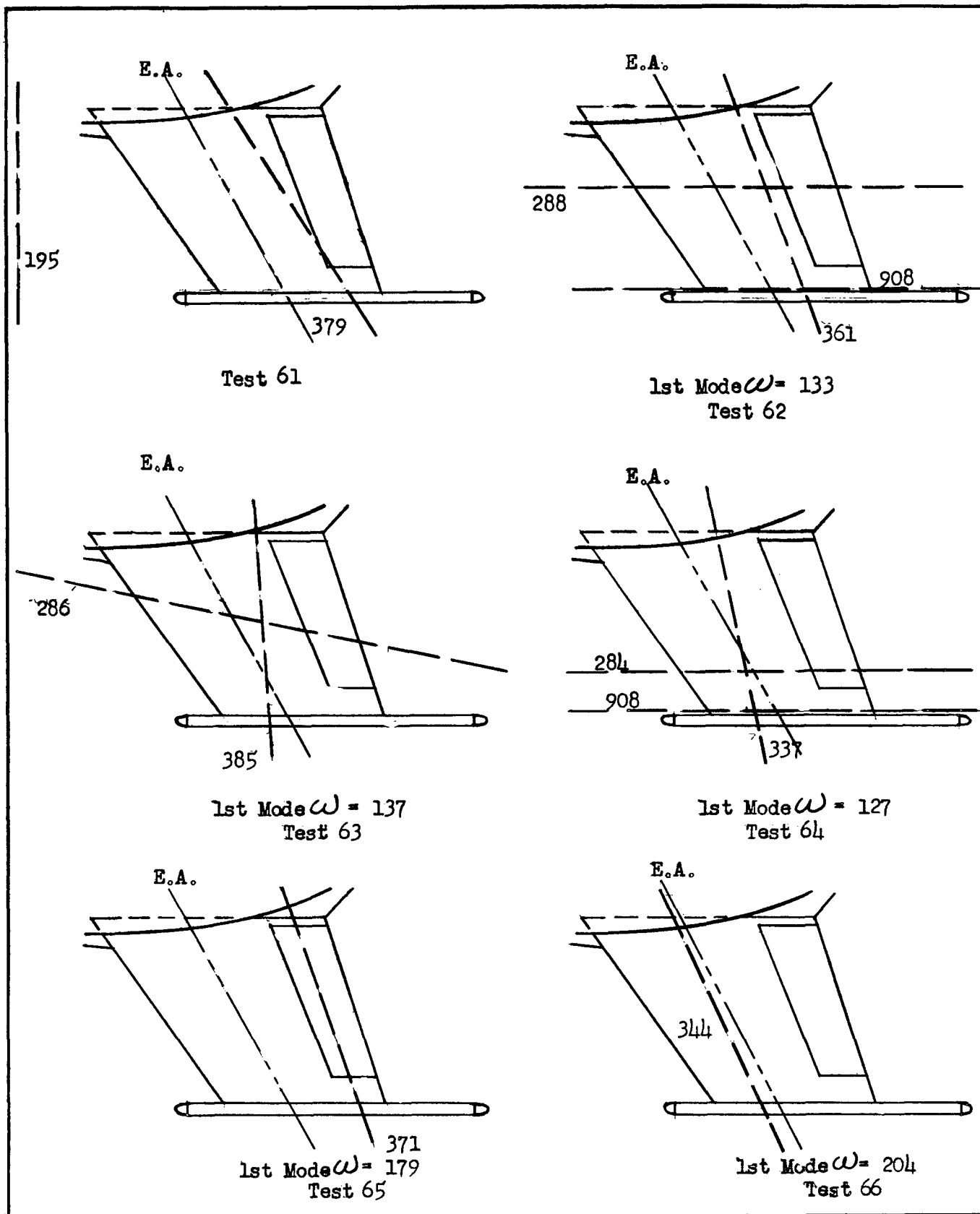
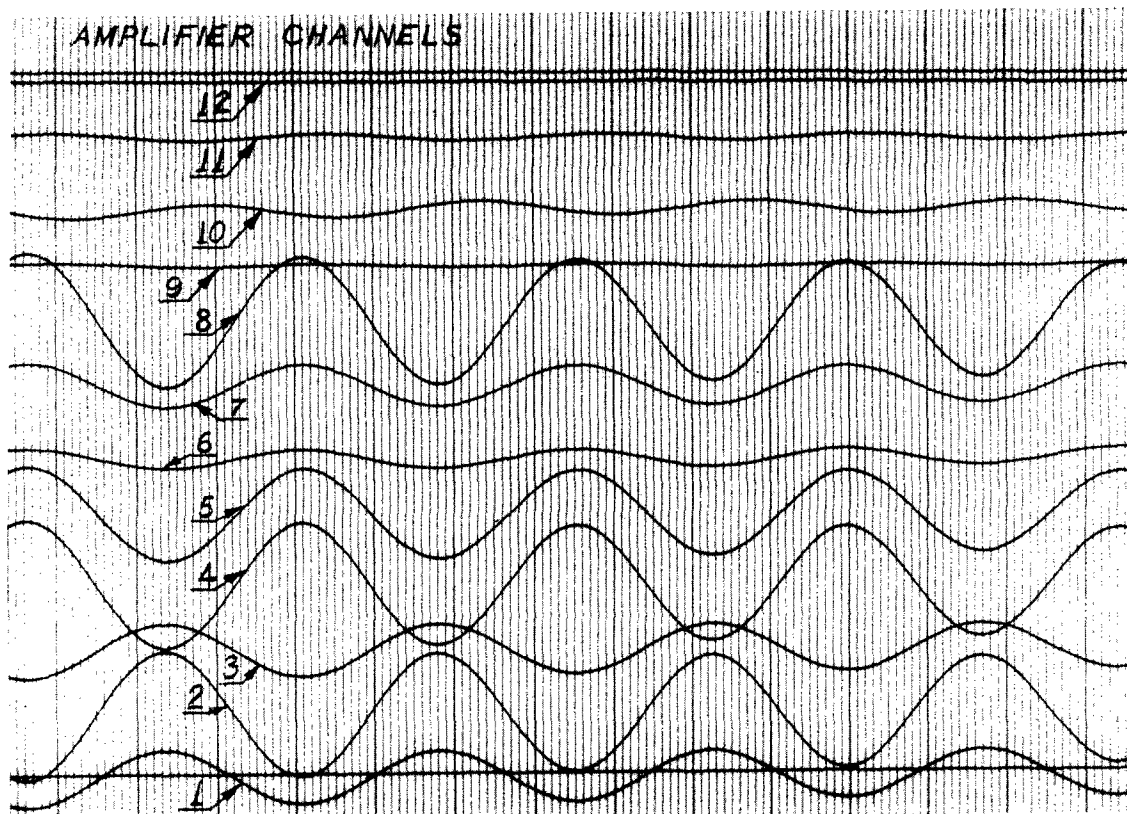
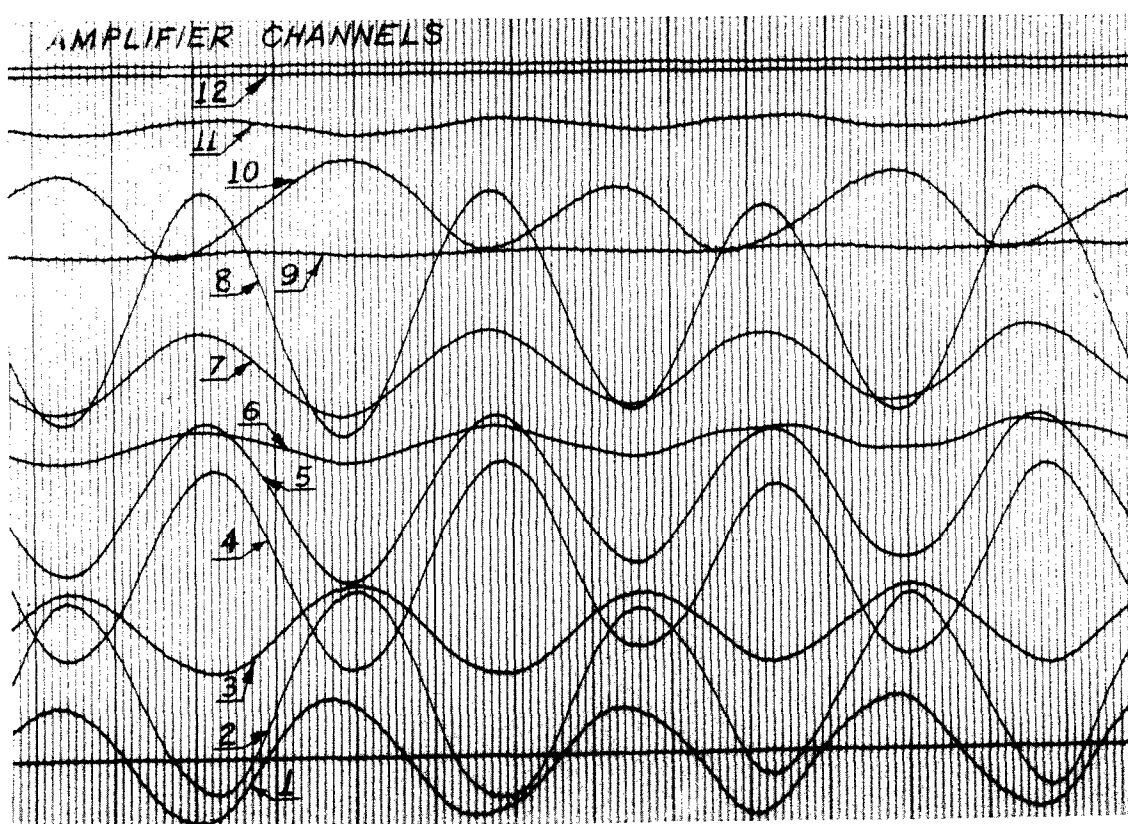


Fig. 3lh Zero Airspeed Vibration Node Lines and Frequencies



Zero Airspeed Record



Flutter Record

Fig. 32 Typical Zero Airspeed and Flutter Oscillograph Records

III. DISCUSSION

A. General

At the time the wind tunnel tests reported herein were conducted, it was most efficient and judicious to slightly alter the sequence of tests as originally scheduled and as listed in Table 3. In most instances the deciding factor in altering the sequence was the relative ease of making configuration changes. In the case of Test Nos. 10, 11, and 12, however, which involved replacing the stabilizer with equivalent weights, the decision to postpone these wind tunnel tests until the very end of the program was due to a combination of the radical nature of the configuration change and recognition of the more catastrophic type of flutter which might be encountered. By scheduling Tests 10, 11, and 12 at the end of the program, the running of the other tests was not being jeopardized by the possibility of having the model destroyed in Tests 10, 11, or 12 in the middle of the test program.

This precaution turned out to be extremely worthwhile since the model was seriously damaged during the running of Test No. 10. Throughout the testing program the model was subjected to rather mild excitations which produced fin tip lateral motions of the order of magnitude of plus or minus two inches. While conducting Test 10, which was run after the completion of Tests 1 through 9 and 13 through 32, a tunnel speed was reached at which the model appeared to be completely stable when excited in the usual manner. With essentially no change in tunnel speed, it was arbitrarily decided to subject the model to a somewhat more violent excitation. Immediately, catastrophic flutter was encountered which resulted in the destruction of the entire empennage of the model as well as the safety system. The same type of safety system which had been adequate for damping out the other cases of flutter proved surprisingly inadequate for the type of flutter encountered in this test. The remaining two tests, which were also configurations involving the stabilizer equivalent weights, were postponed and performed later.

A spare fin and stabilizer were available to run additional tests. These additional tests would have the purpose of trying to clarify certain peculiarities that had been exhibited in the tests with the unlocked rudder and also of trying to determine the significance of the fact that the Test No. 10 flutter condition was a function of the violence of the initial excitation. Accordingly, the spare stabilizer and fin were installed and a minimum of instrumentation necessary to identify flutter conditions was put into operating condition. The Dynamics Branch, WADC personnel then continued with the testing program.

During the course of running other tests the Dynamics Branch repeated part of the test schedule with the simplified instrumentation, for the purpose of checking the flutter speeds and flutter frequencies, using more violent excitations. In most instances a marked decrease in flutter speed was obtained while the flutter frequency and phase relationships remained essentially unchanged. For purposes of correlation with theoretical results, the flutter speeds and flutter frequencies from the latter tests were used while the amplitude ratios and phase relationships determined in the original tests were used whenever available.

B. Experimental Results

The yawing moment of inertia of the stabilizer about a line through the stabilizer center of gravity is approximately 4.5 times the total moment of inertia of the fin-rudder assembly about the fin elastic axis. (Table I-1)

Fore and aft movements of this relatively large mass and inertia over a range of 40% of the fin chord (aft of the fin elastic axis) would normally be expected to alter the flutter characteristics of the model radically. The following tabulated results are obtained from Figures 2 and 5 for the configurations having the stabilizer located at the fin tip.

Item	Fuselage Configuration	Stabilizer C.G. Fore & Aft Location (Per Cent Fin Chord Aft of E.A.)		
		8	28	48
$V/B_r \omega_r / (V/B_r \omega_r)_8$	Locked	1.000	1.034	0.980
$V/(V)_8$	Locked	1.000	.995	.871
$V/B_r \omega_r / (V/B_r \omega_r)_8$	Free	1.000	1.042	1.040
$V/(V)_8$	Free	1.000	1.000	.923

These experimental results show that the critical $V/B_r \omega_r$ varied a maximum of only 5.4% while the stabilizer was moved all the way from 8% to 48% of the fin chord aft of the fin elastic axis. These results also show that V , critical flutter speed, varied a maximum of 12.9% while the stabilizer position was changed from 8.0% to 48% of the fin chord aft of the fin elastic axis. In both the fuselage locked and fuselage free condition, V remains essentially unchanged with the stabilizer center of gravity 8% and 28% of the fin chord aft of the fin elastic axis; in moving the stabilizer from 28% to 48% of the fin chord aft of the fin elastic axis, however, V

is reduced by 12.9% of the forward location value with the fuselage locked and by 7.7% with the fuselage free. Although the reduction in V is not as great as might be expected for this large chordwise movement of the stabilizer aft of the fin elastic axis, the results show that, for a fin having fixed torsion and bending stiffnesses, aft movements (aft of the fin elastic axis) of the stabilizer are accompanied by progressively lower flutter speeds. These results reflect the effect of changing fin bending to fin torsion frequency ratio since the fin bending frequency remained practically constant for chordwise stabilizer movements while the fin torsion frequency changed appreciably. However, since this ratio changes only about 11% for the 40% change in stabilizer movement, it is believed the frequency ratio effect is of a secondary nature (the theoretical results plotted in Figures 20, 22 and 26 confirm this belief).

These results also show that whether the fuselage is free to bend and twist or locked relatively rigidly makes no significant difference on the critical $V/B_r \omega_r$ as the stabilizer is moved fore and aft between 8% and 48% of the fin tip chord aft of the elastic axis. The theoretical results of Figure 2 indicate the same insensitiveness of $V/B_r \omega_r$ to large changes in stabilizer location.

Considering the cases involving the stabilizer at the 58% fin span locations, Figures 2 and 5 yield the following:

Item	Fuselage Configuration	Stabilizer C.G. Fore & Aft Location (Per Cent Fin Chord Aft of E.A.)		
		8	28	48
$V/B_r \omega_r / (V/B_r \omega_r)_8$	Locked	1.000	0.925	0.895
$V/(V)_8$	Locked	1.000	0.875	0.760
$V/B_r \omega_r / (V/B_r \omega_r)_8$	Free	1.000	0.991	1.035
$V/(V)_8$	Free	1.000	0.938	0.885

Here, a decrease of 10.5% in the critical $V/B_r \omega_r$ is experienced as the stabilizer is moved from forward to aft positions with the fuselage locked. When the fuselage is freed, however, the effect is again insignificant; $V/B_r \omega_r$ varying through the range of minus about 1% to plus 3.5%. In view of the foregoing, it appears that from the standpoint of $V/B_r \omega_r$, it makes little difference where the stabilizer is located chordwise, in the range of from 8% to 48% of the fin chord aft of the fin elastic axis. For a fin of fixed torsion and bending stiffnesses such as these results represent, as much as a 24% decrease in critical flutter speed, V , is experienced in moving the stabilizer center of gravity from 8% to 48% of the fin chord aft of the fin elastic axis. The decrease in V

with aft movement of the stabilizer when the stabilizer is at the 58% fin span location is approximately two times as much as when the stabilizer is at the 100% fin span location. This is indicative of the reduced aerodynamic damping effect of the stabilizer when located at the inboard location.

Replacing the stabilizer with the stabilizer equivalent weights, which removed the effect of stabilizer aerodynamic damping from the system, the following effects are noted from Figures 8 and 11:

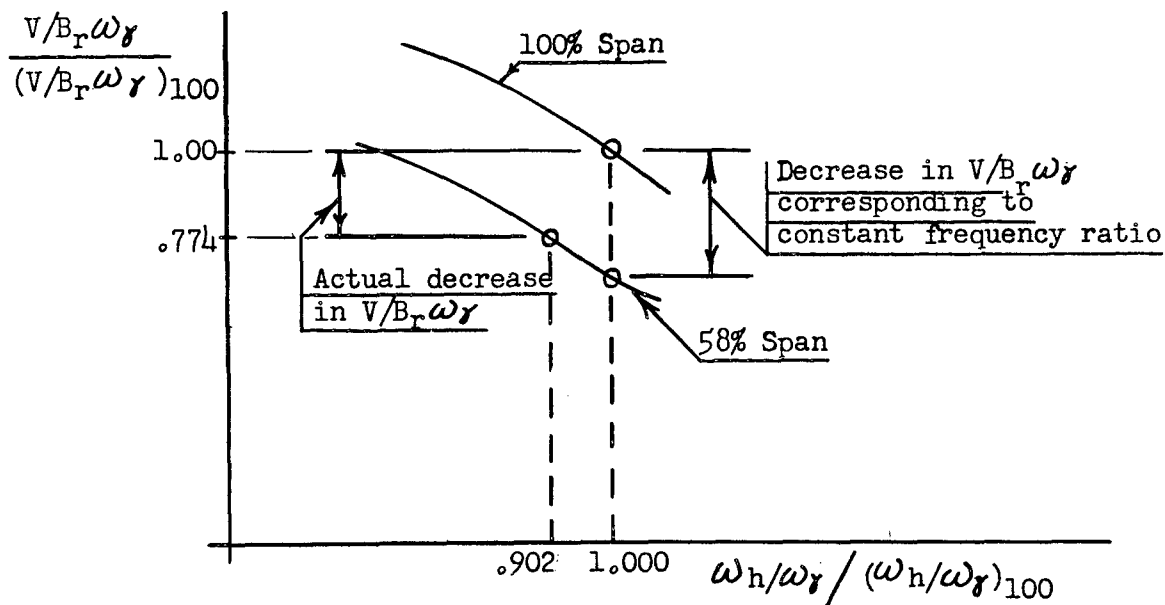
Item	Fuselage Configuration	Weight C.G. Fore & Aft Location (Per Cent of Fin Chord Aft of E.A.)		
		8	28	48
$V/B_r \omega_r / (V/B_r \omega_r)_8$	Locked	1.000	1.090	1.213
$V/(V)_8$	Locked	1.000	1.050	1.080
$V/B_r \omega_r / (V/B_r \omega_r)_8$	Free	1.000	0.901	1.071
$V/(V)_8$	Free	1.000	0.869	0.954

An increase of approximately 21% in the critical $V/B_r \omega_r$ (with locked fuselage) results from aft stabilizer equivalent weight movement, the variation being nearly linear with fore and aft position. When the fuselage is free, a quite different situation results in which $V/B_r \omega_r$ decreases approximately 10% in going from the 48% to the 68% fin chord locations and then increases 17% between the 68% and 88% fin chord locations. Apparently, the critical location is somewhere in the vicinity of the 68% fin chord (28% aft of elastic axis).

The effect of fin spanwise location of the stabilizer on $V/B_r \omega_r$ and critical flutter speed, V , (Fig.2) can best be demonstrated by the following table:

Item	Stabilizer Chordwise Location (per cent fin chord aft of fin EA)	Stabilizer Spanwise Location (per cent fin span)	
		100	58
$V/B_r \omega_r / (V/B_r \omega_r)_{100}$	8	1.000	0.865
$V/(V)_{100}$	8	1.000	1.340
$\omega_h / \omega_r / (\omega_h / \omega_r)_{100}$	8	1.000	0.885
$V/B_r \omega_r / (V/B_r \omega_r)_{100}$	28	1.000	0.774
$V/(V)_{100}$	28	1.000	1.176
$\omega_h / \omega_r / (\omega_h / \omega_r)_{100}$	28	1.000	0.902
$V/B_r \omega_r / (V/B_r \omega_r)_{100}$	48	1.000	0.791
$V/(V)_{100}$	48	1.000	1.168
$\omega_h / \omega_r / (\omega_h / \omega_r)_{100}$	48	1.000	0.940

These values indicate an appreciable decrease in critical $V/B_r \omega_f$ in moving the stabilizer from the fin tip to the 58% span. In addition, a decrease in fin bending-torsion frequency ratio also was experienced. Using the 68% fin chord (28% aft of fin EA) location as an example and assuming the following curve shapes in the vicinity of a frequency ratio of 0.6,



it becomes apparent that had the fin bending and torsion frequencies remained constant, the decrease in critical $V/B_r \omega_f$ would have been even greater as the stabilizer moved inboard. This case is typical of the other two chordwise locations with locked fuselage and of all chordwise locations with a free fuselage.

Therefore, for constant fin bending and fin torsion frequencies, the test results show that the 58% fin span is a more critical stabilizer location than the fin tip for the chordwise positions considered in this report.

If the values of the table are discussed in terms of a fin having fixed torsion and bending stiffnesses, the critical flutter speed, V , becomes the basis for comparison. For a fin of fixed torsion and bending stiffnesses, V increases as much as 34% when the stabilizer is moved from the fin tip to the 58% fin span location. This maximum increase is with the stabilizer in its most forward location (8% of the fin chord aft of the fin elastic axis). In the other two available stabilizer chordwise locations on the fin, approximately a 17% increase in V is realized in moving the stabilizer from the fin tip to the 58% fin span location.

The graphical results contained in Figures 13 and 14 show no appreciable change in either $V/B_r \omega_r$ or $V/B_r \omega_r$ with stabilizer rocking frequency for any of the fin tip chordwise stabilizer positions.

Unlocking the fuselage results generally in a decreased critical $V/B_r \omega_r$ as evidenced by Figures 2 and 5, and the table below.

Item	Stabilizer Spanwise Location (% Fin Span)	Stabilizer Chordwise Location (% Chord Aft of EA)	Fuselage Configuration	
			Locked	Free
$V/B_r \omega_r / (V/B_r \omega_r)_{\text{Locked}}$	100	8	1.000	0.941
$V/B_r \omega_r / (V/B_r \omega_r)_{\text{Locked}}$	100	28	1.000	0.950
$V/B_r \omega_r / (V/B_r \omega_r)_{\text{Locked}}$	100	48	1.000	1.000
$V/B_r \omega_r / (V/B_r \omega_r)_{\text{Locked}}$	58	8	1.000	0.872
$V/B_r \omega_r / (V/B_r \omega_r)_{\text{Locked}}$	58	28	1.000	0.935
$V/B_r \omega_r / (V/B_r \omega_r)_{\text{Locked}}$	58	48	1.000	1.009

The fuselage stiffness appears to be of most importance when the stabilizer is located forward on the fin. As the stabilizer moves aft, the effect of fuselage stiffness on $V/B_r \omega_r$ becomes insignificant.

With the stabilizer equivalent weights on the model, the fuselage stiffness effect on the critical $V/B_r \omega_r$ appears to be more pronounced with the weights 28% aft of the elastic axis and decreasing with movement in either direction (Fig. 8 and 11).

Item	Weight Spanwise Location (% Fin Span)	Weight Chordwise Location (% Chord Aft of EA)	Fuselage Configuration	
			Locked	Free
$V/B_r \omega_r / (V/B_r \omega_r)_{\text{Locked}}$	100	8	1.000	1.040
$V/B_r \omega_r / (V/B_r \omega_r)_{\text{Locked}}$	100	28	1.000	0.860
$V/B_r \omega_r / (V/B_r \omega_r)_{\text{Locked}}$	100	48	1.000	0.918

For the most forward weight location freeing the fuselage actually increases the critical $V/B_r \omega_f$ by 4%.

Even though the rudder was mass balanced by elements, a considerable decrease in flutter speed was obtained when the rudder was unlocked. The results of Tests 1 and 2, Table 5, show the flutter speed decreasing from 205 mph to 117 mph as a result of going from a locked rudder to a rudder rotational frequency of 100 cpm. The rudder dynamic balance with respect to both fin bending and fin torsion was considerably improved by the addition of weights to the rudder, but this change did not result in an appreciable increase in the rudder flutter speed. A chord extension at the rudder trailing edge eliminated the rudder flutter, even though the rudder was appreciably dynamically unbalanced, indicating that this type of flutter was possibly being caused by a high degree of rudder aerodynamic balance. In this final extended chord condition the bending-torsion flutter speed was higher than for the locked rudder condition.

The same low rudder flutter speed was experienced with the other stabilizer locations at the fin tip. However, when the stabilizer was moved to the fin 58% span this rudder flutter mode disappeared and unlocking the rudder resulted, in general, in an increased fin bending-torsion flutter speed.

C. Theoretical Results

A comparison of the velocity-damping curves in Figures 16 and 17, which are for the cases involving the stabilizer and the stabilizer equivalent weights, respectively, at the fin tip 68% chord position, shows the aerodynamic damping effect of the stabilizer. The negative slope of the theoretical g vs. $V/B_r \omega_f$ curve for the stabilizer equivalent weights case tends to emphasize the catastrophic nature of the flutter which was experienced with this configuration. The large degree of aerodynamic damping which was present with the stabilizer attached was reflected throughout in the flatness of the approximate $g - V$ curves plotted during the tests. This is borne out by relative flatness (compared to the equivalent weights case) of the g vs. $V/B_r \omega_f$ curves of Figures 15, 16, and 18.

The degree of correlation obtained between theoretical and experimental results is considered satisfactory in view of the lack of aspect ratio corrections and the complexity of the model. Before conducting the flutter analysis for each configuration, the stability determinant was solved for zero $V/B_r \omega$ in order to check the zero airspeed coupled modes; in each case satisfactory checks were obtained. On the basis of this, it is believed that the type of analysis described in this report is valid for predicting the flutter characteristics of a T-tail, but that the accuracy could be improved by incorporating aspect ratio corrections.

The extreme insensitiveness of the results to radical changes of stabilizer location on the fin are attributed to the aerodynamic damping of the stabilizer and its large mass moment of inertia about the fin elastic axis.

Although theoretical analyses were conducted of too few configurations to permit firm general statements, the data indicate that the theoretical accuracy may range from about 20% conservative to about 20% unconservative. The best agreement between theory and experiment was obtained for the equivalent weight configuration where an excellent correlation was realized between test and calculated values of the nondimensional parameters, $V/B_r \omega$ (0.1%), $V/B_r \omega_r$ (4.5%), and ω/ω_r (4.4%), (Table 7); the calculated values being lower than the test values for each of the three parameters.

IV. CONCLUSIONS AND RECOMMENDATIONS

A. Conclusions

On the basis of the results presented herein, the following conclusions are drawn:

1. If a constant fin bending-torsion frequency ratio is maintained the critical $V/B_r \omega_r$ for T-Tails is relatively independent of stabilizer fore and aft location in the range of locations tested regardless of the stabilizer spanwise location on the fin.
2. If constant or fixed fin torsion and bending stiffnesses are maintained, the critical flutter velocity, V , for T-tails decreases as much as 12.9% with the stabilizer located at the fin tip, and as much as 24.0% with the stabilizer located at the 58% fin span as the stabilizer center of gravity is moved from 8 to 48% of the fin chord aft of the fin elastic axis. The reduction in V is approximately two times as great with a very rigid fuselage (fuselage locked) as with a fuselage which is relatively flexible in side bending and torsion (fuselage free).
3. The fin 58% span is the more critical stabilizer spanwise location by as much as 23% in critical $V/B_r \omega_r$ if constant fin bending and fin torsion frequencies are maintained.
4. If constant or fixed fin torsion and bending stiffnesses are maintained, the critical flutter velocity, V , for T-tails may be increased as much as 34% by changing the location of the stabilizer from the fin tip to the 58% fin span location. This maximum increase was realized with the stabilizer center of gravity at 8% of the fin chord aft of the fin elastic axis. An approximate 17% increase in V was realized with the stabilizer center of gravity located 28 and 48% of the fin chord aft of the fin elastic axis.
5. Relative stiffness in roll of the stabilizer attachment to the fin on this T-tail configuration has a negligible effect on the critical $V/B_r \omega_r$ over the wide range of stiffnesses investigated in these tests.
6. Reducing the fuselage side bending and torsion stiffnesses results generally in decreased critical $V/B_r \omega_r$ values in all instances except for the most rearward stabilizer location configurations tested where the effect was negligible. Reductions in critical $V/B_r \omega_r$ of as much as 13% were experienced.

7. Since the rudder on this model did not seem to function as a normal rudder should, no conclusions can be drawn with respect to the effect of the rudder on critical values of $V/B_r \omega_r$.

Conclusion No. 2 set forth in the original version of Reference 3, which is a preliminary report on the wind tunnel tests of the model described herein, were somewhat prematurely drawn and should be disregarded. A more thorough study of the experimental and theoretical results yielded factors which were unforeseen at the time of writing of the reference report.

B. Recommendations

1. T-tail fins should be as stiff in torsion as is possible.
2. When a T-tail configuration is contemplated in the design of an airplane, a flutter analysis should be made to evaluate the flutter margin of safety and to establish the optimum stabilizer location.
3. Flutter model tests and/or flight flutter tests should be undertaken to establish the critical flutter speed on any given airplane having a T-tail, provided the flutter analysis does not yield an ample margin of safety.
4. Further investigation should be made, if practical, to determine why critical flutter is a function of the degree of violence and duration of the initial excitation.
5. Flutter analyses which include aspect ratio corrections should be made to see if better correlation could be realized between experimental and theoretical results.

V. REFERENCES

1. Smilg, Benjamin and Wasserman, Lee S., Application of Three Dimensional Flutter Theory to Aircraft Structures. Army Air Forces Technical Report No. 4798, July 1942.
2. Arnold, Lee, A Vector Solution of the Flutter Stability Determinant. Navy Department Bureau of Aeronautics Structures Memorandum 26, 22 May 1944.
3. Haviland, George P., Wind Tunnel Tests of a 'Tee' Tail Flutter Model. WADC Technical Note WCLS 52-21. Wright Air Development Center, Wright-Patterson Air Force Base, Ohio.

APPENDIX I

DATA

Tables I-1 through I-3 and Figures I-1 through I-7 constitute a complete listing of basic data on the T-tail flutter model. As is noted in these Figures and Tables, the majority of data were obtained experimentally. The basic data of Tables I-1, and I-2 and Figures I-1 through I-7 were used in evaluation of the numerical values of determinant elements summarized in Table I-3. Appendix III is the derivation of the formulas for the determinant elements.

MODEL PARAMETERS

Geometric Characteristics

Fig. II-5, II-5a, II-8

Fuselage Characteristics (Items 1,2, & 3 do not include fin, rudder or stabilizer).

- | | | |
|----|--|------------------------------|
| 1. | Weight * | 95 lbs. |
| 2. | Moment of inertia in yaw about vertical axis through flexure beam centerline * | 120,800 lb.-in. ² |
| 3. | Moment of inertia in roll about fuselage longitudinal axis * | 4,934 lb.-in. ² |
| 4. | Side bending frequency (stabilizer at fin tip, 68% chord.) | 172 cpm |
| 5. | Torsion frequency (stabilizer at fin tip, 68% chord) | 210 cpm |

Fin, including Rudder, Characteristics

1. Section Properties * (Fig. I-1)

<u>Section</u>	<u>Weight</u>	<u>X(a)</u>	<u>Y(b)</u>	<u>I_{CG}(c)</u>
<u>Boundaries</u>				
(X) (inches)	Lb.	In.	In.	Lb.-In. ²
13.50-19.55	6.82	15.05	19.40	963.92
19.55-24.12	2.50	21.21	17.32	103.23
24.12-29.10	2.28	26.80	14.68	122.78
29.10-36.72	9.80	32.28	14.26	336.59
36.72-41.40	2.18	39.16	13.31	87.02
41.40-44.64	1.73	42.70	15.32	80.46
44.64-49.15	7.46	47.73	10.50	638.46
Total	32.77			2332.4

- a. Fuselage centerline is station zero for all spanwise (X) coordinates.
- b. Fin leading edge is station zero for all chordwise (Y) coordinates.
- c. I_{CG} is taken about an axis through the section C.G. perpendicular to the stream direction, along the span.

Table I-1 - SUMMARY OF MODEL PARAMETERS

MODEL PARAMETERS

Fin, including Rudder, Characteristics (cont'd)

2.	Static unbalance about elastic axis* (Fig. I-2)	33.78 lb.-in.
3.	Moment of inertia about elastic axis* (Fig. I-3)	1900.00 lb.-in.
4.	Bending frequency	
	Stabilizer at fin tip (Table I-2)	
	48% Chord	184 cpm
	68% Chord	184 cpm
	88% Chord	181 cpm
	Stabilizer at 58% fin span	
	48%, 68% and 88% Chord	252 cpm
	Equivalent weights at fin tip (Table I-2)	
	68% Chord	211 cpm
5.	Torsional frequency	
	Stabilizer at fin tip (Table I-2)	
	48% Chord	302 cpm
	68% Chord	290 cpm
	88% Chord	268 cpm
	Stabilizer at 58% fin span	
	48% Chord	466 cpm
	68% Chord	440 cpm
	88% Chord	397 cpm
	Equivalent weights at fin tip	
	48% Chord	353 cpm
	68% Chord	339 cpm
	88% Chord	313 cpm
6.	Elastic Axis	40% Chord

Rudder

1.	Section Properties *			
	<u>Section</u>	<u>Weight</u>	<u>X(a)</u>	<u>Y(b)</u>
	<u>Boundaries</u>			
	(X) inches	Lb.	In.	In.
	14.80-19.55	.964	15.23	2.35
	19.55-24.12	.314	22.10	2.38
	24.12-29.10	.255	26.70	2.58
	29.10-36.72	.428	33.50	2.84
	36.72-41.40	.339	39.40	3.00
	Total	2.300		

Table I-1 - (continued)

MODEL PARAMETERS

Rudder (cont'd)

- a. Fuselage center line is station zero for all spanwise (X) coordinates.
- b. Rudder leading edge is station zero for all chordwise (Y) coordinates.
2. Static unbalance about hinge line* -0.69 lb.in.
3. Moment of inertia about hinge line* 12.6 lb.in.²
4. Frequency Variable

Stabilizer

1. Section Properties *

<u>Section</u>	<u>Weight</u>	<u>X (a)</u>	<u>Y (b)</u>
<u>Boundaries</u>			
(X)in.	lb.	In.	In.
2.00-9.1	4.4386	3.75	11.8
9.1-15.0	.7041	11.47	8.5
15.0-23.1	1.1975	18.20	7.0
23.1-33.1	.9955	27.00	7.3
33.1-40.8	1.6544	36.15	7.58
Total	8.9901 per side		
	18.0 both sides		

- a. Fin Chord line is station zero for all spanwise (X) coordinates.
- b. Stabilizer leading edge is station zero for all chordwise (Y) coordinates.
2. Total yawing moment of inertia about stabilizer C.G.* 8,596 lb.in.²
3. Total rolling moment of inertia about stabilizer center line* 7,054 lb.in.²
4. Symmetrical bending frequency* 452 cpm
5. Rocking frequency

Locked	High
.75 ω_y fitting*	214 cpm
.50 ω_y fitting*	138 cpm

Table I-1 - (continued)

MODEL PARAMETERS

Stabilizer (cont'd)

- | | | |
|----|--|---------------------|
| 6. | Center of Gravity* (Aft of leading edge
root chord) | 75.5% Root
Chord |
| 7. | Elastic axis | 40 % Chord |

Stabilizer Equivalent Weights

- | | | |
|----|---|-----------|
| 1. | Weight (Total) | 18.38 lb. |
| 2. | Yawing moment of inertia about the center of
gravity of the system on the fin center line
(total) | 7,592 lb. |

* Experimentally determined. All other values were
calculated. Frequencies are uncoupled.

Table I-1 - (concluded)

Test No.	Uncoupled Frequencies (cpm)					Damping Coefficients				
	ω_h	ω_r	ω_y	ω_ϕ	ω_θ	g_h	g_r	g_y	g_ϕ	g_θ
1	184	290	---	---	---	.013	.017	---	---	---
3	184	290	214	---	---	.013	.017	.030	---	---
10	211	339	---	---	---	.014	.022	---	---	---
13	184	302	---	---	---	.017	.022	---	---	---
17	181	268	---	---	---	.015	.018	---	---	---
45	184	290	---	172	210	.013	.017	---	.020	.014

Table I-2 - SUMMARY OF UNCOUPLED FREQUENCIES AND
DAMPING COEFFICIENTS USED IN ANALYSES

Fin Bending-Fin Torsion Flutter, Stabilizer at 100% Fin Span and 48% Fin Chord									
$V/B_T \omega$ Element	Aerodynamic Parts (inches)								Structural Parts (in.)
	1.25	2.50	3.33	4.17	5.00	6.25	8.33	10.00	
D_{11}	4.6320 -65.1958j	-32.1548 -146.2617j	-62.4043 -203.5950j	-97.8306 -262.0018j	-138.5148 -320.6731j	-210.4290 -408.4326j	-361.2272 -553.3201j	-511.0234 -667.6754j	$1170[-(\frac{25}{16})X(-1.92)]$
D_{12}	-10.2842 21.7875j	-31.7568 60.5470j	-62.3752 92.7656j	-106.7416 128.8329j	-165.4036 167.8721j	-280.3434 230.9017j	-544.3236 345.1179j	-820.9567 442.7142j	95
D_{21}	1.7413 35.2897j	19.5931 81.7261j	32.5843 115.2507j	46.7524 149.7926j	62.0878 184.7916j	87.8701 237.6124j	139.3038 325.8442j	188.7778 396.2243j	95
D_{22}	5.1730 -27.5848j	6.9531 -64.7317j	13.5111 -92.5245j	24.4952 -121.9727j	40.0953 -152.5830j	71.9999 -200.1316j	147.6880 -282.5867j	228.3672 -350.6222j	$1170[-(\frac{25}{16})X(-1.92)]$

Fin Bending-Fin Torsion Flutter, Stabilizer at 100% Fin Span and 68% Fin Chord									
$V/B_T \omega$ Element	Aerodynamic Parts (inches)								Structural Parts (in.)
	1.25	2.50	3.33	4.17	5.00	6.25	8.33	10.00	
D_{11}	4.6320 -65.1958j	-32.1548 -146.2617j	-62.4043 -203.5950j	-97.8306 -262.0018j	-138.5148 -320.6731j	-210.4290 -408.4326j	-361.2272 -553.3201j	-511.0234 -667.6754j	$1170[-(\frac{25}{16})X(-1.92)]$
D_{12}	-10.2842 21.7875j	-31.7568 60.5470j	-62.3752 92.7656j	-106.7416 128.8329j	-165.4036 167.8721j	-280.3434 230.9017j	-544.3236 345.1179j	-820.9567 442.7142j	240
D_{21}	1.7413 35.2897j	19.5931 81.7261j	32.5843 115.2507j	46.7524 149.7926j	62.0878 184.7916j	87.8701 237.6124j	139.3038 325.8442j	188.7778 396.2243j	240
D_{22}	5.1730 -27.5848j	6.9531 -64.7317j	13.5111 -92.5245j	24.4952 -121.9727j	40.0953 -152.5830j	71.9999 -200.1316j	147.6880 -282.5867j	228.3672 -350.6222j	$1170[-(\frac{25}{16})X(-1.92)]$

NOTE: Nondimensional Determinant Elements obtained by dividing Elements in Appendix III by appropriate values of $\pi^2 B_T^2$, $\pi^2 B_T^3$ and $\pi^2 B_T^4$.

Table I-3 - SUMMARY OF NUMERICAL VALUES OF DETERMINANT ELEMENTS-INFINITE ASPECT RATIO

Fin Bending-Fin Torsion Flutter, Stabilizer Equivalent Weights at 100% Fin Span and 68% Fin Chord								
V/B _r ^ω Element	Aerodynamic Parts (inches)							Structural Parts (in.)
	1.25	2.50	3.33	4.17	5.00	6.25	8.33	10.00
D ₁₁	1.8288 -15.1958j	-17.9788 -29.8457j	-38.7243 -38.7950j	65.7986 -46.9858j	-99.3788 -54.4331j	-162.2690 -64.2726j	-301.1792 -77.5873j	-443.5034 -85.9154j
D ₁₂	8.3412 -12.8683j	-41.5825 -20.1438j	-78.7884 -21.4614j	-128.9438 -20.2001j	-192.5297 -16.6655j	-313.7263 -7.6442j	-585.9444 15.3756j	-867.7565 39.4818j
D ₂₁	3.6843 0.6334j	9.7674 1.0353j	16.1711 1.0237j	24.5502 0.7596j	34.9617 0.2540j	54.4892 -0.9335j	97.6830 -3.8981j	141.9780 -7.0081j
D ₂₂	3.8257 -3.5535j	13.7664 -8.7793j	24.8923 -13.3175j	39.8906 -18.6306j	58.9050 -24.6214j	95.1468 -34.7197j	176.5486 -53.9376j	260.8190 -71.0138j

Fin Bending-Fin Torsion Flutter, Stabilizer at 100% Fin Span and 88% Fin Chord								
V/B _r ^ω Element	Aerodynamic Parts (inches)							Structural Parts (in.)
	1.25	2.50	3.33	4.17	5.00	6.25	8.33	10.00
D ₁₁	4.6320 -65.1958j	-32.1548 -146.2617j	-62.4043 -203.5950j	-97.8306 -262.0018j	-138.5148 -320.6731j	-210.4290 -408.4326j	-361.2272 -553.3201j	-511.0234 -667.6754j
D ₁₂	-10.2842 21.7875j	-31.7568 60.5470j	-62.3753 92.7656j	-106.7416 128.8329j	-165.4036 167.8721j	-280.3434 230.9017j	-544.3236 345.1179j	-820.9567 442.7142j
D ₂₁	1.7413 35.2897j	19.5931 81.7261j	32.5843 115.2507j	46.7524 149.7926j	62.0878 184.7916j	87.8701 237.6124j	139.3038 325.8442j	188.7778 396.2243j
D ₂₂	5.1730 -27.5848j	6.9531 -64.7317j	13.5111 -92.5245j	24.4952 -121.9727j	40.0953 -152.5830j	71.9999 -200.1316j	147.6880 -282.5867j	228.3672 -350.6222j

Note: Nondimensional Determinant₂ Elements obtained by dividing Elements in Appendix III by appropriate values of $\pi \rho B_r^3$, $\pi \rho B_r$ and $\pi \rho B_r^4$.

Table I-3 - (continued)

Fin Bending-Fin Torsion-Stabilizer Rocking Flutter, Stabilizer at 100% Fin Span and 68% Fin Chord

V/B _r Element	Aerodynamic Parts (inches)								Structural Parts (in.)
	1.25	2.50	3.33	4.17	5.00	6.25	8.33	10.00	
D ₁₁	4.6320 -65.1958j	-32.1548 -146.2617j	-62.4043 -203.5950j	-97.8306 -262.0018j	-138.5148 -320.6731j	-210.4290 -408.4326j	-361.2272 -553.3201j	-511.0234 -667.6754j	1170 [-125/1.99j]
D ₁₂	-10.2842 21.7875j	-31.7568 60.5470j	-62.3752 92.7656j	-106.7416 128.8329j	-165.4036 167.8721j	-280.3434 230.9017j	-514.3236 345.1179j	-820.9567 442.7142j	240
D ₁₃	4.0822 -72.8125j	-20.6438 -169.5308j	-34.4840 -239.9900j	-46.6466 -313.1171j	-56.9918 -387.7120j	-70.1330 -501.1830j	-87.4449 -692.7859j	-98.3260 -847.1880j	385
D ₂₁	1.7413 35.2897j	19.5931 81.7261j	32.5843 115.2507j	46.7524 149.7926j	62.0878 184.7916j	87.8701 237.6124j	139.3038 325.8442j	188.7778 396.2243j	240
D ₂₂	5.1730 -27.5848j	6.9531 -64.7317j	13.5111 -92.5245j	24.4952 -121.9727j	40.0953 -152.5830j	71.9999 -200.1316j	147.6880 -282.5867j	228.3672 -350.6222j	1175 [-125/1.99j]
D ₂₃	-2.8295 50.4688j	14.3089 117.5074j	23.9020 166.3450j	32.3323 217.0318j	39.5029 268.7360j	48.6115 347.3865j	60.6110 480.1928j	68.1530 587.2140j	-266
D ₃₁	4.0822 -72.8125j	-20.6438 -169.5308j	-34.4840 -239.9900j	-46.6466 -313.1171j	-56.9918 -387.7120j	-70.1330 -501.1830j	-87.4449 -692.7859j	-98.3260 -847.1880j	385
D ₃₂	-2.8295 50.4688j	14.3089 117.5074j	23.9020 166.3450j	32.3323 217.0318j	39.5029 268.7360j	48.6115 347.3865j	60.6110 480.1928j	68.1530 587.2140j	-266
D ₃₃	5.9568 -106.2500j	-30.1240 -247.3840j	-50.3200 -350.2000j	-68.0680 -456.9090j	-83.1640 -565.7600j	-102.3400 -731.3400j	-127.6020 -1,010.932j	-143.4800 -1,236.240j	1170 [-125/1.99j]

NOTE: Nondimensional Determinant Elements obtained by dividing Elements in Appendix III by appropriate values of $\pi/\rho B_r$, $\pi/\rho B_r^3$ and $\pi/\rho B_r^4$.

Table I-3 -- (continued)

Fin Bending-Fin Torsion-Fuselage Side Bending-Fuselage Torsion Flutter, Stabilizer at 100% Fin Span and 68% Fin Chord										
V/B _r ω Element	Aerodynamic Parts (inches)									
	1.25	2.50	3.33	4.17	5.00	6.25	8.33	10.00	Structural Parts (in.)	
<u>D₁₁</u>	4.6320 -65.1958j	-32.1548 -146.2617j	-62.4043 -203.5950j	-97.8306 -262.0018j	-138.5148 -320.6731j	-210.4290 -408.4326j	-361.2272 -533.3201j	-511.0234 -667.6754j	$1/170 [-(\frac{23}{100})(1+1.94)]$	
<u>D₁₂</u>	-10.2842 21.7875j	-31.7558 60.5470j	-62.3752 92.7656j	-106.7416 128.8329j	-165.4036 167.8721j	-280.3454 230.9017j	-544.3236 345.1179j	-820.9567 442.7142j	240	
<u>D₁₄</u>	13.5182 -60.3440j	-56.2814 -120.8375j	-128.3255 -159.2442j	-221.6405 -195.5575j	-336.7675 -229.7048j	-551.4459 -276.8922j	-1,023.618 -345.9136j	-1,506.108 -393.7360j	2,930	
<u>D₁₅</u>	24.5839 -101.4189j	-11.1609 -234.0623j	-32.6458 -331.5376j	-52.1804 -433.3868j	-69.4227 -537.9614j	-92.0423 -698.0808j	-122.9212 -970.2909j	-142.9709 -1,190.804j	2,410	
<u>D₂₁</u>	1.7413 35.2897j	19.5931 81.7261j	32.5843 115.2507j	46.7524 149.7926j	62.0878 184.7916j	87.8701 237.6124j	139.3038 325.8442j	188.7778 396.2243j	240	
<u>D₂₂</u>	5.1730 -27.5848j	6.9531 -64.7317j	13.5111 -92.5245j	24.4952 -121.9727j	40.0953 -152.5830j	71.9999 -200.1316j	147.6880 -282.5867j	228.3672 -350.6222j	$1/170 [-(\frac{23}{100})(1+1.94)]$	
<u>D₂₄</u>	16.2927 5.4037j	40.9882 10.6600j	66.5801 13.3956j	99.7975 15.3264j	140.8397 16.4513j	217.4643 16.6477j	386.1954 13.4502j	558.7421 8.1984j	1,282	
<u>D₂₅</u>	3.4524 59.6118j	24.1526 138.1324j	36.1890 195.6048j	46.9755 255.4715j	56.3505 316.7576j	68.4885 410.3175j	84.8242 568.8869j	95.2966 697.0380j	164	

Note: Nondimensional Determinant Elements obtained by dividing Elements in Appendix III by appropriate values of $\pi P B_r^2$, $\pi P B_r^3$ and $\pi P B_r^4$.

Table I-3 -- (continued)

Fin Bending-Fin Torsion-Fuselage Side Bending-Fuselage Torsion Flutter, Stabilizer at 100% Fin Span and 68% Fin Chord (continued)										
Element $V/B_T \omega$	Aerodynamic Parts (Inches)									
	1.25	2.50	3.33	4.17	5.00	6.25	8.33	10.00	Structural Parts (in.)	
D_{41}	1.4826 -73.8576j	-107.6745 -142.0344j	-223.3649 -181.7483j	-375.2636 -216.5348j	-564.4502 -246.6385j	-919.9711 -283.6085j	-1,707.8211 -326.6237j	-2,516.691 -347.2070j	2,930	
D_{42}	-44.5531 -62.9137j	-218.8278 -96.5000j	-413.8877 -100.3730j	-676.8380 -90.7236j	-1,010.202 -69.1564j	-1,645.601 -17.3066j	-3,072.764 110.9696j	-4,550.226 243.4240j	1,282	
D_{44}	58.7704 -466.9656j	-551.0898 -919.8750j	-1,188.414 -1,197.927j	-2,019.234 -1,453.389j	-3,048.884 -1,686.564j	-4,976.006 -1,996.206j	-9,229.928 -2,418.965j	-13,586.684 -2,686.680j	$21050 \sqrt{\frac{100}{125} \times \frac{1}{1.196}}$	
D_{45}	121.9160 -183.5523j	51.2140 -414.0625j	2,1625 -587.4123j	-45.1400 -771.7065j	-89.3950 -964.0700j	-150.2125 -1,263.388j	-237.2650 -1,780.601j	-296.0950 -2,204.800j	7,500	
D_{51}	0.8565 -128.0600j	-112.4788 -275.8502j	-220.0091 -375.9028j	-355.0373 -474.7421j	-518.2829 -571.3450j	-818.5633 -711.3216j	-1,471.777 -932.2622j	-2,135.265 -1,099.0751j	2,410	
D_{52}	-41.0092 9.6456j	-165.8724 59.7574j	-315.2170 112.3964j	-521.0425 177.9083j	-785.5015 254.1456j	-1,294.126 385.489j	-2,445.000 640.2109j	-3,641.315 869.078j	164	
D_{54}	8.6392 -310.7389j	-432.4860 -613.5625j	-892.3255 -799.2155j	-1,491.004 -969.1401j	-2,232.291 -1,123.446j	-3,618.685 -1,326.601j	-6,676.817 -1,599.049j	-9,807.471 -1,766.880j	7,500	
D_{55}	89.1841 -268.9119j	-9.5520 -614.3215j	-73.2169 -870.7581j	-132.8838 -1,140.787j	-187.1981 -1,420.108j	-260.2699 -1,850.940j	-362.6768 -2,588.881j	-430.6893 -3,190.109j	$6500 \sqrt{\frac{100}{125} \times \frac{1}{1.196}}$	

Note: Nondimensional Determinant Elements obtained by dividing Elements in Appendix III by appropriate values of $\pi \rho B_T^2$, $\pi \rho B_T^3$ and $\pi \rho B_T^4$.

Table I-3 (concluded)

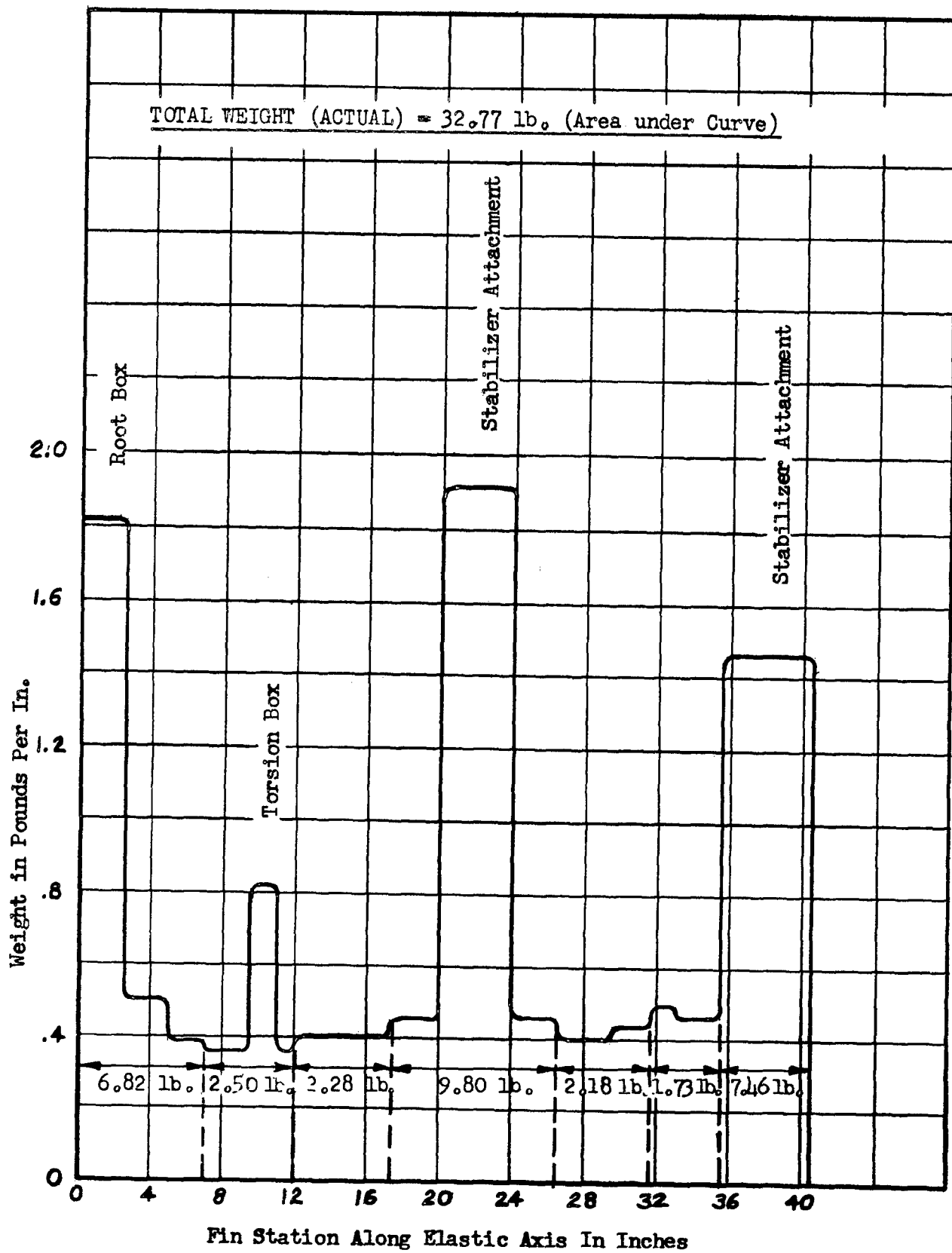


Fig. I-1 Fin-Rudder Weight Distribution

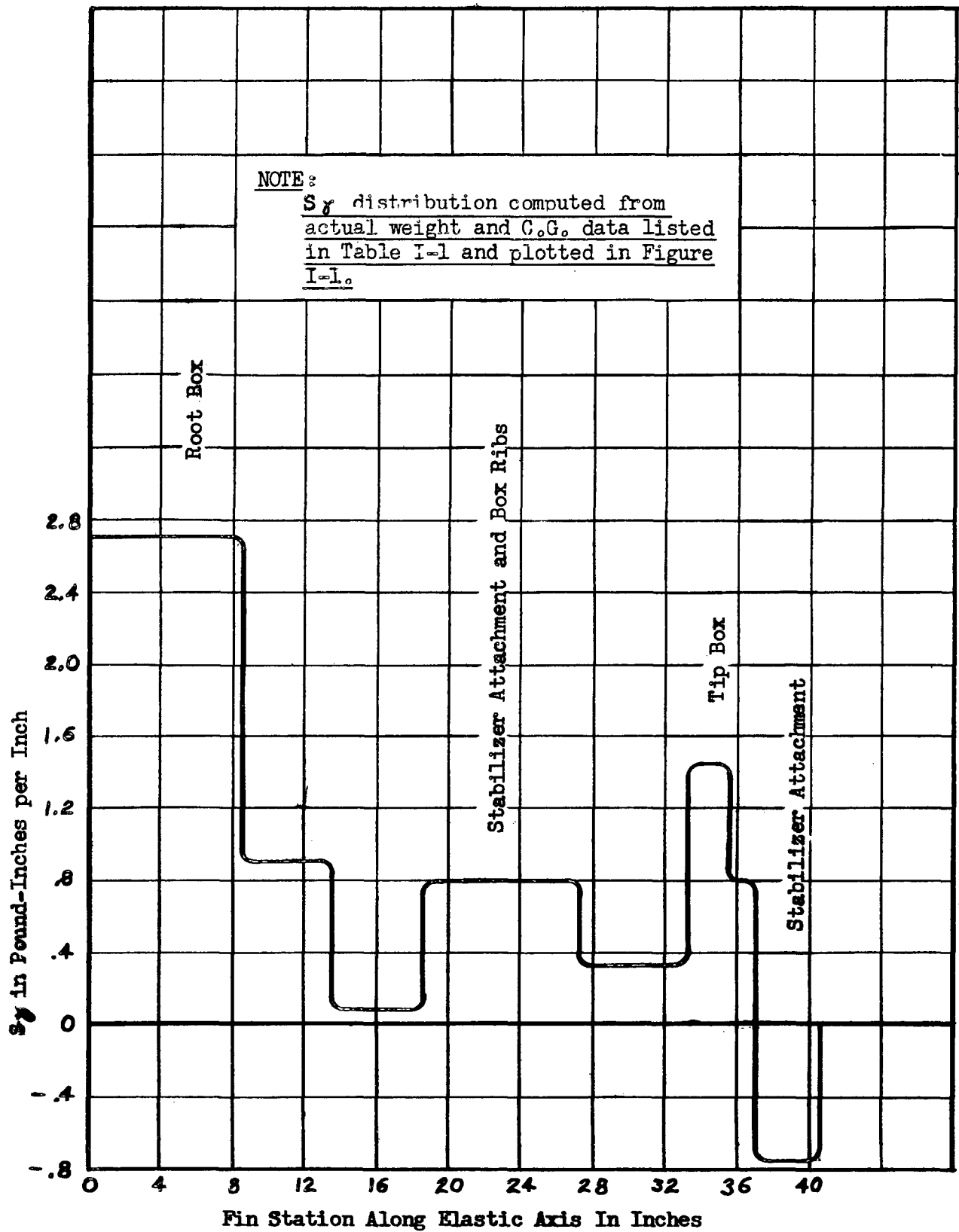


Fig. I-2 Fin Rudder S_y
 Distribution

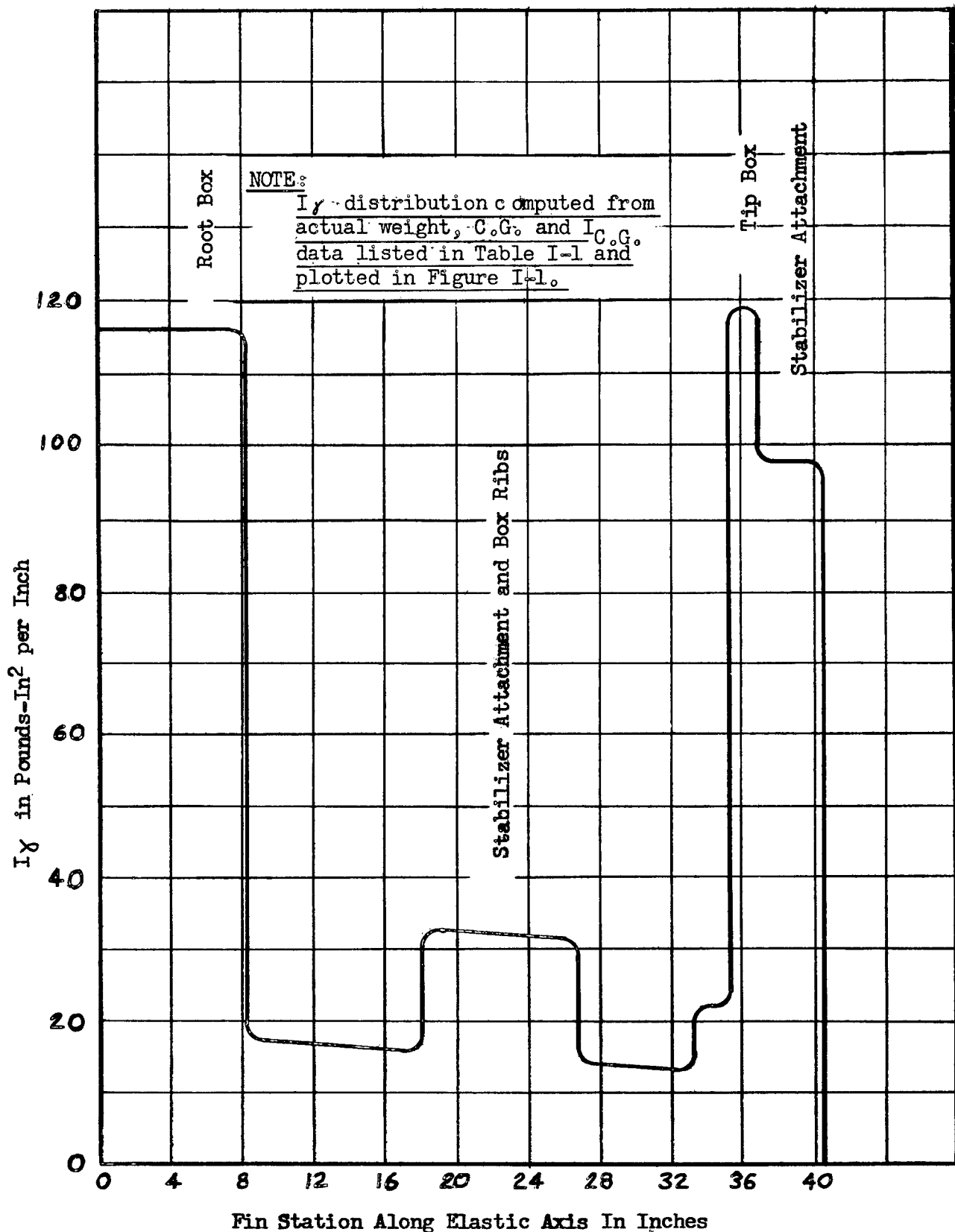


Fig. I-3 Fin-Rudder I_x Distribution

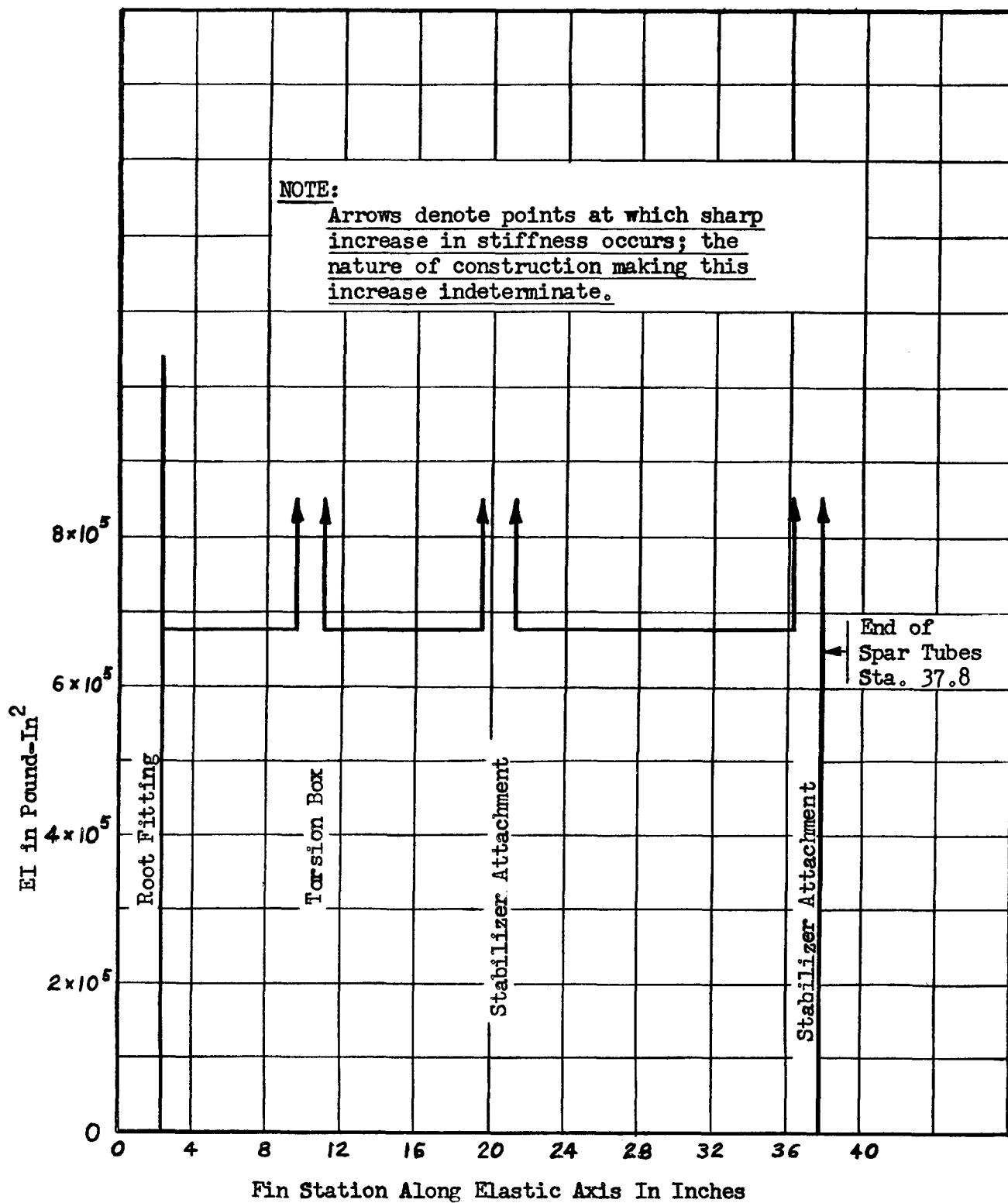


Fig. I-h Fin EI Distribution

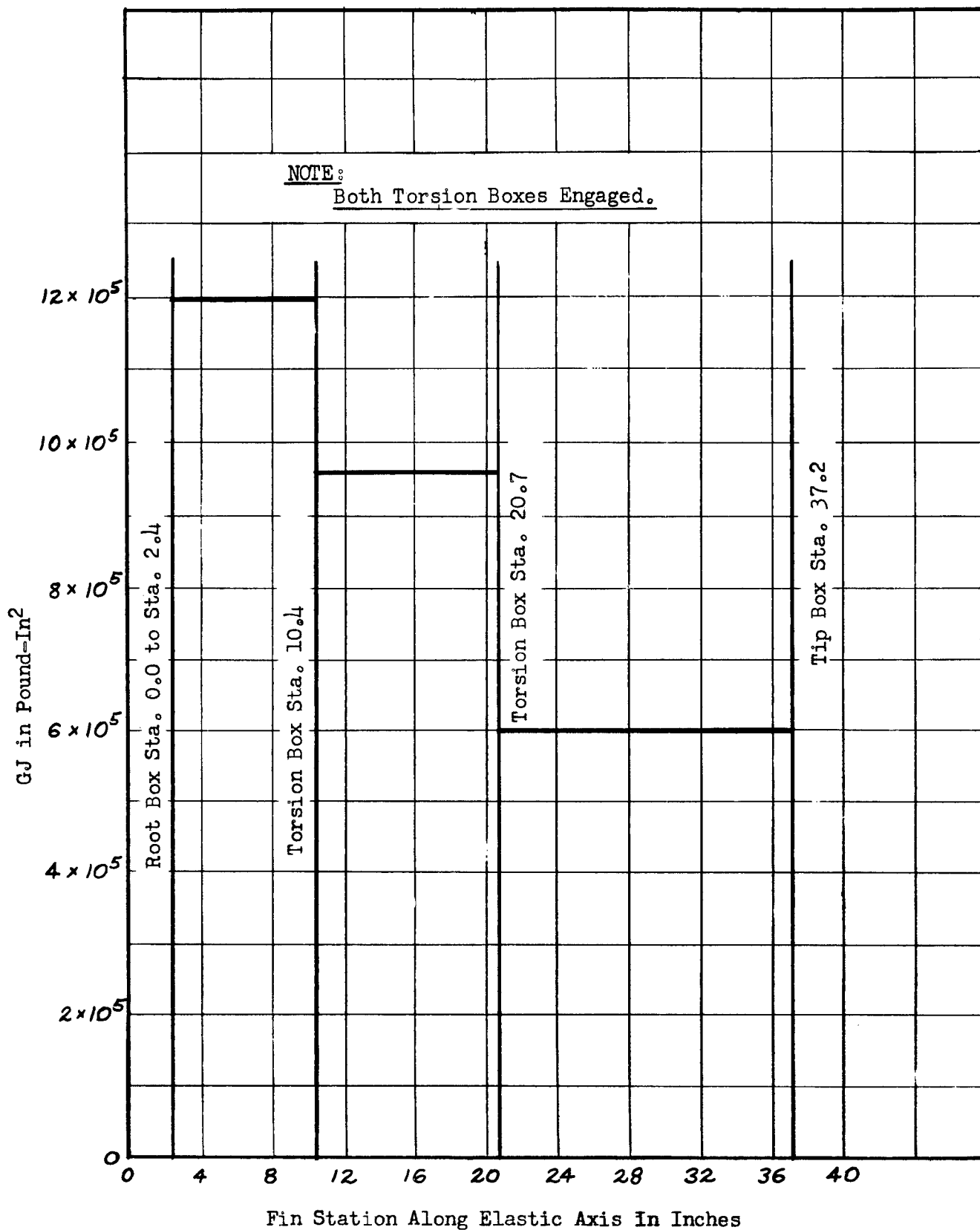


Fig. I-5 Fin GJ Distribution

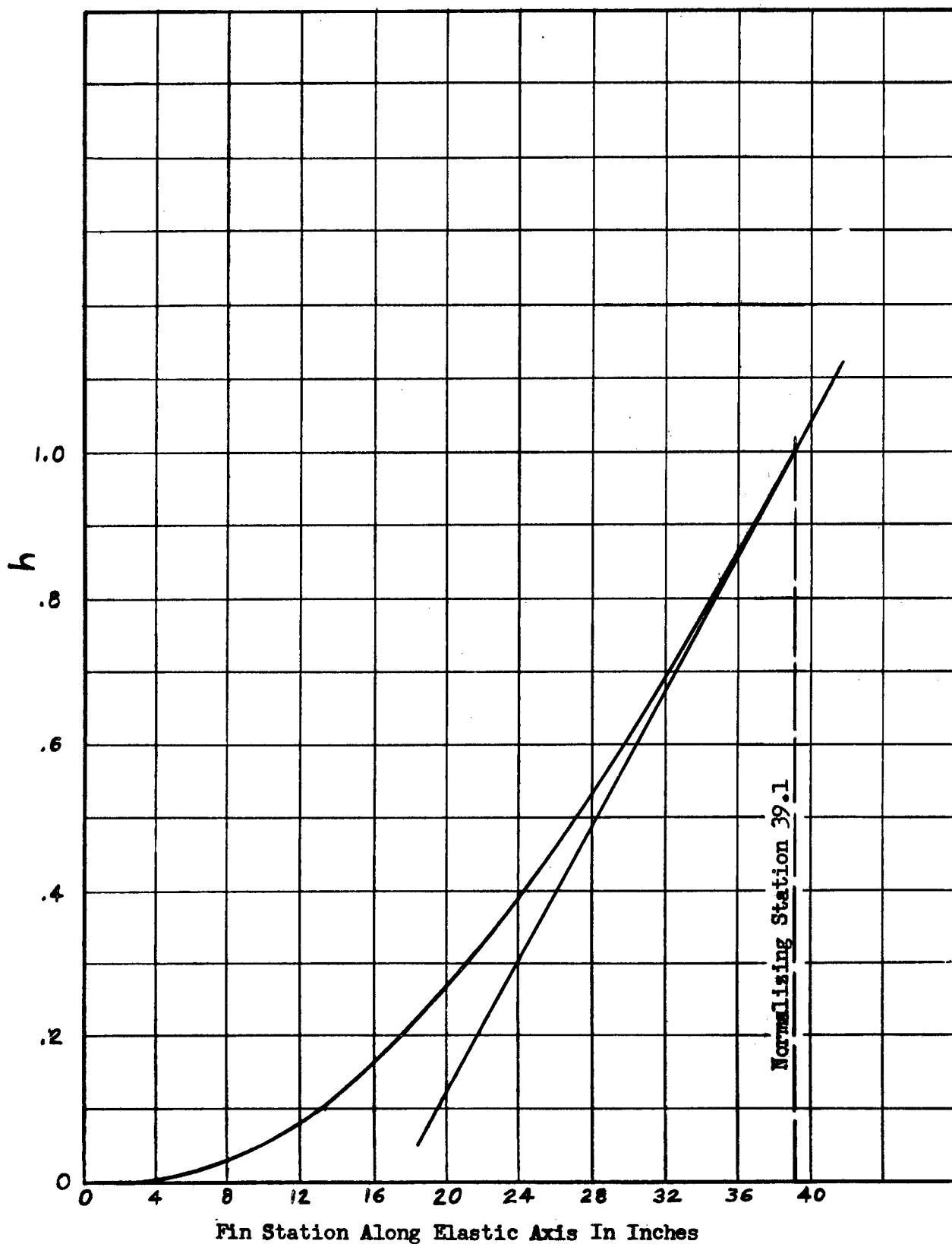


Fig. I-6 Fin Bending Mode Shape

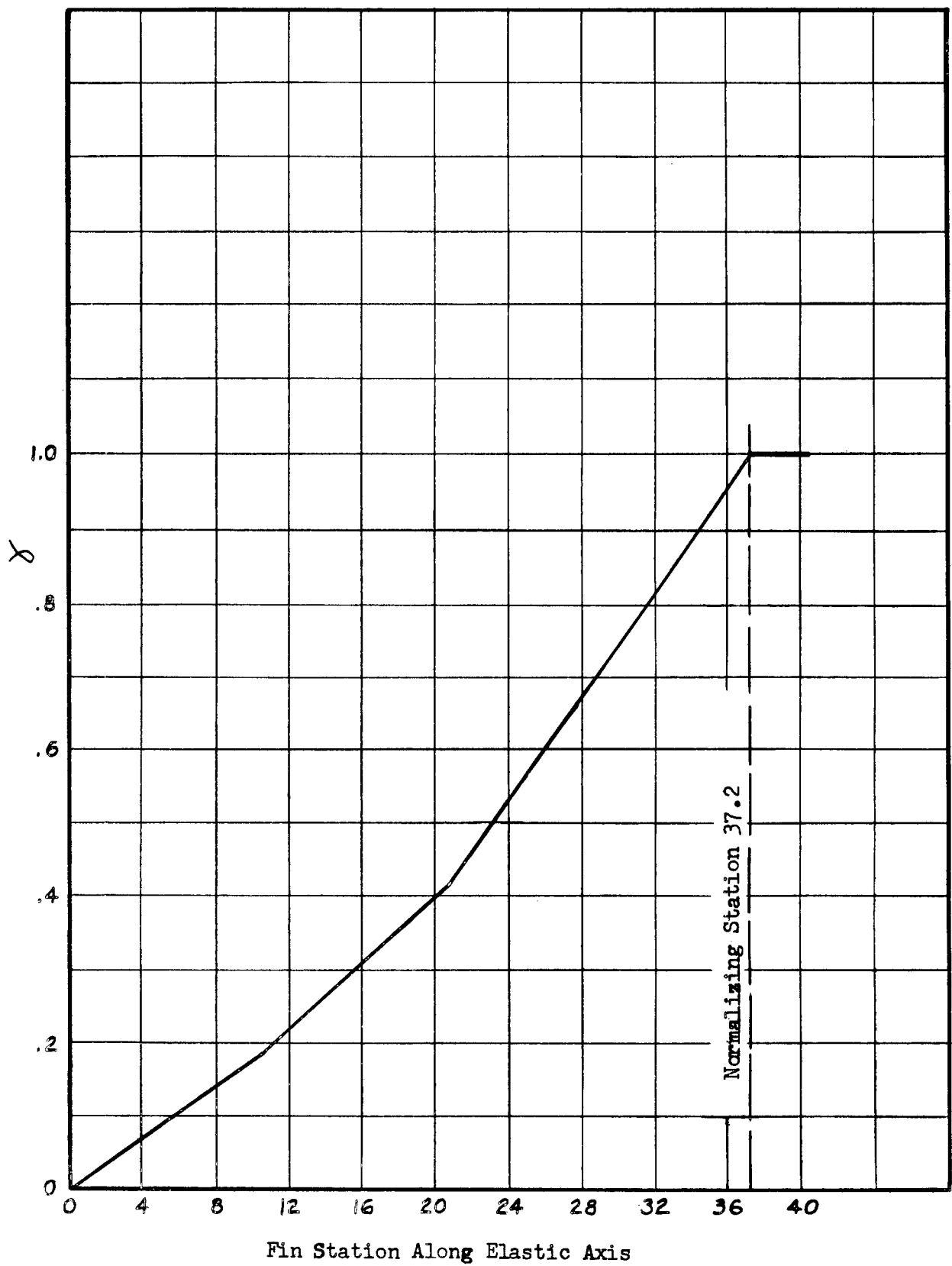


Fig. I-7 Fin Torsion Mode Shape

APPENDIX II

MODEL DESCRIPTION

1. Model Structure

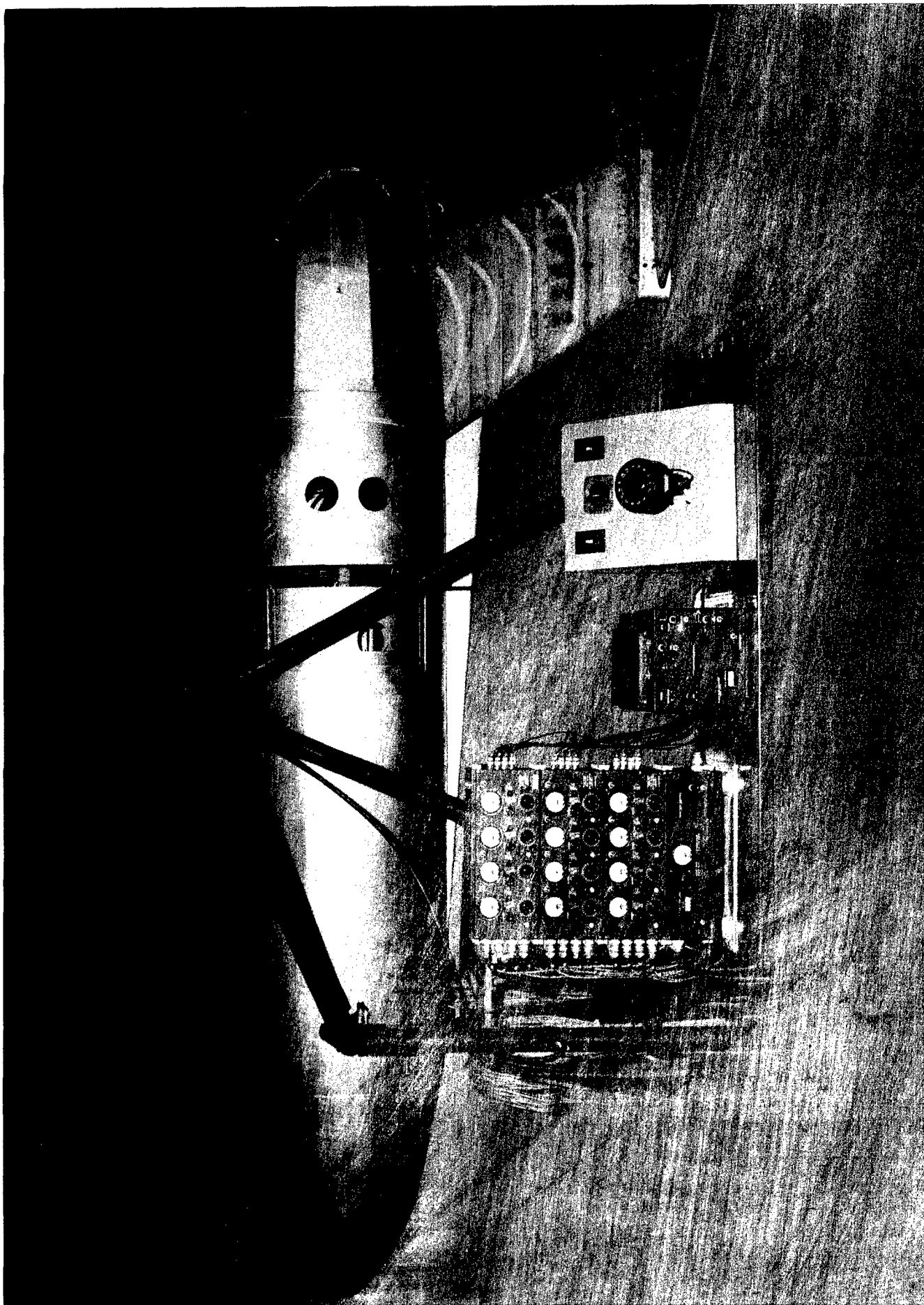
(All model components were designed to have ample margins of safety at a maximum tunnel speed of 250 mph and stabilizer tip amplitudes of ± 2.0 inches fore or aft, laterally or vertically.)

a. Fuselage:

Figure II-1 is a photograph of the completed assembled T-tail flutter model. The forward or nose section of the model consisted of a tubular steel frame covered with a combination wood nose and plywood surface; the surface being connected to the frame by means of plywood bulkheads. The frame was provided with three attachment points for the support structure.

The fuselage tail cone was connected to the nose section by means of an I beam which was designed to provide the required fuselage side bending and fuselage torsional stiffnesses and yet be relatively rigid in vertical bending. The tail cone was made up of a tubular steel frame, which carried a plywood and doped fabric fairing supported by a stringer-bulkhead framework. Steel plates were bolted to the tubular steel frame to obtain required mass properties. Figure II-2 shows the, partially uncovered tail cone section in which the frame, weights, plywood bulkheads, stringers and the partial plywood cover can be seen. Both nose and tail sections were bolted to the ends of the flexure (I) beam.

Means were provided for locking together the nose and tail sections in order to eliminate the two fuselage degrees of freedom. The side bending locks consisted of two heavy steel straps lying in a horizontal plane containing the flexure beam centerline and spaced outboard from the centerline approximately ± 3.6 inches. The bolt holes in the straps were located so that the straps were preloaded when attached to the nose and tail frames with tapered bolts. The torsion lock consisted of tubular frames extending from each end of the flexure beam and sloping upward on top and downward on the bottom toward the center of the beam. Attachments were provided for bolting together the forward and aft frames to effectively prevent twist occurring in the beam. The forward portion of the bending and torsion locks and the flexure beam can be seen in Figure II-3.



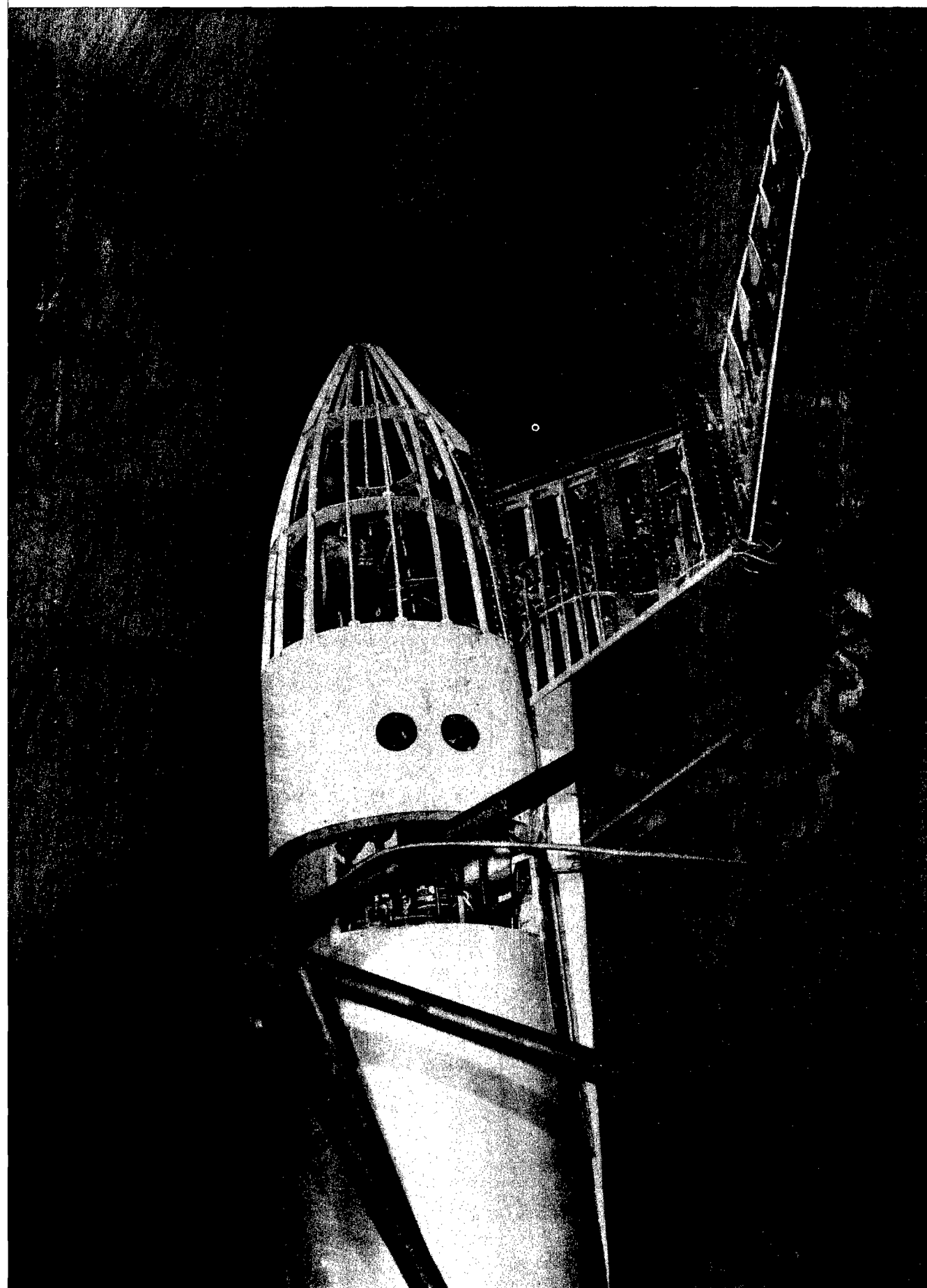


Fig. II-2 Uncovered Model

b. Fin:

Figure II-4 is a photograph of the fin spar with rib clips and stabilizer rocking fittings attached. The fin was of single spar construction, the spar being made up of two main steel tubes and two stiffener tubes connected by a scalloped steel shear web. The stiffener tubes were located in the center of the spar and were intended to provide bending stiffness only. All parts of the spar assembly were silver soldered or brazed together to minimize structural damping.

Rocking fittings for the stabilizer were provided at the fin tip and at 58% of the fin span. Each of these fittings consisted of two steel tubes with the longitudinal axes parallel to the stabilizer chord plane. One tube was silver soldered to the fin spar while the other was free to move. Silver soldered to the latter were small tubes to provide for attaching the stabilizer at the three different chordwise locations. The fixed and the moving tubes were connected with two sets of crossed leaf springs located at each end of the fitting and thereby providing considerable resistance to yawing or pitching of the stabilizer. In order to obtain greater rocking stiffness an additional set of springs could be installed in the center of the fitting. The tubes also could be locked together at each end with screws to prevent any appreciable relative motion between the stabilizer root and the fin.

In order that alterations in the fin torsional stiffness could be made without appreciably changing the bending stiffness, a torsionally stiff tube with longitudinal axis perpendicular to the axis of the spar was silver soldered to the fin main spar tubes about ten inches from the fin root. The tube was cut at its lengthwise center and provided with bolt attachments so that it could be locked or unlocked. A second means of stiffness alteration was incorporated in the fixed tube part of the 58% span rocking fitting. These tubes and the locking mechanisms are visible in Figure II-4. The tubes remained locked throughout the test program since it was found to be unnecessary to use this adjustment.

The spar tubes extended through the root fitting, which provided a means for attaching the fin to the aft fuselage frame, and were welded on the inboard side and silver soldered on the outboard side. SAE 4130 steel was used throughout the spar and fitting structure.

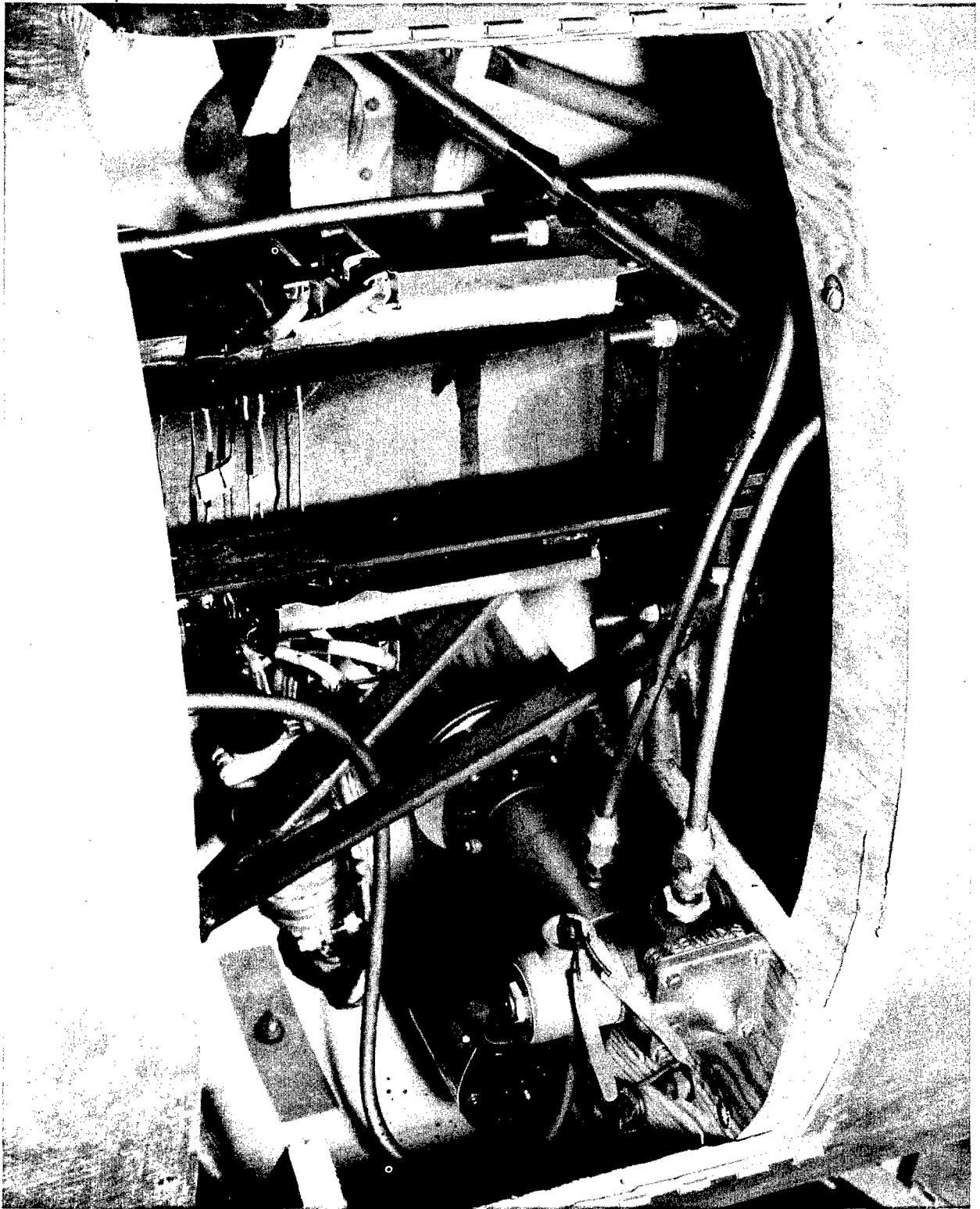


Fig. II-3 Fuselage Flexure Beam and Air Valve Installation

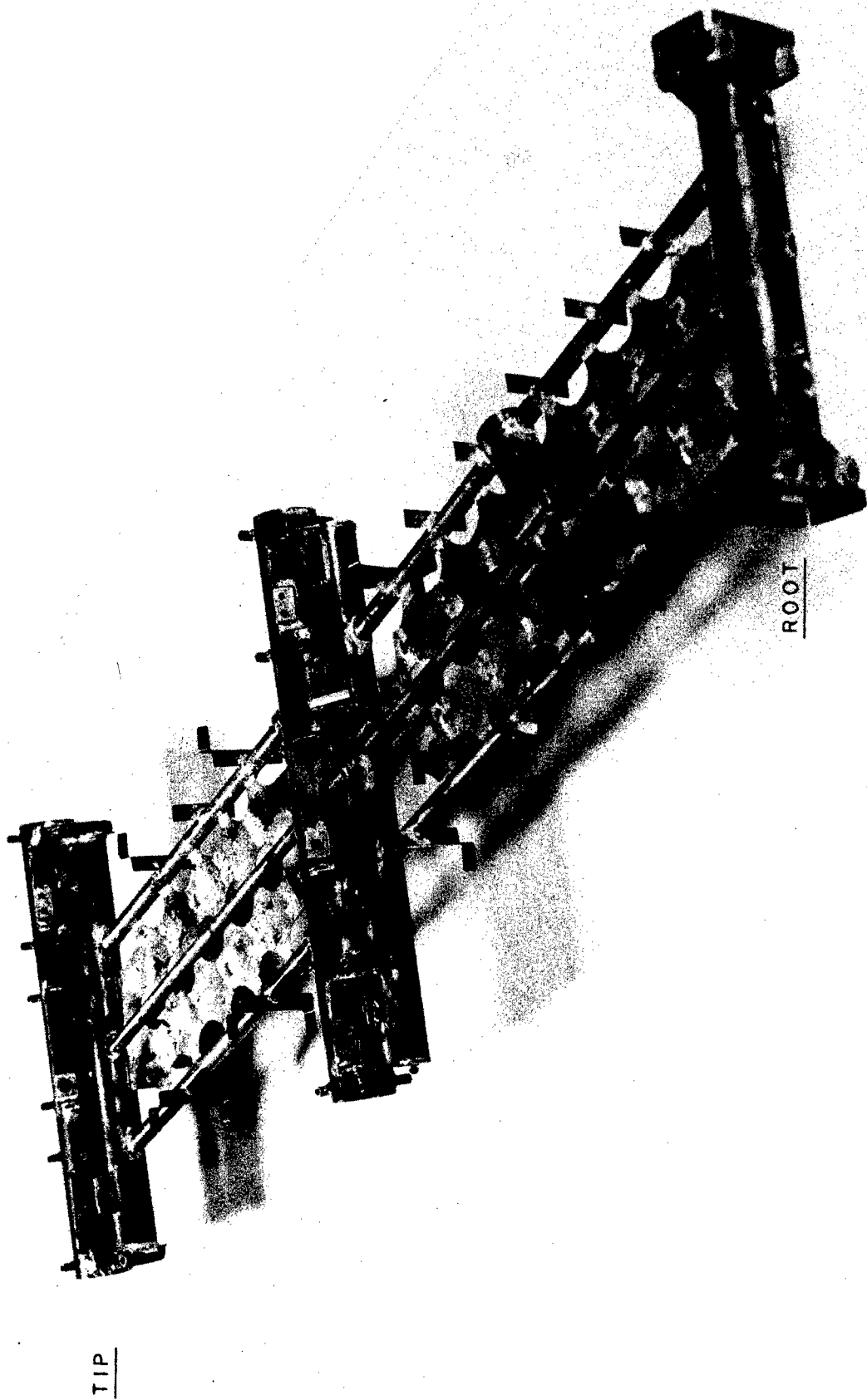


Fig. II-4 Fin Spar

Aluminum alloy channel main ribs and support ribs were riveted to the spar rib clips which were in turn brazed to the main spar tubes. The leading and trailing edges were formed of aluminum alloy sheet and cut into segments so as to offer no appreciable torsional stiffness. The spar and rib structure was covered with nylon net which was impregnated with Goodyear Chemigum Latex 101A. The nylon was stretched on and sewed with the threads running parallel to the elastic axis and parallel to the ribs. The latex was then painted on in several coats until the cover was sealed. The orientation of the threads served to minimize the effect of the cover on the fin torsional stiffness. No serious ballooning difficulties were encountered with this type of covering at wind velocities up to 250 mph. Zippers were installed at various points to provide access to the internal structure and to the instrumentation.

The elastic axis was located at 40% fin chord and had a 28.37° sweepback. Details of the geometry are included in Figure II-5.

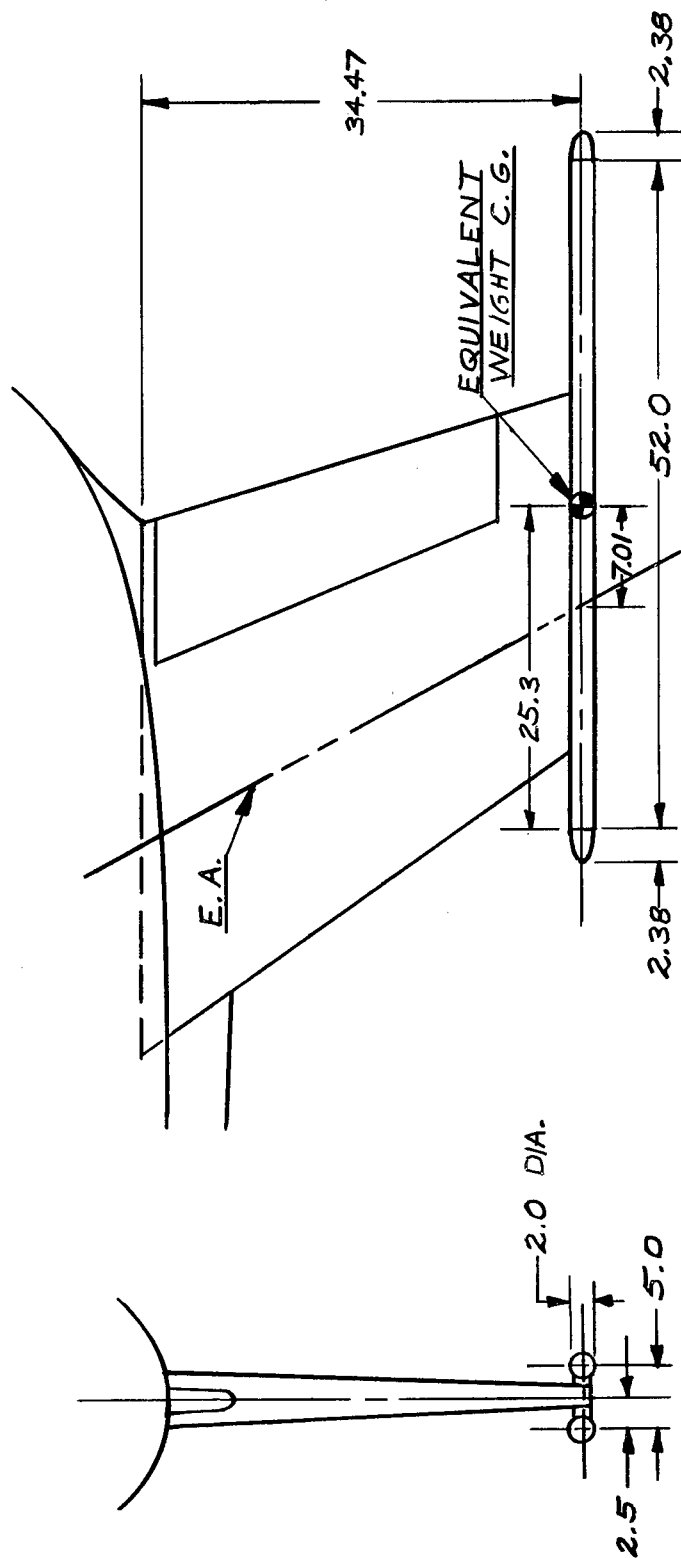
c. Stabilizer:

The stabilizer structure shown in Figure II-7 was quite similar to that of the fin. The spar was made up of two steel tubes connected by a steel sheet web. To prevent warping of the thin sheet due to heat, clips were silvered soldered to the tubes so that alternate clips would be on the same side of the web. The web was then inserted and riveted in place to the clips. All spar components were of SAE 4130 steel. Ribs, leading edge, and trailing edge channels were of aluminum alloy. The leading edge contour, not shown in Figure II-7, was formed of aluminum alloy sheet and riveted to the leading edge channel. Ballast weights necessary to bring the stabilizer up to the specified weight, balance and inertia condition, and consisting of lead slugs, were bolted into place in the root box assembly.

The stabilizer was bolted to the fin with four bolts through the root box. The spar and rib structure was covered with latex impregnated nylon net in the same manner as the fin. Zippers were installed to provide access to the instrumentation



Fig. II-5 Fin and Fuselage Geometry and Pickup Locations



NOTE: WEIGHTS SHOWN AT 68% FIN CHORD POSITION

Fig. II - 5a Stabilizer Equivalent Weight Geometry

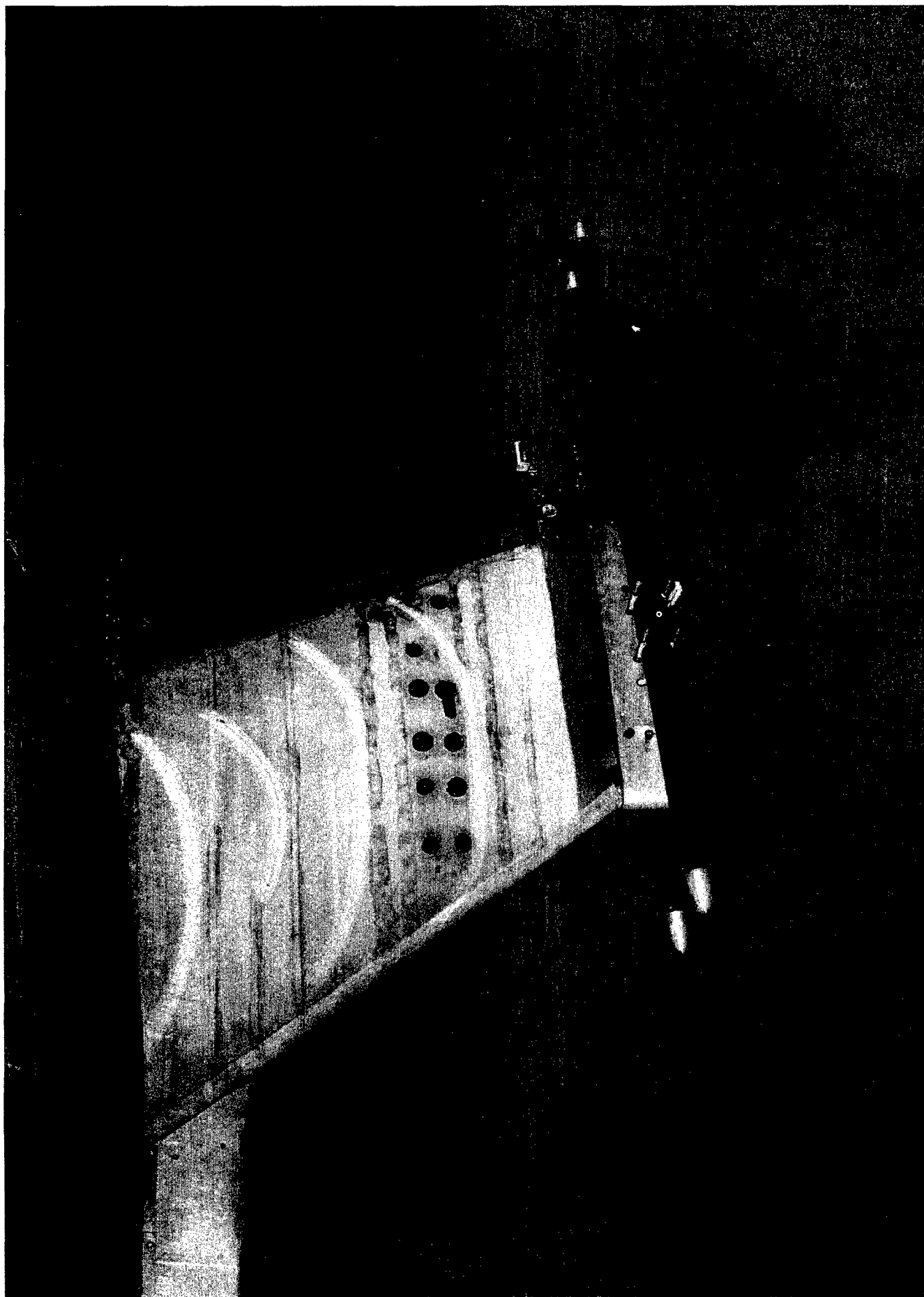


Fig. II-6 Mounted Stabilizer Equivalent Weights

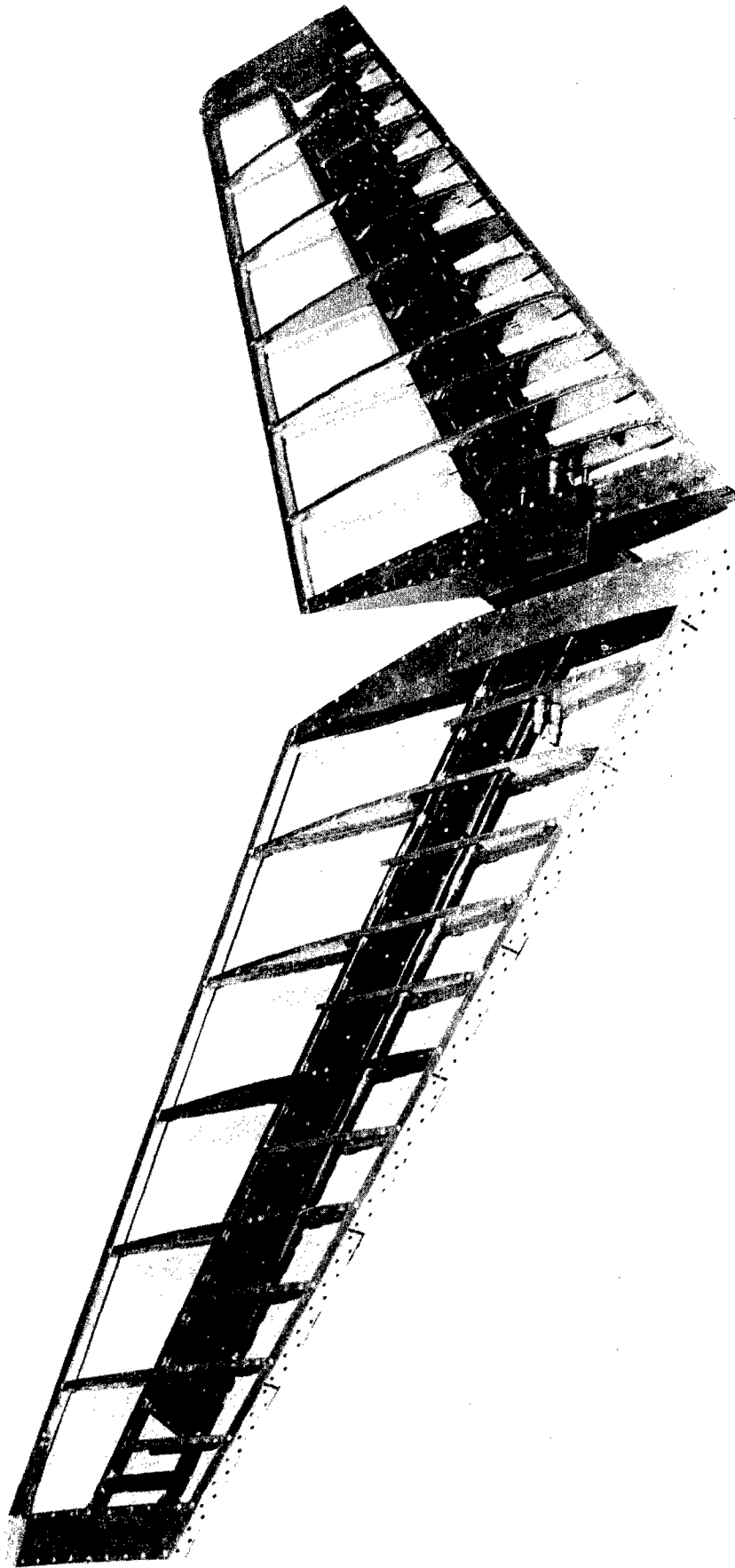


Fig. II-7 Uncovered Stabilizer

and to the root attachment bolts. Figure II-8 is a drawing showing the stabilizer dimensions.

Stabilizer equivalent weights which simulated the stabilizer weight and yawing moment of inertia were constructed of two 2-inch O. D. steel tubes with lead inserts at either end. Figure II-6 is a photograph of the weights in place on the model.

d. Rudder

The rudder was of mahogany plywood construction and was attached at each end to the fin with flexure hinges. One of the hinge platforms is visible in Figure II-9 which is a photograph of the assembled rudder. Additional variable rotational stiffness was provided by means of a torsion spring connecting the rudder root tube to the fuselage frame. The dimensions of the rudder are shown in Figure II-5.

2. Instrumentation

Eight William Miller Type 402C accelerometers located as shown in Figures II-5 and II-8 were used with amplifier double integration circuits to measure displacements. In addition, four strain gage installations, with locations as shown in Figure II-5, were used to measure fuselage side bending, fuselage torsion, stabilizer rocking and rudder rotation.

Recording equipment consisted of the following:

- a. Three units of four channels each, Type CD-2 Amplifiers and Power Supply (William Miller).
- b. One Model W, 16 channel Oscillograph equipped with 180 cps high sensitivity galvanometers (William Miller).

This equipment is shown in Figure II-1.

All accelerometers located in the fin were oriented so as to be sensitive to lateral motion. Three of the stabilizer accelerometers were sensitive to vertical motion and one to fore and aft motion. Table II-1 identifies each pickup by the type, location, and channel number.

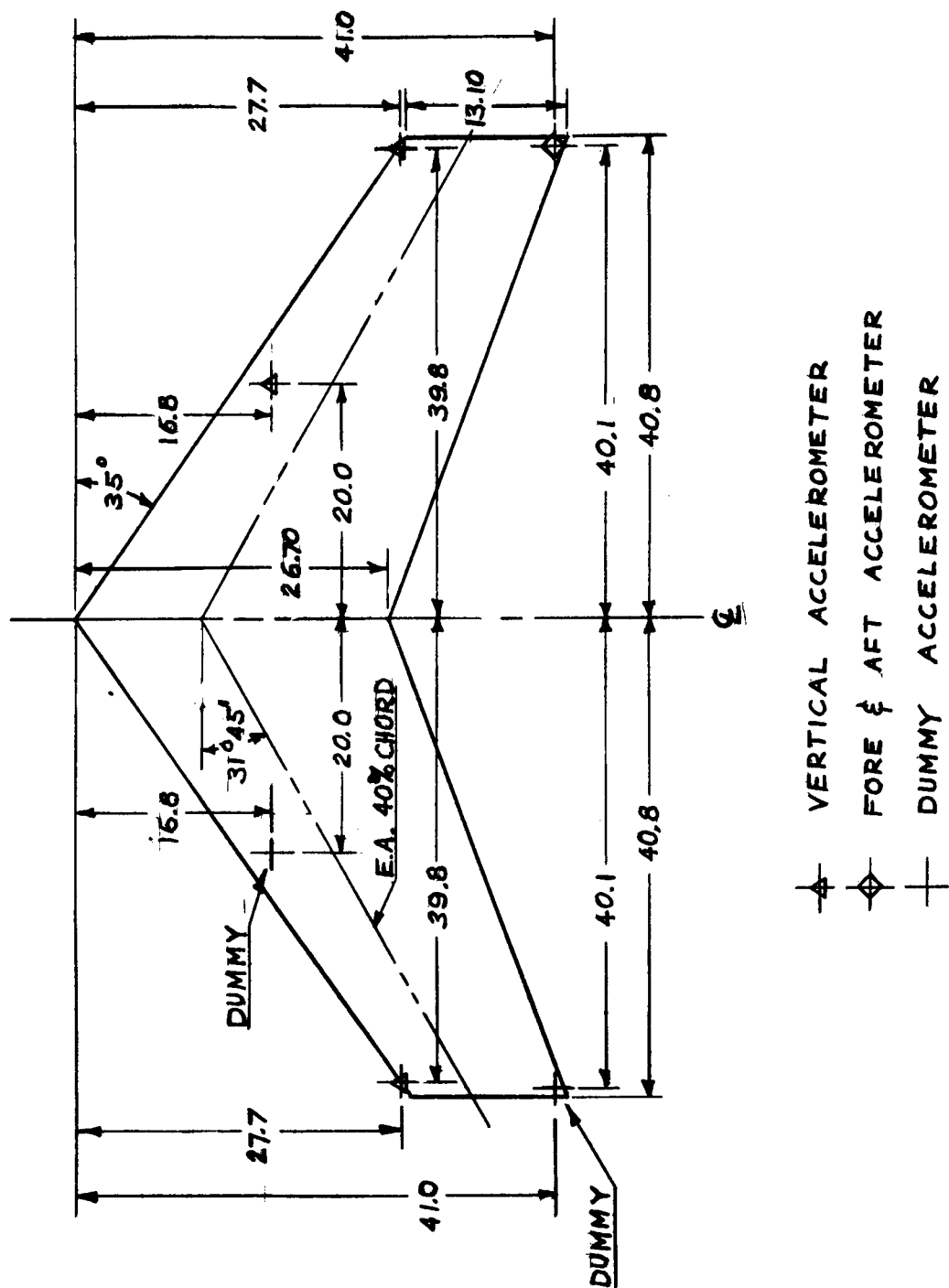


Fig. II-8 Stabilizer Geometry and Pickup Locations

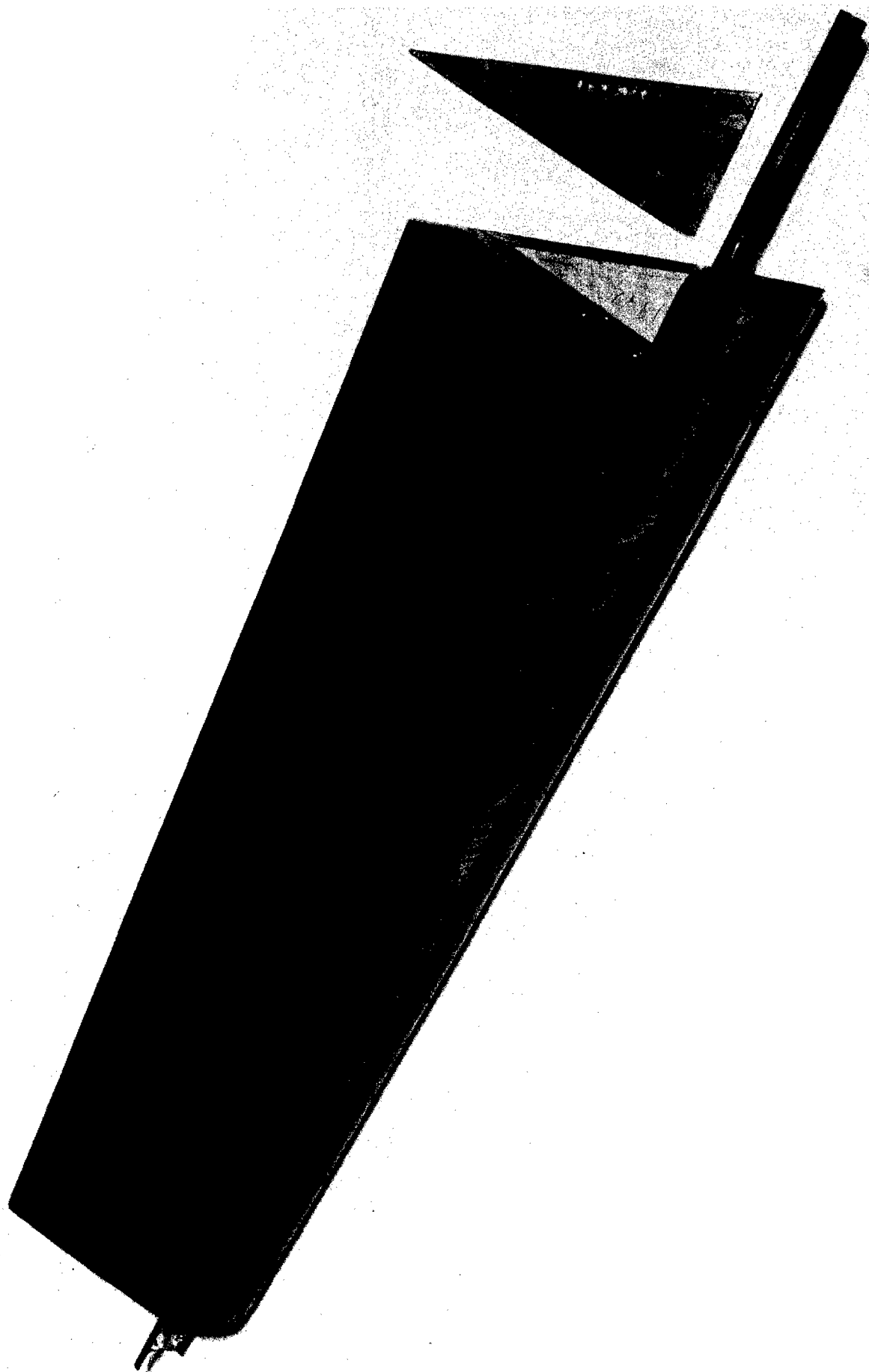


Fig. II-9 Assembled Rudder

Pickup			Con- duc- tor	Ampli- fier Channel	Oscillo- graph Channel
No.	Type	Location and Direction	No.	No.	No.
					1 Ref.
1	Accel.	Right Hand Stab. Tip Trailing Edge Fore and Aft	1	1	2
2	Accel.	Right Hand Stab. Tip Leading Edge Vertical	2	2	3
3	Accel.	Right Hand Stab. Mid-Span Leading Edge-Vertical	3	3	4
4	Accel.	Left Hand Stab. Tip Leading Edge Vertical	4	4	5
					6 Ref.
5	Accel.	Fin Tip Leading Edge Lateral	5	5	7
6	Accel.	Fin Mid-Span Leading Edge Lateral	6	6	8
7	Accel.	Fin Mid-Span Trailing Edge Lateral	7	7	9
8	Accel.	Fin Tip Trailing Edge Lateral	8	8	10
					11 Ref.
9	Strain Gage	Stabilizer Rocking Fitting	9	9	12
10	Strain Gage	Rudder Hinge Line Rudder Rotation	10	10	13
11	Strain Gage	Flexure Beam Fuselage Side Bending	11	11	14
12	Strain Gage	Flexure Beam Fuselage Torsion	12	12	15
					16 Ref.

Table II-1 - Pickup and Channel Identification

Each strain gage installation consisted of four SR-4, Type A-7 strain gages wired to form a Wheatstone bridge. Figure II-10 shows the manner in which the gages were located on the stabilizer flexure springs and is typical also of the rudder spring installation. Two sets of gages were installed on the vertical edges of the fuselage flexure I-beam flanges. One set was wired so as to be sensitive to side bending of the fuselage while the other set was wired to be torsion sensitive. Portions of the fuselage gage installations are visible in the center of Figure II-3.

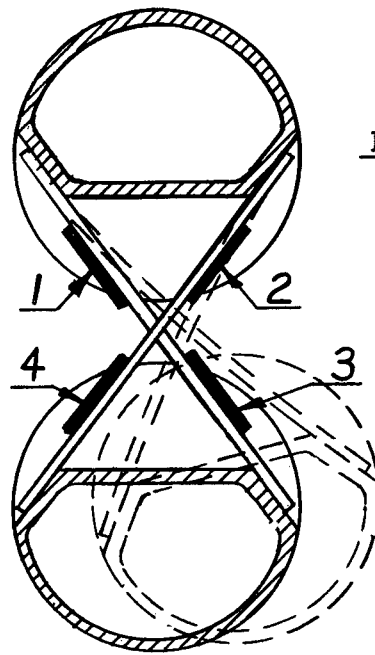
Figures II-11 through II-14 are typical static calibration curves for the strain gage installations. Figure II-15 is a typical accelerometer response curve. The phase response of the accelerometers is shown in Figure II-16 as a plot of strain gage signal phase lag relative to accelerometer signal.

3. Exciting System

Excitation of the model was accomplished by means of a compressed air vibrator installed within the model itself. A supply of compressed air was supplied to a rotary air valve, located in the nose section of the fuselage, just forward of the flexure beam, through a solenoid valve. The solenoid valve was actuated by a toggle switch on the control panel. The rotary air valve was driven by a small variable speed electric motor which was controlled by a Variac on the control panel. A Kollsman Aircraft Tachometer was also located on the control panel and connected electrically to the tachometer generator which was driven through a short flexible shaft by the rotary air valve motor. The rotary air valve produced two alternate pulses of air per cycle to the model. These pulses were delivered to the tips of the stabilizer through two air tubes running from the rotary valve to the stabilizer. At the center of the stabilizer each tube was divided into two tubes by a Y connection and routed to opposite stabilizer tips: one to the stabilizer upper surface and one to the lower surface. By this means it was possible to excite the model by ejecting the pulses of air upward and downward from the four air tubes at the stabilizer tips. By different arrangements of the tubes at the Y connections it was possible to obtain either symmetrical or unsymmetrical excitation.

Figure II-17 is a schematic diagram of the exciting system. The variable speed motor, rotary air valve, and solenoid air valve, can be seen in Figure II-3. The control panel is visible in Figure II-1.

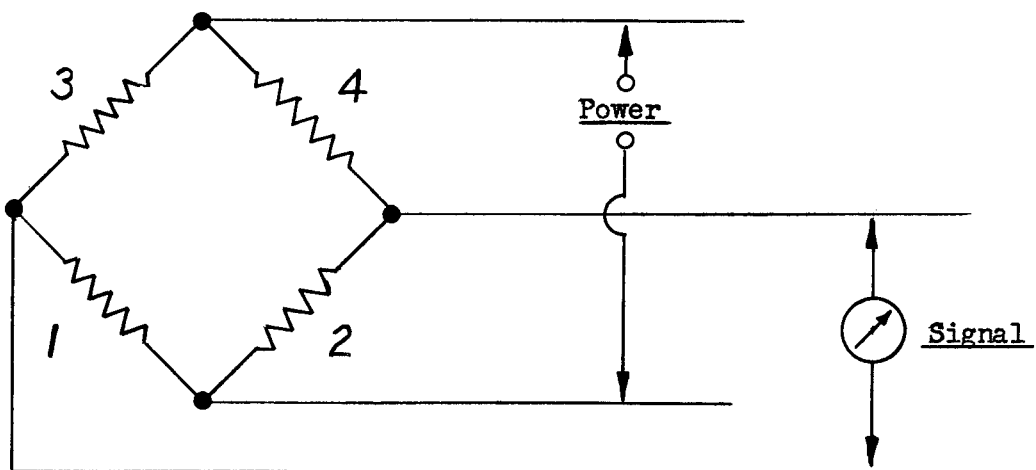
Means were also provided for exciting the model by hand. This consisted merely of a wire attached near the leading edge or trailing edge of the fin tip and extending through the tunnel wall.



Fin Fitting - Fixed

Stabilizer Fitting
Moveable

View Looking Forward



Four Arm Bridge

Fig. II-10 Stabilizer Rocking Fitting Strain Gage
Installation

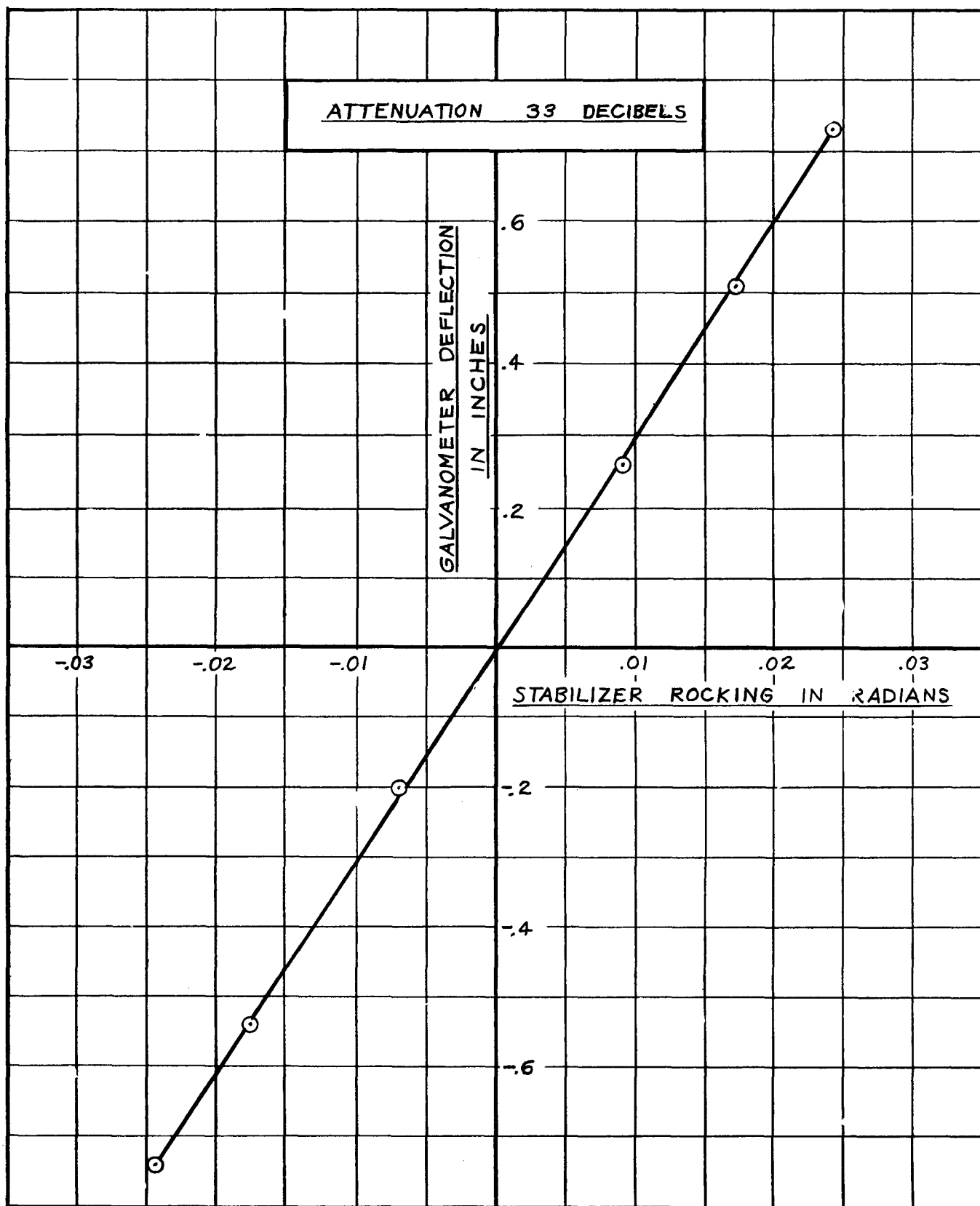


Fig. II-11 Stabilizer Rocking Strain Gage Installation Characteristics

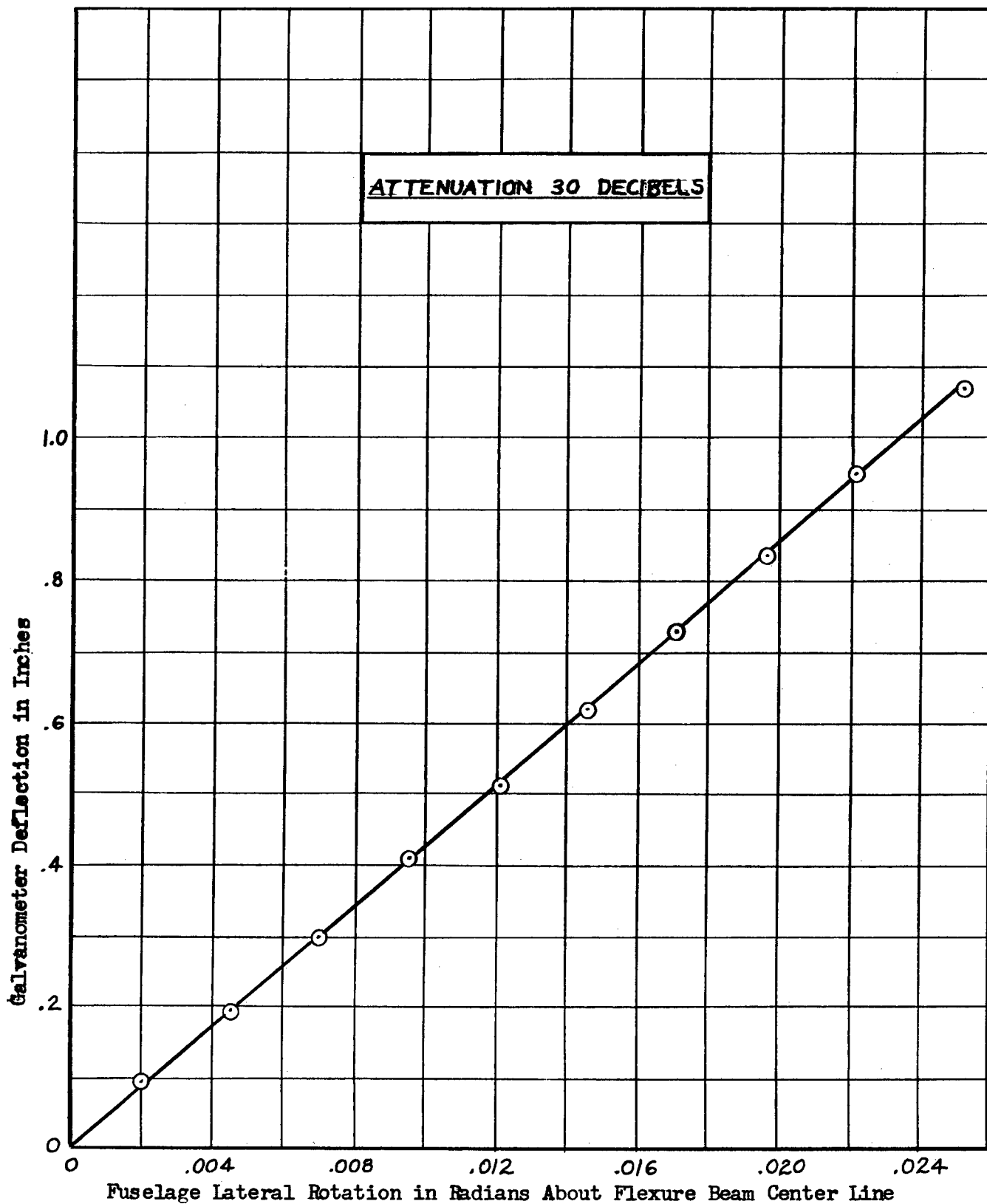


Fig. II-12 Fuselage Side Bending Strain Gage Installation Characteristics

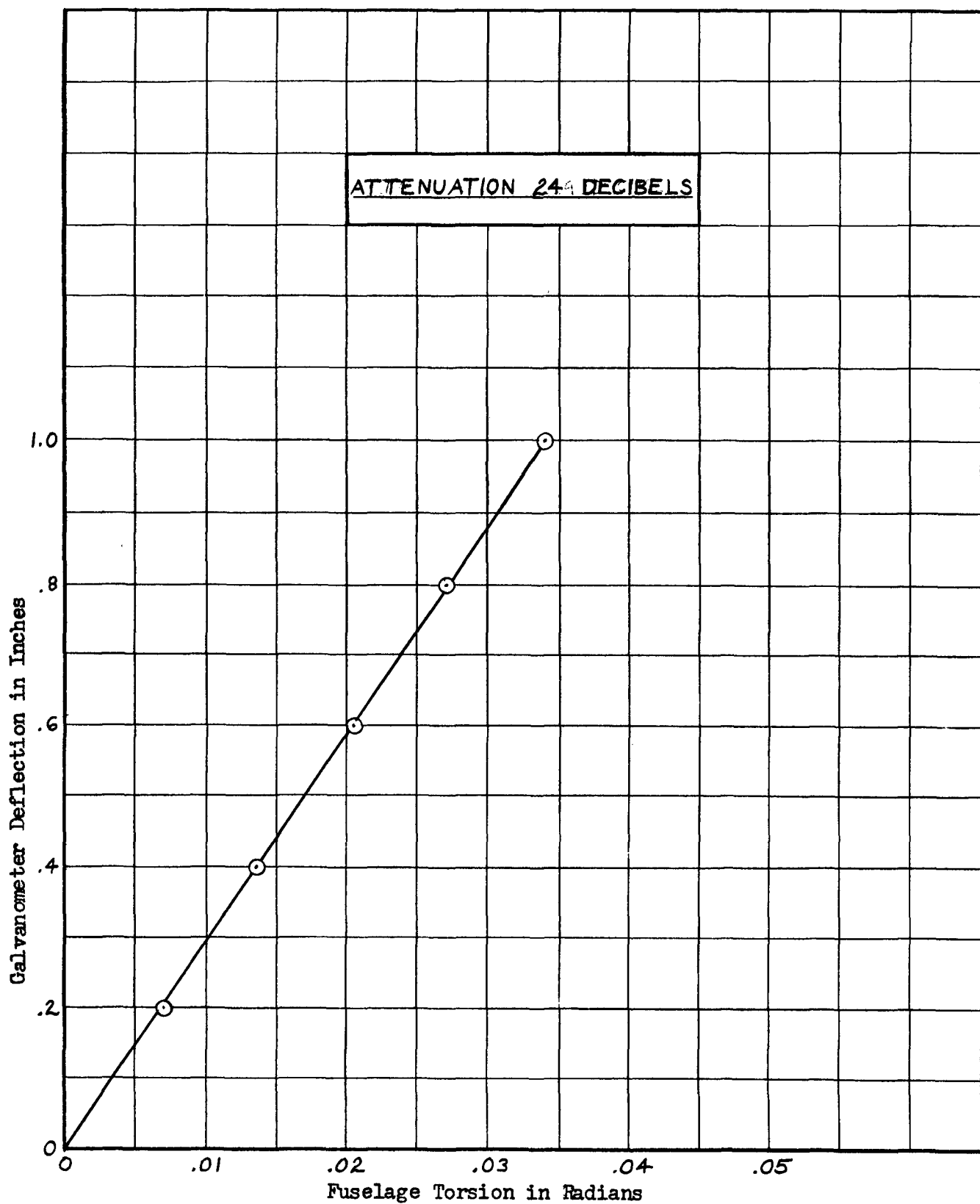


Fig. II-13 Fuselage Torsion Strain Gage Installation Characteristics

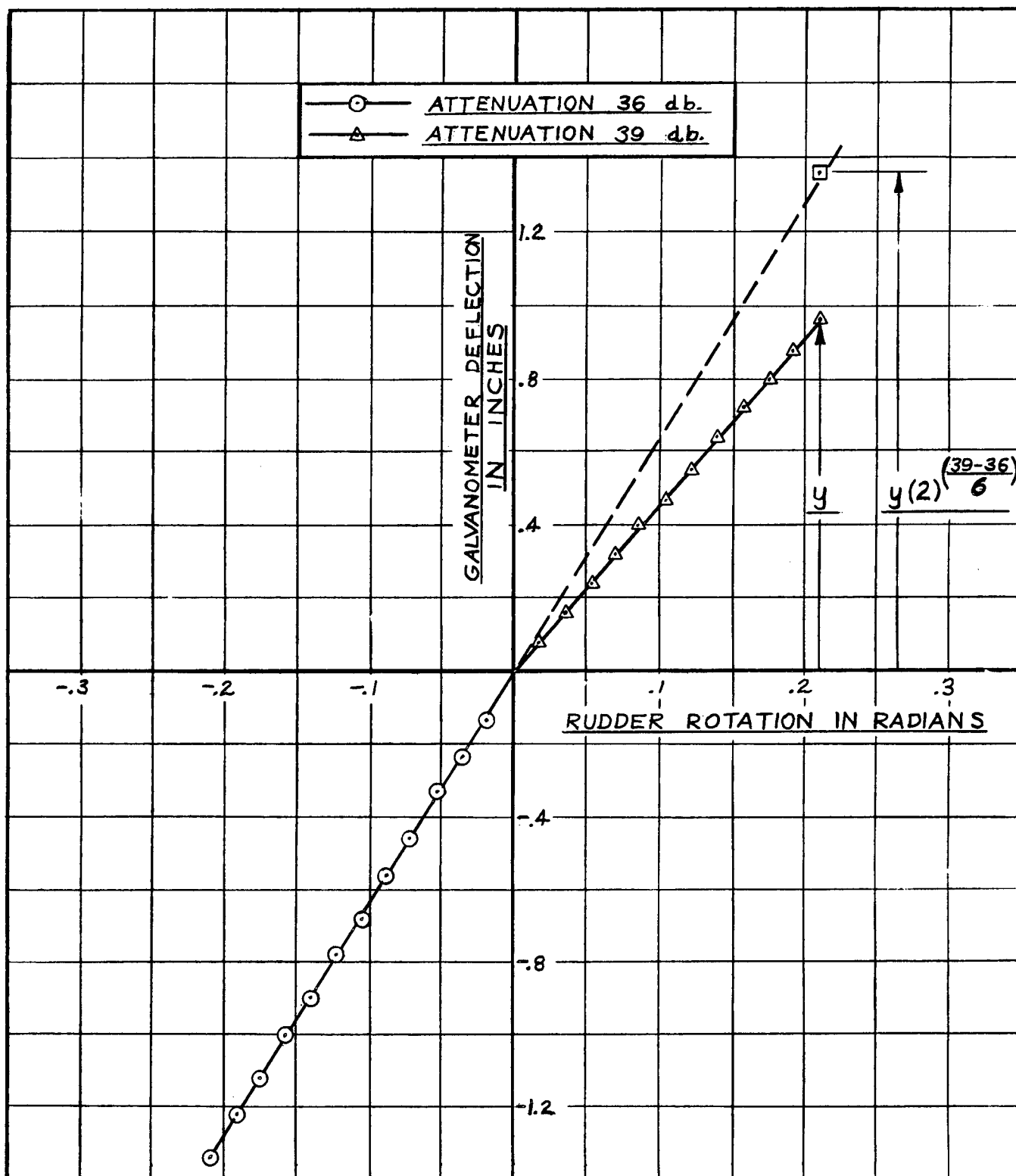


Fig. II-14 Rudder Rotation Strain Gage Installation Characteristics

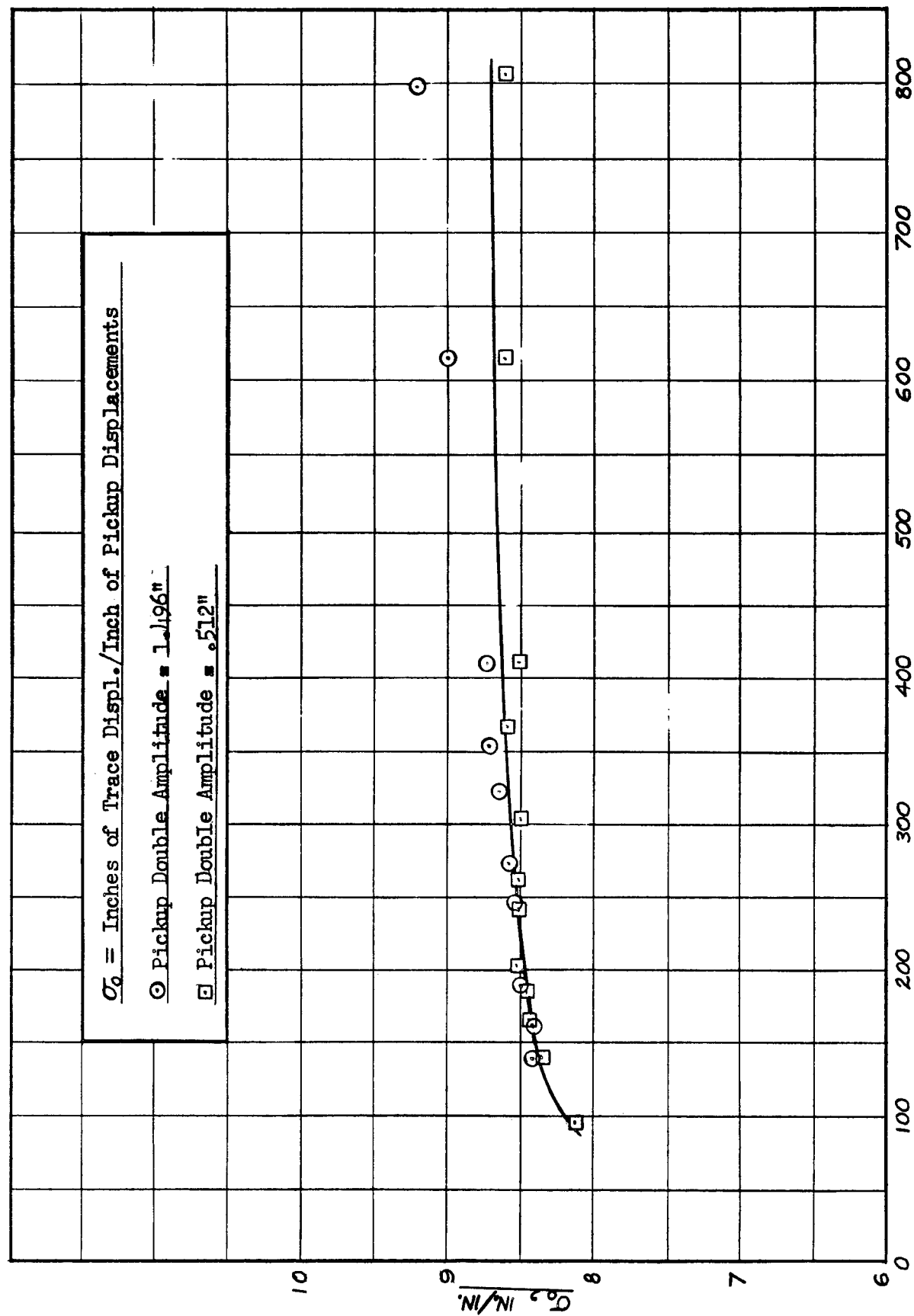


Fig. II-15 Typical Accelerometer Response Curve

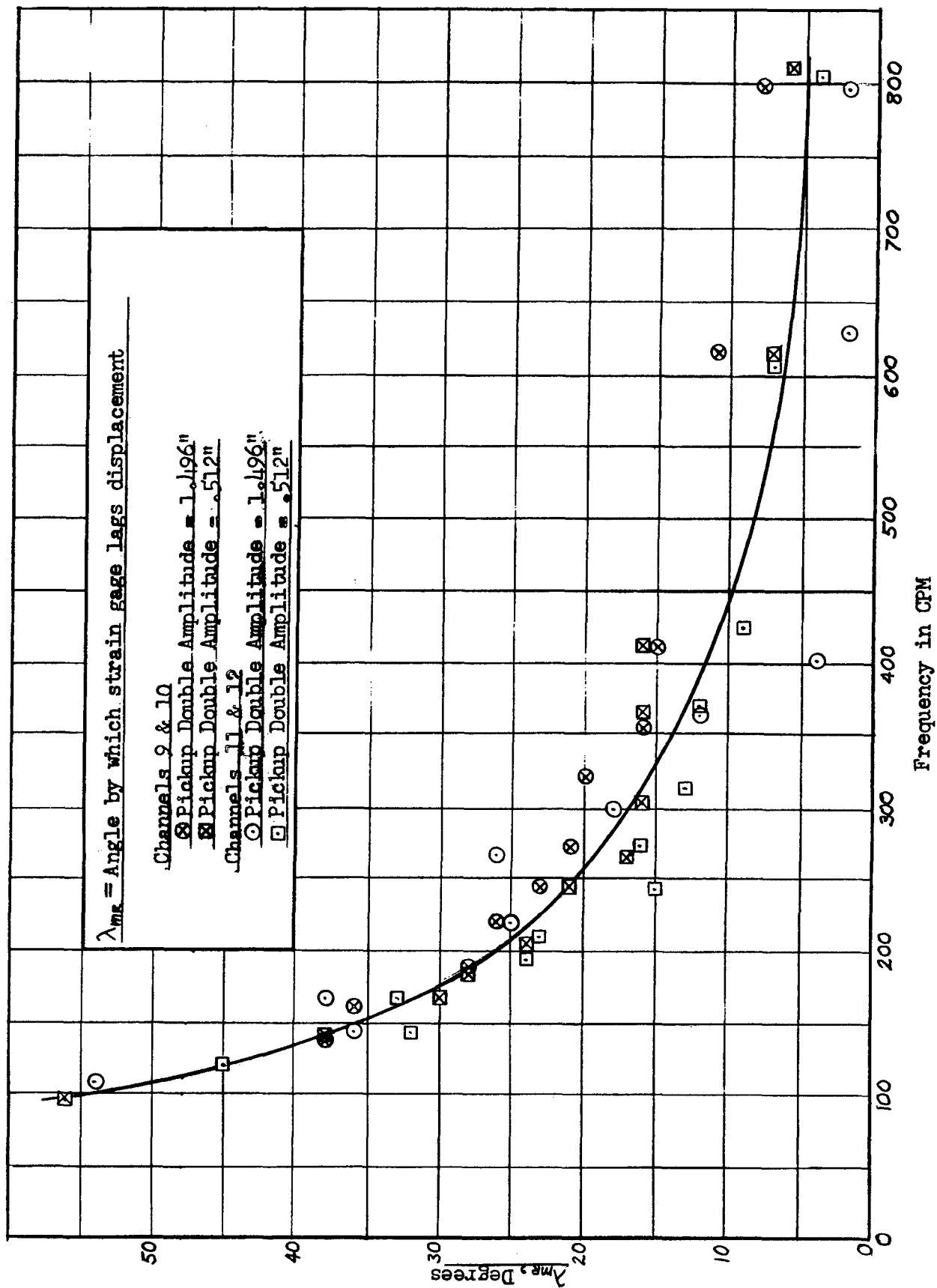


Fig. II-16 Phase Angle Calibration Curve

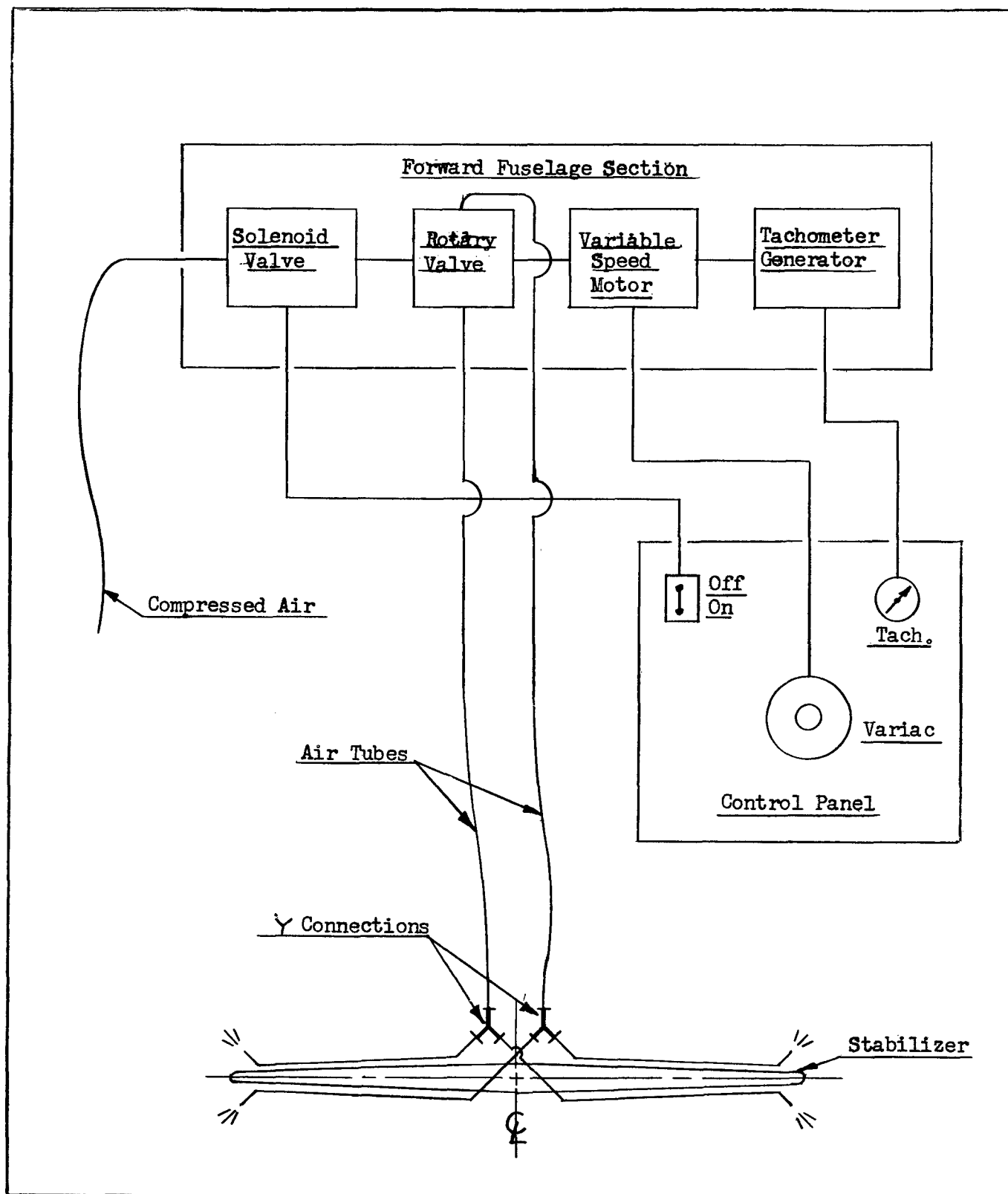


Fig. II-17 Schematic Diagram of Air Exciting System

4. Safety System

The safety system used for curbing the motion of the model when divergent flutter was incurred consisted of a spring-loaded, electrically operated piano wire rigging which, when released, introduced damping into the vibrating system by bringing a rough rubbing surface in contact with the stabilizer tips. The stops were held in the off position by electromagnets in the two cocking mechanisms located on either side of the tunnel. The system was triggered by a switch on the control panel but had to be cocked by hand from outside the walls of the tunnel.

A portion of the system is shown in Figure II-18 for the fin tip stabilizer location and in Figure II-19 for a 58% fin span stabilizer location. The cocking mechanisms are visible in the lower part of Figure II-18. Figure II-20 is a photograph of a cocking mechanism showing the spring, transformer for the electromagnet, cocking cable and the rigging wire. Tension on the cocking cable, which is shown going through the tunnel wall, rotated the pulley which simultaneously loaded the spring, withdrew the rubbing surfaces, and engaged a holding bar with the electromagnet. The system was released or actuated by breaking the circuit which included the electromagnet.

A somewhat similar method was employed for configurations involving the stabilizer equivalent weights. The rubbing surface was applied in a horizontal plane to the top surface of the weights. This configuration can be seen in Figure II-21.

5. Model Support Structure

The model was supported from the tunnel wall by a framework made up of eight struts. The struts were 5.25 in. X 2.50 in., 12-gage streamline tubing which was formed on a press brake from SAE 1020 steel sheet. The assembled structure can be seen in Figures II-18 and II-21.

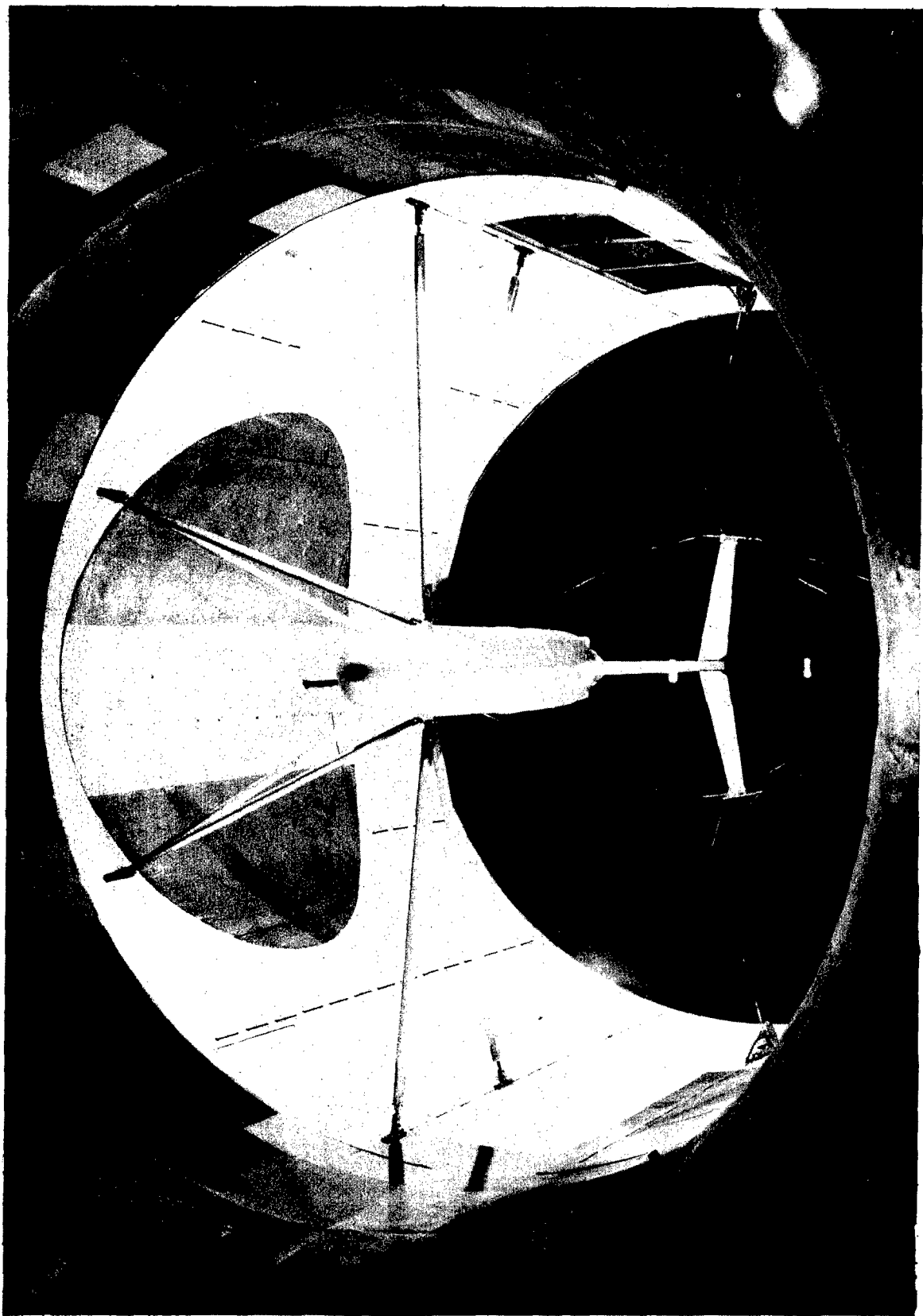


Fig. II-18 Model and Safety System, Stabilizer at Fin Tip

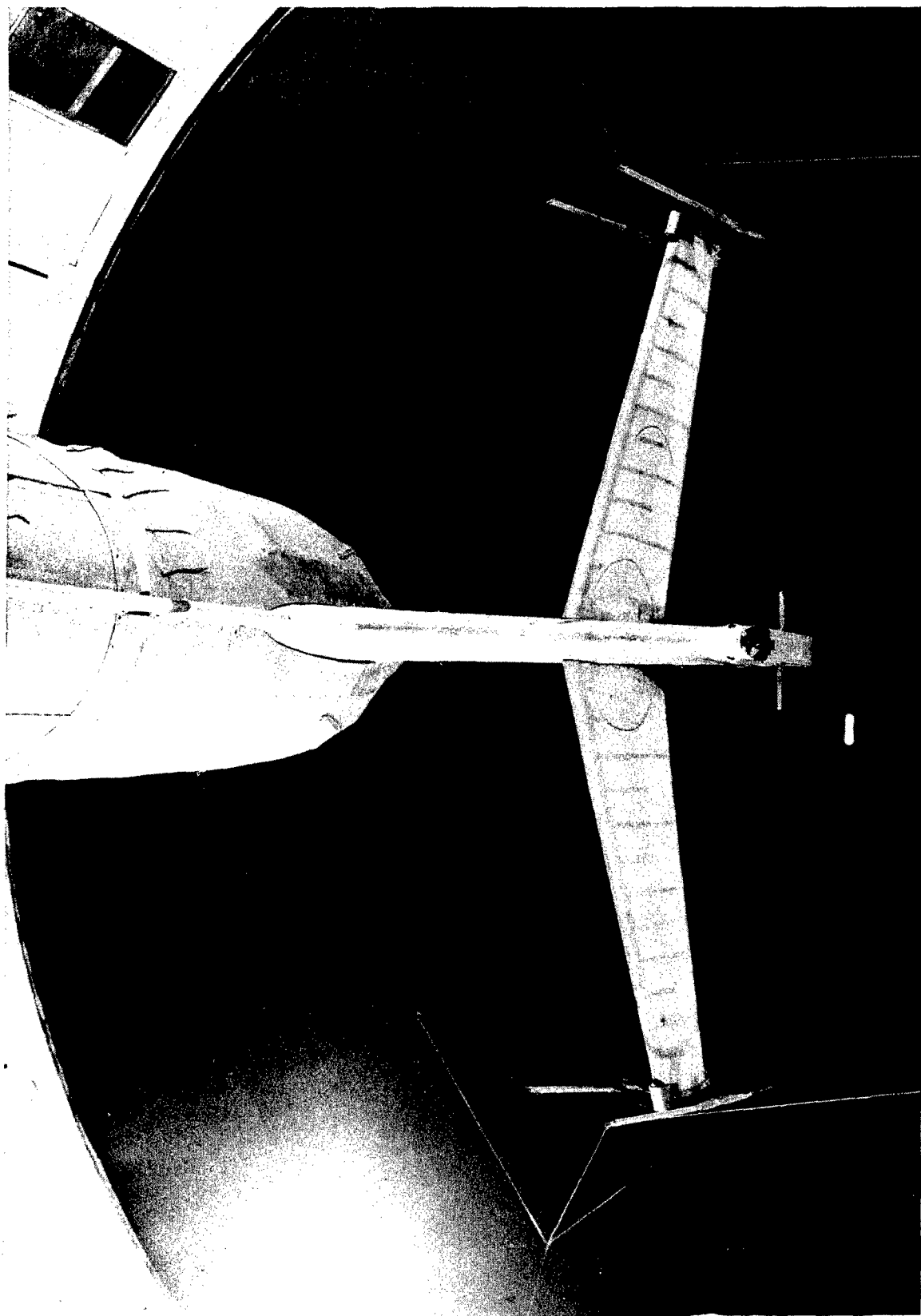


Fig. II-19 Model and Safety System, Stabilizer at 58% Fin Span

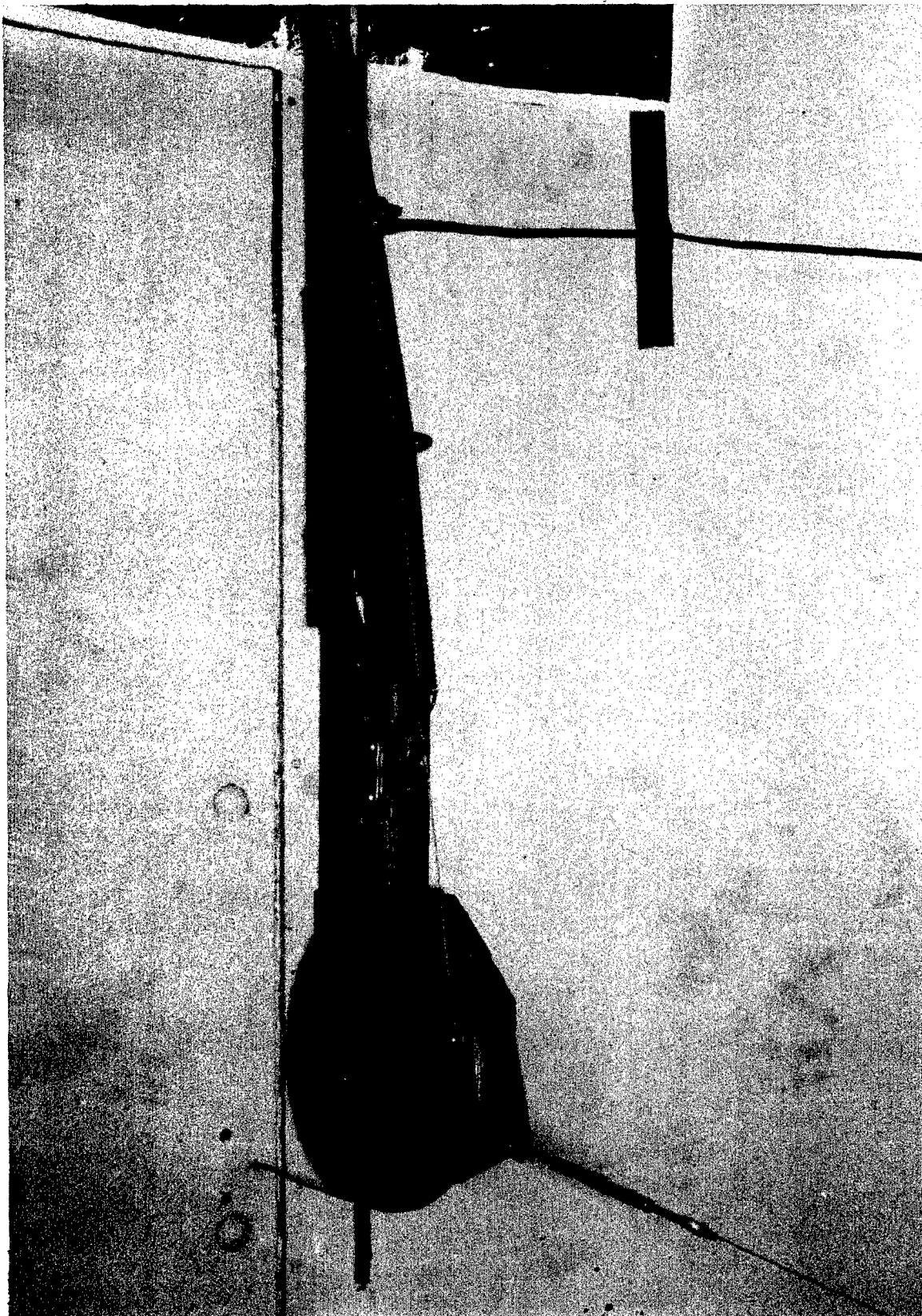


Fig. II-20 Safety System Cocking Mechanism

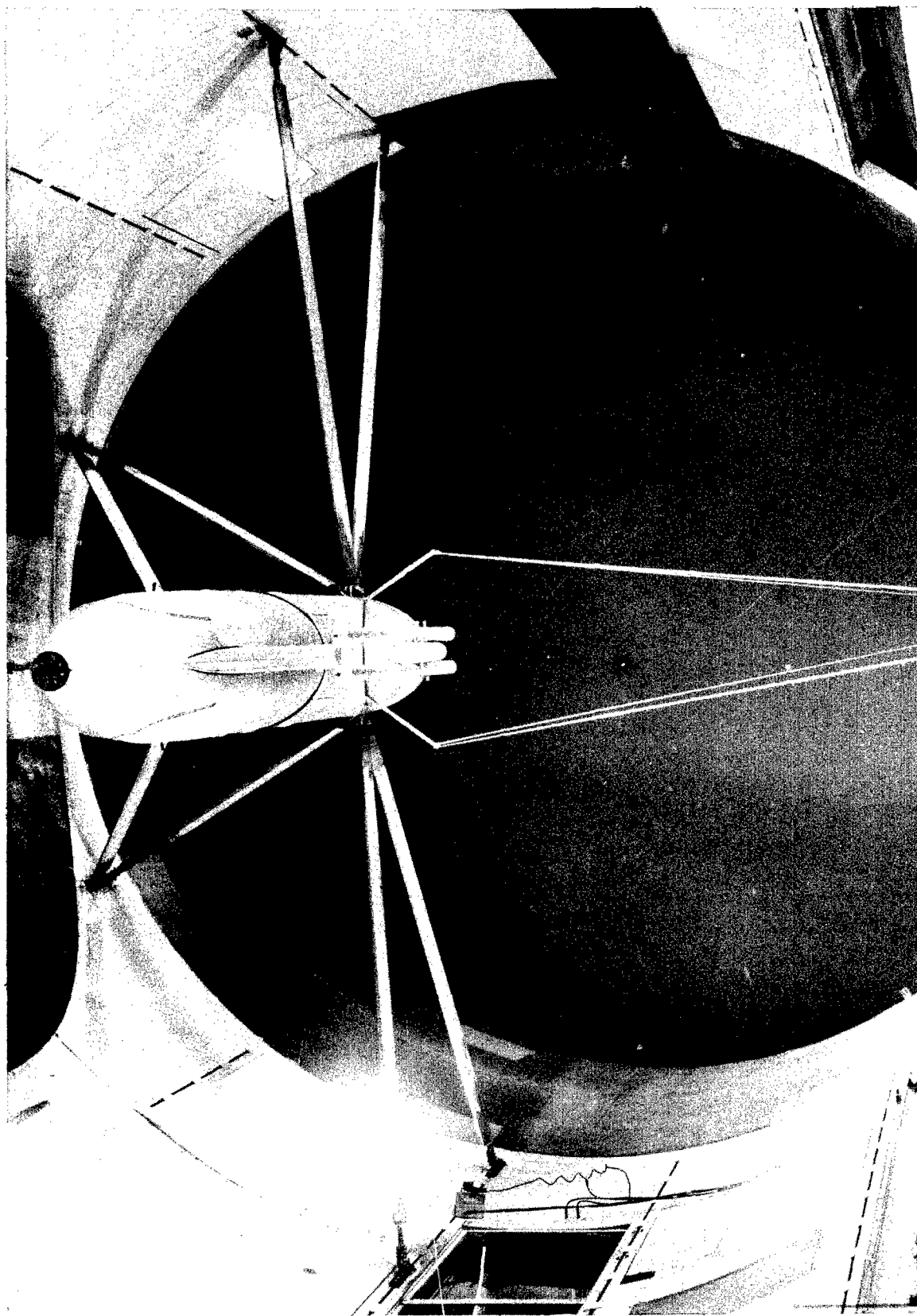


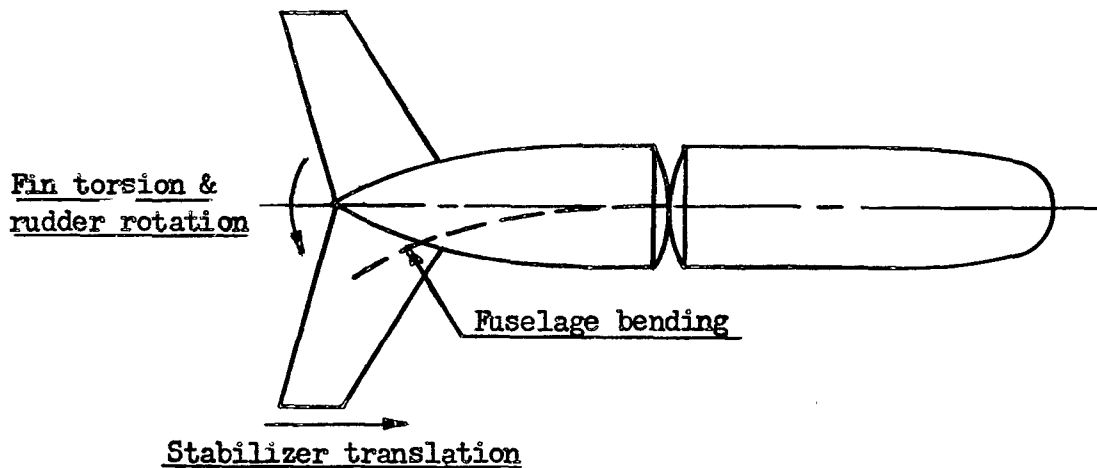
Fig. II-21 Model and Safety System for Stabilizer
Equivalent Weights Configurations

APPENDIX III

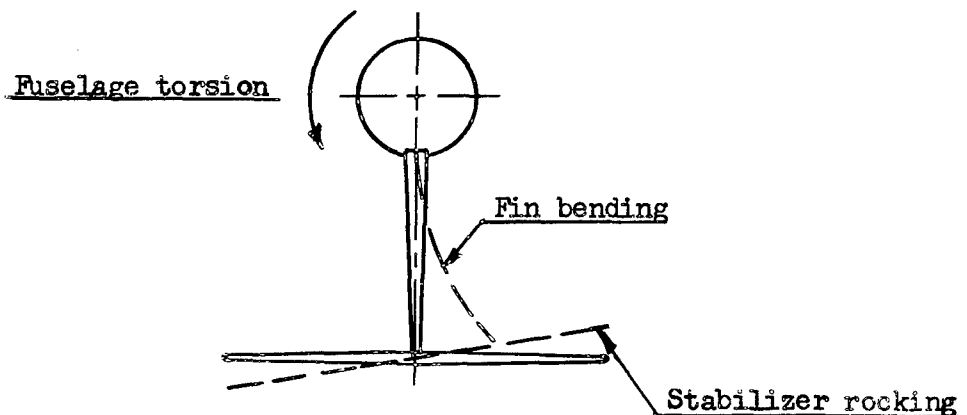
DERIVATION OF DETERMINANT ELEMENTS

1. GENERAL

The following positive directions have been assumed:



Looking Down



Looking Upstream

The various degrees of freedom are described by the following generalized coordinates:

- q_1 -- fin bending along the elastic axis
- q_2 -- fin torsion about the elastic axis
- q_3 -- stabilizer rocking
- q_4 -- fuselage side bending
- q_5 -- fuselage torsion

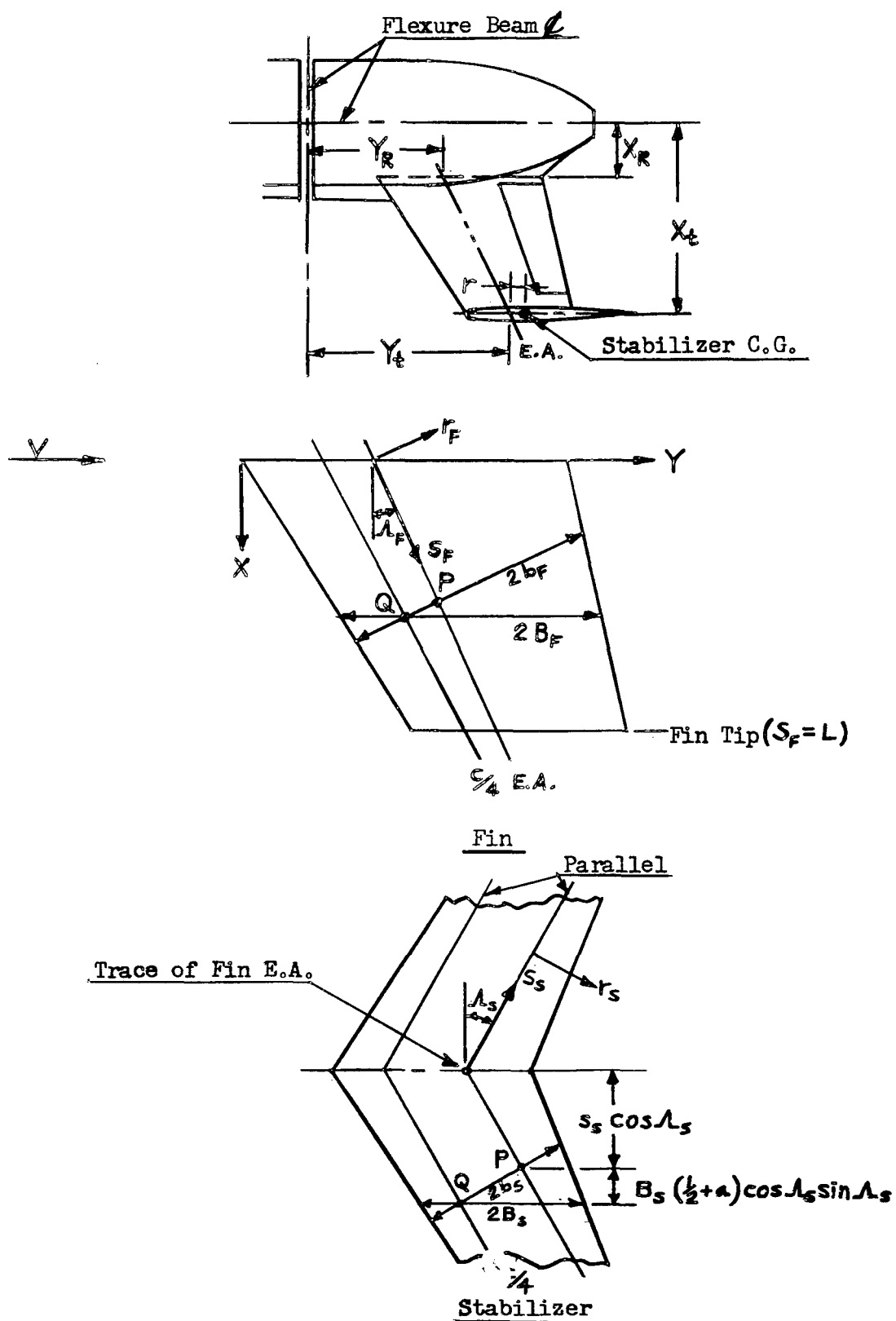


Fig. III-1 Fin and Stabilizer Nomenclature

2. AERODYNAMIC PARTS:

(a) Fin Bending and Torsion

Considering first the aerodynamic terms for fin bending and fin torsion and referring to Figure III-1

$$\begin{aligned}\left(\frac{dL_{c/4}}{d\alpha}\right)_F &= (B_F^2 h_{c/4_F} L_h + B_F^3 \alpha_F L_\alpha) \pi \rho \omega^2 \\ \left(\frac{dM_{c/4}}{d\alpha}\right)_F &= (B_F^3 h_{c/4_F} M_h + B_F^4 \alpha_F M_\alpha) \pi \rho \omega^2 \\ \left(\frac{dL_{c/4}}{d\alpha}\right)_S &= (B_S^2 h_{c/4_S} L_h + B_S^3 \alpha_S L_\alpha) \pi \rho \omega^2 \\ \left(\frac{dM_{c/4}}{d\alpha}\right)_S &= (B_S^3 h_{c/4_S} M_h + B_S^4 \alpha_S M_\alpha) \pi \rho \omega^2\end{aligned}\quad (1 \text{ a-d})$$

The bending deflection at $P_F = q_1 h$ and the torsional deflection at $P_F = q_2 \gamma$. The components of stabilizer motion due to fin motion will be:

$$\begin{aligned}\text{Stabilizer yaw} &= \gamma_L \cos \Lambda_F + \left(\frac{\partial h}{\partial S_F}\right)_L \sin \Lambda_F \\ \text{Stabilizer roll} &= -\gamma_L \sin \Lambda_F + \left(\frac{\partial h}{\partial S_F}\right)_L \cos \Lambda_F\end{aligned}\quad (2 \text{ a-b})$$

If

$$\psi = -\gamma_L q_2 \sin \Lambda_F + \left(\frac{\partial h}{\partial S_F}\right)_L \cos \Lambda_F q_1 \quad (3)$$

the vertical deflection of the stabilizer due to roll at P_S is

$$\psi S_S \cos \Lambda_S$$

and the torsional deflection of the stabilizer due to roll at P_S is

$$-\psi \sin \Lambda_S$$

or,

$$\begin{aligned}\text{vertical deflection at } P_S &= q_1 \left(\frac{\partial h}{\partial S_F}\right)_L S_S \cos \Lambda_S \cos \Lambda_F \\ &\quad - q_2 \gamma_L S_S \cos \Lambda_S \sin \Lambda_F\end{aligned}\quad (4 \text{ a})$$

and

$$\text{torsional deflection at } P_s = q_2 \gamma_L \sin \Lambda_F \sin \Lambda_s - q_1 \left(\frac{\partial h}{\partial s_F} \right)_L \cos \Lambda_F \sin \Lambda_s \quad (4 \text{ b})$$

$$\text{Since } B \cos \Lambda \cong b$$

$$(h_{c/4})_F = q_1 h - B_F (\frac{1}{2} + a) q_2 \gamma \cos \Lambda_F$$

$$(\alpha_{c/4})_F = q_1 \left(\frac{\partial h}{\partial s_F} \right) \sin \Lambda_F + q_2 \gamma \cos \Lambda_F$$

$$(h_{c/4})_s = q_1 \left(\frac{\partial h}{\partial s_F} \right)_L s_s \cos \Lambda_s \cos \Lambda_F - q_2 \gamma_L s_s \cos \Lambda_s \sin \Lambda_F \quad (5 \text{ a-d})$$

$$- B_s (\frac{1}{2} + a) \cos \Lambda_s \left[q_2 \gamma_L \sin \Lambda_F \sin \Lambda_s - q_1 \left(\frac{\partial h}{\partial s_F} \right)_L \cos \Lambda_F \sin \Lambda_s \right]$$

$$(\alpha_{c/4})_s = \left[q_1 \left(\frac{\partial h}{\partial s_F} \right)_L \cos \Lambda_s \cos \Lambda_F - q_2 \gamma_L \sin \Lambda_F \cos \Lambda_s \right] \sin \Lambda_s$$

$$+ \left[q_2 \gamma_L \sin \Lambda_F \sin \Lambda_s - q_1 \left(\frac{\partial h}{\partial s_F} \right)_L \cos \Lambda_F \sin \Lambda_s \right] \cos \Lambda_s$$

$$= 0$$

Thus $(\alpha_{c/4})_s$ is zero as would be expected since ψ has no component perpendicular to the stabilizer center line. It should be noted that "a" for the stabilizer is measured from the pseudoelastic axis on the stabilizer which is parallel to the stabilizer quarter chord line and passes through the fin elastic axis trace.

By rewriting

$$\begin{aligned} (h_{c/4})_s = & q_1 \left\{ \left(\frac{\partial h}{\partial s_F} \right)_L \cos \Lambda_F \left[s_s \cos \Lambda_s + B_s (\frac{1}{2} + a) \cos \Lambda_s \sin \Lambda_s \right] \right\} \\ & - q_2 \left\{ \gamma_L \sin \Lambda_F \left[s_s \cos \Lambda_s + B_s (\frac{1}{2} + a) \cos \Lambda_s \sin \Lambda_s \right] \right\} \end{aligned} \quad (6)$$

and letting

$$(B \gamma)_s = s_s \cos \Lambda_s + B_s (\frac{1}{2} + a) \cos \Lambda_s \sin \Lambda_s \quad (7)$$

which is the perpendicular distance from the stabilizer center line to the point Q,

$$\begin{aligned}
\left(\frac{dL_{c4}}{d\chi}\right)_F &= \pi \rho \omega^2 \left\{ q_1 \left[B_F^2 h L_h + B_F^3 \left(\frac{\partial h}{\partial S_F}\right) \sin \Lambda_F L_\alpha \right] \right. \\
&\quad \left. + q_2 \left[-B_F^3 \left(\frac{1}{2} + a\right) \gamma \cos \Lambda_F L_h + B_F^3 \gamma \cos \Lambda_F L_\alpha \right] \right\} \\
\left(\frac{dM_{c4}}{d\chi}\right)_F &= \pi \rho \omega^2 \left\{ q_1 \left[B_F^3 h M_h + B_F^4 \left(\frac{\partial h}{\partial S_F}\right) \sin \Lambda_F M_\alpha \right] \right. \\
&\quad \left. + q_2 \left[-B_F^4 \left(\frac{1}{2} + a\right) \gamma \cos \Lambda_F M_h + B_F^4 \gamma \cos \Lambda_F M_\alpha \right] \right\} \quad (8 \text{ a-d}) \\
\left(\frac{dL_{c4}}{d\chi}\right)_s &= \pi \rho \omega^2 \left\{ B_s^2 \left[q_1 \left(\frac{\partial h}{\partial S_F}\right)_L \cos \Lambda_F (B\chi_\psi)_s - q_2 \gamma_L \sin \Lambda_F (B\chi_\psi)_s \right] L_h \right. \\
&\quad \left. + B_s^3 (0) L_\alpha \right\} \\
&= \pi \rho \omega^2 \left\{ q_1 \left[B_s^2 (B\chi_\psi)_s \left(\frac{\partial h}{\partial S_F}\right)_L \cos \Lambda_F L_h \right] \right. \\
&\quad \left. - q_2 \left[B_s^2 (B\chi_\psi)_s \gamma_L \sin \Lambda_F L_h \right] \right\} \\
\left(\frac{dM_{c4}}{d\chi}\right)_s &= \pi \rho \omega^2 \left\{ B_s^3 \left[q_1 \left(\frac{\partial h}{\partial S_F}\right)_L \cos \Lambda_F (B\chi_\psi)_s - q_2 \gamma_L \sin \Lambda_F (B\chi_\psi)_s \right] M_h \right\} \\
&= \pi \rho \omega^2 \left\{ q_1 \left[B_s^3 \left(\frac{\partial h}{\partial S_F}\right)_L \cos \Lambda_F (B\chi_\psi)_s M_h \right] - q_2 \left[B_s^3 \gamma_L \sin \Lambda_F (B\chi_\psi)_s M_h \right] \right\}
\end{aligned}$$

The virtual work can be expressed as:

$$\begin{aligned}
\delta W_h &= \delta q_1 \left\{ \int_0^{L_F \cos \Lambda_F} h \left(\frac{dL_{c4}}{d\chi}\right)_F d\chi + \sin \Lambda_F \int_0^{L_F \cos \Lambda_F} \left(\frac{\partial h}{\partial S_F}\right) \left(\frac{dM_{c4}}{d\chi}\right)_F d\chi \right. \\
&\quad \left. + \cos \Lambda_F \int_{-L_S \cos \Lambda_S}^{L_S \cos \Lambda_S} (B\chi_\psi)_s \left(\frac{\partial h}{\partial S_F}\right)_L \left(\frac{dL_{c4}}{d\chi}\right)_s d\chi \right\} \quad (9 \text{ a-b})
\end{aligned}$$

and

$$\begin{aligned}
\delta W_\gamma &= \delta q_2 \left\{ \int_0^{L_F \cos \Lambda_F} -B_F \left(\frac{1}{2} + a\right) \gamma \cos \Lambda_F \left(\frac{dL_{c4}}{d\chi}\right)_F d\chi + \cos \Lambda_F \int_0^{L_F \cos \Lambda_F} \gamma \left(\frac{dM_{c4}}{d\chi}\right)_F d\chi \right. \\
&\quad \left. - \sin \Lambda_F \int_{-L_S \cos \Lambda_S}^{L_S \cos \Lambda_S} (B\chi_\psi)_s \gamma_L \left(\frac{dL_{c4}}{d\chi}\right)_s d\chi \right\}
\end{aligned}$$

Substituting the lift and moment expressions into the virtual work equations and rearranging,

$$\begin{aligned}
Q_h = \frac{\delta W_h}{\delta q_1} = \pi \rho \omega^2 q_1 \left\{ \int_0^{L_F \cos \Lambda_F} \left[B_F^2 h^2 L_h + B_F^3 \left(\frac{\partial h}{\partial S_F} \right) h \sin \Lambda_F (L_\alpha + M_h) \right. \right. \\
\left. \left. + B_F^4 \left(\frac{\partial h}{\partial S_F} \right)^2 \sin^2 \Lambda_F M_\alpha \right] dx \right. \\
\left. + \int_{-L_S \cos \Lambda_S}^{L_S \cos \Lambda_S} B_S^2 (B \chi \psi)_S^2 \left(\frac{\partial h}{\partial S_F} \right)_L^2 \cos^2 \Lambda_F L_h dx \right\} \\
+ \pi \rho \omega^2 q_2 \left\{ \int_0^{L_F \cos \Lambda_F} \left[B_F^3 h \gamma \cos \Lambda_F \{ L_\alpha - (\frac{1}{2} + a) L_h \} \right. \right. \\
\left. \left. + B_F^4 \left(\frac{\partial h}{\partial S_F} \right) \gamma \cos \Lambda_F \sin \Lambda_F \{ M_\alpha - (\frac{1}{2} + a) M_h \} \right] dx \right. \\
\left. - \int_{-L_S \cos \Lambda_S}^{L_S \cos \Lambda_S} B_S^2 (B \chi \psi)_S^2 \left(\frac{\partial h}{\partial S_F} \right)_L \cos \Lambda_F \gamma_L \sin \Lambda_F L_h dx \right\}
\end{aligned}$$

(10 a-b)

$$\begin{aligned}
Q_\gamma = \frac{\delta W_\gamma}{\delta q_2} = \pi \rho \omega^2 q_1 \left\{ \int_0^{L_F \cos \Lambda_F} \left[B_F^3 h \gamma \cos \Lambda_F \{ M_h - (\frac{1}{2} + a) L_h \} \right. \right. \\
\left. \left. + B_F^4 \left(\frac{\partial h}{\partial S_F} \right) \gamma \cos \Lambda_F \sin \Lambda_F \{ M_\alpha - (\frac{1}{2} + a) L_\alpha \} \right] dx \right. \\
\left. - \int_{-L_S \cos \Lambda_S}^{L_S \cos \Lambda_S} B_S^2 (B \chi \psi)_S^2 \left(\frac{\partial h}{\partial S_F} \right)_L \cos \Lambda_F \gamma_L \sin \Lambda_F L_h dx \right\} \\
+ \pi \rho \omega^2 q_2 \left\{ \int_0^{L_F \cos \Lambda_F} B_F^4 \cos^2 \Lambda_F \gamma^2 \left[M_\alpha - (\frac{1}{2} + a) (L_\alpha + M_h) + (\frac{1}{2} + a)^2 L_h \right] dx \right. \\
\left. + \int_{-L_S \cos \Lambda_S}^{L_S \cos \Lambda_S} B_S^2 (B \chi \psi)_S^2 \gamma_L^2 \sin^2 \Lambda_F L_h dx \right\}
\end{aligned}$$

Stabilizer Rocking

If the stabilizer rocking degree of freedom is added:

$$\begin{aligned} \text{Vertical deflection at } P_s = & q_1 \left(\frac{\partial h}{\partial s_F} \right)_L s_s \cos \Lambda_s \cos \Lambda_F - q_2 x_L s_s \cos \Lambda_s \sin \Lambda_F \\ & + q_3 \psi s_s \cos \Lambda_s \end{aligned} \quad (11 \text{ a-b})$$

$$\begin{aligned} \text{Torsional deflection at } P_s = & q_2 x_L \sin \Lambda_F \sin \Lambda_s - q_1 \left(\frac{\partial h}{\partial s_F} \right)_L \cos \Lambda_F \sin \Lambda_s \\ & - q_3 \psi \sin \Lambda_s \end{aligned}$$

$$\begin{aligned} (h_{c/s})_s = & q_1 \left(\frac{\partial h}{\partial s_F} \right)_L s_s \cos \Lambda_s \cos \Lambda_F - q_2 x_L s_s \cos \Lambda_s \sin \Lambda_F + q_3 \psi s_s \cos \Lambda_s \\ & - B_s \left(\frac{1}{2} + a \right) \cos \Lambda_s \left[q_2 x_L \sin \Lambda_F \sin \Lambda_s - q_1 \left(\frac{\partial h}{\partial s_F} \right)_L \cos \Lambda_F \sin \Lambda_s - q_3 \psi \sin \Lambda_s \right] \\ = & q_1 \left(\frac{\partial h}{\partial s_F} \right)_L \cos \Lambda_F \left[s_s \cos \Lambda_s + B_s \left(\frac{1}{2} + a \right) \cos \Lambda_s \sin \Lambda_s \right] \\ & - q_2 x_L \sin \Lambda_F \left[s_s \cos \Lambda_s + B_s \left(\frac{1}{2} + a \right) \cos \Lambda_s \sin \Lambda_s \right] \\ & + q_3 \psi \left[s_s \cos \Lambda_s + B_s \left(\frac{1}{2} + a \right) \cos \Lambda_s \sin \Lambda_s \right] \\ = & \left[q_1 \left(\frac{\partial h}{\partial s_F} \right)_L \cos \Lambda_F - q_2 x_L \sin \Lambda_F + q_3 \psi \right] (B \chi \psi)_s \end{aligned} \quad (12 \text{ a-b})$$

$$(\alpha_{c/s})_s = 0$$

$$\begin{aligned} \left(\frac{dL_{c/s}}{d\chi} \right)_s = & \pi \rho \omega^2 \left\{ q_1 \left[B_s^2 (B \chi \psi)_s \left(\frac{\partial h}{\partial s_F} \right)_L \cos \Lambda_F L_h \right] - q_2 \left[B_s^2 (B \chi \psi)_s x_L \sin \Lambda_F L_h \right] \right. \\ & \left. + q_3 \left[B_s^2 (B \chi \psi)_s \psi L_h \right] \right\} \end{aligned} \quad (13 \text{ a-b})$$

$$\begin{aligned} \left(\frac{dM_{c/s}}{d\chi} \right)_s = & \pi \rho \omega^2 \left\{ q_1 \left[B_s^3 (B \chi \psi)_s \left(\frac{\partial h}{\partial s_F} \right)_L \cos \Lambda_F M_h \right] - q_2 \left[B_s^3 (B \chi \psi)_s x_L \sin \Lambda_F M_h \right] \right. \\ & \left. + q_3 \left[B_s^3 (B \chi \psi)_s \psi M_h \right] \right\} \end{aligned}$$

The virtual work expression in the q_3 degree of freedom becomes

$$\delta W_\gamma = \delta q_3 \int_{-L_s \cos \Lambda_s}^{L_s \cos \Lambda_s} (B\chi_\gamma)_s \psi \left(\frac{dL_s}{d\chi} \right)_s d\chi \quad (14)$$

δW_h and δW_γ remain as before except for the additional term due to the lift and moment on the stabilizer caused by the additional degree of freedom.

For δW_h the extra term is:

$$\begin{aligned} Q_h = \frac{\delta W_h}{\delta q_1} &= \cos \Lambda_F \int_{-L_s \cos \Lambda_s}^{L_s \cos \Lambda_s} (B\chi_\gamma)_s \left(\frac{\partial h}{\partial s_F} \right)_L \left(\frac{dL_s}{d\chi} \right)_s d\chi \\ &= q_3 \pi \rho \omega^2 \cos \Lambda_F \int_{-L_s \cos \Lambda_s}^{L_s \cos \Lambda_s} B_s^2 (B\chi_\gamma)_s^2 \left(\frac{\partial h}{\partial s_F} \right)_L \psi L_h d\chi \end{aligned}$$

For δW_γ the extra term is:

$$\begin{aligned} Q_\gamma = \frac{\delta W_\gamma}{\delta q_2} &= -\sin \Lambda_F \int_{-L_s \cos \Lambda_s}^{L_s \cos \Lambda_s} (B\chi_\gamma)_s \chi_L \left(\frac{dL_s}{d\chi} \right)_s d\chi \\ &= -q_3 \pi \rho \omega^2 \sin \Lambda_F \int_{-L_s \cos \Lambda_s}^{L_s \cos \Lambda_s} B_s^2 (B\chi_\gamma)_s^2 \chi_L \psi L_h d\chi \end{aligned} \quad (15 \text{ a-c})$$

and

$$\begin{aligned} Q_\gamma = \frac{\delta W_\gamma}{\delta q_3} &= \pi \rho \omega^2 \int_{-L_s \cos \Lambda_s}^{L_s \cos \Lambda_s} \left\{ q_1 [B_s^2 (B\chi_\gamma)_s^2 \left(\frac{\partial h}{\partial s_F} \right)_L \cos \Lambda_F \psi L_h] \right. \\ &\quad - q_2 [B_s^2 (B\chi_\gamma)_s^2 \chi_L \sin \Lambda_F \psi L_h] \\ &\quad \left. + q_3 [B_s^2 (B\chi_\gamma)_s^2 \psi^2 L_h] \right\} d\chi \end{aligned}$$

(c) Fuselage Side Bending

Adding the fuselage side bending degree of freedom, q_4

$$\text{Bending deflection at } P_F = q_1 h + q_4 \phi (Y_R + S_F \sin \Lambda_F)$$

$$\text{Torsional deflection at } P_F = q_2 x + q_4 \phi \cos \Lambda_F$$

(16 a-b)

Vertical and torsional deflection at P_S remain as before.

$$\begin{aligned} (h_{c/4})_F &= q_1 h + q_4 \phi (Y_R + S_F \sin \Lambda_F) - B_F (\frac{1}{2} + a) \cos \Lambda_F (q_2 x + q_4 \phi \cos \Lambda_F) \\ (\alpha_{c/4})_F &= \frac{\partial}{\partial S_F} [q_1 h + q_4 \phi (Y_R + S_F \sin \Lambda_F)] \sin \Lambda_F + (q_2 x + q_4 \phi \cos \Lambda_F) \cos \Lambda_F \\ &= q_1 \left(\frac{\partial h}{\partial S_F} \right) \sin \Lambda_F + q_2 x \cos \Lambda_F + q_4 \phi \end{aligned} \quad (17 \text{ a-b})$$

$(h_{c/4})_S$ and $(\alpha_{c/4})_S$ remain as before.

$$\begin{aligned} \left(\frac{dL_{c/4}}{dx} \right)_F &= \pi \rho \omega^2 \left\{ B_F^2 [q_1 h + q_4 \phi (Y_R + S_F \sin \Lambda_F) - B_F (\frac{1}{2} + a) \cos \Lambda_F (q_2 x + q_4 \phi \cos \Lambda_F)] L_h \right. \\ &\quad \left. + B_F^3 [q_1 \left(\frac{\partial h}{\partial S_F} \right) \sin \Lambda_F + q_2 x \cos \Lambda_F + q_4 \phi] L_\alpha \right\} \\ &= \pi \rho \omega^2 \left\{ q_1 [B_F^2 h L_h + B_F^3 \left(\frac{\partial h}{\partial S_F} \right) \sin \Lambda_F L_\alpha] \right. \\ &\quad \left. + q_2 [-B_F^3 (\frac{1}{2} + a) x \cos \Lambda_F L_h + B_F^3 x \cos \Lambda_F L_\alpha] \right. \\ &\quad \left. + q_4 [B_F^2 \phi (Y_R + S_F \sin \Lambda_F) L_h - B_F^3 \phi (\frac{1}{2} + a) \cos^2 \Lambda_F L_h + B_F^3 \phi L_\alpha] \right\} \\ \left(\frac{dM_{c/4}}{dx} \right)_F &= \pi \rho \omega^2 \left\{ B_F^3 [q_1 h + q_4 \phi (Y_R + S_F \sin \Lambda_F) - B_F (\frac{1}{2} + a) \cos \Lambda_F (q_2 x + q_4 \phi \cos \Lambda_F)] M_h \right. \\ &\quad \left. + B_F^4 [q_1 \left(\frac{\partial h}{\partial S_F} \right) \sin \Lambda_F + q_2 x \cos \Lambda_F + q_4 \phi] M_\alpha \right\} \\ &= \pi \rho \omega^2 \left\{ q_1 [B_F^3 h M_h + B_F^4 \left(\frac{\partial h}{\partial S_F} \right) \sin \Lambda_F M_\alpha] \right. \\ &\quad \left. + q_2 [-B_F^4 (\frac{1}{2} + a) x \cos \Lambda_F M_h + B_F^4 x \cos \Lambda_F M_\alpha] \right. \\ &\quad \left. + q_4 [B_F^3 \phi (Y_R + S_F \sin \Lambda_F) M_h - B_F^4 \phi (\frac{1}{2} + a) \cos^2 \Lambda_F M_h + B_F^4 \phi M_\alpha] \right\} \end{aligned} \quad (18 \text{ a-b})$$

δW_ψ will remain as before. δW_h and δW_γ will remain as before except for the additional terms due to the lift and moment on the fin produced by the q_4 degree of freedom.

For δW_h the extra terms are:

$$\begin{aligned}
 Q_h = \frac{\delta W_h}{\delta q_1} &= \int_0^{L_F \cos \Lambda_F} h \left(\frac{dL_{c/4}}{dx} \right)_F dx + \sin \Lambda_F \int_0^{L_F \cos \Lambda_F} \left(\frac{\partial h}{\partial s_F} \right) \left(\frac{dM_{c/4}}{dx} \right)_F dx \\
 &= q_4 \pi \rho \omega^2 \left\{ \int_0^{L_F \cos \Lambda_F} \left[B_F^2 h \phi (Y_R + s_F \sin \Lambda_F) L_h - B_F^3 h \phi \left(\frac{1}{2} + a \right) \cos^2 \Lambda_F L_h + B_F^3 h \phi L_\alpha \right] dx \right. \\
 &\quad \left. + \sin \Lambda_F \int_0^{L_F \cos \Lambda_F} \left[B_F^3 \phi \left(\frac{\partial h}{\partial s_F} \right) (Y_R + s_F \sin \Lambda_F) M_h - B_F^4 \phi \left(\frac{\partial h}{\partial s_F} \right) \left(\frac{1}{2} + a \right) \cos^2 \Lambda_F M_h \right. \right. \\
 &\quad \left. \left. + B_F^4 \phi \left(\frac{\partial h}{\partial s_F} \right) M_\alpha \right] dx \right\} \\
 &= q_4 \pi \rho \omega^2 \int_0^{L_F \cos \Lambda_F} \left\{ B_F^2 h \phi (Y_R + s_F \sin \Lambda_F) L_h + B_F^3 h \phi [L_\alpha - \left(\frac{1}{2} + a \right) \cos^2 \Lambda_F L_h] \right. \\
 &\quad \left. + B_F^3 \phi \left(\frac{\partial h}{\partial s_F} \right) (Y_R + s_F \sin \Lambda_F) \sin \Lambda_F M_h \right. \\
 &\quad \left. + B_F^4 \phi \left(\frac{\partial h}{\partial s_F} \right) \sin \Lambda_F [M_\alpha - \left(\frac{1}{2} + a \right) \cos^2 \Lambda_F M_h] \right\} dx \quad (19 a)
 \end{aligned}$$

For δW_γ the extra terms are:

$$\begin{aligned}
 Q_\gamma = \frac{\delta W_\gamma}{\delta q_2} &= \int_0^{L_F \cos \Lambda_F} -B_F \left(\frac{1}{2} + a \right) \gamma \cos \Lambda_F \left(\frac{dL_{c/4}}{dx} \right)_F dx + \cos \Lambda_F \int_0^{L_F \cos \Lambda_F} \gamma \left(\frac{dM_{c/4}}{dx} \right)_F dx \\
 &= q_4 \pi \rho \omega^2 \left\{ \int_0^{L_F \cos \Lambda_F} \left[-B_F^3 \gamma \phi \left(\frac{1}{2} + a \right) (Y_R + s_F \sin \Lambda_F) \cos \Lambda_F L_h \right. \right. \\
 &\quad \left. \left. + B_F^4 \gamma \phi \left(\frac{1}{2} + a \right)^2 \cos^3 \Lambda_F L_h - B_F^4 \gamma \phi \left(\frac{1}{2} + a \right) \cos \Lambda_F L_\alpha \right] dx \right. \\
 &\quad \left. + \cos \Lambda_F \int_0^{L_F \cos \Lambda_F} \left[B_F^3 \gamma \phi (Y_R + s_F \sin \Lambda_F) M_h - B_F^4 \gamma \phi \left(\frac{1}{2} + a \right) \cos^2 \Lambda_F M_h \right. \right. \\
 &\quad \left. \left. + B_F^4 \gamma \phi M_\alpha \right] dx \right\} \quad (19 b) \\
 &= q_4 \pi \rho \omega^2 \cos \Lambda_F \int_0^{L_F \cos \Lambda_F} \left\{ B_F^3 \gamma \phi (Y_R + s_F \sin \Lambda_F) [M_h - \left(\frac{1}{2} + a \right) L_h] \right. \\
 &\quad \left. + B_F^4 \gamma \phi [M_\alpha - \left(\frac{1}{2} + a \right) L_\alpha] \right. \\
 &\quad \left. - \left(\frac{1}{2} + a \right) \cos^2 \Lambda_F [M_h - \left(\frac{1}{2} + a \right) L_h] \right\} dx
 \end{aligned}$$

The virtual work in the q_4 degree of freedom can be expressed as:

$$\delta W_\phi = \delta q_4 \left\{ \int_0^{L_F \cos \Lambda_F} \phi \left[(Y_R + S_F \sin \Lambda_F) - B_F \left(\frac{1}{2} + a \right) \cos^2 \Lambda_F \right] \left(\frac{dL_{\phi_4}}{d\chi} \right)_F d\chi \right. \\ \left. + \int_0^{L_F \cos \Lambda_F} \phi \left(\frac{dM_{\phi_4}}{d\chi} \right)_F d\chi \right\} \quad (20)$$

Substituting the lift and moment expressions and combining terms:

$$Q_\phi = \frac{\delta W_\phi}{\delta q_4} = q_1 \pi \rho \omega^2 \int_0^{L_F \cos \Lambda_F} \left\{ B_F^2 h \phi (Y_R + S_F \sin \Lambda_F) L_h \right. \\ + B_F^3 \left(\frac{\partial h}{\partial S_F} \right) \phi (Y_R + S_F \sin \Lambda_F) \sin \Lambda_F L_\alpha \\ + B_F^3 h \phi [M_h - (\frac{1}{2} + a) \cos^2 \Lambda_F L_h] \\ + B_F^4 \phi \left(\frac{\partial h}{\partial S_F} \right) \sin \Lambda_F [M_\alpha - (\frac{1}{2} + a) \cos^2 \Lambda_F L_\alpha] \Big\} d\chi \quad (21) \\ + q_2 \pi \rho \omega^2 \cos \Lambda_F \int_0^{L_F \cos \Lambda_F} \left\{ B_F^3 \gamma \phi (Y_R + S_F \sin \Lambda_F) [L_\alpha - (\frac{1}{2} + a) L_h] \right. \\ + B_F^4 \gamma \phi \left[\{ M_\alpha - (\frac{1}{2} + a) M_h \} - (\frac{1}{2} + a) \cos^2 \Lambda_F \{ L_\alpha - (\frac{1}{2} + a) L_h \} \right] \Big\} d\chi \\ + q_4 \pi \rho \omega^2 \int_0^{L_F \cos \Lambda_F} \left\{ B_F^2 \phi^2 (Y_R + S_F \sin \Lambda_F)^2 L_h \right. \\ + B_F^3 \phi^2 (Y_R + S_F \sin \Lambda_F) [(L_\alpha + M_h) - 2(\frac{1}{2} + a) \cos^2 \Lambda_F L_h] \\ + B_F^4 \phi^2 [M_\alpha - (\frac{1}{2} + a) \cos^2 \Lambda_F (L_\alpha + M_h) + (\frac{1}{2} + a)^2 \cos^4 \Lambda_F L_h] \Big\} d\chi$$

(d) Fuselage Torsion

Considering finally the fuselage torsion degree of freedom and ignoring the stabilizer rocking degree of freedom since none of the analyses involved simultaneously stabilizer rocking and fuselage torsion:

$$\text{Bending deflection at } P_F = q_1 h + q_4 \phi (Y_R + S_F \sin \Lambda_F) + q_5 \theta (X_R + S_F \cos \Lambda_F)$$

$$\text{Torsional deflection at } P_F = q_2 \gamma + q_4 \phi \cos \Lambda_F - q_5 \theta \sin \Lambda_F \quad (22 \text{ a-d})$$

$$\begin{aligned} \text{Vertical deflection at } P_S = & q_1 \left(\frac{\partial h}{\partial S_F} \right)_L \cos \Lambda_F S_S \cos \Lambda_S - q_2 \gamma_L \sin \Lambda_F S_S \cos \Lambda_S \\ & + q_5 \theta S_S \cos \Lambda_S \end{aligned}$$

$$\begin{aligned} \text{Torsional deflection at } P_S = & q_2 \gamma_L \sin \Lambda_F \sin \Lambda_S - q_1 \left(\frac{\partial h}{\partial S_F} \right)_L \cos \Lambda_F \sin \Lambda_S \\ & - q_5 \theta \sin \Lambda_S \end{aligned}$$

$$(h_{\frac{3}{4}})_F = q_1 h + q_4 \phi (Y_R + S_F \sin \Lambda_F) + q_5 \theta (X_R + S_F \cos \Lambda_F)$$

$$- B_F \left(\frac{l}{2} + a \right) \cos \Lambda_F (q_2 \gamma + q_4 \phi \cos \Lambda_F - q_5 \theta \sin \Lambda_F)$$

$$(\alpha_{\frac{3}{4}})_F = \frac{\partial}{\partial S_F} [q_1 h + q_4 \phi (Y_R + S_F \sin \Lambda_F) + q_5 \theta (X_R + S_F \cos \Lambda_F)] \sin \Lambda_F$$

$$+ q_2 \gamma \cos \Lambda_F + q_4 \phi \cos^2 \Lambda_F - q_5 \theta \sin \Lambda_F \cos \Lambda_F$$

$$= q_1 \left(\frac{\partial h}{\partial S_F} \right) \sin \Lambda_F + q_2 \gamma \cos \Lambda_F + q_4 \phi \quad (23 \text{ a-d})$$

$$(h_{\frac{3}{4}})_S = q_1 \left(\frac{\partial h}{\partial S_F} \right)_L \cos \Lambda_F S_S \cos \Lambda_S - q_2 \gamma_L \sin \Lambda_F S_S \cos \Lambda_S + q_5 \theta S_S \cos \Lambda_S$$

$$- B_S \left(\frac{l}{2} + a \right) \cos \Lambda_S [q_2 \gamma_L \sin \Lambda_F \sin \Lambda_S - q_1 \left(\frac{\partial h}{\partial S_F} \right)_L \cos \Lambda_F \sin \Lambda_S$$

$$- q_5 \theta \sin \Lambda_S]$$

$$(\alpha_{\frac{3}{4}})_S = 0$$

The lift and moment expressions become:

$$\begin{aligned} \left(\frac{dL_{\%}}{d\chi}\right)_F = \pi \rho \omega^2 \bigg\{ & q_1 [B_F^2 h L_h + B_F^3 \left(\frac{\partial h}{\partial S_F}\right) \sin \Lambda_F L_\alpha] \\ & + q_2 [B_F^3 \gamma \cos \Lambda_F \{L_\alpha - (\frac{1}{2} + a) L_h\}] \\ & + q_4 [B_F^2 \phi (\gamma_R + S_F \sin \Lambda_F) L_h + B_F^3 \phi \{L_\alpha - (\frac{1}{2} + a) \cos^2 \Lambda_F L_h\}] \\ & + q_5 [B_F^2 \theta (\chi_R + S_F \cos \Lambda_F) L_h + B_F^3 (\frac{1}{2} + a) \theta \sin \Lambda_F \cos \Lambda_F L_h] \bigg\} \end{aligned}$$

$$\begin{aligned} \left(\frac{dM_{\%}}{d\chi}\right)_F = \pi \rho \omega^2 \bigg\{ & q_1 [B_F^3 h M_h + B_F^4 \left(\frac{\partial h}{\partial S_F}\right) \sin \Lambda_F M_\alpha] \\ & + q_2 [B_F^4 \gamma \cos \Lambda_F \{M_\alpha - (\frac{1}{2} + a) M_h\}] \\ & + q_4 [B_F^3 \phi (\gamma_R + S_F \sin \Lambda_F) M_h + B_F^4 \phi \{M_\alpha - (\frac{1}{2} + a) \cos^2 \Lambda_F M_h\}] \\ & + q_5 [B_F^3 \theta (\chi_R + S_F \cos \Lambda_F) M_h + B_F^4 (\frac{1}{2} + a) \theta \sin \Lambda_F \cos \Lambda_F M_h] \bigg\} \end{aligned}$$

(24 a-d)

$$\begin{aligned} \left(\frac{dL_{\%}}{d\chi}\right)_s = \pi \rho \omega^2 \bigg\{ & q_1 B_s^2 \left(\frac{\partial h}{\partial S_F}\right)_L \cos \Lambda_F (B \chi \psi)_s L_h \\ & - q_2 B_s^2 \gamma_L \sin \Lambda_F (B \chi \psi)_s L_h \\ & + q_5 B_s^2 \theta (B \chi \psi)_s L_h \bigg\} \end{aligned}$$

$$\begin{aligned} \left(\frac{dM_{\%}}{d\chi}\right)_s = \pi \rho \omega^2 \bigg\{ & q_1 B_s^3 \left(\frac{\partial h}{\partial S_F}\right)_L \cos \Lambda_F (B \chi \psi)_s M_h \\ & - q_2 B_s^3 \gamma_L \sin \Lambda_F (B \chi \psi)_s M_h \\ & + q_5 B_s^3 \theta (B \chi \psi)_s M_h \bigg\} \end{aligned}$$

Substituting the lift and moment expressions into the virtual work equations and rearranging, the following additional terms are obtained by virtue of the q_5 degree of freedom:

For δW_h the extra terms are:

$$Q_h = \frac{\delta W_h}{\delta q_1} = q_5 \pi \rho \omega^2 \left\{ \int_0^{L_F \cos \Lambda_F} \left[B_F^2 h \theta (X_R + S_F \cos \Lambda_F) L_h + B_F^3 \left(\frac{1}{2} + a \right) h \theta \sin \Lambda_F \cos \Lambda_F L_h \right. \right. \\ \left. \left. + B_F^3 \left(\frac{\partial h}{\partial S_F} \right) \theta (X_R + S_F \cos \Lambda_F) \sin \Lambda_F M_h \right. \right. \\ \left. \left. + B_F^4 \left(\frac{1}{2} + a \right) \left(\frac{\partial h}{\partial S_F} \right) \theta \sin^2 \Lambda_F \cos \Lambda_F M_h \right] d\chi \right. \\ \left. + \int_{-L_S \cos \Lambda_S}^{L_S \cos \Lambda_S} B_S^2 \left(\frac{\partial h}{\partial S_F} \right)_L \cos \Lambda_F \theta (B \chi \psi)_S^2 L_h d\chi \right\}$$

For δW_γ the extra terms are:

$$Q_\gamma = \frac{\delta W_\gamma}{\delta q_2} = q_5 \pi \rho \omega^2 \left\{ \int_0^{L_F \cos \Lambda_F} \left[-B_F^3 \left(\frac{1}{2} + a \right) \theta (X_R + S_F \cos \Lambda_F) \gamma \cos \Lambda_F L_h \right. \right. \\ \left. \left. - B_F^4 \left(\frac{1}{2} + a \right)^2 \theta \sin \Lambda_F \gamma \cos^2 \Lambda_F L_h + B_F^3 \theta (X_R + S_F \cos \Lambda_F) \gamma \cos \Lambda_F M_h \right. \right. \\ \left. \left. + B_F^4 \left(\frac{1}{2} + a \right) \theta \sin \Lambda_F \gamma \cos^3 \Lambda_F M_h \right] d\chi \right. \\ \left. - \int_{-L_S \cos \Lambda_S}^{L_S \cos \Lambda_S} B_S^2 \gamma_L \sin \Lambda_F \theta (B \chi \psi)_S^2 L_h d\chi \right\} \quad (25 \text{ a-c})$$

For δW_ϕ the extra terms are:

$$Q_\phi = \frac{\delta W_\phi}{\delta q_4} = q_5 \pi \rho \omega^2 \left\{ \int_0^{L_F \cos \Lambda_F} \left[B_F^2 \theta (X_R + S_F \cos \Lambda_F) \phi (Y_R + S_F \sin \Lambda_F) L_h \right. \right. \\ \left. \left. + B_F^3 \left(\frac{1}{2} + a \right) \theta \sin \Lambda_F \phi \cos \Lambda_F (Y_R + S_F \sin \Lambda_F) L_h \right. \right. \\ \left. \left. - B_F^3 \left(\frac{1}{2} + a \right) \theta (X_R + S_F \cos \Lambda_F) \phi \cos^2 \Lambda_F L_h \right. \right. \\ \left. \left. - B_F^4 \left(\frac{1}{2} + a \right)^2 \theta \sin \Lambda_F \phi \cos^3 \Lambda_F L_h \right. \right. \\ \left. \left. + B_F^3 \phi \theta (X_R + S_F \cos \Lambda_F) M_h \right. \right. \\ \left. \left. + B_F^4 \left(\frac{1}{2} + a \right) \phi \theta \sin \Lambda_F \cos \Lambda_F M_h \right] d\chi \right\}$$

The virtual work in the q_5 degree of freedom can be expressed as:

$$\delta W_\theta = \delta q_5 \left\{ \int_0^{L_F \cos \Lambda_F} \theta \left[(\chi_R + s_F \cos \Lambda_F) + B_F \left(\frac{1}{2} + a \right) \sin \Lambda_F \cos \Lambda_F \right] \left(\frac{dL_{\frac{5}{4}}}{d\chi} \right)_F d\chi \right. \\ \left. + \int_{-L_S \cos \Lambda_S}^{L_S \cos \Lambda_S} \theta (B\chi_\psi)_s \left(\frac{dL_{\frac{5}{4}}}{d\chi} \right)_s d\chi \right\} \quad (26)$$

Substituting the lift expressions and combining terms:

$$Q_\theta = \frac{\delta W_\theta}{\delta q_5} = \pi \rho \omega^2 q_1 \left\{ \int_0^{L_F \cos \Lambda_F} \left[B_F^2 h \theta (\chi_R + s_F \cos \Lambda_F) L_h + B_F^3 \left(\frac{\partial h}{\partial s_F} \right) \sin \Lambda_F \theta (\chi_R + s_F \cos \Lambda_F) L_\alpha \right. \right. \\ \left. \left. + B_F^3 \left(\frac{1}{2} + a \right) h \theta \sin \Lambda_F \cos \Lambda_F L_h + B_F^4 \left(\frac{1}{2} + a \right) \chi \left(\frac{\partial h}{\partial s_F} \right) \theta \sin^2 \Lambda_F \cos \Lambda_F L_\alpha \right] d\chi \right. \\ \left. + \int_{-L_S \cos \Lambda_S}^{L_S \cos \Lambda_S} B_s^2 \left(\frac{\partial h}{\partial s_F} \right)_L \cos \Lambda_F \theta (B\chi_\psi)_s^2 L_h d\chi \right\} \\ + \pi \rho \omega^2 q_2 \left\{ \int_0^{L_F \cos \Lambda_F} \left[B_F^3 \chi \cos \Lambda_F \theta (\chi_R + s_F \cos \Lambda_F) \{ L_\alpha - \left(\frac{1}{2} + a \right) L_h \} \right. \right. \\ \left. \left. + B_F^4 \left(\frac{1}{2} + a \right) \theta \sin \Lambda_F \chi \cos^2 \Lambda_F \{ L_\alpha - \left(\frac{1}{2} + a \right) L_h \} \right] d\chi \right. \\ \left. + \int_{-L_S \cos \Lambda_S}^{L_S \cos \Lambda_S} -B_s^2 \alpha_L \sin \Lambda_F \theta (B\chi_\psi)_s^2 L_h d\chi \right\} \\ + \pi \rho \omega^2 q_4 \int_0^{L_F \cos \Lambda_F} \left\{ B_F^2 \theta (\chi_R + s_F \cos \Lambda_F) \phi (\chi_R + s_F \sin \Lambda_F) L_h \right. \\ \left. + B_F^3 \theta \phi (\chi_R + s_F \cos \Lambda_F) [L_\alpha - \left(\frac{1}{2} + a \right) \cos^2 \Lambda_F L_h] \right. \\ \left. + B_F^3 \theta \phi (\chi_R + s_F \sin \Lambda_F) \left(\frac{1}{2} + a \right) \sin \Lambda_F \cos \Lambda_F L_h \right. \\ \left. + B_F^4 \theta \phi \left(\frac{1}{2} + a \right) \sin \Lambda_F \cos \Lambda_F [L_\alpha - \left(\frac{1}{2} + a \right) \cos^2 \Lambda_F L_h] \right\} d\chi \\ + \pi \rho \omega^2 q_5 \left\{ \int_0^{L_F \cos \Lambda_F} \left[B_F^2 \theta^2 (\chi_R + s_F \cos \Lambda_F)^2 L_h \right. \right. \\ \left. \left. + 2 B_F^3 \left(\frac{1}{2} + a \right) \theta^2 (\chi_R + s_F \cos \Lambda_F) \sin \Lambda_F \cos \Lambda_F L_h \right. \right. \\ \left. \left. + B_F^4 \left(\frac{1}{2} + a \right)^2 \theta^2 \sin^2 \Lambda_F \cos^2 \Lambda_F L_h \right] d\chi \right. \\ \left. + \int_{-L_S \cos \Lambda_S}^{L_S \cos \Lambda_S} B_s^2 \theta^2 (B\chi_\psi)_s^2 L_h d\chi \right\} \quad (27)$$

3. Mechanical Parts:

The maximum kinetic energy of the system can be expressed in parts in the following manner:

(a) Fuselage

$$T_{fus.} = \frac{1}{2} I_{\phi x} \dot{q}_4^2 \phi^2 + \frac{1}{2} I_{\theta y} \dot{q}_5^2 \theta^2 \quad (28)$$

(b) Fin

Since the normal velocity of any point on the fin

$$= h\dot{q}_1 + r_F \gamma \dot{q}_2 + \phi(Y_R + s_F \sin \Lambda_F + r_F \cos \Lambda_F) \dot{q}_4 + \theta(X_R + s_F \cos \Lambda_F - r_F \sin \Lambda_F) \dot{q}_5 \quad (29)$$

$$T_F = \frac{1}{2} \int_0^{L_F} \int_{-b_F}^{b_F} [h\dot{q}_1 + r_F \gamma \dot{q}_2 + \phi(Y_R + s_F \sin \Lambda_F + r_F \cos \Lambda_F) \dot{q}_4 + \theta(X_R + s_F \cos \Lambda_F - r_F \sin \Lambda_F) \dot{q}_5]^2 \sigma dr_F ds_F \quad (30)$$

Where σ = mass per unit area

(c) Stabilizer

$$\text{Yawing angular velocity} = \left(\frac{\partial h}{\partial s_F}\right)_L \sin \Lambda_F \dot{q}_1 + \gamma_L \cos \Lambda_F \dot{q}_2 + \phi \dot{q}_4$$

$$\text{Rolling angular velocity} = \left(\frac{\partial h}{\partial s_F}\right)_L \cos \Lambda_F \dot{q}_1 - \gamma_L \sin \Lambda_F \dot{q}_2 + \psi \dot{q}_3 + \theta \dot{q}_5 \quad (31 \text{ a-c})$$

$$\begin{aligned} \text{Translational velocity} &= h_L \dot{q}_1 + \left(\frac{\partial h}{\partial s_F}\right)_L \sin \Lambda_F r \dot{q}_1 + \gamma_L \cos \Lambda_F r \dot{q}_2 \\ &\quad + \phi(Y_t + r) \dot{q}_4 + \theta X_t \dot{q}_5 \end{aligned}$$

$$\begin{aligned}
T_s = & \frac{1}{2} I_{yaw_s} \left[\left(\frac{\partial h}{\partial s_F} \right)_L \sin \Lambda_F \dot{q}_1 + x_L \cos \Lambda_F \dot{q}_2 + \phi \dot{q}_4 \right]^2 \\
& + \frac{1}{2} I_{roll_s} \left[\left(\frac{\partial h}{\partial s_F} \right)_L \cos \Lambda_F \dot{q}_1 - x_L \sin \Lambda_F \dot{q}_2 + \psi \dot{q}_3 + \theta \dot{q}_5 \right]^2 \\
& + \frac{1}{2} M_s \left[h_L \dot{q}_1 + \left(\frac{\partial h}{\partial s_F} \right)_L \sin \Lambda_F r \dot{q}_1 + x_L \cos \Lambda_F r \dot{q}_2 + \phi (Y_t + r) \dot{q}_4 \right. \\
& \quad \left. + \theta x_t \dot{q}_5 \right]^2
\end{aligned} \tag{32}$$

The total kinetic energy is

$$T = T_{fus.} + T_F + T_s \tag{33}$$

The mass and inertia terms are obtained from $\frac{d}{dt} \left(\frac{\partial T}{\partial \dot{q}_i} \right)$

4. Determinant Elements

By expanding the expression for the total kinetic energy and applying the Lagrange equation to the energy expressions the determinant elements below are obtained.

It should be noted that the following substitutions have been made:

$$\begin{aligned} \psi_g &= \gamma_L \sin \Lambda_F & I_y &= \int_{-b_F}^{b_F} r_F^2 \sigma dr_F \\ \psi_h &= \left(\frac{\partial h}{\partial s_F} \right)_L \cos \Lambda_F & m &= \int_{-b_F}^{b_F} \sigma dr_F \\ h' &= \left(\frac{\partial h}{\partial s_F} \right) & S_y &= \int_{-b_F}^{b_F} r \sigma dr_F \\ \eta_g &= \gamma_L \cos \Lambda_F & S_{ys} &= M_s r \\ \eta_h &= \left(\frac{\partial h}{\partial s_F} \right)_L \sin \Lambda_F & I_Y &= I_{Y_{aw_s}} + M_s r^2 \\ \Omega_i &= \left(\frac{\omega_i}{\omega} \right)^2 (1 + j g_i) & I_{sx} &= I_{Y_{aw_s}} + M_s (Y_t + r)^2 \\ & & I_{sy} &= I_R + M_s X_t^2 \end{aligned}$$

Integrating along ds and multiplying by $\cos \Lambda$ is in effect integrating along dX

Thus

$$\int_0^{L \cos \Lambda} f(x) dx = \cos \Lambda \int_0^L f(s) ds$$

DETERMINANT:

Fin Bending (h) vs. Fin Torsion (γ) vs. Stabilizer
 Rocking (ψ) vs. Fuselage Side Bending (ϕ)
 vs. Fuselage Torsion (θ)

	h	γ	ψ	ϕ	θ
h	D_{11}	D_{12}	D_{13}	D_{14}	D_{15}
γ	D_{21}	D_{22}	D_{23}	D_{24}	D_{25}
ψ	D_{31}	D_{32}	D_{33}	D_{34}	D_{35}
ϕ	D_{41}	D_{42}	D_{43}	D_{44}	D_{45}
θ	D_{51}	D_{52}	D_{53}	D_{54}	D_{55}

1 - h - Fin Bending

2 - γ - Fin Torsion

3 - ψ - Stabilizer Rocking

4 - ϕ - Fuselage Side Bending

5 - θ - Fuselage Torsion

DETERMINANT ELEMENTS:

$$D_{11} = (1 - \Omega_1) \left[\int_0^{L_F} m h^2 ds_F + I_Y \eta_h^2 + I_R \psi_h^2 + M_S h_L^2 + 2 S_{\gamma s} h_L \eta_h \right] \\ + \pi \rho \cos \Lambda_F \int_0^{L_F} \left[B_F^2 h^2 L_h + B_F^3 h h' \sin \Lambda_F (L_\alpha + M_h) + B_F^4 h'^2 \sin^2 \Lambda_F M_\alpha \right] ds_F \\ + 2 \pi \rho \cos \Lambda_S \psi_h^2 \int_0^{L_S} B_S^2 (B \chi_\psi)_S^2 L_h ds_S$$

$$D_{12} = \int_0^{L_F} S_\gamma h \gamma ds_F + I_Y \eta_\gamma \eta_h - I_R \psi_\gamma \psi_h + S_{\gamma s} h_L \eta_\gamma \\ + \pi \rho \cos^2 \Lambda_F \int_0^{L_F} \left\{ B_F^3 h \gamma [L_\alpha - (\frac{1}{2} + a) L_h] + B_F^4 h' \gamma \sin \Lambda_F [M_\alpha - (\frac{1}{2} + a) M_h] \right\} ds_F \\ - 2 \pi \rho \cos \Lambda_S \psi_h \psi_\gamma \int_0^{L_S} B_S^2 (B \chi_\psi)_S^2 L_h ds_S$$

$$D_{13} = I_R \psi \psi_h + 2 \pi \rho \cos \Lambda_S \psi \psi_h \int_0^{L_S} B_S^2 (B \chi_\psi)_S^2 L_h ds_S$$

$$D_{14} = \int_0^{L_F} [m h \phi Y_R + m h \phi s_F \sin \Lambda_F + S_\gamma h \phi \cos \Lambda_F] ds_F \\ + \phi [I_{Yaw} + S_{\gamma s} (Y_t + r)] \eta_h + M_S \phi (Y_t + r) h_L \\ + \pi \rho \cos \Lambda_F \int_0^{L_F} \left\{ B_F^2 h \phi (Y_R + s_F \sin \Lambda_F) L_h + B_F^3 h \phi [L_\alpha - (\frac{1}{2} + a) \cos^2 \Lambda_F L_h] \right. \\ \left. + B_F^3 h' \phi (Y_R + s_F \sin \Lambda_F) \sin \Lambda_F M_h \right. \\ \left. + B_F^4 h' \phi \sin \Lambda_F [M_\alpha - (\frac{1}{2} + a) \cos^2 \Lambda_F M_h] \right\} ds_F$$

$$\begin{aligned}
 D_{15} = & \int_0^{L_F} [mh\theta X_R + mh\theta s_F \cos \Lambda_F - S_Y h\theta \sin \Lambda_F] ds_F + I_R \theta \psi_h + M_S \theta \chi_t h_L + S_{Y_S} \theta \chi_t \eta_h \\
 & + \pi \rho \cos \Lambda_F \int_0^{L_F} [B_F^2 h\theta (X_R + s_F \cos \Lambda_F) L_h + B_F^3 h\theta (\frac{1}{2} + a) \sin \Lambda_F \cos \Lambda_F L_h \\
 & + B_F^3 h' \theta (X_R + s_F \cos \Lambda_F) \sin \Lambda_F M_h \\
 & + B_F^4 h' \theta (\frac{1}{2} + a) \sin^2 \Lambda_F \cos \Lambda_F M_h] ds_F \\
 & + 2\pi \rho \cos \Lambda_S \psi_h \theta \int_0^{L_S} B_S^2 (B\chi_\psi)_S^2 L_h ds_S
 \end{aligned}$$

$$\begin{aligned}
 D_{21} = & \int_0^{L_F} S_Y h \gamma ds_F + I_Y \eta_Y \eta_h - I_R \psi_Y \psi_h + S_{Y_S} h_L \eta_Y \\
 & + \pi \rho \cos^2 \Lambda_F \int_0^{L_F} \{ B_F^3 h \gamma [M_h - (\frac{1}{2} + a) L_h] + B_F^4 h' \gamma \sin \Lambda_F [M_\alpha - (\frac{1}{2} + a) L_\alpha] \} ds_F \\
 & - 2\pi \rho \cos \Lambda_S \psi_h \psi_Y \int_0^{L_S} B_S^2 (B\chi_\psi)_S^2 L_h ds_S
 \end{aligned}$$

$$\begin{aligned}
 D_{22} = & (1 - \Omega_2) \left[\int_0^{L_F} I_Y \gamma^2 ds_F + I_Y \eta_Y^2 + I_R \psi_Y^2 \right] \\
 & + \pi \rho \cos^3 \Lambda_F \int_0^{L_F} B_F^4 \gamma^2 \left[M_\alpha - (\frac{1}{2} + a) (L_\alpha + M_h) + (\frac{1}{2} + a)^2 L_h \right] ds_F \\
 & + 2\pi \rho \cos \Lambda_S \psi_Y^2 \int_0^{L_S} B_S^2 (B\chi_\psi)_S^2 L_h ds_S
 \end{aligned}$$

$$D_{23} = -I_R \psi \psi_Y - 2\pi \rho \cos \Lambda_S \psi \psi_Y \int_0^{L_S} B_S^2 (B\chi_\psi)_S^2 L_h ds_S$$

$$\begin{aligned}
 D_{24} = & \int_0^{L_F} [S_Y \gamma \phi Y_R + S_Y \gamma \phi s_F \sin \Lambda_F + I_Y \gamma \phi \cos \Lambda_F] ds_F + \phi [I_{YAW} + S_{YS} (Y_t + r)] \eta_Y \\
 & + \pi \rho \cos^2 \Lambda_F \int_0^{L_F} \left\{ B_F^3 \gamma \phi (Y_R + s_F \sin \Lambda_F) [M_h - (\frac{1}{2} + a) L_h] \right. \\
 & \left. + B_F^4 \gamma \phi [\{M_\alpha - (\frac{1}{2} + a) L_\alpha\} - (\frac{1}{2} + a) \cos^2 \Lambda_F \{M_h - (\frac{1}{2} + a) L_h\}] \right\} ds_F
 \end{aligned}$$

$$\begin{aligned}
 D_{25} = & \int_0^{L_F} [S_Y \gamma \theta X_R + S_Y \gamma \theta s_F \cos \Lambda_F - I_Y \gamma \theta \sin \Lambda_F] ds_F - I_R \theta \psi_Y + S_{YS} \theta X_t \eta_Y \\
 & + \pi \rho \cos^2 \Lambda_F \int_0^{L_F} \left\{ B_F^3 \gamma \theta (X_R + s_F \cos \Lambda_F) [M_h - (\frac{1}{2} + a) L_h] \right. \\
 & \left. + B_F^4 \gamma \theta (\frac{1}{2} + a) \sin \Lambda_F \cos \Lambda_F [M_h - (\frac{1}{2} + a) L_h] \right\} ds_F \\
 & - 2 \pi \rho \cos \Lambda_s \psi_Y \theta \int_0^{L_F} B_s^2 (B \chi_Y)_s^2 L_h ds_s
 \end{aligned}$$

$$D_{31} = I_R \psi \psi_h + 2 \pi \rho \cos \Lambda_s \psi \psi_h \int_0^{L_s} B_s^2 (B \chi_Y)_s^2 L_h ds_s = D_{13}$$

$$D_{32} = -I_R \psi \psi_Y - 2 \pi \rho \cos \Lambda_s \psi \psi_Y \int_0^{L_s} B_s^2 (B \chi_Y)_s^2 L_h ds_s = D_{23}$$

$$D_{33} = (1 - \Omega_3) I_R \psi^2 + 2 \pi \rho \cos \Lambda_s \psi^2 \int_0^{L_s} B_s^2 (B \chi_Y)_s^2 L_h ds_s$$

$$D_{34} = 0$$

$$\begin{aligned}
 D_{41} = & \int_0^{L_F} [mh\phi Y_R + mh\phi s_F \sin \Lambda_F + S_y h\phi \cos \Lambda_F] ds_F \\
 & + \phi [I_{yaw} + S_{ys} (Y_t + r)] \eta_h + M_s \phi (Y_t + r) h_L \\
 & + \pi \rho \cos \Lambda_F \int_0^{L_F} \left\{ B_F^2 h\phi (Y_R + s_F \sin \Lambda_F) L_h + B_F^3 h\phi [M_h - (\frac{1}{2} + a) \cos^2 \Lambda_F L_h] \right. \\
 & \quad + B_F^3 h\phi (Y_R + s_F \sin \Lambda_F) \sin \Lambda_F L_\alpha \\
 & \quad \left. + B_F^4 h\phi \sin \Lambda_F [M_\alpha - (\frac{1}{2} + a) \cos^2 \Lambda_F L_\alpha] \right\} ds_F
 \end{aligned}$$

$$\begin{aligned}
 D_{42} = & \int_0^{L_F} [S_y \gamma \phi Y_R + S_y \gamma \phi s_F \sin \Lambda_F + I_y \gamma \phi \cos \Lambda_F] ds_F \\
 & + \phi [I_{yaw} + S_{ys} (Y_t + r)] \eta_y \\
 & + \pi \rho \cos^2 \Lambda_F \int_0^{L_F} \left\{ B_F^3 \gamma \phi (Y_R + s_F \sin \Lambda_F) [L_\alpha - (\frac{1}{2} + a) L_h] \right. \\
 & \quad \left. + B_F^4 \gamma \phi [\{M_\alpha - (\frac{1}{2} + a) M_h\} - (\frac{1}{2} + a) \cos^2 \Lambda_F \{L_\alpha - (\frac{1}{2} + a) L_h\}] \right\} ds_F
 \end{aligned}$$

$$D'_{43} = 0 = D_{34}$$

$$\begin{aligned}
 D_{44} = (1 - \Omega_4) \bigg\{ & \int_0^{L_F} [m\phi^2 s_F^2 \sin^2 \Lambda_F + 2m\phi^2 Y_R s_F \sin \Lambda_F + 2S_y \phi^2 Y_R \cos \Lambda_F \\
 & + 2S_y \phi^2 s_F \sin \Lambda_F \cos \Lambda_F] ds_F + \phi^2 \cos^2 \Lambda_F I_F + \phi^2 Y_R^2 M_F \\
 & + I_{\phi x} \phi^2 + I_{s x} \phi^2 \bigg\} + \pi \rho \cos \Lambda_F \int_0^{L_F} \bigg\{ B_F^2 \phi^2 (Y_R + s_F \sin \Lambda_F)^2 L_h \\
 & + B_F^3 \phi^2 (Y_R + s_F \sin \Lambda_F) [(M_h + L_\alpha) - 2(\frac{1}{2} + a) \cos^2 \Lambda_F L_h] \\
 & + B_F^4 \phi^2 [M_\alpha - (\frac{1}{2} + a) \cos^2 \Lambda_F \{ (M_h + L_\alpha) - (\frac{1}{2} + a) \cos^2 \Lambda_F L_h \}] \bigg\} ds_F
 \end{aligned}$$

$$\begin{aligned}
 D_{45} = \int_0^{L_F} & [ms_F \phi \theta (Y_R \cos \Lambda_F + X_R \sin \Lambda_F) + ms_F^2 \phi \theta \sin \Lambda_F \cos \Lambda_F \\
 & + S_y \phi \theta (X_R \cos \Lambda_F - Y_R \sin \Lambda_F) + S_y s_F \phi \theta (\cos^2 \Lambda_F - \sin^2 \Lambda_F)] ds_F \\
 & + \phi Y_R \theta X_R M_F + \phi (Y_t + r) \theta X_t M_S - \phi \theta \sin \Lambda_F \cos \Lambda_F I_F \\
 & + \pi \rho \cos \Lambda_F \int_0^{L_F} \bigg\{ B_F^2 \theta (X_R + s_F \cos \Lambda_F) \phi (Y_R + s_F \sin \Lambda_F) L_h \\
 & + B_F^3 \phi (Y_R + s_F \sin \Lambda_F) \theta (\frac{1}{2} + a) \sin \Lambda_F \cos \Lambda_F L_h \\
 & + B_F^3 \phi \theta (X_R + s_F \cos \Lambda_F) [M_h - (\frac{1}{2} + a) \cos^2 \Lambda_F L_h] \\
 & + B_F^4 \phi \theta (\frac{1}{2} + a) \sin \Lambda_F \cos \Lambda_F [M_h - (\frac{1}{2} + a) \cos^2 \Lambda_F L_h] \bigg\} ds_F
 \end{aligned}$$

DETERMINANT ELEMENTS (cont'd.)

$$D_{51} = \int_0^{L_F} [mh\theta\chi_R + mh\theta s_F \cos\Lambda_F - S_Y h\theta \sin\Lambda_F] ds_F + I_R \theta \psi_h + M_s \theta \chi_t h_t + S_{Ys} \theta \chi_t \eta_h \\ + \pi \rho \cos\Lambda_F \int_0^{L_F} [B_F^2 h\theta (\chi_R + s_F \cos\Lambda_F) L_h + B_F^3 h\theta (\frac{1}{2} + a) \sin\Lambda_F \cos\Lambda_F L_h \\ + B_F^3 h\theta (\chi_R + s_F \cos\Lambda_F) \sin\Lambda_F L_\alpha + B_F^4 h\theta (\frac{1}{2} + a) \sin^2\Lambda_F \cos\Lambda_F L_\alpha] ds_F \\ + 2\pi \rho \cos\Lambda_s \psi_h \int_0^{L_s} B_s^2 (B\chi_\psi)_s^2 L_h ds_s$$

$$D_{52} = \int_0^{L_F} [S_Y \gamma \theta \chi_R + S_Y \gamma \theta s_F \cos\Lambda_F - I_Y \gamma \theta \sin\Lambda_F] ds_F - I_R \theta \psi_Y + S_{Ys} \theta \chi_t \eta_Y \\ + \pi \rho \cos^2\Lambda_F \int_0^{L_F} \{B_F^3 \gamma \theta (\chi_R + s_F \cos\Lambda_F) [L_\alpha - (\frac{1}{2} + a) L_h] \\ + B_F^4 \gamma \theta (\frac{1}{2} + a) \sin\Lambda_F \cos\Lambda_F [L_\alpha - (\frac{1}{2} + a) L_h]\} ds_F \\ - 2\pi \rho \cos\Lambda_s \psi_Y \int_0^{L_s} B_s^2 (B\chi_\psi)_s^2 L_h ds_s$$

$$D_{54} = \int_0^{L_F} [ms_F \phi \theta (Y_R \cos\Lambda_F + \chi_R \sin\Lambda_F) + ms_F^2 \phi \theta \sin\Lambda_F \cos\Lambda_F \\ + S_Y \phi \theta (\chi_R \cos\Lambda_F - Y_R \sin\Lambda_F) + S_Y s_F \phi \theta (\cos^2\Lambda_F - \sin^2\Lambda_F)] ds_F \\ + \phi Y_R \theta \chi_R M_F + \phi (Y_t + r) \theta \chi_t M_s - \phi \theta \sin\Lambda_F \cos\Lambda_F I_F \\ + \pi \rho \cos\Lambda_F \int_0^{L_F} \{B_F^2 \theta (\chi_R + s_F \cos\Lambda_F) \phi (Y_R + s_F \sin\Lambda_F) L_h \\ + B_F^3 \phi \theta (Y_R + s_F \sin\Lambda_F) (\frac{1}{2} + a) \sin\Lambda_F \cos\Lambda_F L_h \\ + B_F^3 \phi \theta (\chi_R + s_F \cos\Lambda_F) [L_\alpha - (\frac{1}{2} + a) \cos^2\Lambda_F L_h] \\ + B_F^4 \phi \theta (\frac{1}{2} + a) \sin\Lambda_F \cos\Lambda_F [L_\alpha - (\frac{1}{2} + a) \cos^2\Lambda_F L_h]\} ds_F$$

$$\begin{aligned}
 D_{55} = (1 - \Omega_5) \Big\{ & \int_0^{L_F} \left[m\theta^2 s_F^2 \cos^2 \Lambda_F + 2m\theta^2 X_R s_F \cos \Lambda_F - 2S_y \theta^2 X_R \sin \Lambda_F \right. \\
 & \left. - 2S_y \theta^2 s_F \sin \Lambda_F \cos \Lambda_F \right] ds_F + I_{\theta Y} \theta^2 + \theta^2 X_R^2 M_F + \theta^2 \sin^2 \Lambda_F I_F \\
 & + \theta^2 I_{sY} \Big\} + \pi \rho \cos \Lambda_F \int_0^{L_F} \left[B_F^2 \theta^2 (X_R + s_F \cos \Lambda_F)^2 L_h \right. \\
 & + 2 B_F^3 \theta^2 (X_R + s_F \cos \Lambda_F) (\tfrac{1}{2} + a) \sin \Lambda_F \cos \Lambda_F L_h \\
 & + B_F^4 \theta^2 (\tfrac{1}{2} + a)^2 \sin^2 \Lambda_F \cos^2 \Lambda_F L_h \Big] ds_F \\
 & + 2\pi \rho \cos \Lambda_s \theta^2 \int_0^{L_s} B_s^2 (B\pi r)_s^2 L_h ds_s
 \end{aligned}$$